Texas A&M University
Mechanical Engineering Department

Thermohydrodynamic Analysis of Cryogenic Liquid Turbulent Flow Fluid Film Bearings (Phase II)

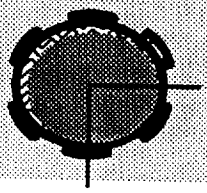

NASA Grant NAG3-1434

1994 Annual Research Progress Report to
NASA Lewis Research Center

Contract Monitor: Mr. James Walker

Luis San Andres
Associate Professor
December 1994

Period of performance: January 1 to December 31, 1994

THERMOHYDRODYNAMIC ANALYSIS OF CRYOGENIC LIQUID TURBULENT FLOW FLUID FILM BEARINGS
PHASE II

Luis San Andres
Associate Professor, Texas A&M University
College Station, TX 77843-3123

Annual Report to NASA-Lewis Research Center
NASA Grant NAG3-1434
Contract Monitor: Mr. James Walker

EXECUTIVE SUMMARY

This Phase II (1994) **Annual Progress Report** presents two major report - sections describing the **thermal** analysis of tilting- and flexure-pad hybrid bearings, and the unsteady flow and transient response of a point mass rotor supported on fluid film bearings. A literature review on the subject of two-phase flow in fluid film bearings and part of the proposed work for 1995 are also included.

The programs delivered at the end of 1994 are named **hydroflext** and **hydrotran**. Both codes are fully compatible with the **hydrosealt** (1993) program. The new programs retain the same calculating options of **hydrosealt** plus the added bearing geometries, and unsteady flow and transient forced response.

Refer to the **hydroflext & hydrotran User's Manual** and **Tutorial** for basic information on the analysis and instructions to run the programs. The **Examples Handbook** contains the test bearing cases along with comparisons with experimental data or published analytical values.

The following major tasks were completed on 1994 (Phase II):

a) Extension of the thermohydrodynamic analysis and development of computer program **hydroflext** to model the following bearing geometries:

   tilting-pad hydrodynamic journal bearings,
   flexure-pad cylindrical bearings (hydrostatic and hydrodynamic), and
   cylindrical pad bearings with a simple elastic matrix (ideal foil bearings).

b) Improved thermal model including radial heat transfer through the bearing stator.

c) Calculation of the **unsteady** bulk-flow field in fluid film bearings and the **transient response** of a point mass rotor supported on bearings.

d) A literature review on the subject of two-phase flows and homogeneous - mixture flows in thin-film geometries.

Brief description of hydroflext program

The motion of a cryogenic liquid on the thin film annular region of a fluid film bearing is described by a set of mass and momentum conservation, and energy transport equations for the turbulent bulk-flow velocities and pressure, and accompanied by thermophysical state equations for evaluation of the fluid material properties. Zeroth-order equations describe the fluid flow field for a journal static equilibrium position, while first-order (linear) equations govern the fluid flow for small amplitude journal center translational motions. Solution to the zeroth-order flow field equations provides the bearing flow rate, load capacity, drag torque and temperature rise. Solution to the first-order equations determines the rotordynamic force coefficients due to journal radial motions.

The **hydroflext** program calculates the static load and dynamic force coefficients for the following bearing geometries:

1. hydrostatic bearings with orifice compensation and rectangular recesses (single row or two-parallel recess row),

2. annular pressure seals (damper seals) (cylindrical and multilobe),

3. plain cylindrical hydrodynamic bearings (cylindrical and multilobe),

4. fixed arc hydrodynamic bearings with arbitrary preload,

5. tilting-pad journal bearings,

6. flexure-pad journal bearings (hydrostatic and hydrodynamic),

7. cylindrical pad bearings with a simple elastic matrix (ideal foil bearing).

hydroflext includes the following thermal models:

- adiabatic surfaces, i.e. insulated journal and bearing surfaces.

- isothermal journal at specified temperature and insulated (adiabatic) bearing.

- isothermal bearing at specified temperature and insulated (adiabatic) journal.

- isothermal journal and bearing surfaces.

- isothermal journal and radial heat flow through bearing (stator).

- adiabatic journal and radial heat flow through bearing (stator).

hydroflext calculates

1) bearing flowrate or seal leakage
2) friction torque, power dissipation and temperature rise
3) load capacity (fluid film forces and moments) if journal eccentricity

is given, or
journal equilibrium eccentricity components if the external loads are given.

4) 16 complex impedance coefficients due to dynamic journal center displacements and journal axis rotations. The real and imaginary parts of the impedances correspond to the stiffness and damping coefficients evaluated at a specified excitation frequency.
5) Stability indicator or whirl frequency ratio for lateral journal motions and equivalent stiffness at operating speed.
6) Pressure and temperature fields on the bearing surface, and density and viscosity field variations, within ranges of fluid flow Reynolds numbers and Mach numbers.

for

1) isothermal flow with barotropic fluid,
2) thermohydrodynamic adiabatic or radial heat flow and/or isothermal journal and bearing surfaces
in the single phase flow regime.

with the following fluids:

1) liquid hydrogen,	2) liquid nitrogen,
3) liquid oxygen,	4) liquid methane,
5) water,	6) oil,
7) air,	8) barotropic liquid.

For cryogenic liquids, the fluid properties (density, viscosity and specific heat) are calculated with the miprops program from NBS Standard Reference Database 12.

hydroflext handles the following boundary conditions at the bearing exit planes:

1) periodic pressure asymmetry in the axial direction.
2) local discharge end seal effects via an orifice like model to simulate wear-ring hydrostatic bearings or annular seals.
3) inlet specified circumferential pre-swirl velocity distribution.

The axial clearance functions included are of the type:

a) uniform, b) tapered,
c) stepped, or, d) arbitrary via spline interpolation.

Cylindrical bearings can be specified as multi-lobe geometries, and bearing pads can have a specified assembly preload.

For tilting-pads and flexure-pad bearings, pad mass moment of inertia and flexure rotational stiffness and damping coefficientc are needed for full specification of the bearing geometry.

Brief description of hydrotran program

The extended computer program **hydrotran** calculates the dynamic (transient) force response of a rigid rotor supported on fluid film bearings. The code calculates at each time step of numerical integration the unsteady bulk-flow field and the fluid film bearing forces due to prescribed time-varying external loads. **The transient analysis is restricted to isothermal flows and rigid pad bearings, i.e., the current model does not account for transient thermal effects and can not handle the transient dynamics of tilting pad bearings.** These restrictions on the code are due to the large computational times required to determine a transient solution with small time steps.

The equations of motion solved are:

$$M\,AX = FX + WX(t) \quad (1)$$

$$M\,AY = FY + WY(t)$$

where M: rotor point mass [kg],

WX,WY: external time dependent loads [N],

AX,AY(t): rotor accelerations [m/s^2], and

FX,FY(t): are the fluid film bearing reaction forces [N].

The external load cases considered are:

1 periodic forcing function
WX=Fmag cos(wt), WY=Fmag sin(wt)

2 ramp loading along X direction
WX=Fmag t/T if t<T, WX=Fmag if t>=T ; WY=0

3 step loading along X direction
WX=Fmag for t>=0, WY=0.

4 rotor weight along X + sudden unbalance forcing function
WX=Weight+ Funbal cos(ωt); WY= 0 + Funbal sin(ωt)

Weight=M·g , Funbal= Mrotor x UNBmag [m] x ω^2

5 impulse load along Y direction applied over To (secs)
WX=Weight=M·g , WY=Fimpulse exp[-.5x(t/to)^2]

The Wilson-Θ method is used to perform the numerical integration of equations (1). A simpler program (**TWOdof**) uses the (linear) rotordynamic force coefficients at an equilibrium position and calculates an approximate transient response. This program executes much faster than the full numerical nonlinear solution and can be used efficiently for rotors supported on externally pressurized bearings, i.e. bearings which do not show great variation of their

force coefficients with the applied load or journal position.

List of technical publication for cryogenic fluid film bearings - 1994

Directly supported by NASA Grant NAG3-1434:

San Andres, L., "Thermohydrodynamic Analysis of Fluid Film Bearings for Cryogenic Applications," accepted for publication at AIAA Journal of Propulsion and Power, September 1994.

San Andres, L., 1994, "Turbulent Flow Foil Bearings for Cryogenic Applications," ASME Transactions Paper 94-TRIB-33, to be published at the ASME Journal of Tribology.

San Andres, L., and Yang, Z., "Thermohydrodynamic Analysis of Fluid Film Bearings for Cryogenic Applications," 6th NASA Conference on Advanced Earth-to-Orbit Propulsion Technology, Huntsville, Alabama, May 1994.

San Andres, L., "Analysis of Arbitrary Recess Geometry Hydrostatic Bearings," 6th NASA Conference on Advanced Earth-to-Orbit Propulsion Technology, Huntsville, Alabama, May 1994.

Yang, Z., L. San Andres and D. Childs, "Thermohydrodynamic Analysis of Process Liquid Hydrostatic Bearings in Turbulent Regime, Part I: Theory, Part II: Numerical Solution and Results," accepted at ASME Journal of Applied Mechanics, April 1994.

Other past funding sources

San Andres, L., Z. Yang, and D. Childs, "Turbulent Flow Hydrostatic Bearings: Analysis and Experimental Results," accepted for publication at International Journal of Mechanical Sciences, October 1994.

Hill., D., E. Baskharone, and L. San Andres, 1994, "Inertia Effects in a Hybrid Bearing with a 45 degree Entrance Region," accepted for publication at ASME Journal of Tribology, July 1994.

Yang, Z., L. San Andres, and D. Childs, "Process Liquid Turbulent Flow Hydrostatic Bearings: Analysis and Tests for Rotordynamic Coefficients," Proceedings of the 4th International IFToMM Rotordynamics Conference, pp. 233-242, Chicago, September, 1994.

Franchek, N., D. Childs, and L. San Andres, 1994, "Theoretical and Experimental Comparisons for Rotordynamic Coefficients of a High-Speed, High-Pressure, Orifice-Compensated Hybrid Bearings," ASME Transactions Paper 94-TRIB-43, to be published on the ASME Journal of Tribology.

San Andres, L., "Dynamic Force Response of Spherical Hydrostatic Journal Bearings for Cryogenic Applications", STLE Tribology Transactions, Vol 37, 3, pp. 463-470, 1994.

TABLE OF CONTENTS

THERMOHYDRODYNAMIC ANALYSIS OF CRYOGENIC LIQUID TURBULENT FLOW FLUID FILM BEARINGS PHASE II

TABLE OF CONTENTS (continued)

TABLE OF CONTENTS (continued)

Texas A&M University
Mechanical Engineering Department

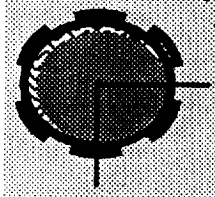

Turbulent Flow, Flexure Pad Fluid Film Bearings for Cryogenic Applications

NASA Lewis Research Center
NASA Grant NAG3-1434
Contract Monitor: Mr. James Walker

Luis San Andres
Associate Professor
December 1994

Thermohydrodynamic Analysis of Cryogenic Liquid Turbulent Flow Fluid Film Bearings (Phase II)

Turbulent Flow, Flexure-Pad Fluid Film Bearings

for Cryogenic Applications

Luis San Andres
Associate Professor
Texas A&M University
December 1994

prepared for NASA Lewis Research Center
NASA Grant NAG3-1434, Phase II
Year II
Contract Monitor: Mr. James Walker

ABSTRACT

The thermal analysis of flexure pivot tilting-pad hybrid (combination hydrostatic - hydrodynamic) fluid film bearings for cryogenic liquid applications is presented. Turbulent bulk-flow, variable properties, momentum and energy transport equations of motion govern the flow in the thin film lands. Zeroth-order equations describe the fluid flow field for a journal static equilibrium position, while first-order linear equations govern the fluid flow for small amplitude journal center translational motions. Solution to the zeroth-order flow field equations provides the fluid film bearing flow-rate, load capacity, drag torque, and temperature rise. Solution to the first-order equations determines the linearized force coefficients due to journal radial motions. An elegant method to determine the tilting-pad moment coefficients from the force displacement coefficients, and an iterative Newton-Raphson scheme to balance the pad moments are detailed. Numerical predictions correlate well with experimental measurements for tilting-pad hydrodynamic bearings. A design of a flexure-pad hydrostatic bearing for a cryogenic application is shown to have a reduced whirl frequency ratio without loss in load capacity or reduction in direct stiffness and damping coefficients.

This report extends the previous analysis (Mid-Year Progress Report, June 1993) of tilting- and flexure-pad bearings to include **thermal** effects. The Results section is identical to that of the original Mid-Year Report.

For a lucid discussion on the importance and advantages of fluid film bearings in cryogenic turbomachinery see the Research Progress Report, Phase I, to the present project (San Andres, 1993).

Refer to **hydroflext User's Manual and Tutorial** for information and instructions to run the program. Also if you are in charge of installing the program on your system please browse the **README** file enclosed on the **hydroflext** documentation.

NOMENCLATURE

A_o	$Cd\ \pi\ d_o^2/4$. Equivalent orifice area [m^2].
A_r	$l \cdot R_* \cdot \Theta_r$. Recess area [$m^2$].
C_d	empirical orifice discharge coefficient.
$C_p, C_*, \bar{C}_p$	Pad clearance function, characteristic clearance [m], C_p/C_*
C_m	Assembled bearing radial clearance [m]
$C^k_{XX}, C^k_{XY}, C^k_{YX}, C^k_{YY}$	Pad Force damping coefficients due to displacements [Ns/m]
$C^k_{\delta X}, C^k_{\delta Y}$	Pad Moment damping coefficients due to displacements [N-s]
$C^k_{\delta\delta}$	Pad Moment damping coefficient due to pad rotation [N-m-s/rad]
$C^k_{X\delta}, C^k_{Y\delta}$	Pad Force damping coefficients due to pad rotation [N-s/rad]
$C^k_{R\alpha\beta}$	Reduced pad damping coefficients at frequency ω; $\alpha, \beta = X, Y$
$C_{R\alpha\beta}$	Reduced bearing damping coefficients; $\alpha, \beta = X, Y$ [N·s/m]
Cr_k	Pad rotational damping coefficient [N-m-s/rad]
$c_p, \bar{c}_p$	specific heat [J/kg·°K], c_p/c_{p*}
D	$2 \cdot R$. Bearing diameter [m].
d_o	Orifice diameter [m]
e_X, e_Y	Journal displacements in X and Y directions [m].
E_c	$(U^2/T \cdot c_p)_*$. Eckert number.
$f_{J,B}$	$a_M \left[1 + \left(c_M \frac{r_{J,B}}{H} + \frac{b_M}{R_{J,B}} \right)^{e_M} \right]$; $a_M = 0.001375$, $b_M = 500{,}000$; $c_M = 10{,}000$, $e_M = 1/3.00$
	Turbulent flow friction factors at journal and bearing surfaces.
F^k_X, F^k_Y	Pad fluid film forces along {X,Y} axes [N].
F_X, F_Y	Film forces along {X,Y} axes [N].
i	$\sqrt{-1}$. Imaginary unit.
I_k	Pad mass moment of Inertia [$kg \cdot m^2$].
H,h	Film thickness [m], H/C_*.

H_r	Recess depth [m].
h_o	H_o/C_*. Dimensionless zeroth-order film thickness.
h_1	$e^{i\tau}\ \Delta_\alpha\ h\alpha$. Circumferential fluid film thickness functions.
h_X, h_Y, h_δ^k	$\cos\theta$, $\sin\theta$, $\sin(\theta_p^k-\theta)$. Perturbed film thickness components.
h_B, h_J	Convection heat transfer coefficients [$W/m^2\cdot°K$].
$\bar{h}_B, \bar{h}_J$	$(h_B, h_J)C_*/(P_{e*}K_*)$.
$K, \bar{K}$	Fluid thermal conductivity [$W/m\cdot°K$], K/K_*
$K_{XX}^k, K_{XY}^k, K_{YX}^k, K_{YY}^k$	Pad Force stiffness coefficients due to displacements [N/m]
$K_{\delta X}^k, K_{\delta Y}^k$	Pad Moment stiffness coefficients due to displacements [N]
$K_{\delta\delta}^k$	Pad Moment stiffness coefficient due to pad rotation [N-m/rad]
$K_{X\delta}^k, K_{Y\delta}^k$	Pad Force stiffness coefficients due to rotations [N/rad]
$K_{R\alpha\beta}^k$	Reduced pad stiffness coefficients at frequency ω; α,β=X,Y
$K_{R\alpha\beta}$	Reduced bearing stiffness coefficients; α,β=X,Y [N/m]
Kr_k	Pad rotational structural stiffness coefficient [N·m/rad]
L, L_R, L_L	Bearing axial length = L_R+L_L, Right and Left axial side lengths measured from recess center [m]
l	Recess axial length [m].
M	$U_\theta\cdot\sqrt{\beta_p\cdot\rho_r}$. Orifice circumferential velocity Mach number.
M^k	$R\{\sin\theta_p^k\ F_X - \cos\theta_p^k\ F_Y\}$. Pad Moment due to fluid film forces [N·m]
N_{pad}	Number of pads on bearing.
N_{recess}	Number of recesses on pad.
P, Pr	Fluid pressure, recess pressure [N/m^2].
P_e^-, P_e^+	Pressures just before and after recess edge [N/m^2].
P_L, P_R	Discharge pressures on left and right sides of bearing[N/m^2].
P_s	External supply pressure [N/m^2].
P_a	$\mathrm{Min}\{P_L, P_R\}$. Characteristic discharge pressure [N/m^2].
P_{sa}	characteristic pressure, = $Ps-P_a$ for hydrostatic bearings; = $\mu\Omega(R/C_*)^2$ for hydrodynamic bearings.

p	$(P-P_*)/(P_{sa})$. Dimensionless fluid film pressure.
p_X, p_Y, p_δ	Dimensionless dynamic (first-order) pressures.
P_{e*}	$(\rho \cdot U \cdot C^2 c_p/K \cdot R)_*$. Characteristic Peclet Number.
Q_s	heat flow to bearing and journal surfaces [W/m^2].
q_{rl}	$Q_{rl}/(\rho UCR)_* = \int \rho \bar{h} \vec{u} . \vec{n} \cdot d\bar{\Gamma}_r$. Recess to land mass flow rate
q_{ro}	$Q_{ro}/(\rho UCR)_* = \delta_* \sqrt{\rho_{ro}(1-p_{ro})}$. Orifice mass flow rate
R	Bearing radius [m].
Re	$(\rho \cdot \Omega \cdot C \cdot R/\mu)_*$. Nominal circumferential flow Reynolds number.
Re_H	$(\rho \cdot \Omega \cdot H \cdot R \cdot/\mu)_*$. Film Reynolds number due to journal rotation.
Re_p	$(\rho \cdot U \cdot C \cdot/\mu)_*$. Reference flow Reynolds number.
Re_p^*	$Re_p \cdot (C/R)_*$. Modified reference flow Reynolds number.
Re_s	$(\rho \cdot \omega \cdot C^2/\mu)_*$. Nominal Squeeze film Reynolds number
R_J, R_B	$(\rho/\mu)H\sqrt{[(U_\theta - \Omega \cdot R)^2 + U_z^2]}$; $(\rho/\mu)H\sqrt{[U_\theta^2 + U_z^2]}$
	Flow Reynolds numbers relative to journal and bearing surfaces.
r_J, r_B	Mean roughness depths at journal and bearing surfaces [m].
$T, \bar{T}$	Fluid bulk-flow temperature [°K], T/T_*
T_B, T_J	Temperature at bearing and journal surfaces [°K].
$T_* = T_s$	Characteristic (supply) temperature [°K].
U_*	$C_*^2 P_{sa}/(\mu_* R_*)$. Characteristic flow speed [m/s].
u_z, u_θ	$(U_z, U_\theta)/U_*$. Dimensionless bulk-flow velocities in axial and circumferential (θ) directions.
V_r	$(H_r+H)A_r+V_s$. Total recess volume [m^3].
V_s	Volume of orifice supply line [m^3].
{X,Y,Z}	Inertial coordinate system.
z	Z/R. Dimensionless axial coordinate.
$Z^k_{\alpha\beta}$	$K^k_{\alpha\beta} + i\omega C^k_{\alpha\beta}$. kth-pad impedance coefficients, $\alpha, \beta = X, Y, \delta$

$ZZ^k_{\delta\delta}$	$Kr_k + K^k_{\delta\delta} - \omega^2 I_k + i\omega\,(Cr_k + C^k_{\delta\delta})$.
$Z^k_{R\alpha\beta}$	$[ZZ_{\alpha\beta} - Z_{\alpha\delta}\cdot Z_{\delta\beta}/Z_{\delta\delta}]^k$. Pad reduced impedance coefficients, α,β=X,Y
α	Circumferential velocity entrance swirl factor.
$\beta_P, \bar{\beta}_P$	$(1/\rho)(\partial\rho/\partial P)$. Liquid compressibility coefficient [m^2/N], $\beta_P \cdot P_{sa}$.
$\beta_T, \bar{\beta}_T$	$-(1/\rho)(\partial\rho/\partial T)$. Liquid volumetric expansion factor [1/°K], $\beta_T \cdot T_*$.
δ^k	Pad rotation angle [rad].
δ_*	$\dfrac{A_o \cdot \mu_* \sqrt{2}}{C_*^3 \sqrt{\rho_* P_{sa}}}$. Dimensionless Orifice parameter.
$\varepsilon_X,\ \varepsilon_Y$	$(e_X, e_Y)/C_*$. Dimensionless journal eccentricities in X & Y directions.
$\Delta\varepsilon_X, \Delta\varepsilon_Y, \Delta\delta^k$	Dynamic (perturbed) journal eccentricities and pad rotation
η	$H/(H_r+H)$. Ratio of land film thickness to recess depth.
θ	x/R. Circumferential or angular coordinate.
θ_k	k-th pad angular length [rad].
θ_{1k}	kth-pad angular position of pad leading edge [rad]
θ_{pk}	kth-pad angular position of pivot [rad]
θ^k_r	rth-recess angular length [rad] in kth-pad [rad].
$\kappa_z = \kappa_\theta$	$\frac{1}{2}(\kappa_J + \kappa_B)$. Turbulence shear factors in (z,θ) flow directions.
$\kappa_J,\ \kappa_B$	$f_J \cdot R_J,\ f_B \cdot R_B$. Turbulent shear parameters at journal and bearing surfaces.
κ_r	$\dfrac{Re_r^{0.681}}{7.753}$. Turbulent shear flow parameter at recess.
κ_P	Pad leading edge pressure recovery factor.
$\rho, \rho_*, \bar{\rho}$	Fluid density [Kg/m^3], characteristic density [kg/m^3], ρ/ρ_*.
$\bar{\mu}, \mu_*, \mu$	Fluid viscosity [Ns/m^2], characteristic viscosity [Ns/m^2], μ/μ_*.
$\xi_{\theta u}, \xi_{\theta d}$	Empirical recess-edge entrance loss coefficients in circumferential (upstream,downstream) direction.
ξ_{zL}, ξ_{zR}	Empirical recess-edge entrance loss coefficients in axial

	direction (left and right of recess).
λ_1	$\omega \cdot V_r/(U \cdot R \cdot C)_*$. Frequency parameter at recess volume.
λ_{11}	$\sigma \cdot l/R$. Modified frequency parameter at recess volume.
λ_2	$\lambda_1 \cdot \bar{\beta}_{Pr}$. Combination of frequency and compressibility parameters.
λ_T	Thermal mixing coefficient for pad heat carry-over.
Ω, ω	Rotational speed of journal, excitation or whirl frequency [1/s]
Λ	$\Omega \cdot R/U_*$. Dimesionless journal surface velocity parameter.
σ	$\omega \cdot R/U_*$. Film frequency parameter.
τ	ωt. Dimensionless time coordinate
Γ_r	Recess boundary with outward normal $\vec{n}$.

Subscripts refer to:

*	Characteristic values or supply (inlet) conditions.
z,θ	In direction of local axial and circumferential coordinates in plane of bearing {y,θ}.
J,B	Journal and bearing surfaces.
o	Zero-th order solution
α,β	First order solution for perturbations in (X,Y) displacements and pad rotation (δ).
r,e	bearing recesses and edges (entrance).
L,R	Left and right axial planes of bearing
u,d	Upstream and downstream edges of recess in θ dir.

Superscripts refer to:

k	kth- pad on bearing.

LIST OF TABLES

LIST OF FIGURES

LIST OF FIGURES (continued)

INTRODUCTION

The technology of externally pressurized bearings for cryogenic liquid turbopump applications has steadily advanced in the past years. Computational bearing design programs have been validated with a wealth of experimental data obtained at the TAMU Hydrostatic Bearing Test Facility (Kurtin et al., 1993, Childs and Hale, 1994, Franchek et al. 1994). Advanced cryogenic turbomachinery designs already demand an all-fluid-film-bearing technology to improve efficiency, reduce size and weight, and with lesser impact on the environment. The progress achieved brings needed verification to promote the use of externally pressurized, process-liquid bearings for use in commercial high-performance rotating machinery. This type of machinery eliminates expensive oil-based lubrication systems as well as rolling element bearings of limited success in high-speed applications. Magnetically driven canned and sealess pumps of proven superior performance and reliability are examples of these new advances. In other high performance applications, hydrostatic bearings and damping bearing seals are the primary candidates to provide this quantum step in machinery performance.

Despite the attactive features provided by hybrid (combination hydro - static and hydrodynamic) journal bearings (HJBs), fluid film bearing stability considerations and thermal phenomena accompanied by fluid phase change are issues of primary concern for high speed operation with large pressure differentials (San Andres, 1993). Bearing dynamic stability is related to hydrodynamic and liquid compressibility effects limiting severely the maximum operating speed of a rotating structure to a value close to the system first critical speed divided by the whirl frequency ratio (WFR). The WFR is a stability indicator which, for conventional incompressible liquid hybrid bearings, is typically equal to 0.50. Innovative fixed geometry hybrid bearings

with improved stability have been designed and tested (Franchek, 1992). Some of these bearing configurations include rough-surface bearings, anti-swirl liquid injection HJBs, and bearings with structural stiffness asymmetry.

The flexure-pad hybrid bearing concept (Zeidan, 1992), see Figure 1, constitutes a promising alternative for use in high speed applications and without stability restrictions. The major advantage of this bearing over conventional tilting-pad technology derives from its structured design and single-piece EDM manufacturing. The thin webs provide enough radial stiffness to support aplied loads while allowing for rotational pad motions. Tilting-pad bearings are mechanically complex due to their many parts, and on assembly, tolerances stack-up requiring a high degree of manufacturing accuracy to yield acceptable clearances. Furthermore, these bearings are supported on ball and socket type joints which are prone to rapid wear if the fluid media has no lubricity. This is precisely the case with liquid cryogens as well as with most process liquid applications. The flexure-pad structural arrangement offers a unique advantage to ensue combined hydrostatic and hydrodynamic actions with supply ports directly machined on the thin webs for delivery of a pressurized lubricant. The flexure-pad bearing technology applies advanced automated machining processes to manufacture bearings of any specified tolerance for shape and film clearance as well as structural properties (Zeidan, 1992). In addition, the dynamic variation of external pressure and flow through the bearing orifice ports can lead to the concept of a **SMART BEARING**, i.e. a self-adapting, low friction, mechanical support able to modify the entire rotor-bearing system frequency response by controlling its stiffness and suppressing critical speeds.

Literature Review

Tilting-pad hydrodynamic journal bearings are used frequently as support elements in high speed rotating machinery requiring maximum stability. The ability of the bearing pads to rotate (about an individual pad pivot) determines a reduction or complete elimination of the undesirable cross-coupled stiffnesses which produce bearing instability in fixed geometry fluid film bearings. Flack et al. (1984), and Fillon et al. (1987, 1991) offer lucid reviews of the extensive theoretical literature relevant to tilting-pad bearings. Shapiro et al. (1977) and Nicholas et al.(1979, 1994) discuss practical design issues in tilting-pad bearings and refer extensively to the benefits these bearings have brought to rotating machinery.

The theoretical models used to describe the performance of tilting-pad journal bearings have steadily increased in complexity. The number of independent parameters required to fully represent the flow are virtually countless. Three-dimensional thermohydrodynamic (THD) and structural effects as well as the lubricant feed and mixing mechanism are thought to be necessary for accurate prediction of peak pressure, minimum film thickness and temperature rise. Theoretical models currently account for variable properties, heat transfer through the bearing pads, pad thermoelastic deformations, and pivot wear and flexibility. The analyses of Ettles et al. (1980, 1992), Knight and Barrett (1988), and Taniguchi et al. (1990) are representative of these advanced developments. Pinkus (1990) offers a scholarly account of the major developments in the area of thermal effects in fluid film lubrication.

Tilting-pad bearings have many more degrees of freedom than fixed geometry bearings, and consequently, their analysis is complicated and subject to a number of assumptions regarding the dynamic motion of journal and pads. Lund (1964) introduced rotordynamic force coefficients for tilting-pad

bearings using an assembly method from a single generic fixed pad. Barrett et al. (1988) and White and Chan (1992) discuss the effect of excitation frequency on the bearing reduced force coefficients. Rouch (1983) includes pivot flexibility, and Lund and Bo-Pedersen (1987) and Kim and Palazzolo (1993) account for pad flexibility on the THD evaluation of rotordynamic coefficients. These investigations show that thermoelastic deformations affect significantly the bearing damping force coefficients. Nicholas and Barrett (1986) also demonstrate, both theoretically and experimentally, that support flexibility has a profound effect on the critical speeds and dynamic performance of rotors supported on tilting-pad bearings.

Orcutt (1967) and Pinkus (1984/85) present analyses for prediction of tilting-pad bearing performance for turbulent flow and isothermal conditions. Taniguchi et al. (1990) provide tilting-pad bearing pressure and temperature experimental data and detailed correlations to numerical predictions from a complex three-dimensional, turbulent flow, thermohydrodynamic analysis including heat conduction through the bearing pads. Bouard et al. (1994) compare different turbulent flow models to the test data of Taniguchi et al. with no major diffrences among the models used. Recently, Ha et al. (1994) include a pad leading edge-ram pressure effect to improve the prediction of pressure and film thickness on large scale, turbulent flow tilting-pad bearings.

Relevant experimental investigations in tilting-pad bearings are given by Someya (1988), Brockwell and Leinbub (1989), and Fillon et al. (1991) for laminar flow conditions, and by Orcutt (1967), Taniguchi et al. (1990), and Ha et al. (1994) for both laminar and turbulent flows. The detailed experimental works have concentrated on the static performance of tilting pad bearings under various conditions of load and shaft speed with attention to the film and pads surface temperature and pressure evolution. In general, theoretical predictions

agree well with measurements if all bearing parameters are known accurately. Actual operating clearance and preload, and the inlet pad temperature are perhaps the most important factors affecting tilting-pad bearing performance. Isothermal models suffice to predict well bearing performance for small loads (or large Sommerfeld numbers), while apparently a complete elasto-thermohydrodynamic model becomes mandatory for large loads (small Sommerfeld numbers) accompanied by very small minimum film thickness and large temperature rises.

Measurements of tilting-pad journal bearing force coefficients have been relatively scarce in the technical literature until recently, see for example the relevant works of Someya (1988), Brockwell et al.(1990), Parkins and Horner (1992), and Arumugan et al. (1994). Test stiffness coefficients agree reasonably well with theoretical predictions. Measured damping coefficients are typically lower than calculated values. Pad thermoelastic deformations, and pivot and shaft flexibilities appear to affect greatly the measured results. Flack and Zuck (1988) report experimental rotordynamic responses of two flexible rotors supported on tilting-pad bearings. These fundamental tests demonstrate unstable rotor-bearing behavior as a whip condition with whirl frequency equal to the first critical speed. The instabilities are thought to be bearing induced, but the physical mechanism or bearing parameter(s) producing this highly unusual behavior (in tilting-pad bearings) are yet to be identified.

Zeidan (1992), and Zeidan and Paquette (1994) introduce flexure-pivot, tilting-pad bearings and discuss their advantages over conventional tilting-pad bearings. Armentrout and Paquette (1993) and Chen (1994) present analyses for evaluation of rotordynamic force coefficients in isothermal flow, flexure-pad bearings. Experimental bearing force coefficients are yet to be reported in the archival literature. Zeidan (1992) and Chen (1994) describe applications in which flexure-pad bearings provided stability to otherwise unstable rotating

machinery and with a performance superior to that of conventional tilting-pad bearings. De Choudhury et al. 1992) demonstrate experimentally that a flexure-pad bearing brings a lower temperature rise and frictional power loss when compared to a similar size five shoe tilting pad journal bearing. This fact allowed the flexure-pad bearing to operate at a lower oil flow rate while providing acceptable oil throwoff temperatures.

The analytical work on fluid film bearings at Texas A&M University has lead both the experimental verification and the practical application of hybrid bearing technology. Many of the relevant and some times surprising analytical results have been later verified on the test stand. Most notably the reduced whirl frequency ratio ($\simeq$0.50) has been of primary concern (San Andres, 1990). The measures to fix or avoid the instability condition which limits severely the application of hybrid bearings to cryogenic turbopumps have been discussed in detail elsewhere (San Andres, 1993). Tilting-pad journal bearings with hydrostatic pressurization were originally proposed by Greenhill (1991) as ideal bearing candidates with no hydrodynamic stability restriction. However, the mechanical complexity of conventional tilting pad bearings prevented their consideration as a suitable replacement for fixed geometry hybrid bearings. The appearance of flexure-pivot tilting-pad bearings on the commercial bearing market has relaxed the concerns for their potential use in cryogenic liquid turbopumps. The present technical development then presents the relevant analysis and computational predictions which demonstrate the feasibility of this type of bearing configuration for aerospace applications.

ANALYSIS

Consider the flow of a variable properties liquid in the thin film annular region between an inner rotating journal and a hydrostatic/hydrodynamic tilting pad bearing. The bearing pads provide rotational stiffness and viscous damping (see Figure 1) but are regarded as rigid in the radial direction. Each pad may contain one or more recesses and orifice restrictors for radial liquid supply to the bearing. A liquid at high pressure (P_s) is supplied **radially** through orifices and flows into the bearing recesses. For hydrostatic operation, the recess pressure (P_r) is uniform over the entire recess volume, while at the recess edges, an inertial pressure drop occurs due to the sudden transition from the recess of depth (H_r) into the film land region of small thickness (H). For hybrid operation (combined hydrodynamic - hydrostatic), the pressure within the recess downstream of the supply line rises due to viscous shear effects. The viscous pressure rise occurs for the small recess depths typical of cryogenic HJBs and closely parallels the pressure development in step bearings (Constantinescu et al., 1975, 1987). The liquid then flows into the film lands and a pressure drop to the discharge (sump) value follows. On the thin film region, hydrostatic and hydrodynamic effects are important, and for the high speed - high pressure conditions typical of cryogenic liquid environments, the fluid flow in the bearing is fully turbulent and dominated by fluid inertia effects.

The analysis studies the fully developed turbulent **bulk-flow** of a cryogenic liquid whose material properties depend on its local thermophysical state of pressure and temperature. Cryogenic liquids have low viscosities, and thermal(energy transport) effects due to friction heating and kinetic energy variations are expected to be of minor importance for pure hydrostatic

performance. This assertion is not fully justified for especial operating conditions (see for example San Andres et al., 1993, and Yang et al., 1993).

Coordinate system and film thickness

A local coordinate system is placed on the unwrapped plane of the bearing with the {x,z} axes pointing in the circumferential and axial directions, respectively. This cartesian coordinate system is a logical consequence of the smallness of the film thickness relative to the bearing diameter and length, and constitutes the fundamental assumption of lubrication theory.

A characteristic tilting pad of angular extent Θ_k and axial length equal to $L=L_L+L_R$ is shown in Figure 2. The leading edge of the k-th pad is defined by the coordinate Θ_{lk}, and Θ_{pk} denotes the position of the pad pivot or rotational flexural node . At operating conditions, the journal position relative to the bearing housing is described with reference to the inertial axes {X,Y,Z} by the journal center displacements (e_X,e_Y). Simple geometrical relationships determine the film thickness in the flow region of the k-th bearing pad to be given by:

$$H^k(Z,\theta,t) = C_p(Z) + e_X \cos(\theta) + e_Y \sin(\theta) - r_{pk}\cos(\theta-\Theta_p^k) - R\cdot\delta^k\sin(\theta-\Theta_p^k) \quad (1)$$

where $\theta=x/R$ and δ^k is the pad rotational angle; C_p is the pad machined radial clearance, in general a function of the axial coordinate (Z); $r_p=C_p-C_m$, corresponds to the bearing preload with C_m known as the bearing assembled clearance. The journal center displacement components (e_X,e_Y) and pad rotational angle (δ^k) are functions only of time. Note that no journal misalignment has been considered on the description of the film thickness. This ommission is due only for simplicity in the presentation of the analysis.

The equations of motion

The fluid flow on the film lands of a bearing pad is considered as fully developed with a turbulent character due to the large axial pressure drop, high rotor surface speed and the low viscosity typical of cryogenic liquids. The equations of motion for the turbulent bulk-flow on the thin film land of the k-th bearing pad are given by (San Andres, 1992, 1993, Yang, 1992):

equation of continuity:

$$\frac{\partial}{\partial t}(\rho H)^k + \frac{\partial}{\partial z}(\rho H U_z)^k + \frac{\partial}{\partial x}(\rho H U_\theta)^k = 0 \qquad (2)$$

axial momentum equation:

$$-H^k \frac{\partial P^k}{\partial z} = \frac{\mu}{H^k}\left\{ \kappa_z U_z \right\}^k + \frac{\partial(\rho H U_z)^k}{\partial t} + \left\{ \frac{\partial(\rho H U_z U_z)}{\partial z} + \frac{\partial(\rho H U_\theta U_z)}{\partial x} \right\}^k \qquad (3)$$

circumferential momentum equation:

$$-H^k \frac{\partial P^k}{\partial x} = \frac{\mu}{H^k}\left\{ \kappa_\theta U_\theta - \kappa_J \frac{\Omega R}{2} \right\}^k + \frac{\partial(\rho H U_\theta)^k}{\partial t} + \left\{ \frac{\partial(\rho H U_z U_\theta)}{\partial z} + \frac{\partial(\rho H U_\theta U_\theta)}{\partial x} \right\}^k \qquad (4)$$

energy tranport equation:

$$c_p \left\{ \frac{\partial}{\partial t}\left(\rho H T\right) + \frac{\partial}{\partial x_i}\left(\rho H U_i T\right) \right\}^k + Q_s = \beta_T H T \left\{ \frac{\partial P}{\partial t} + U_i \frac{\partial P}{\partial x_i} \right\}^k + \Omega \cdot R \frac{H}{2} \frac{\partial P}{\partial x}$$

$$+ \frac{\mu}{H}\left\{ \kappa_x \left(U_x^2 + U_y^2 + \frac{1}{2}\Omega \cdot R \cdot U_x \right) + \kappa_J \Omega R \left(\frac{1}{4}\Omega R - U_x \right) \right\}^k \qquad (5)$$

$$i = x, y$$

$$k = 1, \ldots, N_{pad}$$

on the flow region $\{-L_L \le Z \le L_R;\ \theta_{1k} \le \theta \le \theta_{1k} + \theta_k\}$; and where, $\kappa_z = \kappa_\theta = (k_J + k_B)/2$ are

the wall shear stress difference coefficients as local functions of the turbulent friction factors, bearing and journal surface conditions, and the flow Reynolds numbers relative to the rotating (R_J) and stationary (R_B) surfaces, i.e $\kappa_J=f_J R_J$, $\kappa_B=f_B R_B$ (Hirs, 1973). The cryogenic liquid properties are calculated from the Benedict-Web-Rubin equation of state as given in the standard data base of McCarty(1986). In the energy equation,

$$Q_s = h_B(T-T_B) + h_J\,(T-T_J) \qquad (6)$$

denotes the heat flow from the fluid film to the bearing and journal surfaces at temperatures (T_B) and (T_J), respectively, and with (h_B,h_J) as the bulk-flow convection heat transfer coefficients. A description of these parameters in turbulent bulk-flows is detailed by Yang (1992).

Hydrostatic Bearing, Recess Flow and Pressure equations

A mass conservation equation at each bearing recess of area $(l\cdot R\cdot \theta_r)^k$ and depth H_r is defined by the global balance between the mass flow through the orifice restrictor (Q_{ro}), the mass flow into the film lands and the time rate of change of liquid mass within the recess volume V_r. This equation is given as:

$$Q_{ro}^k = A_o\sqrt{2\,\rho_r(P_s-P_r)}^k = \int_{\Gamma_r}\left[\rho\, H\, \vec{\mathbf{U}}\cdot\vec{\mathbf{n}}\right]^k d\Gamma_r + \rho_r^k\frac{\partial V_r^k}{\partial t} + \rho_r^k V_r^k\left\{\beta_P\frac{\partial P_r}{\partial t} - \beta_T\frac{\partial P_r}{\partial t}\right\}^k \qquad (7)$$

for r=1,2..., Nrecess on the k-th pad

where $A_o=C_d\pi d^2/4$ is the effective orifice area, and $\beta_P=(1/\rho)\partial\rho/\partial P$ and $\beta_T=-(1/\rho)\partial\rho/\partial T$ represent the fluid compressibility and volumetric expansion coefficients, respectively. Γ_r represents the closure of the recess volume with the film lands and with normal **n** along the boundary line. Note that the orifice

flow equation is valid only for small changes of the liquid density. A more accurate relationship should be used for large variations in fluid material properties across the orifice. A fundamental relationship is yet unknown for compressible cryogenic liquids, although a general thermophysical model is available in the literature (Hall et al., 1986). In equation (7) above, the orifice discharge coefficient C_d is of extreme importance since experimental measurements at Texas A&M University and elsewhere have shown that numerical predictions require accurate C_d values to provide meaningful results. Needless to say that this orifice coefficient depends not only on the flow structure and Reynolds numbers, but also on the fluid used and the closeness of the orifice to the journal surface. Refer to Kurtin et al. (1993), Franchek (1992) and Mosher (1992) for experimentally based discharge coefficients in high-pressure, high-speed water HJBs, and to Scharrer (1990) for some measurements on liquid freon and liquid nitrogen HJBs.

The fluid edge pressure at the entrance to the film lands is given by the superposition of viscous shear effects on the recess extent and an entrance drop due to fluid inertia. Figure 3 shows the assumed pressure distribution within the recess volume and details the relevant nomenclature. On the circumferential direction, the pressure rise ($\hat{P_e}$) downstream of the recess orifice is given by (Constantinescu et al., 1975, 1987, San Andres, 1992):

$$\left[\bar{P_e} = P_r - \mu_r K_r \frac{R \cdot \theta_r}{2 H_r^2} \left(U_\theta \, (\bar{\rho_e}/\rho_r) \, \eta - \frac{\Omega \cdot R}{2} \right) \frac{1}{(1-M^2)} \right]^k \qquad (8.a)$$

$$r=1,2..,N_{rec} \text{ on k-th pad}$$

where, M is the circumferential flow local Mach number at the orifice discharge

and defined as the ratio between the azimuthal velocity U_θ and the liquid sound speed $(1./\sqrt{[\beta_P \rho_r]})$.

The entrance pressures (P_e^+) to the film lands in the circumferential and axial directions are given by:

$$\left[P_e^+ = P_e^- - \frac{\rho_e^+}{2}(1+\xi_\theta)\left\{1- (\rho_e^+/\rho_e^-)^2\eta^2\right\} U_\theta^2 \right]^k \qquad (8.b)$$

$$\left[P_e^+ = P_r - \frac{\rho_e^+}{2}(1+\xi_z)\left\{1- (\rho_e^+/\rho_e^-)^2\eta^2\right\} U_z^2 \right]^k \qquad (8.c)$$

for r=1,2..., Nrecess on k-th pad

The analysis generalizes equations (8) for uneven empirical entrance loss factors ξ in the axial direction (Z) and also circumferentially upstream(u) and downstream(d) of the recess. The Bernoulli like pressure drop occurs only if fluid flows from the recess towards the film lands. On the contrary, if fluid enters from the film lands into the bearing recess, then the edge pressure is regarded as equal to the recess pressure.

A simplified form of the energy transport equation at a bearing recess is esily derived from equation (5). A detailed exposition of the energy transport process in a bearing recess is given by San Andres (1993).

Boundary Conditions

At low rotational speeds, the pressure at the side (right and left) boundaries of the k-th pad is essentially constant and equal to a specified value of ambient or sump pressure, i.e.,

$$P^k(L_R,\theta) = P_R^k; \qquad P^k(-L_L,\theta) = P_L^k \qquad (9.a)$$

and at the pad leading and trailing edges,

$$P^k(Z,\theta_{1k}) = P^k(Z,\theta_{1k}+\theta_k) = f_s\,(P_R,\ P_L) \text{ on } -L_L \le Z \le L_R \qquad (9.b)$$

where (f_s) denotes a linear pressure variation along the axial side of the bearing pad leading and trailing edges. At high journal surface speeds ($\Omega \cdot R$) significant momentum changes occur at the pad leading edge (θ_{lk}). Inmediately upstream of the pad, the fluid entering the film lands can develop a dynamic head equal to some fraction of a reference dynamic pressure based on the bearing surface speed (Burton and Carper, 1967, Smalley et al., 1974, Mori et al., 1991, Ettles et al., 1968), i.e.

$$\Delta P^k(Z,\theta_{lk}) = \frac{1}{2}\, \kappa_p \cdot \rho^k \left(\frac{\Omega \cdot R}{2}\right)^2 \qquad (9.c)$$

The coefficient (κ_p) is an empirical ram pressure factor. Burton and Carper (1967) suggest a value of κ_p=0.64 for high speed flows with large turbulence levels. The appearance of this ram pressure effect due to journal rotation at the leading edge of a bearing pad is of fundamental importance on the analysis of high speed pad bearings. The model introduced is very simple. A more accurate knowledge of the entrance entrance condition requires the analysis of the complex flow field on the axial groove and feeding port separating the bearing pads (Ha et al., 1994).

A further assumption about the external flow is necessary to fully specify the flow variables. The flow at the inlet(leading edge) to the film land in the pad bearing is assumed to be parallel to the direction of surface motion. This simplification implies that on the line,

$$-L_L \le Z \le L_R, \qquad U_z^k(Z,\theta_{lk}) = 0; \quad k=1,..,N_{pad} \qquad (10)$$

In the thermal analysis, the inlet bulk-flow temperature to a bearing pad is obtained using mass flow and energy balances of the upstream pad flow and

temperature and incoming fresh fluid at a supply temperature (T_s). The pad inlet bulk-flow temperature depends on the specification of a thermal mixing parameter ($0 \leq \lambda_T \leq 1$) as given by Mitsui et al. (1983).

The boundary conditions noted refer only to the fluid film flow within the bearing pad. At an equilibrium journal position due to an imposed external load, each individual tilting- or flexure-pad must be balanced, i.e. the fluid induced moments and elastic restoring moments must add to zero. This item will be discussed later in the analysis.

Perturbation Analysis

Consider the motion of the journal as the superposition of small ampitude periodic motions around an equilibrium static position. That is, we let the journal center displacements and pad rotation be given as

$$e_X(t) = e_{Xo} + \Delta e_X\, e^{i\omega t}, \qquad e_Y(t) = e_{Yo} + \Delta e_Y\, e^{i\omega t}$$
$$\delta^k(t) = \delta_o^k + \Delta\delta^k e^{i\omega t}, \qquad i=\sqrt{-1} \tag{11}$$

where ω denotes the frequency of the whirl motion. The magnitudes of the dynamic perturbations in journal displacements and pad rotations are very small, i.e., $|\{\Delta e_X, \Delta e_Y, R\cdot\Delta\delta^k\}|/C_* \ll 1$. Then, the film thickness can be thought as the superposition of steady-state(h_o) and dynamic (h_1) components given by the real part of the following dimensionless expression:

$$h^k = h_o^k + h_1^k\, e^{i\omega t} \tag{12}$$

with

$$h_o^k = \bar{C}_p(z) + \varepsilon_{Xo}\cos(\theta) + \varepsilon_{Yo}\sin(\theta) - \bar{r}_p^k \cos(\theta-\theta_p^k) - [R\cdot\delta_o^k/C_*]\sin(\theta-\theta_p^k) \tag{13}$$

$$h_1^k = \left\{ \Delta\varepsilon_X + (R/C_*)\,\Delta\delta^k \sin(\theta_p^k)\right\}\cos(\theta) + \left\{\Delta\varepsilon_Y - (R/C_*)\,\Delta\delta^k\cos(\theta_p^k)\right\}\sin(\theta) \tag{14.a}$$

or

$$h_1 = \Delta_\alpha \cdot h_\alpha = \Delta\varepsilon_X\, h_X + \Delta\varepsilon_Y\, h_Y + (R/C_*)\ \Delta\delta^k h_\delta^k \qquad (14.b)$$

with

$$h_X = \cos\theta; \quad h_Y = \sin\theta,$$

$$h_\delta^k = \sin(\theta_p^k)\cdot h_X - \cos(\theta_p^k)\cdot h_Y = \sin(\theta_p^k - \theta) \qquad (15)$$

and $\quad \bar{C}_p = C_p(Z)/C_*, \ \bar{r}_p = [C_p - C_m]/C_*, \qquad$ on $\theta_{1k} \le \theta \le \theta_{1k} + \theta_k$

where C_* is a characteristic clearance for the bearing. The functions defined in equations (14-15) facilitate the understanding of the perturbed flow field equations and the resulting rotordynamic force coefficients given latter.

For each bearing pad the flow field variables (U_z, U_θ, P, T), as well as the fluid properties (ρ, μ) and the shear parameters $(\kappa_\theta, \kappa_z)$ are also formulated as the superposition of zeroth-order and first-order complex number fields describing the equilibrium condition for steady-state flow, and the perturbed condition for small amplitude dynamic journal motions, respectively. In general, these fields are expressed as:

$$\Psi^k = \Psi_o^k + e^{i\omega t}\left\{\Delta\varepsilon_X \Psi_X + \Delta\varepsilon_Y \Psi_Y + (R/C_*)\Delta\delta\Psi_\delta\right\}^k = \Psi_o^k + e^{i\omega t}\ \Delta_\alpha\ \Psi_\alpha^k \qquad (16)$$

$$\alpha = X, Y, \delta^k, \quad k = 1, 2..N_{pad}$$

Substitution of (12) and (16) into the equations of motion (2-7) determines the **zeroth-order dimensionless equations:**

$$\frac{\partial}{\partial z}\left(\bar{\rho}_o h_o u_{zo}\right)^k + \frac{\partial}{\partial\theta}\left(\bar{\rho}_o h_o u_{\theta o}\right)^k = 0 \qquad (17)$$

$$-h_o^k \frac{\partial p_o^k}{\partial z} = \frac{\bar{\mu}_o}{\bar{h}_o^k}\left\{\kappa_{zo} u_{zo}\right\}^k + \mathbf{Re}_p^* \left\{\frac{\partial}{\partial z}\left(\bar{\rho}_o h_o u_{zo} u_{zo}\right) + \frac{\partial}{\partial\theta}\left(\bar{\rho}_o h_o u_{\theta o} u_{zo}\right)\right\}^k \qquad (18)$$

$$-h_o^k \frac{\partial p_o^k}{\partial \theta} = \frac{\bar{\mu}_o}{h_o^k}\left\{k_\theta u_\theta - \kappa_J \frac{\Lambda}{2}\right\}_o^k + \mathbf{Re}_p^* \left\{ \frac{\partial}{\partial z}(\bar{\rho}_o h_o u_{zo} u_{zo}) + \frac{\partial}{\partial \theta}(\bar{\rho}_o h_o u_{\theta o} u_{\theta o}) \right\}^k \qquad (19)$$

$$\frac{\mathbf{Re}_p^*}{E_c}\left\{\bar{c}_{po}\left[\frac{\partial}{\partial \theta}(\bar{\rho}_o h_o u_{\theta o} \bar{T}_o) + \frac{\partial}{\partial z}(\bar{\rho}_o u_{zo} h_o \bar{T}_o)\right] + (\bar{h}_{Bo} + \bar{h}_{Jo}) T_o \right\}^k =$$

$$\bar{\beta}_{To} \bar{T}_o h_o \left\{u_{\theta o} \frac{\partial p_o}{\partial \theta} + v_{zo} \frac{\partial p_o}{\partial z}\right\}^k + h_o \frac{\Lambda}{2} \frac{\partial p_o}{\partial \theta} + \frac{\mathbf{Re}_p^*}{E_c}\left[\bar{h}_{Bo} \bar{T}_{Bo} + \bar{h}_{Jo} \bar{T}_{Jo}\right] +$$

$$\frac{\bar{\mu}_o}{h_o}\left\{k_{\theta o}\left[u_{\theta o}^2 + u_{zo}^2 + \frac{1}{2} u_{\theta o} \Lambda\right] + k_{Jo} \Lambda \left[\frac{1}{4}\Lambda - u_{\theta o}\right]\right\}^k \qquad (20)$$

$$k=1,2..,N_{pad}$$

Refer to the Nomenclature for definition of all dimensionless variables in equations (17-20). On the recess volumes of a hydrostatic bearing, the mass flow through the orifices must equal the mass flow into the bearing lands,

$$\delta_* \sqrt{\bar{\rho}_{ro}(1-p_{ro})}^k = q_{ro}^k = \iint_{\Gamma_r} \left[\bar{\rho}_o \, h_o (\vec{u}_o \cdot \vec{n})\right]^k d\bar{\Gamma}_r \,, \qquad (21)$$

$$r=1,2..\ \text{Nrecess on k-th pad}$$

The circumferential pressure rise at the downstream side edge of a recess is related to the recess pressure and fluid velocity by:

$$\left[\bar{p}_{eo} = p_{ro} - \bar{\mu}_{ro} \, \phi_r \left(u_{\theta o}(\bar{\rho}_e/\rho_r) \cdot \eta - \frac{\Lambda}{2}\right) \frac{1}{(1-M^2)} \right]^k \qquad (22.a)$$

where $\phi_r = \kappa_r \cdot \Theta_r / (2 \cdot h_r^2)$ is a dimensionless recess shear factor. The recess edge - entrance film pressures in the circumferential and axial directions are

given by

$$p^{+}_{eo} = p^{-}_{eo} - \frac{\bar{\rho}^{-+}_{e}}{2}\phi_{\theta}\, u^{2}_{\theta o} \Bigg]^{k} \qquad (22.b)$$

$$p^{+}_{eo} = p_{ro} - \frac{\bar{\rho}^{-+}_{e}}{2}\phi_{z}\, u^{2}_{zo} \Bigg]^{k} \qquad (22.c)$$

where,

$$\phi_{\theta} = (1+\xi_{\theta})\cdot \mathbf{Re}^{*}_{p}\left[1-(\rho^{+}_{e}/\rho^{-}_{e})\eta^{2}\right]\cdot\left\{1+\frac{1.95}{\mathbf{Re}_{H}^{0.43}}\right\} \qquad (22.d)$$

and

$$\phi_{z} = (1+\xi_{z})\cdot \mathbf{Re}^{*}_{p}\left[1-(\rho^{+}_{e}/\rho^{-}_{e})\eta^{2}\right] \qquad (22.e)$$

At the bearing pad discharge (axial) sides and the trailing edge, the pressure takes specified values, see equations (9). The ram pressure jump at the leading edge of a bearing pad is given in dimensionless form as:

$$\Delta p^{k}_{o}(z,\theta_{1k}) = \frac{1}{2}\,\kappa_{p}\cdot\bar{\rho}^{k}_{o}\cdot \mathbf{Re}^{*}_{p}\left(\frac{\Lambda}{2}\right)^{2} \qquad (23.a)$$

Across the line, $-L_{L}/R \leq z \leq L_{R}/R$, (pad leading edge) the inlet flow is regarded as parallel to the bearing pad, i.e.,

$$u^{k}_{zo}(z,\theta_{1k}) = 0 \qquad (23.b)$$

First-order dimensionless equations

The first-order flow equations for perturbations in the film thickness due to journal displacements ($\Delta e_{X}, \Delta e_{Y}$) and pad rotation ($\Delta\delta^{k}$) can be expressed in the unique form:

$$i\cdot\sigma\left\{\bar{\rho}_\alpha h_o+\bar{\rho}_o\cdot h_\alpha\right\}^k+\frac{\partial}{\partial z}\left\{\bar{\rho}_\alpha h_o u_{zo}+\bar{\rho}_o\cdot h_\alpha u_{zo}+\bar{\rho}_o\bar{h}_o u_{z\alpha}\right\}^k$$

$$+\frac{\partial}{\partial\theta}\left\{\bar{\rho}_\alpha h_o u_{\theta o}+\bar{\rho}_o\cdot h_\alpha u_{\theta o}+\bar{\rho}_o\bar{h}_o u_{\theta\alpha}\right\}^k=0 \tag{24}$$

$$-h_o^k\frac{\partial p_\alpha^k}{\partial z}=\left[\left\{\gamma_{zz}+i\cdot Re_s\bar{\rho}_o h_o\right\}u_{z\alpha}+\gamma_{z\theta}\,u_{\theta\alpha}+\gamma_{zh}\,h_\alpha+\gamma_{z\rho}\bar{\rho}_\alpha+\gamma_{z\mu}\bar{\mu}_\alpha\right.$$

$$\left.+Re_p^*\left\{\frac{\partial}{\partial z}(\bar{\rho}_o h_o u_{zo}u_{z\alpha})+\frac{\partial}{\partial\theta}(\bar{\rho}_o h_o u_{\theta o}u_{z\alpha})+\bar{\rho}_o h_o\left[u_{z\alpha}\frac{\partial u_{zo}}{\partial z}+u_{\theta\alpha}\frac{\partial u_{zo}}{\partial\theta}\right]\right\}\right]^k \tag{25}$$

$$-h_o^k\frac{\partial p_\alpha^k}{\partial\theta}=\left[\left\{\gamma_{\theta\theta}+i\cdot Re_s\bar{\rho}_o h_o\right\}u_{\theta\alpha}+\gamma_{\theta z}\,u_{z\alpha}+\gamma_{\theta h}\,h_\alpha+\gamma_{\theta\rho}\,\bar{\rho}_\alpha+\gamma_{\theta\mu}\bar{\mu}_\alpha\right.$$

$$\left.+Re_p^*\left\{\frac{\partial}{\partial z}(\bar{\rho}_o h_o u_{zo}u_{\theta\alpha})+\frac{\partial}{\partial\theta}(\bar{\rho}_o h_o u_{\theta o}u_{\theta\alpha})+\bar{\rho}_o h_o\left[u_{z\alpha}\frac{\partial u_{\theta o}}{\partial z}+u_{\theta\alpha}\frac{\partial u_{\theta o}}{\partial\theta}\right]\right\}\right]^k \tag{26}$$

$$\frac{Re_p^*}{E_c}\bar{c}_{po}\left[\frac{\partial}{\partial\theta}(\bar{\rho}_o h_o u_{\theta o}\bar{T}_\alpha)+\frac{\partial}{\partial z}(\bar{\rho}_o u_{zo}h_o\bar{T}_\alpha)\right]+\left\{\gamma_{tt}+i\bar{\rho}_o h o\bar{c}_{po}R_{es}/E_c\right\}\bar{T}_\alpha^k+$$

$$\gamma_{tu}u_{\theta\alpha}+\gamma_{tv}v_{z\alpha}+(\gamma_{tp}-i\sigma\bar{\beta}_{To}\bar{T}_o)p_\alpha+\gamma_{th}h_\alpha-h_o\frac{\Lambda}{2}\frac{\partial p_\alpha}{\partial\theta}=$$

$$\bar{\beta}_{To}\bar{T}_o h_o\left\{u_{\theta o}\frac{\partial p_\alpha}{\partial\theta}+v_{zo}\frac{\partial p_\alpha}{\partial z}\right\}^k+\frac{Re_p^*}{E_c}\left[\bar{h}_{Bo}\bar{T}_{B\alpha}+\bar{h}_{Jo}\bar{T}_{J\alpha}\right]^k \tag{27}$$

for perturbations in the α=X,Y directions and pad rotation $\alpha=\delta^k$, k=1,2..,N_{pad}. In the equations above (h_α) correspond to the perturbation fields in film thickness as defined by equations (15). The coefficients γ_{ij}'s arise from

perturbation of the shear stress factors k_z, k_θ and k_J, and their explicit formulae have been given before (San Andres, 1993, Yang, 1992). The perturbed first-order fluid peoperties are obtained from relationships like:

$$\bar{f}_\alpha = (\partial\bar{f}/\partial p)\big|_o\, p_\alpha + (\partial\bar{f}/\partial\bar{T})\big|_o\, \bar{T}_\alpha; \qquad f=\rho,\mu,c_p \tag{28}$$

On each recess of a kth-pad hydrostatic bearing, the first-order continuity equation takes the linearized form:

$$-p^k_{r\alpha}\left[\frac{\delta_*^2\,\bar{\rho}_{ro}}{2q_{ro}}\left\{1-\bar{\beta}_{po}(1-p_{ro})\right\}+i\cdot\bar{\rho}_{ro}\lambda_2\right]^k = i\cdot\bar{\rho}^k_{ro}\lambda_{11}\cdot\int_{\Gamma r}^k h_{r\alpha}\,d\theta +$$

$$\int_{\Gamma_r}\left\{\bar{\rho}_o h_\alpha\vec{u}_o+\bar{\rho}_o h_o\vec{u}_\alpha+\bar{\rho}_\alpha\vec{u}_o h_o\right\}^k\cdot\vec{n}\,d\bar{\Gamma}_r + \left[(1-p_{ro})\frac{\delta_*\rho^{2-}_{ro}}{2q_{ro}} - i\lambda_1\bar{\rho}_{ro}\right]\bar{\beta}_{To}T_{r\alpha}^- \tag{29}$$

r=1,2...Nrecess on k-th pad

The first-order recess edge (circumferential and axial) pressures into the film lands are given as

$$p^+_{e\alpha}= p^-_{r\alpha}-\phi_\theta\left\{\bar{\rho}_o\cdot u_{\theta o}\cdot u_{\theta\alpha}+\bar{\rho}_\alpha\frac{u^2_{\theta o}}{2}\right\}\Bigg]^k \quad ; \text{ if } u^k_{\theta o}>0 \tag{30.a}$$

$$p^+_{e\alpha}= p^-_{r\alpha}-\phi_z\left\{\bar{\rho}_o\cdot u_{zo}\cdot u_{z\alpha}+\bar{\rho}_\alpha\frac{u^2_{zo}}{2}\right\}\Bigg]^k \quad ; \text{ if } u^k_{zo}\cdot\vec{n}>0 \tag{30.b}$$

for $\alpha=X,Y,\delta^k$

No perturbations on the pad leading edge ram pressure are considered. Thus, the first-order pressure field is null everywhere on the side boundaries of the

bearing kth-pad; i.e. $p_{\alpha}{}^{k}=0$.

Note that the first order equations, (24) to (30) can be written in the general form:

$$L\,(u_{\theta X},\ u_{zX},\ p_X,\ \rho_X,\ \mu_X)^k = h_X \qquad (31.a)$$

$$L\,(u_{\theta Y},\ u_{zY},\ p_Y,\ \rho_Y,\ \mu_Y)^k = h_Y \qquad (31.b)$$

$$L\,(u_{\theta\delta},\ u_{z\delta},\ p_\delta,\ \rho_\delta,\ \mu_\delta)^k = h_\delta^k = h_X \sin(\Theta_p^k) - h_Y \cos(\Theta_p^k) \qquad (31.c)$$

where L are linear differential operators with coefficients depending only on the zeroth order flow field variables $(u_{\theta o}, u_{zo}, p_o, h_o)^k$. Equation (31.c) describing the perturbed flow field due to a pad rotation $(\Delta\delta^k)$ is <u>just</u> a linear combination of the first two equations. Hence, for homogeneous boundary conditions on the perturbed fields, the following statement is correct:

$$\Psi_\delta^k = \sin(\Theta_p^k)\ \Psi_X^k - \cos(\Theta_p^k)\ \Psi_Y^k, \quad \text{where } \Psi_\delta = u_{\theta\delta},\ u_{z\delta},\ p_\delta,\ \rho_\delta,\ \mu_\delta \qquad (32)$$

This equation shows that the first-order flow field due to a pad rotation can be found as the superposition of the perturbed flow fiels due to journal displacements in the {X,Y} directions. Thus, the computational time for the evaluation of force coefficients in tilting (or flexure) pad bearings is considerably reduced.

<u>Pad Fluid Film Forces, and Dynamic Force and Moment Coefficients</u>

The fluid film forces and moment on each bearing pad are calculated by integration of the pressure field, i.e.,

$$\begin{bmatrix} F_X^k \\ F_Y^k \end{bmatrix} = P_{sa}\cdot R^2 \cdot \int_{-L_L}^{L_R} \int_{\theta_{1k}}^{\theta_{1k}+\theta_k} p^k \cdot \begin{bmatrix} \cos\theta \\ \sin\theta \end{bmatrix} dz\cdot d\theta_k \quad [\mathbf{N}] \qquad (33)$$

$$k=1,2\ldots N_{pad}$$

$$M^k = P_{sa} \cdot R^3 \cdot \int_{-L_L}^{L_R} \int_{\theta_{1k}}^{\theta_{1k}+\theta_k} p^k \sin(\theta_p^k - \theta)\, dz \cdot d\theta_k \qquad [N.m] \qquad (34.a)$$

$$k=1,2\ldots N_{pad}$$

where P_{sa} is a characteristic pressure. The pad moment due to fluid film effects can be rewritten as:

$$M^k = R \left\{ \sin(\theta_p^k)\, F_X^k - \cos(\theta_p^k)\, F_Y^k \right\} \qquad (34.b)$$

Substitution of the pressure field, equation (16),

$$p^k = p_o^k + e^{i\tau} \left\{ \Delta\varepsilon_X p_X + \Delta\varepsilon_Y p_Y + \Delta\delta (R/C_*) p_\delta \right\}^k$$

into equations (33) and (34) determines the k-th pad zeroth- and first-order forces and moment due to the fluid film pressure as:

$$\begin{aligned}
F_X^k &= F_{Xo}^k + F_{X1}^k\, e^{i\tau} = F_{Xo}^k - \left\{ Z_{XX}\, \Delta e_X + Z_{XY}\, \Delta eY + Z_{X\delta}\, \Delta\delta \right\}^k e^{i\tau} \\
F_Y^k &= F_{Yo}^k + F_{Y1}^k\, e^{i\tau} = F_{Yo}^k - \left\{ Z_{YX}\, \Delta e_X + Z_{YY}\, \Delta eY + Z_{Y\delta}\, \Delta\delta \right\}^k e^{i\tau} \qquad (35) \\
M^k &= M_o^k + M_1^k\, e^{i\tau} = M_o^k - \left\{ Z_{\delta X}\, \Delta e_X + Z_{\delta Y}\, \Delta eY + Z_{\delta\delta}\, \Delta\delta \right\}^k e^{i\tau}
\end{aligned}$$

where

$$\begin{bmatrix} F_{Xo} \\ F_{Yo} \end{bmatrix}^k = P_{sa} \cdot R^2 \cdot \int_{-L_L}^{L_R} \int_{\theta_{1k}}^{\theta_{1k}+\theta_k} p_o^k \cdot \begin{bmatrix} \cos\theta \\ \sin\theta \end{bmatrix} dz \cdot d\theta_k \qquad [N] \qquad (36)$$

$$k=1,2\ldots N_{pad}$$

and

$$M_o^k = R \left\{ \sin(\theta_p^k)\, F_{Xo}^k - \cos(\theta_p^k)\, F_{Yo}^k \right\} \quad [N\cdot m] \qquad (37)$$

$$k=1,2..N_{pad}$$

are the zeroth order fluid film forces and induced moment for the kth-pad, respectively. The $Z_{\alpha\beta}$ are pad impedance coefficients whose real and imaginary parts correspond to pad fluid film stiffness and damping coefficients, respectively. Analytical expressions for the kth-pad impedance coefficients are given as:

force impedances due to journal displacements Δe_X, Δe_Y:

$$Z^k_{\alpha\beta} = K^k_{\alpha\beta} + i\,\omega\cdot C^k_{\alpha\beta} = -\frac{P_{sa}R^2}{C_*}\int_{-L_L}^{L_R}\int_{\theta_{1k}}^{\theta_{1k}+\theta_k} p^k_\beta\, h_\alpha\, dz\cdot d\theta_k \quad [N/m] \qquad \alpha,\beta = X,Y \qquad (38.a)$$

force impedances due to pad rotation $\Delta\delta^k$:

$$Z^k_{\alpha\delta} = K^k_{\alpha\delta} + i\,\omega\cdot C^k_{\alpha\delta} = -\frac{P_{sa}R^3}{C^2}\int_{-L_L}^{L_R}\int_{\theta_{1k}}^{\theta_{1k}+\theta_k} p^k_\delta\, h_\alpha\, dz\cdot d\theta_k \quad [N/rad] \qquad \alpha = X,Y \qquad (38.b)$$

pad moment impedances due to journal displacements Δe_X, ΔeY:

$$Z^k_{\delta\beta} = K^k_{\delta\beta} + i\,\omega\cdot C^k_{\delta\beta} = -\frac{P_{sa}R^3}{C_*}\int_{-L_L}^{L_R}\int_{\theta_{1k}}^{\theta_{1k}+\theta_k} p^k_\beta\, h^k_\delta\, dz\cdot d\theta \quad [N] \qquad \beta = X,Y \qquad (38.c)$$

pad moment impedance due to pad rotation $\Delta\delta$:

$$Z^k_{\delta\delta} = K^k_{\delta\delta} + i\,\omega\cdot C^k_{\delta\delta} = -\frac{P_{sa}R^4}{C_*}\int_{-L_L}^{L_R}\int_{\theta_{1k}}^{\theta_{1k}+\theta_k} p^k_\delta\, h^k_\delta\, dz\cdot d\theta \quad [N\cdot m/rad] \qquad (38.d)$$

A total of 9 impedance coefficients are determined for each bearing pad. A clear distinction of fluid inertia force or added mass coefficients is not appropriate

for tilting-pad bearings since the stiffness and damping coefficients are frequency dependent. A major simplification in the evaluation of the impedance coefficients is possible by using equation (32) for the dynamic pressure field due to a pad rotation, i.e

$$p_{\delta}^{k} = \sin(\theta_{p}^{k})\ p_{X}^{k} - \cos(\theta_{p}^{k})\ p_{Y}^{k},$$

and allows the impedance coefficients to be expressed as unique functions of the force impedances $Z_{\alpha\beta}$, $\alpha,\beta=X,Y$ as follows:

$$\begin{aligned}
Z_{\delta X}^{k} &= R\ \{\ \sin(\Theta_{p})\ Z_{XX}^{k} - \cos(\Theta_{p})\ Z_{YX}^{k}\ \} \\
Z_{\delta Y}^{k} &= R\ \{\ \sin(\theta_{p})\ Z_{XY}^{k} - \cos(\theta_{p})\ Z_{YY}^{k}\ \} \\
Z_{X\delta}^{k} &= R\ \{\ \sin(\theta_{p})\ Z_{XX}^{k} - \cos(\theta_{p})\ Z_{XY}^{k}\ \} \\
Z_{Y\delta}^{k} &= R\ \{\ \sin(\theta_{p})\ Z_{YX}^{k} - \cos(\theta_{p})\ Z_{YY}^{k}\ \} \\
Z_{\delta\delta}^{k} &= R\ \{\ \sin(\theta_{p})\ Z_{X\delta}^{k} - \cos(\theta_{p})\ Z_{Y\delta}^{k}\ \} \\
&= R^{2}\left[\ \sin^{2}(\theta_{p}^{k})\ Z_{XX}^{k} - \sin(\theta_{p}^{k})\cos(\theta_{p}^{k})(Z_{XY}^{k}+Z_{YX}^{k}) + \cos^{2}(\theta_{p})\ Z_{YY}^{k}\ \right]
\end{aligned} \tag{39}$$

Equations (39) show only four impedance coefficients to be independent, with the other five uniquely determined by the relations defined above. These equations simplify greatly the analysis of tilting-pad bearings since only the dynamic pressure fields for journal center perturbations in the {X,Y} directions are (strictly) required.

Bearing Equilibrium Equation and Pad Equation of Rotational Motion

In a multiple pad bearing, the sum of the individual pad forces must balance the externally applied load **W**. This load has components (W_X, W_Y) on the {X,Y} directions, respectively. Thus, the static equilibrium force equation (in the absence of rotor-inertial effects) is given as:

$$W_X + \sum_{k=1}^{N_{pad}} F_X^k = 0 \quad ; \quad W_Y + \sum_{k=1}^{N_{pad}} F_Y^k = 0 \tag{40}$$

The equation of rotational motion for each bearing pad is given as:

$$I_k \ddot{\delta}^k + Cr_k \dot{\delta}^k + Kr_k \delta^k = M^k = R \{ \sin(\Theta_p^k) F_X^k - \cos(\Theta_p^k) F_Y^k \} \tag{41}$$

$$k=1,\ldots N_{pad}$$

where I_k, Cr_k, Kr_k correspond to the **pad** inertia, and pad rotational viscous damping and structural stiffness coefficients, respectively. (Note that in a conventional tilting pad bearing, $Kr_k=0$).

A static load W_o impossed on the fluid film bearing determines a bearing equilibrium position at a static journal eccentricity (e_{Xo}, e_{Yo}) and a set of stationary pad rotations $\{\delta_o\}^k, k=1,..N_{pad}$. Hence, the bearing force and pad moments equilibrium equations are givens as:

$$0 = W_{Xo} + \sum_{k=1}^{N_{pad}} F_{Xo}^k(e_{Xo}, e_{Yo}, \delta_o^k) \quad ; \quad 0 = W_{Yo} + \sum_{k=1}^{N_{pad}} F_{Yo}^k(e_{Xo}, e_{Yo}, \delta_o^k) \tag{42}$$

$$0 = -Kr_k \delta_o^k + M_o^k = -Kr_k \delta_o^k + R \{ \sin(\Theta_p^k) F_{Xo}^k - \cos(\Theta_p^k) F_{Yo}^k \} \tag{43}$$

$$k=1,2\ldots, N_{pad}$$

In the practical analysis of tilting- and flexure-pad bearings, **reduced** bearing stiffness and damping coefficients are determined at the static equilibrium

position and for a particular frequency of excitation, typically synchronous ($\omega=\Omega$) or subsynchronous ($\omega<\Omega$). For small amplitude journal motions (Δe_X, $\Delta e_Y)e^{i\omega t}$, and pad rotations $\{\Delta\delta^k\}e^{i\omega t}$, k=1, N_{pad} with frequency ω about the equilibrium position ($e_{Xo}, e_{Yo}, \delta_o^k$), the individual pad forces and the pad moment balance equation can be written as (see also equations (35)):

$$\begin{aligned} F_X^k(t) &= F_{Xo}^k - \{ Z_{XX}^k \Delta e_X + Z_{XY}^k \Delta e_Y + Z_{X\delta}^k \Delta\delta^k \} e^{i\omega t} \\ F_Y^k(t) &= F_{Yo}^k - \{ Z_{YX}^k \Delta e_X + Z_{YY}^k \Delta e_Y + Z_{Y\delta}^k \Delta\delta^k \} e^{i\omega t} \end{aligned} \tag{44}$$

$$0 = Kr_k \delta_o^k - M_o^k = \left[\left\{ Kr_k - \omega^2 I_k + i\,\omega\, C_{rk} \right\} \Delta\delta^k + Z_{\delta X}^k \Delta e_X + Z_{\delta Y}^k \Delta e_Y + Z_{\delta\delta}^k \Delta\delta^k \right] e^{i\omega t} \tag{45}$$

where $Z_{\alpha\beta}^k = K_{\alpha\beta}^k + i\,\omega\, C_{\alpha\beta}^k$ are the pad impedance coefficients at frequency ω. Equation (45) indicates that the kth-pad rotational motion is a function of the journal dynamic displacements ($\Delta e_X, \Delta e_Y$).

Let
$$ZZ_{\delta\delta}^k = (K_{\delta\delta}^k + Kr_k - \omega^2 I_k) + i\,\omega\,(C_{\delta\delta}^k + Cr_k) \tag{46}$$

and the relation between the k-th pad dynamic rotations and journal dynamic displacements is given from equation (45) as:

$$\Delta\delta^k = -\left[\frac{Z_{\delta X}}{ZZ_{\delta\delta}} \Delta e_X + \frac{Z_{\delta Y}}{ZZ_{\delta\delta}} \Delta e_Y \right]^k \tag{47}$$

Substitution of (47) into the force equation (44) renders the pad reduced impedance coefficients as:

$$\begin{aligned} F_X^k(t) &= F_{Xo}^k - \left[Z_{RXX}^k \Delta e_X - Z_{RXY}^k \Delta e_Y \right] e^{i\omega t} \\ F_Y^k(t) &= F_{Yo}^k - \left[Z_{RYX}^k \Delta e_X - Z_{RYY}^k \Delta e_Y \right] e^{i\omega t} \end{aligned} \tag{48}$$

where $$Z^k_{R\alpha\beta} = \left[Z_{\alpha\beta} - \frac{Z_{\alpha\delta} \cdot Z_{\delta\beta}}{ZZ_{\delta\delta}} \right]^k = K^k_{R\alpha\beta} + i\,\omega\, C^k_{R\alpha\beta} \qquad \alpha,\beta=X,Y \qquad (49)$$

and, $(K^k_{R\alpha\beta},\ C^k_{R\alpha\beta})^k_{\alpha,\beta=X,Y}$ are the **reduced** force-displacement stiffness and damping coefficients for the kth-pad.

The **reduced** stiffness and damping coefficients for the entire bearing assembly are then given by the summation of all the pad reduced force coefficients, i.e.

$$K_{R\alpha\beta} = \sum_{k=1}^{N_{pad}} K^k_{R\alpha\beta} \quad ; \quad C_{R\alpha\beta} = \sum_{k=1}^{N_{pad}} C^k_{R\alpha\beta} \qquad \alpha,\beta=X,Y \qquad (50)$$

A method to determine the bearing static equilibrium position

A static load with components (W_{Xo}, W_{Yo}) determines the journal center euilibrium coordinates (e_{Xo}, e_{Yo}) and pad rotation angles $\{\delta^k\}$, k=1,.. N_{pad}, such that equations (42) and (43) are satisfied. In practice, an iterative method is needed to determine the equilibrium journal coordinates and pad rotation angles satisfying the applied load and pad moment constraints. The current analysis implements a Newton-Raphson algorithm to reach convergence to the actual solution. Consider at iteration J, the journal center to have an ecentricity defined by its components $(e_X, e_Y)^J$ on the {X,Y} directions, and a set of pad rotational angles $\{\delta^k\}^J$, k=1,..,N_{pad} such that the pad moment equation (43) is satisfied, i.e. the pad moments are balanced. For these conditions, the bearing has a set of reduced static stiffness coefficients (calculated at ω=0) denoted as $\{K_{R\alpha\beta}\}^J$, $\alpha,\beta=X,Y$.

Improved journal center coordinates $(e_X, e_Y)^{J+1}$ converging to the actual values satisfying equation (42) are determined as:

$$e_X^{J+1} = e_X^J + \Delta e_X; \quad e_Y^{J+1} = e_Y^J + \Delta e_Y \qquad (51)$$

where the small changes $(\Delta e_X, \Delta e_Y)$ are determined from solution of the equation

$$\begin{bmatrix} W_{Xo}+F_X \end{bmatrix}^J = \begin{bmatrix} K_{RXX} & K_{RXY} \\ K_{RYX} & K_{RYY} \end{bmatrix}_J \begin{bmatrix} \Delta e_X \\ \Delta e_Y \end{bmatrix} \qquad (52)$$

Improved pad rotations are found from:

$$\delta_k^{J+1} = \delta_k^J + \Delta\delta^k \qquad k=1,2..N_{pad} \qquad (53)$$

where (see also equation 47),

$$\Delta\delta^k = -\left[\frac{K^k_{\delta X}}{Kr_k + K^k_{\delta\delta}} \Delta e_X + \frac{K^k_{\delta Y}}{Kr_k + K^k_{\delta\delta}} \Delta e_Y \right]^J; \quad k=1,..,N_{pad} \qquad (54)$$

Note that at each step in the iterative process the pad moment equation is satisfied, i.e.,

$$\left[Kr_k \, \delta_o^k - M_o^k \right]^J = 0 \qquad k=1,2..N_{pad}$$

The procedure continues with updated journal eccentricities and pad angles until the error in the load equation is within some predetermined range, i.e. $|W_{Xo}+F_X^J| \leq \varepsilon W_o$, $|W_{Yo}+F_Y^J| \leq \varepsilon W_o$ where ε=0.01 typically.

The load-bearing equilibrium position scheme described here has proven to be robust because at every iterative step each pad moment equation is satisfied, and the improved values of journal eccentricity and pad rotation angles are predicted from the stifness coefficients evaluated at zero whirl frequency.

It is important to note that most algorithms for tilting-pad bearing analysis sometimes have difficulty in determining the journal equilibrium position when one or more pads become unloaded (*). This is most frequent for bearings with

(*) ---- A pad is defined as unloaded (fully cavitated) when no fluid pressures (also forces and moments) are generated within the pad for the values of journal eccentricity and pad rotation angle specified. At this condition, it should be clear that all pad stiffness coefficients are zero, in particular $K_{\delta\delta}$.

small, null or even negative preload. The traditional approach artificially increases the pad rotational angle until this becomes "barely" loaded. This procedure only works for tilting-pad bearings, i.e. pads without rotational structural stiffness. On the other hand, for flexure-pad bearings, if the pad becomes unloaded (null fluid film moment), then the only admissible equilibrium solution is $\delta^k=0$.

Another more difficult problem arises when a pad goes from unloaded to loaded in the current iterative step. Here, unless the predicted (new) pad rotation angle is sufficiently large, the iterative scheme will bring the pad to a state of unloading when the actual solution indicates the opposite. The procedure then introduces spurious oscillations, and frequently takes large computing times to reach an "erroneous" solution. The difficulty described is overcome easily by recognizing that a valid equilibrium (stable) pad rotational angle requires a positive pad moment stiffness, i.e.

$$Kr_k + K^k_{\delta\delta} > 0 \qquad (55)$$

Numerical method of solution for the flow equations

The well known control-volume method of Patankar (1980) is used to solve the differential equations of motion. Staggered grids containing control volumes for the primitive flow variables: circumferential and axial velocity, and pressure and temperature are generated. Algebraic difference equations are derived on each control volume for the conservation of circumferential and axial momentum, and transport of energy. A discrete form of the conservation of mass equation allows determination of the pressure field. The SIMPLEC procedure of Van Doormaal and Raithby (1984) is adopted for solution of the non-linear

difference equations along with a scheme for line solution developed by Launder and Leschziner (1978). Further details on the method applied for hybrid (hydrostatic and hydrodynamic) bearing configurations are given by Yang (1992).

Figures 4 shows the thermal bulk-flow models implemented on the computational program. These models include adiabatic (insulated) journal surface or specified (isothermal) journal temperature, as well as isothermal bearing surface or bearing shell with radial heat flow and including an adiabatic surface. Complete details on thermal boundary conditions and numerical treatment are given by San Andres (1993).

The numerical scheme devised to find the equilibrium solution in tilting pads and flexure pad bearings is both elegant and robust. Non-reduced force coefficients for each bearing pad are found from perturbed analytical difference equations for journal displacements in two orthogonal directions. The pad moment coefficients and force coefficients due to pad angular motions are fully defined as linear combinations of the force coefficients due to journal dynamic displacements, see equations (39). The method then avoids numerical evaluation of moment force coefficients due to pad rotations and thus, it is fast and accurate. Recognition that the overall pad moment-rotation stiffness coefficient has to be positive for a true pad equilibrium solution brings robustness to the procedure and avoids the possibility of oscillatory solutions, in particular for unloaded pads.

RESULTS and DISCUSSION

The validaty and usefulness of the analysis and computational program developed can only be assesed by extensive comparisons with relevant experimental data. In the absence of test results, comparisons with predictions from

similar analyses given in the literature are then justified. In any case, the calculations from the computational model implemented can only be as good as the assumptions used in the analysis. It is noted here that the present theoretical development has as its major objective the evaluation of the static and dynamic force performance characteristics of cryogenic liquid fluid film bearings. This particular application is known to require large journal surface speeds or external pressurization to provide the required load capacity since cryogenic liquids are essentially inviscid. At this time there are no experimental results for tilting-pad or flexure-pad hybrid bearings handling cryogens. Measurements of forces and force coefficients for fixed-arc (i.e. rigid surface) hybrid bearings with cryogens and surrogate fluids have appeared recently. The experimental work of Childs and Hale (1994) provides a wealth of test results and pointed out new directives for research and uses in the aerospace industry. Previous publications from the author,San Andres et al. (1990-1993), present extensive comparisons with measurements obtained from the hydrostatic test facility of Childs, as well as from other relevant investigations (Butner and Murphy, 1986, Adams et al., 1992, Chaomleffel et al., 1986).

The experimental work of Taniguchi et al. (1990) is most relevant to the present development since the tilting-pad bearing investigated operates both in the laminar and turbulent flow regimes. Furthermore, the measured pressure shows a "ram" effect due to fluid inertia at the leading edge of the loaded bearing pads. The THD analysis of Taniguchi et al. accounts for the effects of viscosity variation across the film thickness, includes a turbulent flow model based on the Ng and Pan Theory (1969), and a three dimensional energy tranport equation for the fluid film with a differential heat conduction equation for the bearing metal. The model imposses a realistic boundary condition at the shaft interface

and allows for a thermal mixing flow model at the pad leading edges. The analysis does not include thermoelastic pad deformations. The importance of this effect on tilting pad bearing performance has been clearly ellucidated by Fillon et al. (1991).

Table 1 presents the geometry and operating characteristics of Taniguchi et al.(1990) four shoe tilting pad bearing. The large bearing tested (19 inches diameter) is for use in a steam turbine and was loaded to 300 kN (67,500 lbs). Numerical calculations using the present model have been performed using the data shown in Table 1 with an adiabatic bearing and shaft surfaces thermal model, fluid inertia at the film lands and a pad inertia entrance factor K_p=0.25. A pad heat carry-over mixing coefficient equal to 1.0 was assumed in all the calculations. Figure 5 shows the equilibrium journal eccentricity as the load increases from 60kN to 300kN for a shaft speed of 3,000 rpm. The predicted results agree very well with the measurements and also with the theoretical results from Taniguchi et al. (Figure 8 of referred paper). Figure 6 shows the calculated and experimental minimum film thickness for the loaded pads (2 and 3) for the same range of applied external loads. The agreement between the present numerical results and test data follows the same trend as the theoretical values provided by Taniguchi et al.

At a fixed load of 180kN and shaft speed of 3,000 rpm, Taniguchi et al. present detailed measurements of the bearing centerline pressure, film thickness and metal surface temperature. Measured frictional drag loss is equal to 200kW and the present numerical calculations predicts a similar value. The test results correspond to a (slightly) turbulent flow case with a circumferential flow Reynolds number ($\rho\Omega RC/\mu$) equal to 1,430. Figures 7 through 9 show predictions of pressure, film thickness and bulk-flow film temperature from the

present model for two cases. The first case labeled as conventional shows results obtained with a model not including fluid inertia effects at the film lands or at the pads leading edges. This case corresponds to the solution of the Reynolds equation for the pressure field. The second case includes the effects of fluid inertia at the film lands and a "ram" pressure effect at the pad leading egde (κ_p=0.25). Referring to Figure 6 of Taniguchi et al. paper (1988), the present inertial flow model correlates better with the test results for pressure and film thickness. It is noted here that the numerical predictions without fluid inertia are virtually identical to those of Taniguchi et al. Recently, Fillon et al. (1991) performed similar comparisons with Taniguchi's test results and showed better agreement when accounting for the effects of elastic distortion due to thermal growth and pressure loading.

The film temperatures presented in Figure 9 are low compared with the temperature measurements at the pad bearing surface. The error is as large as 10°C for the loaded pads. Note that the present model predicts a film **bulk-flow** temperature , i.e. an average temperature across the film thickness, which is certainly smaller than the measured temperatures on the bearing pads or predicted across the film thickness in a 3-dimensional model. Nonetheless, the results of the present analysis are shown to predict very well the static equilibrium journal position and provide an accurate representation of the film thickness variation with a representative distribution of the film bulk-flow temperature.

Someya's journal bearing databook (1988) is a standard reference for the design of fluid film bearings. The book details the theoretical (numerical calculations) static and dynamic force performance characteristics for a variety of fluid film bearing geometries, and includes test results for a number of

relevant bearing configurations. Test bearing No. 11 of Someya's scholar reference, namely a tilting pad bearing with five pads, has been chosen to validate the numerical predictions from the present analysis. Table 2 shows the geometric and operating characteristics of the test bearing article. Someya presents the test results in a dimensionless form as a function of a Sommerfled number defined as $S=\mu_{eff}\Omega \cdot L \cdot D\ (R/C)_2/[2\pi W]$ where the effective viscosity is assumed to have the value corresponding to the measured fluid outlet temperature. Calculations using the present model have been performed for two flow conditions, a) an isothermal flow model without thermal energy transport and using the effective viscosity provided by Someya; and, b) an adiabatic flow model with null heat flow through the bearing and shaft surfaces, a heat carry-over mixing coefficient equal to 0.50, and an oil viscosity vs. temperature relation based on an exponential formulae. The test bearing operates on the laminar flow regime with no appreciable effects of fluid inertia at film lands or pad leading edges. The isothermal model was carried out to compare results with the analytical predictions presented by Someya (1988).

Figure 10 shows the measured and predicted equilibrium eccentricity versus the bearing Sommerfeld number. The largest Sommerfeld number (S=0.106) denotes test conditions of low load (1.2 kN) and high shaft speed (6,120 rpm), while the lowest Sommerfeld number represents the largest load (9.48kN) and lowest journal speed (2,982 rpm). The isothermal results are virtually identical to those reported by Someya (1988) in his handbook. Note that the adiabatic flow model provides better agreement with the test data for the low speed, high load condition (small S) where thermal effects are expected to be of importance.

The experimental synchronous (direct) stiffness and damping force coefficients obtained by Someya are given in Figures 11 through 14. The

analytical values obtained from the isothermal flow model are similar to those from the theoretical model of Someya and not reproduced for brevity. The figures show a different scaling from those depicted on the databook to emphasize the differences between tests and theory. Figures 11 and 12 show the dimensionless direct stiffness coefficients (K_{XX},K_{YY}) versus the Sommerfeld number, respectively. The adiabatic flow model predicts better the stiffness coefficients in particular at low speeds and high loads (low Sommerfled numbers). The large differences between the isothermal model and the adiabatic model at low S's are due to the heating of the fluid film at large loads which brings a temperature rise as large as 100°C (calculated) on the film lands. The experimental values for the direct stiffness K_{XX} are very low compared with the theoretical results. The large differences are explained in terms of both thermal and elastic deformations since the largest predicted pressure is 20.6 MPa (2,987 psi).

Figures 13 and 14 present the dimensionless damping coefficients (C_{XX}, C_{YY}) versus the effective Sommerfeld number. The predicted damping coefficients C_{YY} agree very well with the test data, while the other direct coefficient C_{XX} shows poor correlation at the lowest values of Sommerfeld number (large load, low speed). The theoretical results for the adiabatic flow model correlate better and at least do not increase as the Sommerfeld number decreases.

It is well known that most analyses overpredict damping coefficients when compared to test results in tilting-pad bearings. The rationale for the large discrepancies is not yet clear although thermoelastic pad deformations and support structural effects are suspect (Nicholas and Barrett, 1986, Kim and Palazzolo, 1993). The comparisons shown in the figures demonstrate the current model to agree well with test results for low loads and high speeds conditions.

Thermoelastic pad deformations could be a major source of discrepancy for large loads. Note that the predictions from the present model are representative of other models available in the literature.

Predictions obtained with the present computational program are identical to those presented by Armentrout and Paquette (1993) and Chen (1994) for flexure-pad bearings operating at high speeds and light viscous fluids under laminar flow conditions. Typical results show, at the design load condition and as as the pad rotational stiffness increases, the variation of force coefficients from a tilting-pad regime passing through a transition zone and leading to a fixed-geometry regime. Designers typically select the value of rotational stiffness which shows the least value of the difference in cross - coupled stiffness coefficients ($K_{XY}-K_{YX}$) just before the transition regime starts. Then a finite element program is used to design the geometry of the flexure pad web which renders the required pad rotational stiffness as well as pad radial stiffness when the case merits. In its simplest form, the flexure pad rotational and radial stiffness are given by the following elementary relations:

$$K_r = E \cdot I_w / h_w \ [N \cdot m/rad]; \quad K_R = A_w \cdot E / h_w \quad [N/m] \qquad (56)$$

where E is the elastic modulus of the web material, h_w is the web height, $A_w = w \cdot L$ is the web cross-sectional area (of width w and axial length L), and $I_w = L \cdot w^3/12$ is the area moment of inertia of the web. The expressions detailed do not account for the geometric stiffness due to the load applied on the pad. Note that the ratio of the radial stiffness to rotational stiffness (K_R/K_r) is equal to $12/w^2$.

The following discussion pertains to the results obtained for a flexure pad hybrid bearing for application in a liquid oxygen (LOx) turbopump. The

geometry and operating conditions for the six pad bearing are given in Table 3. Each pad has a rectangular recess and an orifice fluid supply line machined across the web supporting the flexure pad. The recess to pad ratio of areas is equal to 0.236 as recommended for a LOx application (Butner and Murphy, 1986). The values of supply and discharge pressure and rotational speed correspond to that on an ALS bearing turbopump configuration. The large values of axial flow, circumferential, and squeeze film flow Reynolds numbers show a turbulent flow application with large fluid inertial effects. Calculations for both isothermal conditions and adiabatic heat flow with full pad leading edge thermal mixing were performed simultaneously. The resuls between both models differ little expect for an increment in fluid temperature at the pad sides of 12°K and not sufficient to affect considerably the bearing performance. Henceforth, in the results that follow only the isothermal results are discussed in detail.

At the journal concentric position (e=0), Figure 15 shows the calculated whirl frequency ratio (WFR) and recess pressure ratio for increasing values of the pad rotational stiffness. The lowest value of K_r represents an ideal tilting pad geometry with null restraining moments, while the largest rotational stiffness effectively represents a rigid (fixed) pad bearing configuration. The effect of pad angular stiffness on the stability indicator (WFR) is clear and shows the advantage of a moving pad geometry for this high speed application. As the pad rotational stiffness increases, the recess pressure ratio decreases while the flow rate increases as shown in Figure 16. The (X) marked on this figure represents the flow rate for a conventional fixed HJB with film lands of 360° extent. Figure 17 shows the pad rotation angle and the pad minimum film thickness (occurring at the pad trailing edge) versus the pad rotational stiffness. As this stiffness increases it is clear that the pad is unable to

move and hence the minimum film thickness is that of the fixed pad. The largest rotations are expected in the tilting pad regime with a reduction in film thickness of 40%. The drag torque shown in Figure 18 is shown to decrease with the pad rotational stiffness since the effective film thickness is essentially larger. This result then shows that the flexure pad bearing has lower drag power than the conventional tilting pad bearing.

Figure 19 shows the synchronous force coefficients, i.e. evaluated at $\omega=\Omega$. At the concentric position, the direct coefficients are equal ($K_{XX}=K_{YY}$) while the cross-coupled coefficients differ in sign ($K_{YX}=-K_{XY}$). Note that the direct stiffness is about an order of magnitude larger than the cross-coupled stiffness coefficients for the fixed pad condition. The calculations show the paramount effect of the pad rotational stiffness coefficient on the rise of the cross-coupled coefficients. Figures 20 to 23 show the effect of frequency excitation on the stiffness (K_{XX}, K_{XY}), and damping (C_{XX}, C_{XY}) coefficients, respectively. The results denote calculations at frequency ratios $f=\omega/\Omega$ equal to 0, 0.5, 1 and 2 times the rotational speed. The direct stiffness K_{XX} decreases with the frequency ratio f mainly due to fluid inertia effects, with a maximum direct stiffness at a pad rotational stiffness equal to 10,000 N·m/rad. The excitation frequency appears not to affect the cross-coupled coefficients showing then low values of cross-coupled inertia coefficients.

Next, a pad rotational stiffness (K_r)of 10 KNm/rad was selected to perform calculations for the load capacity of the bearing at the rated operating condition. The load (W) applied to the bearing increased to a maximum of 12 kN (2,700 lbs) denoting a specific load (W/LD) equal to 3.5 MPa (507 psi). Two cases were considered, **(A)** load applied towards the center of a bearing pad - LOP, **(B)** load applied at 30° from the vertical line, i.e. between pads - LBP.

Figure 24 shows the calculated journal eccentricity and the mimimum film thickness occurring on the bottom pad to have a very linear relationship with the applied load. Note that the smallest film thickness is just 40% of the nominal bearing clearance for the largest load applied. The selected flexure pad rotational stiffness has a whirl frequency ratio equal to 0.25. This pad stiffness value although not low enough to elliminate hydrodynamic inestability constitutes a major advancement over the rigid bearing pad configuration.

The flexure pad geometry to provide the selected value of pad rotational stiffness can be obtained using the formulae given by equation (56). Using a conventional steel with an elastic modulus of 20.7E10 N/m^2 (30E6 psi), a web height (h_w) of 1 cm and thickness (w) of 5.4 mm renders a value K_r=10KN·m/rad. The web thickness is enough to allow for the orifice supply line of 2.581 mm diameter. The pad radial stiffness is equal to 4,135 MN/m which is an order of magnitude larger than the fluid film direct stiffness K_{XX}, and hence it will not affect greatly the bearing performance. (Maximum elastic web deformations of less than 3μm are expected for the largest load applied of 12KN).

Figures 25 and 26 show the synchronous stiffness and damping coefficients versus the applied load, respectively. Note that the stiffness coefficients are virtually constant for loads to 8kN (1800 lbs). The cross-coupled stiffnesses for the case of load between pads (B) show the largest deviations at the largest load applied, while the direct damping coefficients decrease slightly with the applied load. The whirl frequency ratio decreases monotonically from 0.25 to 0.22 as the load increases. Figure 27 shows the calculated (dimensionless) centerline pressure and film thickness for a load of 12 kN. The largest film pressures along with minimum film occur at pad 4 where the journal load is applied. The results show a small "ram" pressure at the pads inlet and

hydrodynamic pressure increases in the downstream portion of the bearing recesses. Note also the large inertial pressure drops at the recess edges.

The analysis also includes a pad rotational damping and set to zero in all calculations presented. Flexure-pad bearings due to its automated wire-EDM construction offer the advantage of accurate specification of the gap (g) between the pad inersurface and the bearing housing. A simple one-dimensional analysis shows that the pad rotational damping is approximately equal to:

$$C_r = (1/60)\cdot\mu\cdot L\cdot(\theta_p\cdot\pi D/180)^5(1/g)^3 \qquad [N\cdot m\cdot sec/rad] \quad (57)$$

The rotational damping for a gap (g) equal to 101.6μm (0.004 mils) is equal to 0.05187 N·m·sec/rad and not large enough to affect the dynamics of the LOx flexure pad bearing. However, some commercial applications handling high viscosity lubricants may offer large values of rotational damping. It this damping is large enough it will cause the flexure pad to become overdamped and in fact, it may lock the pad and degrade the dynamic performance of the whole bearing. This condition is very interesting since the flexure-pad bearing will still behave well under static load conditions, i.e. it will show a journal displacement in the same direction as the applied load, but due to excess in rotational damping, it can bring hydrodynamic stability at sufficiently large speeds and whirl frequencies.

The calculations performed show that a flexure-pad bearing keeps virtually all the benefits of a hydrostatic pad application (large direct stiffness and damping coefficients) while offering an accurate control on the cross-coupled stiffness coefficients and reduction in the whirl frequency ratio. The results provide ample evidence on the effect of pad rotational stiffness on the performance of a hybrid - flexure pad bearing.

CONCLUSIONS

This reports details the theoretical analysis for calculation of the dynamic force performance of tilting-pad and flexure-pad hybrid (combination hydrostatic and hydrodynamic) bearings operating in the turbulent flow regime. These types of bearings appear to offer an alternative to improve (and eliminate) the limited stability characteristics of conventional fixed pad geometry bearings. In particular, a flexure pad bearing is best suited to meet this objective since it offers many advantages when compared to a conventional tilting pad bearing. These advantages encompass acuracy of manufacturing without added difficulties for assembly and calibration, adequate control of bearing preload and pad structural stiffnesses (radial and rotational), and absence of wear between shoe and pivot support. Flexure pad bearings lend themselves to a hydrostatic application since the ports for the pressurized fluid can be easily machined on the pad supporting web without added mechanical complexities and at a reduced cost.

Bulk-flow equations of mass conservation, momentum and energy transport describe the motion of a variable properties fluid within the thin film lands of a bearing. A mass conservation equation at the recess volumes with a simple formulation for the recess pressure and temperature fields are also considered. Fluid inertia effects, temporal and advective, are fully accounted for flows with large pressure differentials or large surface speeds. Zeroth- and first-order flow equations are numerically solved to determine the flow field and calculate the pad fluid film forces and force coefficients. An elegant method to determine the journal equilibrium position and the reduced force coefficients for tilting-pad bearings is introduced.

Numerical results from the present development have been compared to similar analyses for laminar flow tilting-pad bearings. Predictions from the model also correlate well with experimental bearing loads and dynamic force coefficients. The comparisons insure the validity of the model implemented and also widen the range of practical applications for the computational program developed.

Predictions for a flexure-pad hybrid bearing handling liquid oxygen at operating conditions typical of a turbopump applications demonstrate the ability of this type of bearing to improve the hydrodynamic stability whirl ratio, without degradation on the static load performance or reduction in direct stiffness and damping coefficients. The test example shows that hybrid bearings satisfy in excess the load requirements typical of present and future cryogenic turbopumps.

The analysis still needs to be improved to account for pad flexibility in the radial direction. Industrial applications with large loads applications may also demand a thermoelastic model for accurate determination of pad surface temperature and minimum film thickness. These considerations may not be of great importance in a cryogenic turbopump application.

REFERENCES:

Adams, M., J. Sawicki, R. Capaldi, 1992, "Experimental Determination of Hydrostatic Journal Bearing Rotordynamic Coefficients," Proc, IMechE, Paper C432/145, pp. 365-374.

Armentrout, R., and D. Paquette, 1993, "Rotordynamic Characteristics of Flexure-Pivot Tiliting Pad Journal Bearings," STLE Tribology Transactions, Vol 36, 3, pp. 443-451.

Arumugam, P., S. Swarnamani, and B.S. Prabhu, 1994, "Experimental Identification of Linearized Oil Film Coefficients of Cylindrical and Tilting Pad Bearings," ASME Paper 94-GT-81.

Barrett, L.E., Allaire P.E.,and B.W. Wilson, 1988, "The Eigenvalue Dependence of Reduced Tilting Pad Bearing Stiffness and Damping Coefficients," STLE tribology Transactions, Vol. 31, 4, pp. 411-419.

Bouard, L., Fillon, M., and J. Frene, 1994, "Comparison Between Three Turbulent Models - Application to Themohydrodynamic Performances of Tilting-Pad Bearings," International Tribology Conference, AUSTRIB '94, Perth, Australia, December, pp. 119-126.

Brockwell,K., and D. Kleibub, 1989, "Measurement of the Steady State Operating Characteristics of the Five Shoe Tilting Pad Journal Bearing," STLE Tribology Transactions, Vol. 32, 2, pp. 267-275.

Brockwell,K., D. Kleibub, W. Dmochowski, 1990, "Measurement and Calculation of the Dynamic Operating Characteristics of the Five Shoe Tilting Pad Journal Bearing," STLE Tribology Transactions, Vol. 33, 4, pp. 481-492.

Burton, R.A., and H.J. Carper, 1967, "An Experimental Study of Annular Flows with Applications in Turbulent Film Lubrication," Journal of Lubrication Technology, pp. 381-391.

Butner, M., and B. Murphy, 1986, "SSME Long Life Bearings," NASA CR Report 179455.

Chaomleffel, J.P., and D. Nicholas, 1986, "Experimental Investigation of Hybrid Journal Bearings," Tribology International, Vol. 19, 5, pp. 253-259.

Chen, W.J., 1994, "Bearing Dynamic Coefficients of Flexible Pad Bearings," STLE Transactions, Preprint No. 94-TC-4D-1.

Childs, 1994, and K. Hale, 1994, "A Test Apparatus and Facility to Identify the Rotordynamic Coefficients of High Speed Hydrostatic Bearings," ASME Journal of Tribology, Vol. 116, 1, pp. 337-344.

Constantinescu, V.N. and S. Galetuse, 1975, "Pressure Drop Due to Inertia Forces in Step Bearings," ASME Paper 75-Lub-34.

Constantinescu, V.N., and F. DiMofte, 1987, "On the Influence of the Mach

Number on Pressure Distribution in Gas Lubricated Step Bearings," Rev. Roum. Sci. Tech. - Mec. Appl., Tome 32, No 1, p. 51-56.

De Choudhury, P., M. Hill, and D. Paquette, "A Flexible Pad Bearing System for a High Speed Centrifugal Compressor," Proceedings of the 21st Turbomachinery Symposium, Dallas, TX, Spetember, 1992, pp. 57-65.

Ettles, C., and A. Cameron, 1968, "Considerations of Flow Across a Bearing Groove, Journal of Lubrication Technology, pp. 312-319.

Ettles, C.M., 1980, "The Analysis and Performance of Pivoted Pad Journal Bearings Considering Thermal and Elastic Effects," ASME Journal of Lubrication Technology, Vol. 102, pp. 182-192.

Ettles, C.M., 1992, "The Analysis of Pivoted Pad Journal Bearing Assemblies Considering Thermoelastic Deformation and Heat Transfer Effects," STLE Tribology Transactions, Vol. 35, 1, pp. 156-162.

Fillon, M., J-C Bligoud, and J. Frene, "Experimental Study of Tilting-Pad Journal Bearings-Comparison with Theoretical Thermoelastohydrodynamic Results," ASME Transactions, Paper 91-trib-17.

Fillon, M., Frene, J., and R. Boncompain, 1987, "Historical Aspects and Present Development on Thermal Effects in Hydrodynamic Bearings," Proceedings of the 13th Leeds-Lyon Symposium, pp. 27-47.

Flack, R.D., and P.E. Allaire, 1984, "Literature Review of Tilting Pad and Turbulent Hydrostatic Journal Bearings for Nuclear Main Coolant Pumps," The Shock and Vibration Digest, Vol. 16, 7, pp. 3-12.

Flack, R.D., and C.J. Zuck, 1988, "Experiments on the Stability of Two Flexible Rotors in Tilting Pad Bearings," STLE Tribology Transactions, Vol. 31; 2, pp. 251-257.

Franchek, N., 1992, "Theory Versus Experimental Results and Comparisons for Five Recessed, Orifice Compensated, Hybrid Bearing Configurations," Texas A&M University, M.S. Thesis, TAMU Turbomachinery Laboratories, August 1992.

Franchek, N., Childs, D., and L. San Andres, 1994, "Theoretical and Experimental Comparisons for Rotordynamic Coefficients at a High-Speed, High-Orifice-Compensated Hybrid Bearings," ASME Paper 94-Trib-43.

Greenhill, L., 1991, Private Communication, Aerojet TechSystems Corp., CA

Ha, H.C., Kim, H.J., and K.W. Kim, 1994, "Inlet Pressure Effects on the Thermohydrodynamic Performance of a Large Tilting Pad Journal Bearing," ASME Paper 94-Trib-26.

Hall, K.R., P. Eubank, J. Holste, K. Marsh, 1986, "Performance Equations for Compressible Flow Through Orifices and Other ΔP Devices: A Thermodynamics Approach," AIChe Journal, Vol.32, No. 3, pp. 517-519.

Hirs, G.G. , 1973, "A Bulk-Flow Theory For Turbulence in Lubricating Films," ASME Journal of Lubrication Technology, pp. 135-146.

Kim, J., and A. Palazzolo, 1993, "Dynamic Characteristics of TEHD Tilt Pad Journal Bearing Simulation Including Multiple Mode Pad Flexibility Model," ASME 1993 Vibrations Conference, Vibrations of Rotating Systems, DE-Vol. 60, pp. 363-379.

Knight, J.D., and L.E. Barrett, 1988, "Analysis of Tilting Pad Journal Bearings with Heat Transfer Effects," ASME Journal of Tribology, Vol. 110, pp. 128-133.

Kurtin, K., Childs, D., San Andres, L.A., and K. Hale, 1993, "Experimental versus Theoretical Characteristics of a High Speed Hybrid (combination Hydrostatic and Hydrodynamic) Bearing," ASME Journal of Tribology, Vol. 115, 2, pp. 160-169.

Launder, B., and M. Leschziner, 1978, "Flow in Finite Width Thrust Bearings Including Inertial Effects," ASME Journal of Lubrication Technology, Vol. 100, pp. 330-345.

Lund, J., 1964, "Spring and Damping Coefficients for the Tilting Pad Journal Bearing," ASLE Transactions, Vol. 7, pp. 342-352.

Lund, J., and L. Bo Pedersen, 1986, "The Influence of Pad Flexibility on the Dynamic Coefficients of a Tilting Pad Journal Bearing," ASME Paper 86-Trib-49

McCarty, R.D., 1986, NBS Standard Reference Data Base 12, Thermophysical Properties of Fluids, MIPROPS 86, Thermophysics Division, Center for Chemical Engineering, National Bureu of Standards, Colorado.

Mori, A., T. Makino, and H. Mori, 1991, "Entry Flow and Pressure Jump in Submerged Multi-Pad Bearings and Grooved Bearings," ASME Paper 90-Trib-42.

Mosher, P., 1992, "Experimental vs. experimental and Theoretical Characteristics of Five Hybrid (Combination Hydrostatic and Hydrodynamic) Bearing Designs for Use in High Speed Turbomachinery," M.S. Thesis, Texas A&M University, December.

Mitsui, J.,Hori, Y., and M. Tanaka, 1983, "Thermohydrodynamic Analysis of Cooling Effect of supply Oil in Circular Journal Bearing," ASME Journal of Lubication Technology, Vol. 105, pp. 414-421.

Ng, C.W., and and C. Pan, 1965, "A Linearized Turbulent Lubrication Theory," ASME Journal of Basic Engineering, Vol. 87, pp. 675-688.

Nicholas, J.C., and L.E. Barrett, 1986, "The Effect of Bearing support Flexibility on Critical Speed Predcition," ASLE Transactions, Vol. 29, 3, pp. 329-338.

Nicholas, J.C., and R.G. Kirk, 1979, "Selection and Design of Tilting Pad and Fixed Lobe Journal Bearings for Optimum Rotordynamics," Proc. of the 8th Turbomachinery Symposium, Turbomachinery Laboratory, Texas A&M University, Dallas, pp. 43-58.

Nicholas, J.C., 1994, "Tilting Pad Design," Proc. of the 23th Turbomachinery Symposium, Turbomachinery Laboratory, Texas A&M University, Dallas, pp. 179-194.

Orcutt, F.K., 1967, "The Steady-State Characteristics of the Tilting-Pad Journal Bearing in Laminar and Turbulent Flow Regimes," ASME Journal of Lubrication Technology, pp. 392-404

Parkins, D. W., and D. Horner, "Tilting pad Journal Bearings - Measured and Predicted Stiffness Coefficients,"STLE Transactions, Pre-print No. 92-TC-3D-2.

Patankar, S., 1980, "Numerical Heat Transfer and Fluid Flow," Hemisphere Publishing Corporation, McGraw-Hill Book Company.

Pinkus, O., 1984/85, "Optimization of Tilting Pad Journal Bearings Including Turbulence and Thermal Effects," Israel Journal of Technology, Vol. 22, pp. 142-154.

Pinkus, O., 1990, "Thermal Aspects of Fluid Film Tribology," ASME Press, NY.

Rouch, K.E., 1983, "Dynamics of Pivoted-Pad Journal Bearings, Including Pad Transalation and Rotation Effects," ASLE Transaction, Vol. 26, 1, pp. 102-109.

San Andres, L.A., 1990, "Turbulent Hybrid Bearings with Fluid Inertia Effects", ASME Journal of Tribology, Vol. 112, pp. 699-707

San Andres, L.A., 1992, "Analysis of Turbulent Hydrostatic Bearings with a Barotropic Fluid," ASME Journal of Tribology, Vol. 114, 4, pp. 755-765.

San Andres, L, 1993, "Thermohydrodynamic Analysis of Cryogenic Liquid, Turbulent Flow Fluid Film Bearings," Annual Progress Report to NASA Lewis Research Center, NASA Grant NAG3-1434.

San Andres, L., Z. Yang, and D. Childs, 1993, "Thermal Effects in Cryogenic Liquid Annular Seals, I: Theory and Approximate Solutions; II: Numerical Solution and Results", ASME Journal of Lubrication Technology, Vol 115, 2, pp. 267-284.

Scharrer,J,K, R. Hibbs, 1990, "Flow Coefficients for the Orifice of a Hydrostatic Bearing," STLE Tribology Transactions, vo. 33, pp. 543-547.

Shapiro, W., and R. Colsher, 1977, "Dynamic Characteristics of Fluid-Film Bearings," Proc. of the 6th Turbomachinery Symposium, Turbomachinery Laboratory, Texas A&M University, pp. 39-51.

Smalley, A.J., J.H. Vohr, V. Castelli, and C. Wachtmann, 1974, "An Analytical and Experimental Investigation of Turbulent Flow in Bearing Films Including Convective Fluid Inertia Forces," Journal of Lubrication Technology, pp. 151-157.

Someya, T., (editor), "Journal-Bearing Databook," Springer-Verlag, pp. 227-229, 1988.

Taniguchi, S., T. Makino, K. Takeshita, T. Ichimura, "A Thermohydrodynamic Analysis of Large Tilting-Pad Journal Bearing in Laminar and Turbulent Flow Regimes with Mixing," ASME Journal of Tribology, Vol. 112, pp. 542-549, 1990.

Van Doormal, J.P., and D. Raithby, 1984, "Enhancements of the SIMPLE Method for Predicting Incompressible Fluid Flows," Numerical Heat Transfer, Vol. 7, pp. 147-163.

White, M.F., and S.H. Chan, 1992, "The Subsynchronous Behavior of Tilting-Pad Journal Bearings," ASME Journal of Tribology, Vol. 114, pp. 167-173.

Yang, Z., 1992, "Thermohydrodynamic Analysis of Product Lubricated Hydrostatic Bearings in the Turbulent Flow Regime," Ph.D. Dissertation, Mechanical Engineering Department, Texas A&M University, December

Yang, Z., L. San Andres, and D. Childs, 1993, "Importance of Heat Transfer from Fluid Film to Stator in Turbulent Flow Annular Seals," WEAR, Vol. 160, pp. 269-277.

Zeidan, F., 1992, "Developments in Fluid Film Bearing Technology," Turbomachinery International Magazine, September/October 1992.

Zeidan, F., and D. J. Paquette, 1994, "Application of High Speed and High Pefformance Fluid Film Bearings in Rotating Mechnery," Proc. of the 23th Turbomachinery Symposium, Turbomachinery Laboratory, Texas A&M University, Dallas, pp. 209-234.

Table 1. Geometry and Operating Conditions of Taniguchi et al. Bearing (1990)

Number of pads = 4
Diameter (D) = 479 mm
Length (L) = 300 mm
Clearance (C_p) = 612 μm, zero preload

Pad Arc: 80°, offset=0.50 (centrally pivoted)
pivots at 45°,135°,225°,315°
Pad thickness=121 mm

Lubricant: Oil ISO VG 32 with ρ=860 kg/m^3
viscosity μ=0.0277 Pa-s at 40°C
oil viscosity-temperature coefficient 0.034 1/°C

Supply conditions: Ps=0.1 MPa at Ts=40°C
flow rate 520 lit/min

Operating speed: 1krpm to 4krpm

Load between pads 2 & 3: 60kN to 300 kN.

Circumferential flow Reynolds number (ρΩRC/μ) = 1,430

- o -

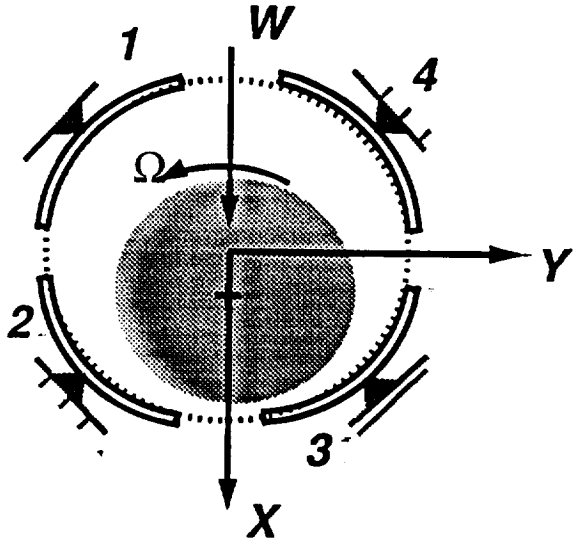

Table 2. **Geometry of Test Bearing No. 11 of Someya (1988), pp. 227-229.**

Number of pads = 5
Diameter (D) = 76.4 mm
Length (L) = 31.6 mm
Clearance (C_p) = 86 μm, zero preload

Pad Arc: 58°, offset=0.50 (centrally pivoted)
pivots at 36°,108°,180°,252°.324°

Lubricant: #140 turbine Oil with ρ=874 kg/m^3

viscosity ν= 61.8 mm^2/sec at 37.8°C
35.4 '' 50.0°C
7.78 '' 98.9°C

Supply conditions: Ps=0.1 MPa

Inlet Temperature: varies between 38.5°C to 41.3°C

Operating speed: varies between 2,980 rpm to 6,240 rpm

Load W on bottom pad (#3): 1.2 kN to 9.48 kN.

$$\text{Sommerfeld Number } S=\frac{\mu_{eff}\ \Omega\ L\ D}{2\pi\quad W}\left(\frac{R}{C_p}\right)^2$$

Dimensionless stiffness coefficients $k_{ij} = K_{ij}\ (C/W)$

damping "" $c_{ij} = C_{ij}\ (C\cdot\Omega/W)$

Réfer to Someya's Databook for a detailed description of test conditions

- o -

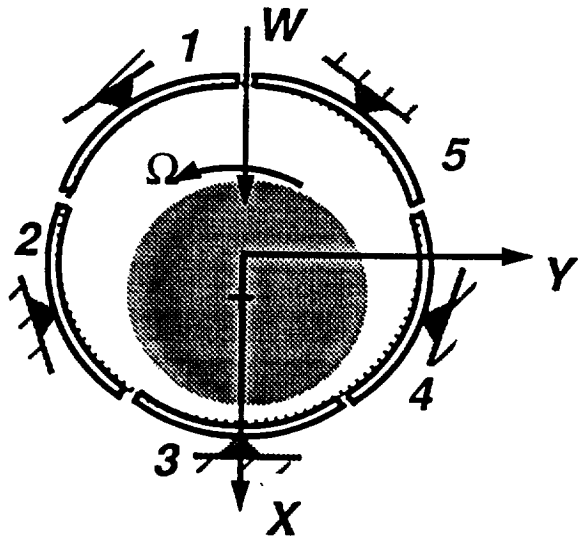

Table 3. Flexure-pad Liquid Oxygen Hybrid Bearing.
Geometry and operating conditions

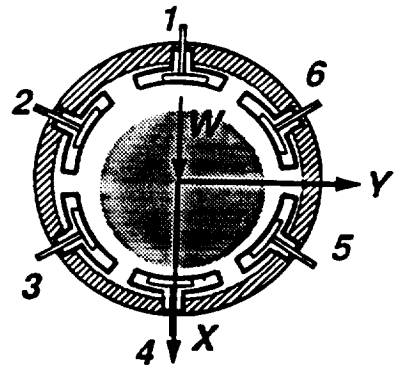

Diameter D=92.71 mm (3.65 in)
Length L=37.08 mm (1.46 in)
Clearance C_p = 76.2 μm (0.003 in), zero preload
Recess depth H_R = 228μm (0.009 in)

6 pads of length 50° and 1 recess per pad
pad offset=0.50
pad pivots at 0°,60°,120°,180°,240°,300°
leading edge ram pressure coefficient κ_p=0.32

recess arc length 23.5° and axial length l= 19mm (0.75 in)

orifice diameter d_o=2.58 mm, C_d=1.0

edge loss coefficients ξ_θ, ξ_y=0.0
swirl ratio α=0.50

Pad rotational stiffness (K_r) varies

damping (C_r)=0 N·m·s/rad

Inertia : 1.017E-4 kg·m^2, mass : 0.283 kg for thickness 0.02 m

Operating speed: 25krpm

Pressure supply P_s = 26.71 MPa (3874 psi)
discharge P_a = 8.81 MPa (1278 psi), ΔP= 2600 psi

Liquid oxygen at inlet temperature T_s=90°K (162°R)

at (P_s,T_s): density ρ_s= 1,192 kg/m^3, viscosity μ_s=0.2459E-03 Pa·s,

Reynolds numbers at concentric position,
Circumferential flow $Re_c=(\rho/\mu)_s \Omega \cdot R \cdot C$= 44,832
Axial flow $Re_a=(\rho/\mu)_s V \cdot C_2$ = 30,487 - 30,801
Squeeze film $Re_s=(\rho/\mu)_s \omega \cdot C^2$ = 73.52 (ω=Ω)

- o -

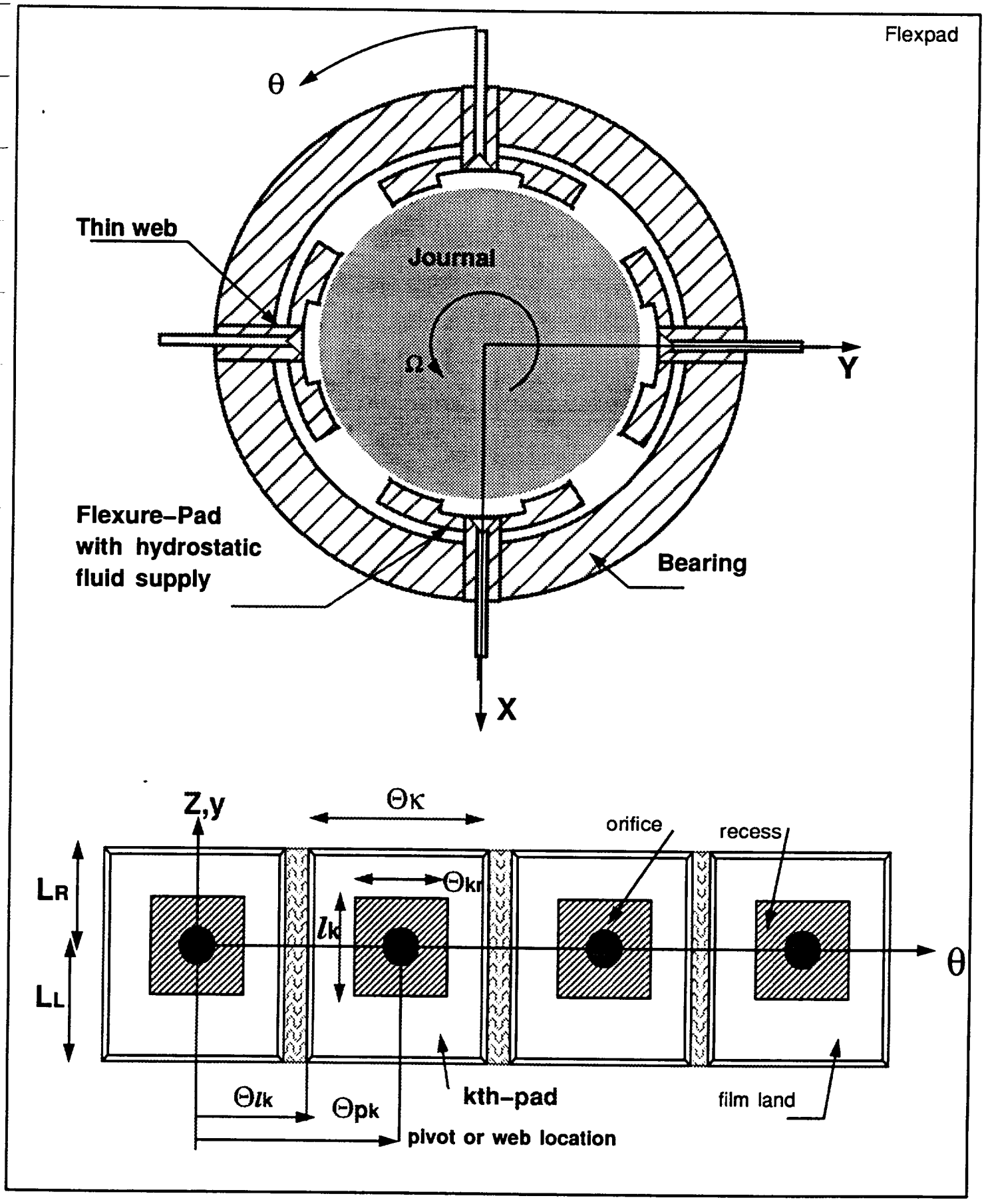

Figure 1. Geometry of flexure pad hybrid bearing

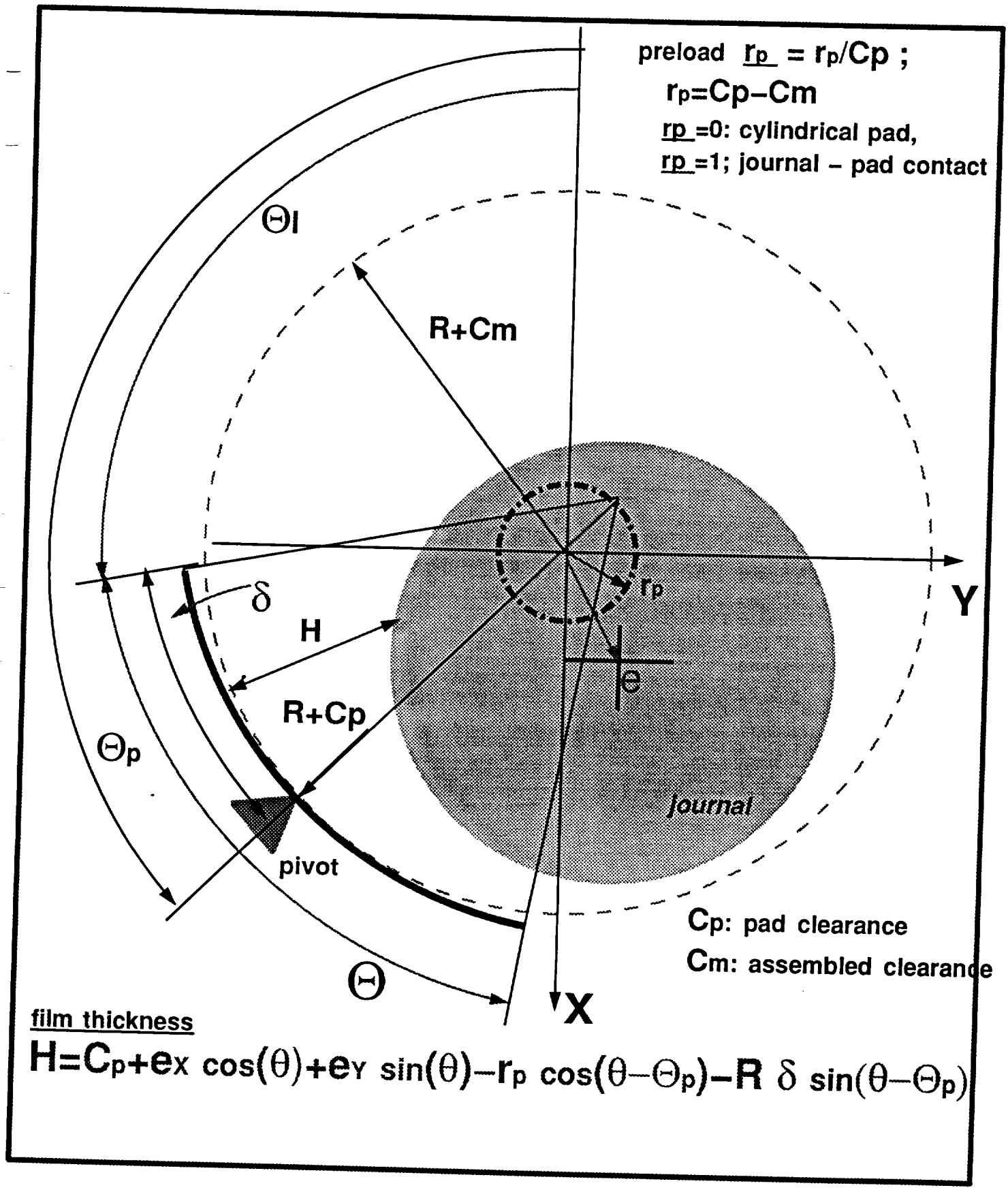

Figure 2. Geometry and nomenclature for tilting–pad

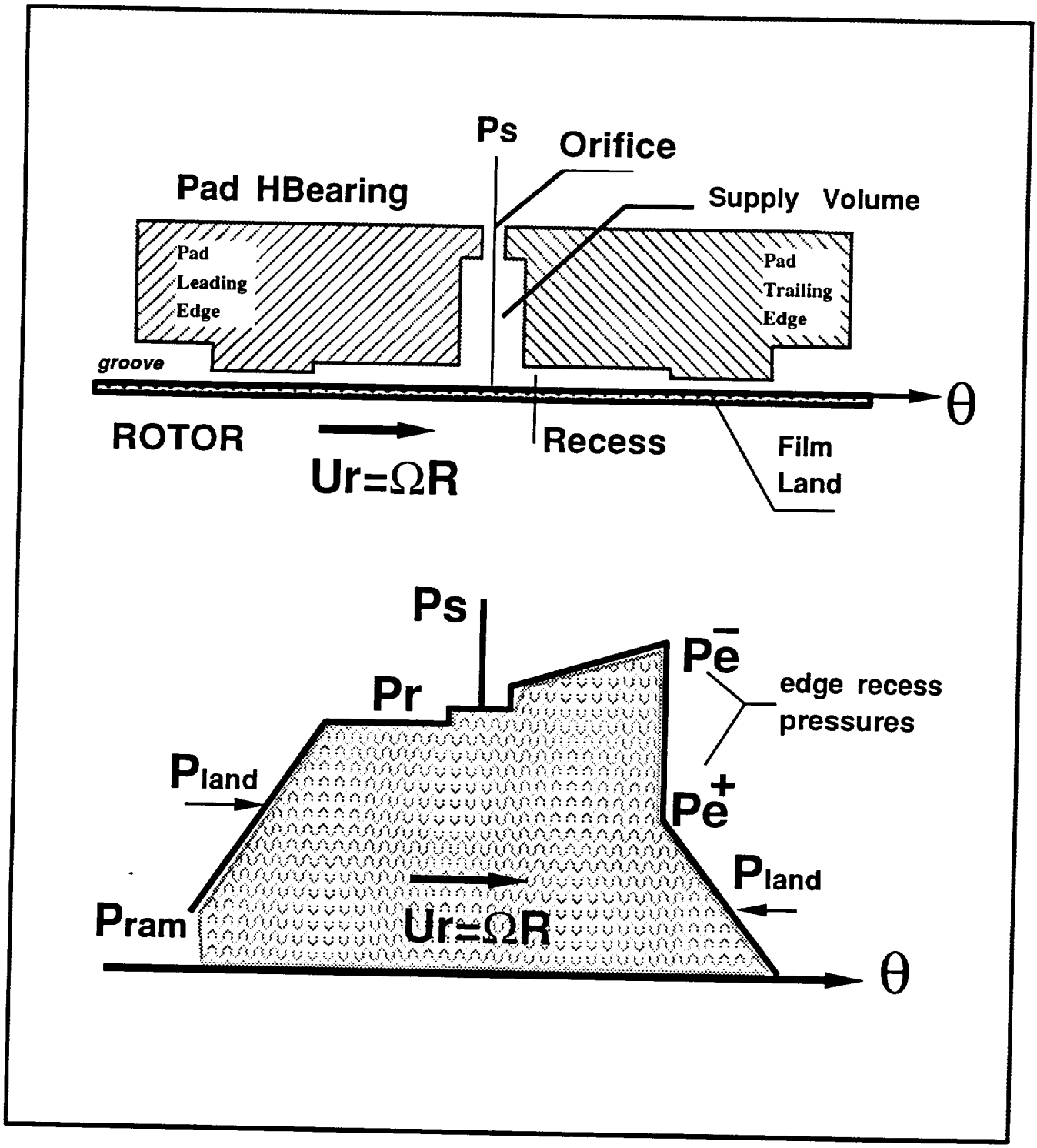

Figure 3. Conceptual description of pressure rise and drop at recess edge of a hydrostatic pad bearing, and pressure ram effect at leading edge of bearing pad..

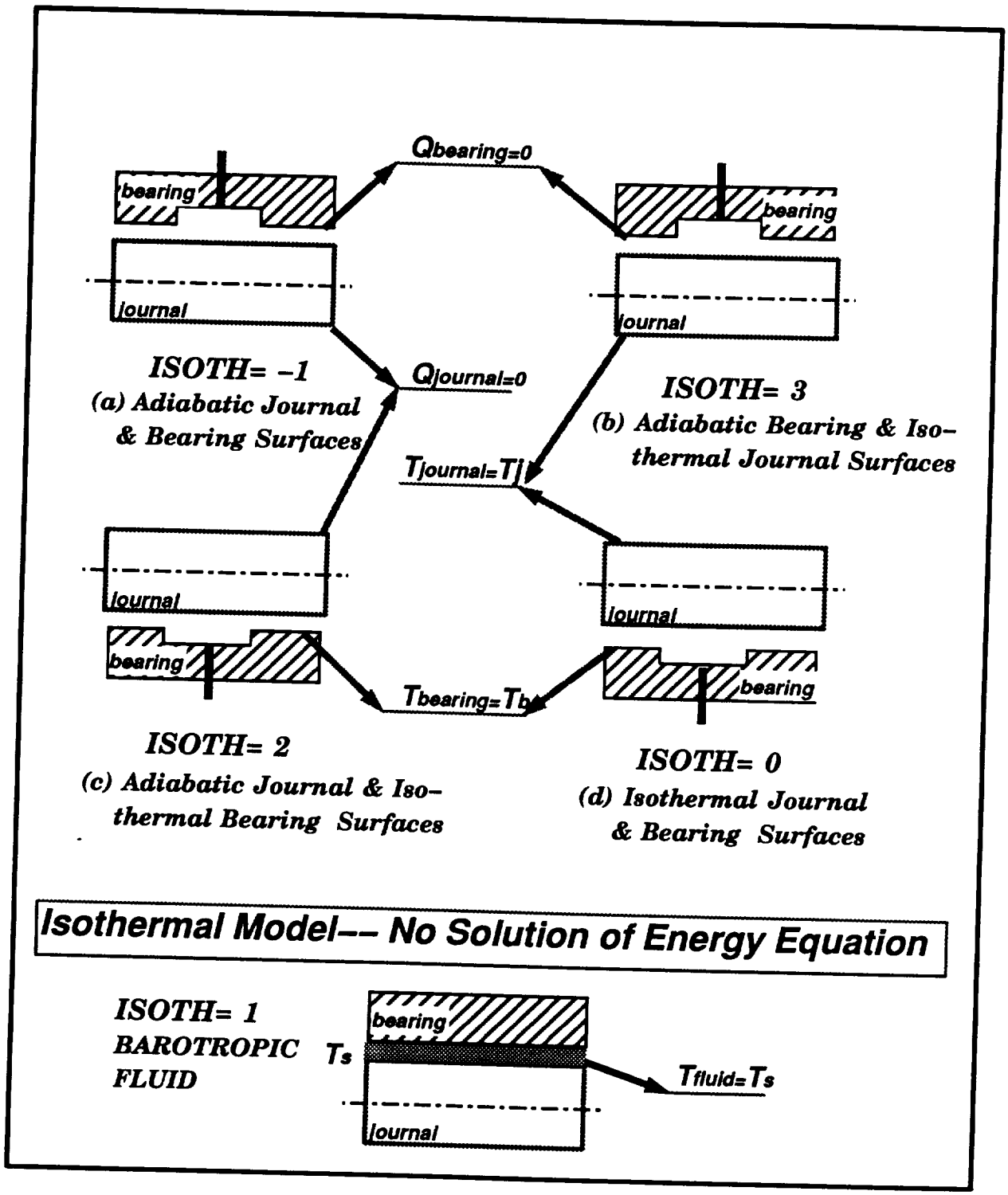

Figure 4a. Thermal bulk-flow models

ISOTH=5, Isothermal journal & Radial heat flow through bearing
ISOTH=4, Adiabatic journal & Radial heat flow through bearing

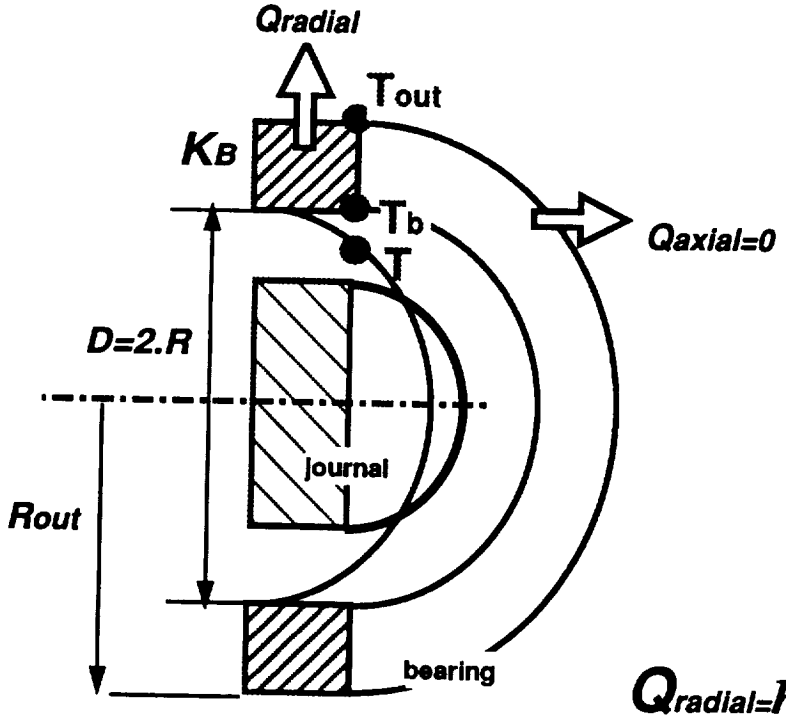

$$Q_{radial} = h_{BT} (T - T_{out})$$

$$h_{BT} = h_B (K_B/R)/\{K_B/R + h_B \ln(R_{out}/R)\}$$

where h_B is the fluid–film to bearing surface convection heat transfer coefficient

Figure 4b. Radial heat flow on bearing shell

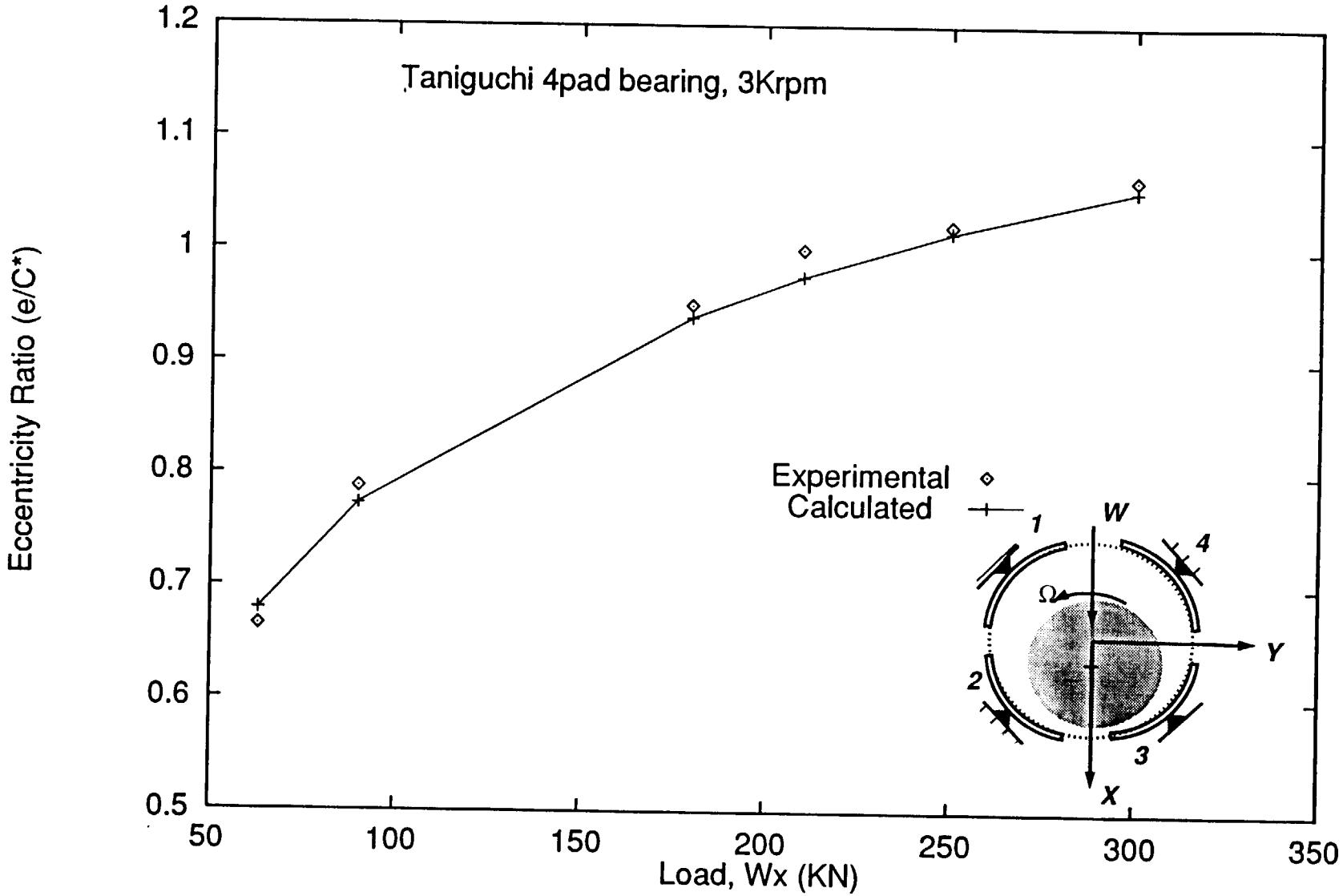

Figure 5. Equilibrium eccentricity vs. applied load
Taniguchi et al. tilt pad bearing. Speed 3krpm

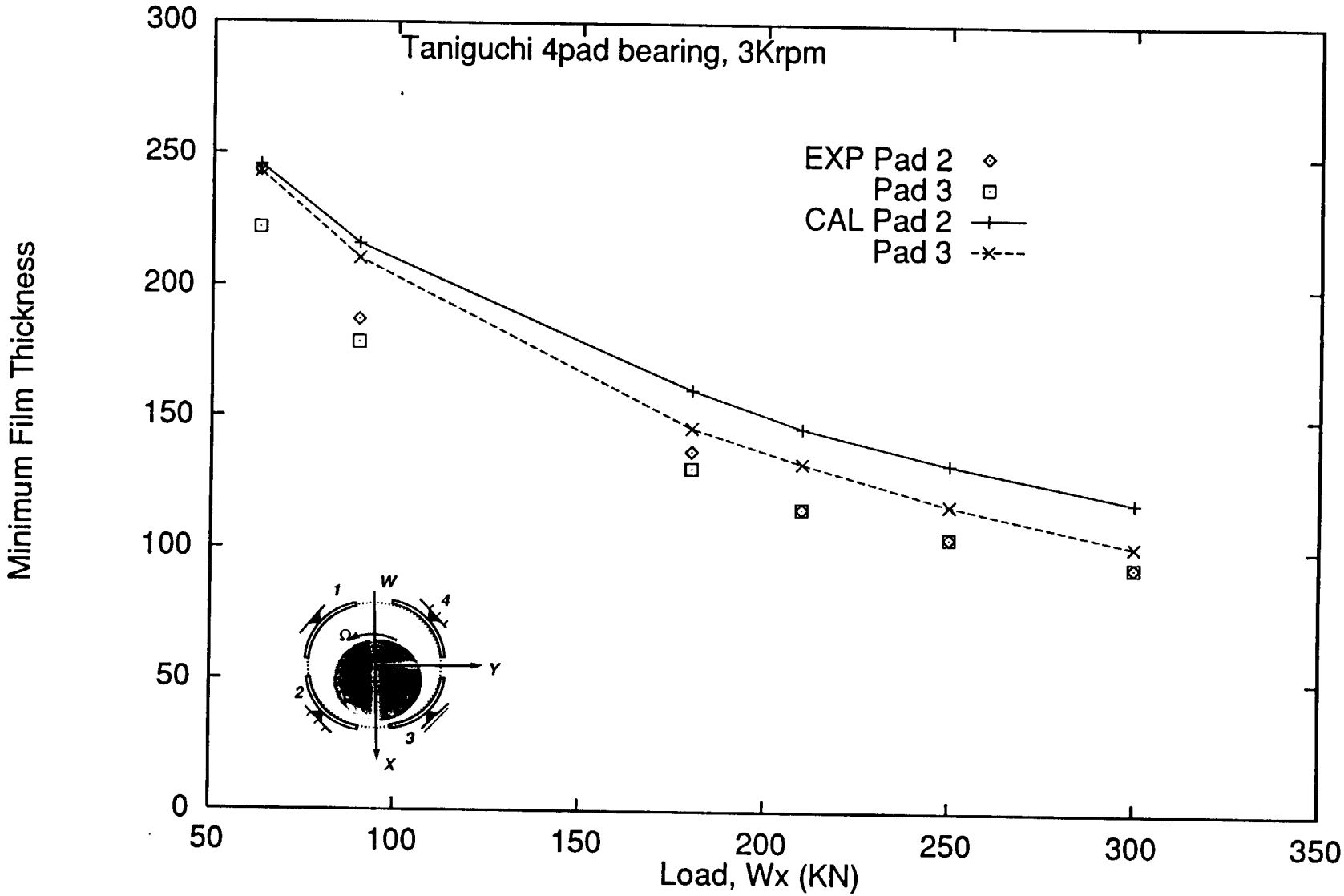

Figure 6. Minimum film thickness (μm) vs. applied load

Taniguchi et al. tilt pad bearing. Speed 3krpm

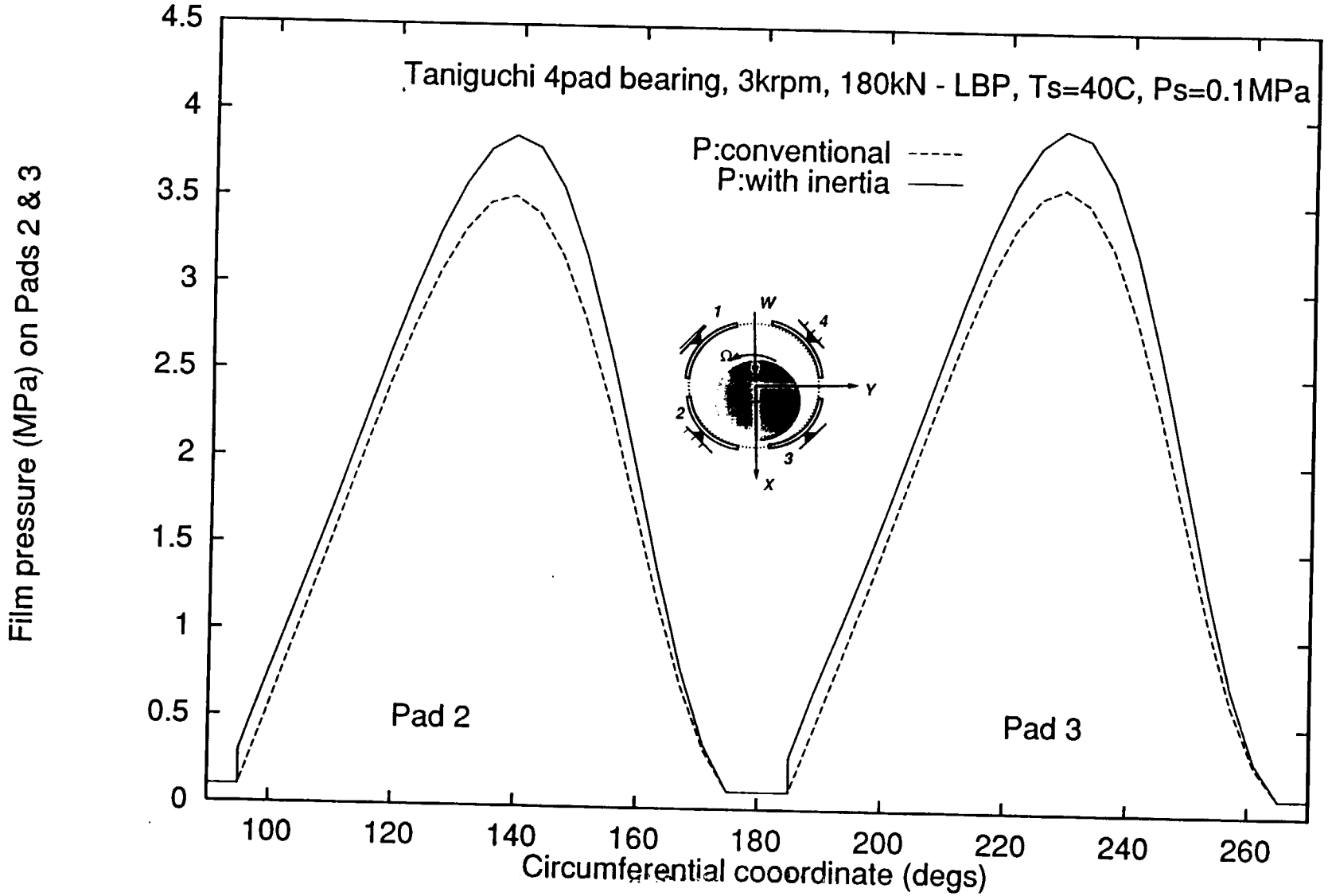

Figure 7. Centerline film pressure (MPa) on loaded pads
Taniguchi et al. tilt pad bearing. Speed 3krpm, Load=180kN

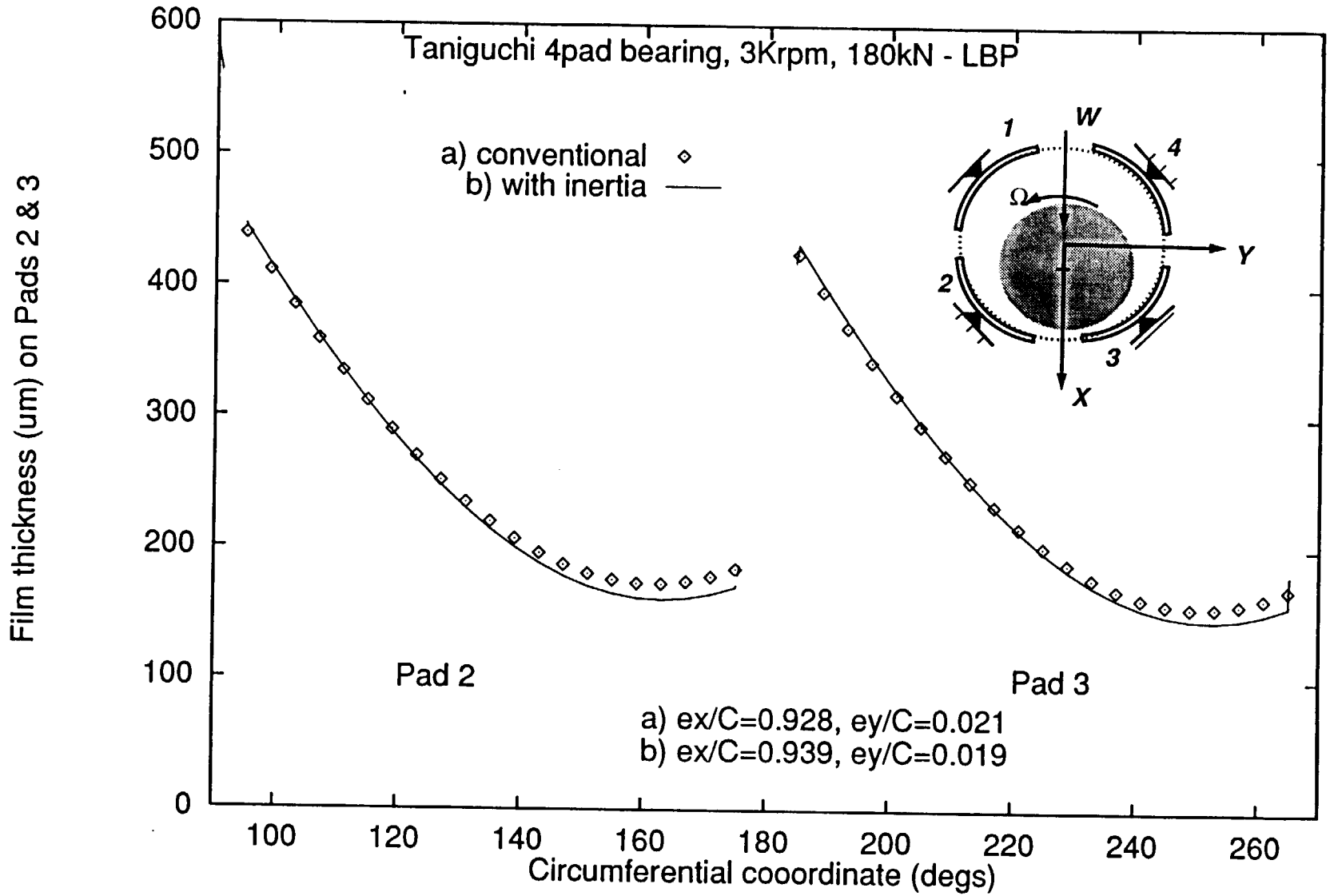

Figure 8. Film thickness (μm) on loaded pads.

Taniguchi et al. tilt pad bearing. Speed 3krpm, Load=180kN

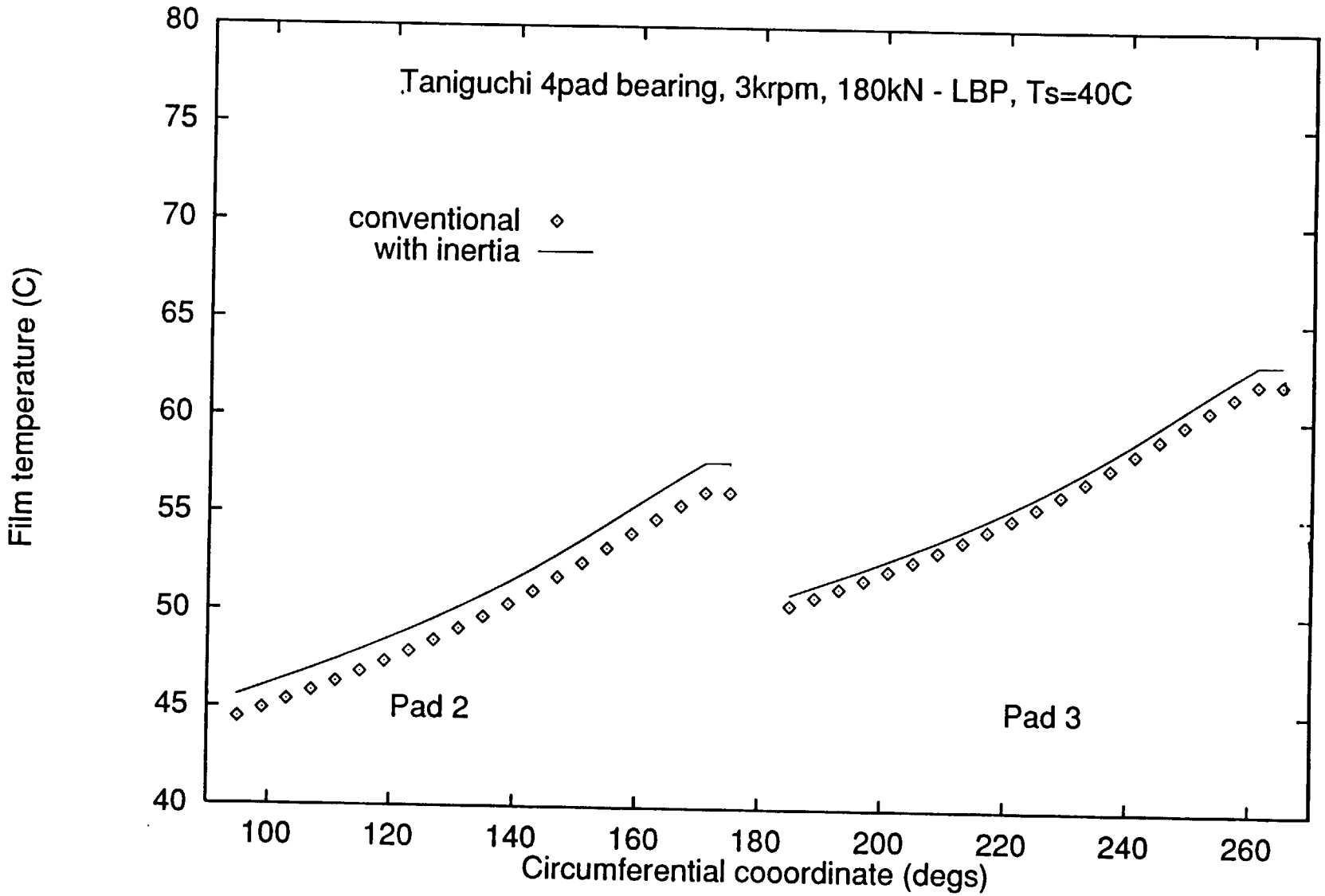

Figure 9. Bulk–flow film temperature on loaded pads.
Taniguchi et al. tilt pad bearing. Speed 3krpm, Load=180kN

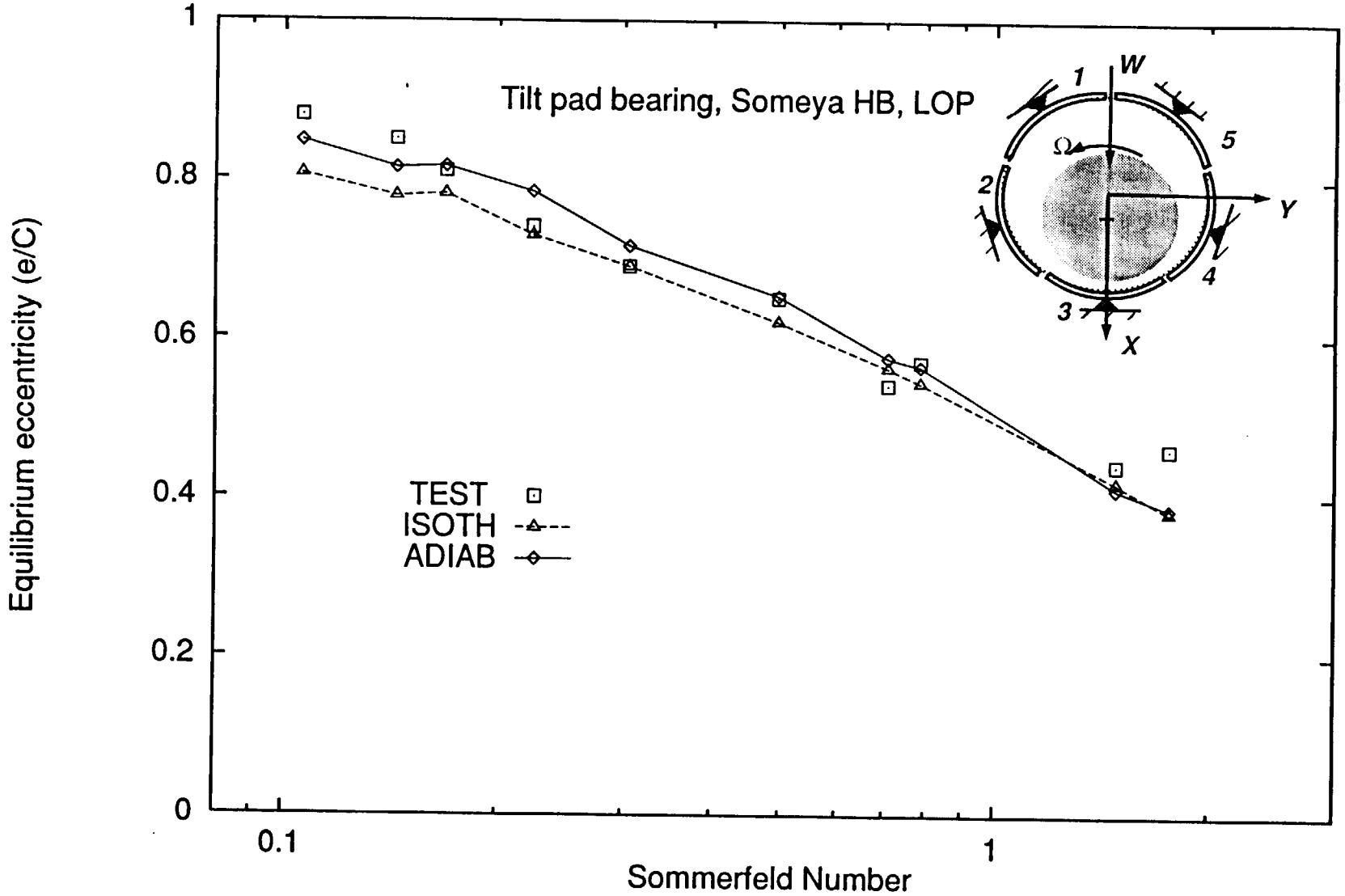

Figure 10. Equilibrium eccentricity vs. Sommerfeld Number

TEST Measurements, ISOthermal and ADIAbatic solutions.
Someya's databook 4 shoe tilt pad bearing – Load on pad

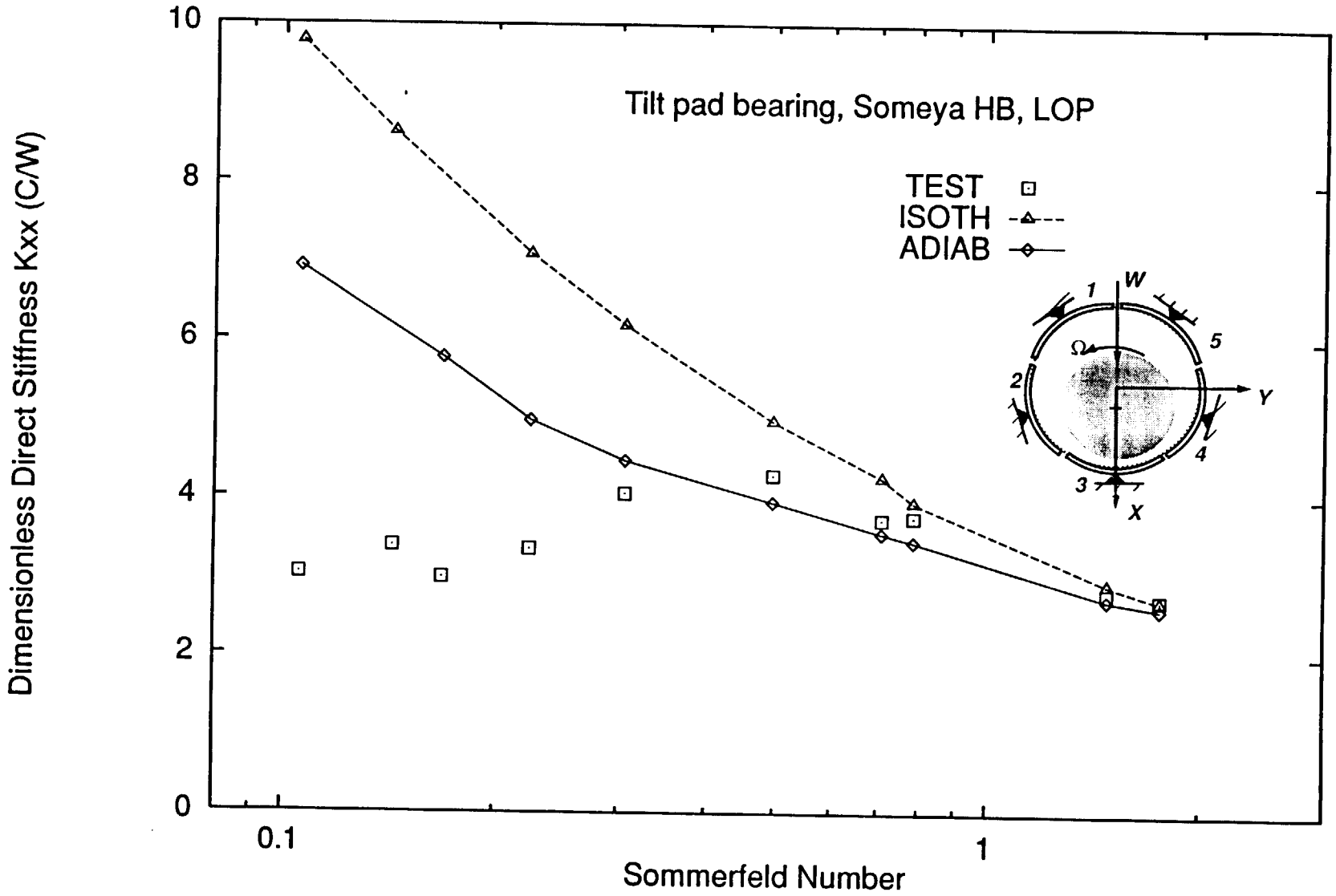

Figure 11. Direct Stiffness Kxx[C/W] vs. Sommerfeld Number

TEST Measurements, ISOthermal and ADIAbatic solutions.
Someya's databook 4 shoe tilt pad bearing – Load on pad

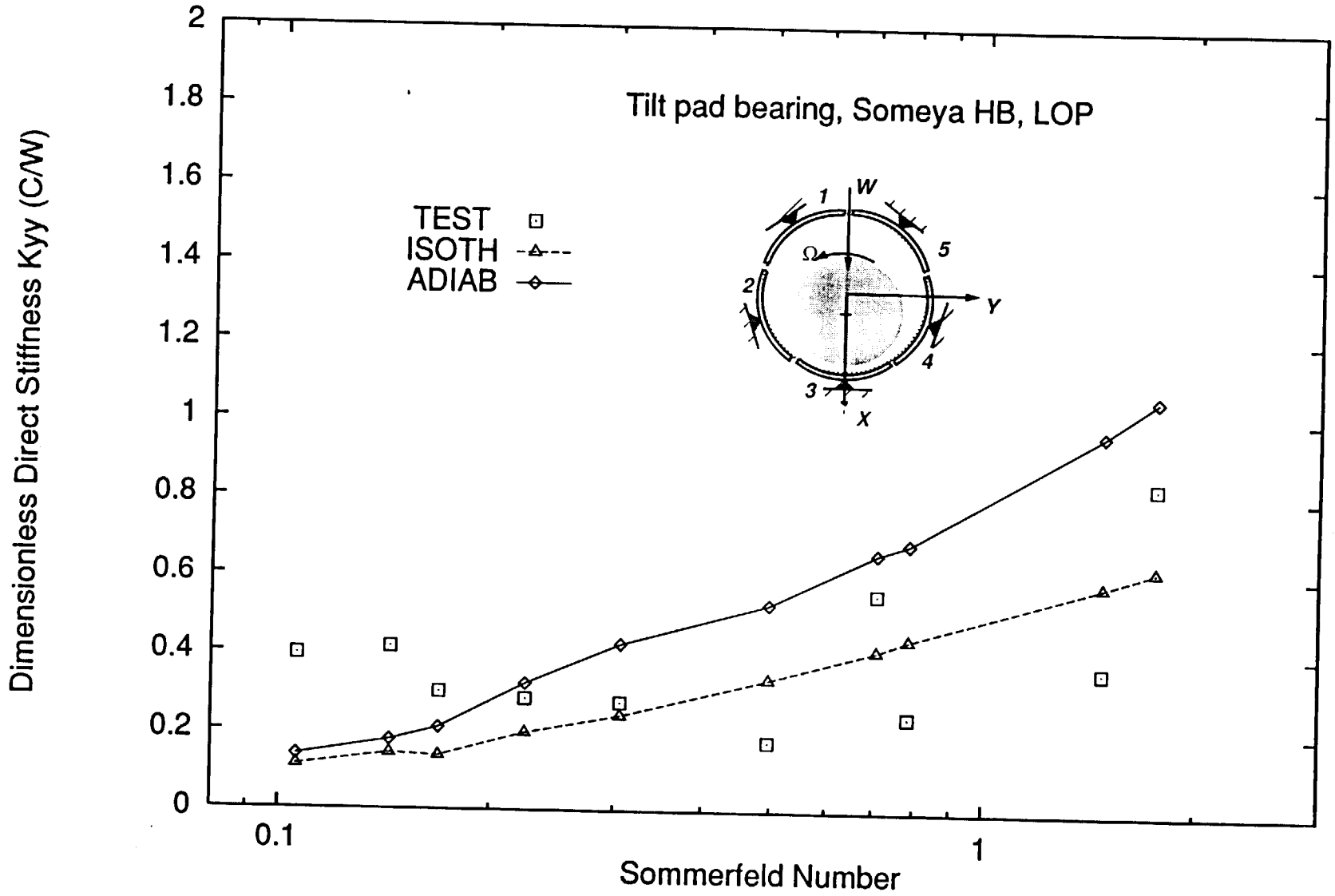

Figure 12. Direct Stiffness K_{YY}[C/W] vs. Sommerfeld Number
TEST Measurements, ISOthermal and ADIAbatic solutions.
Someya's databook 4 shoe tilt pad bearing – Load on pad

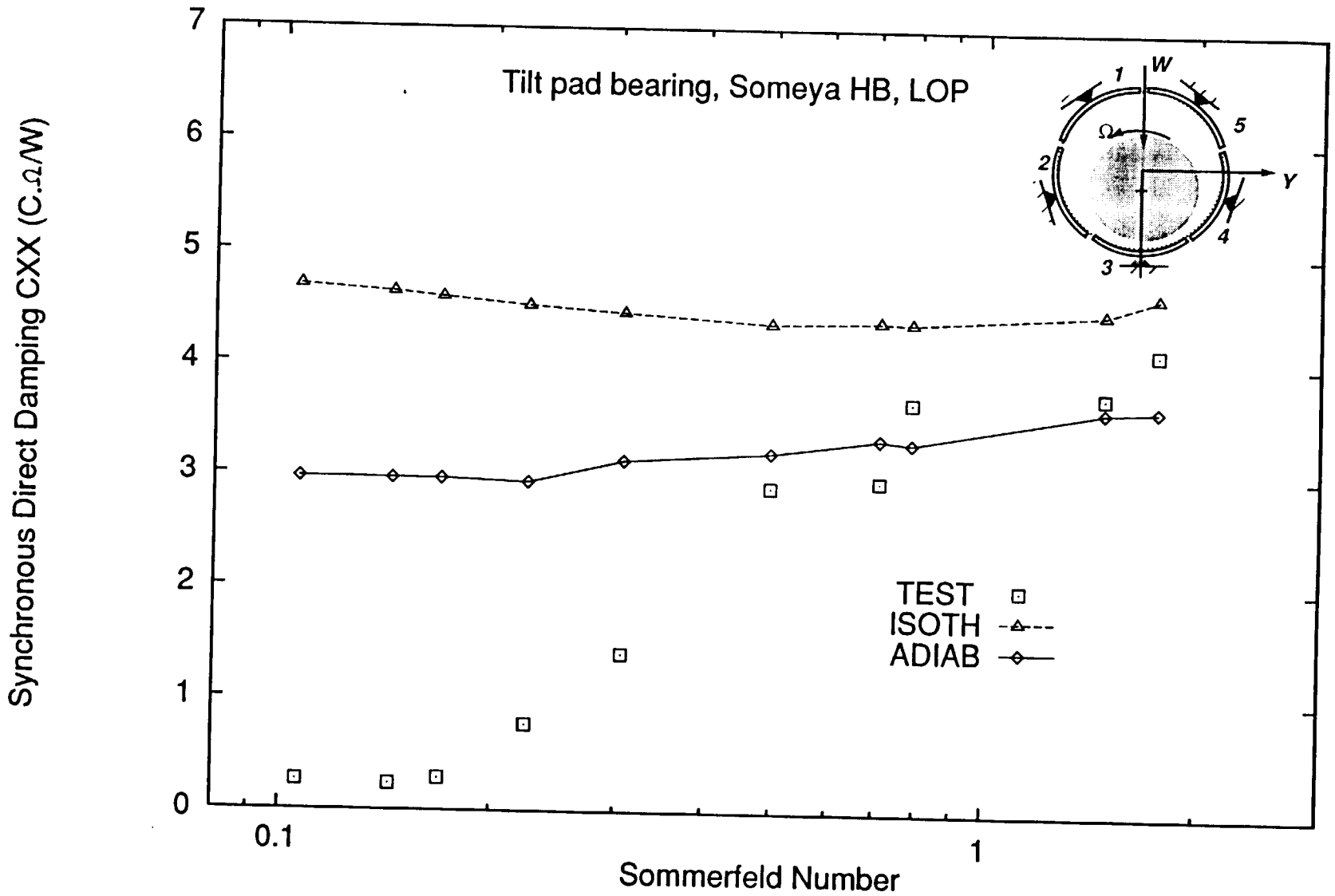

Figure 13. Direct Damping Cxx[CΩ/W] vs. Sommerfeld Number

TEST Measurements, ISOthermal and ADIAbatic solutions.
Someya's databook 4 shoe tilt pad bearing – Load on pad

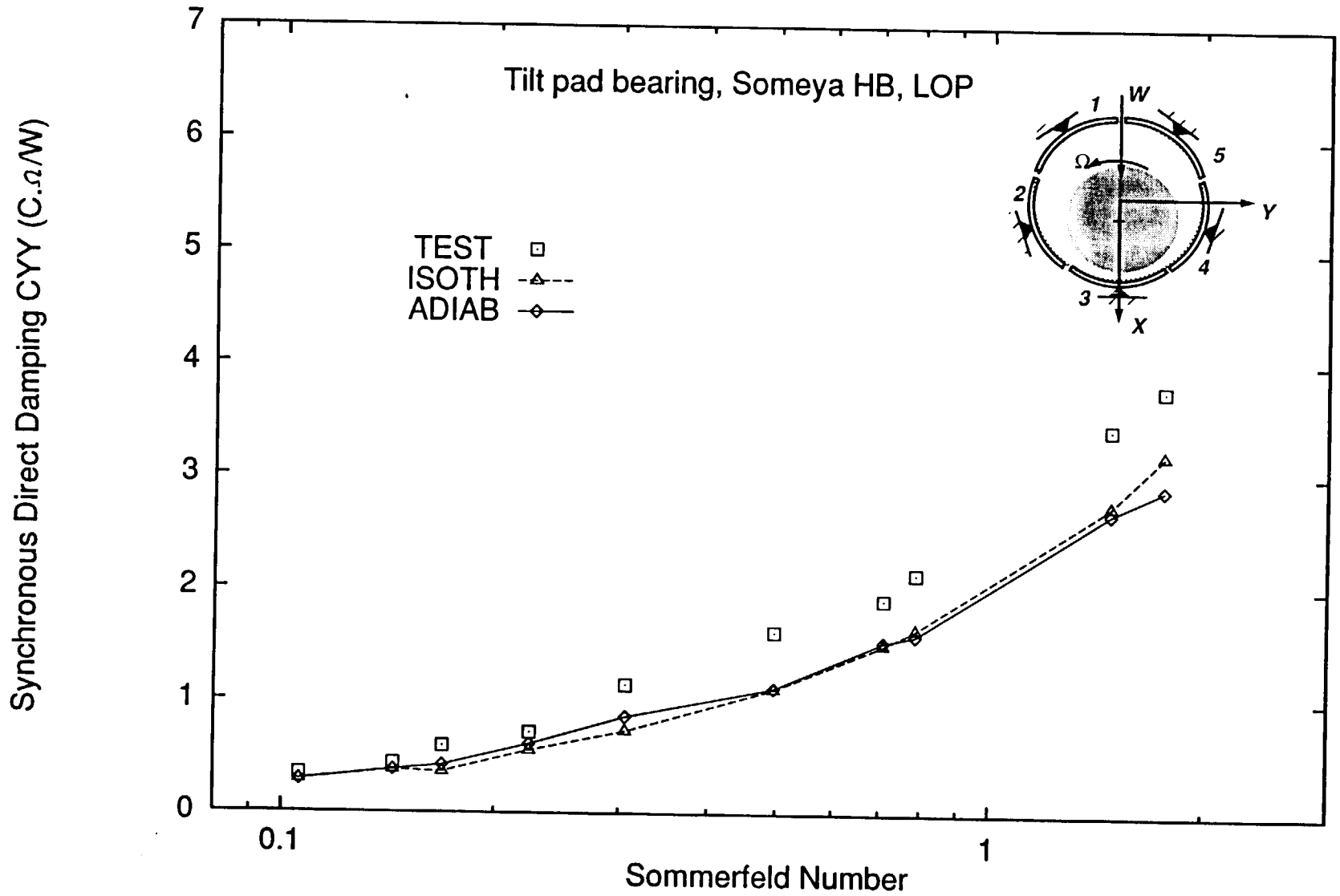

Figure 14. Direct Damping C_{YY}[CΩ/W] vs. Sommerfeld Number

TEST Measurements, ISOthermal and ADIAbatic solutions.
Someya's databook 4 shoe tilt pad bearing – Load on pad

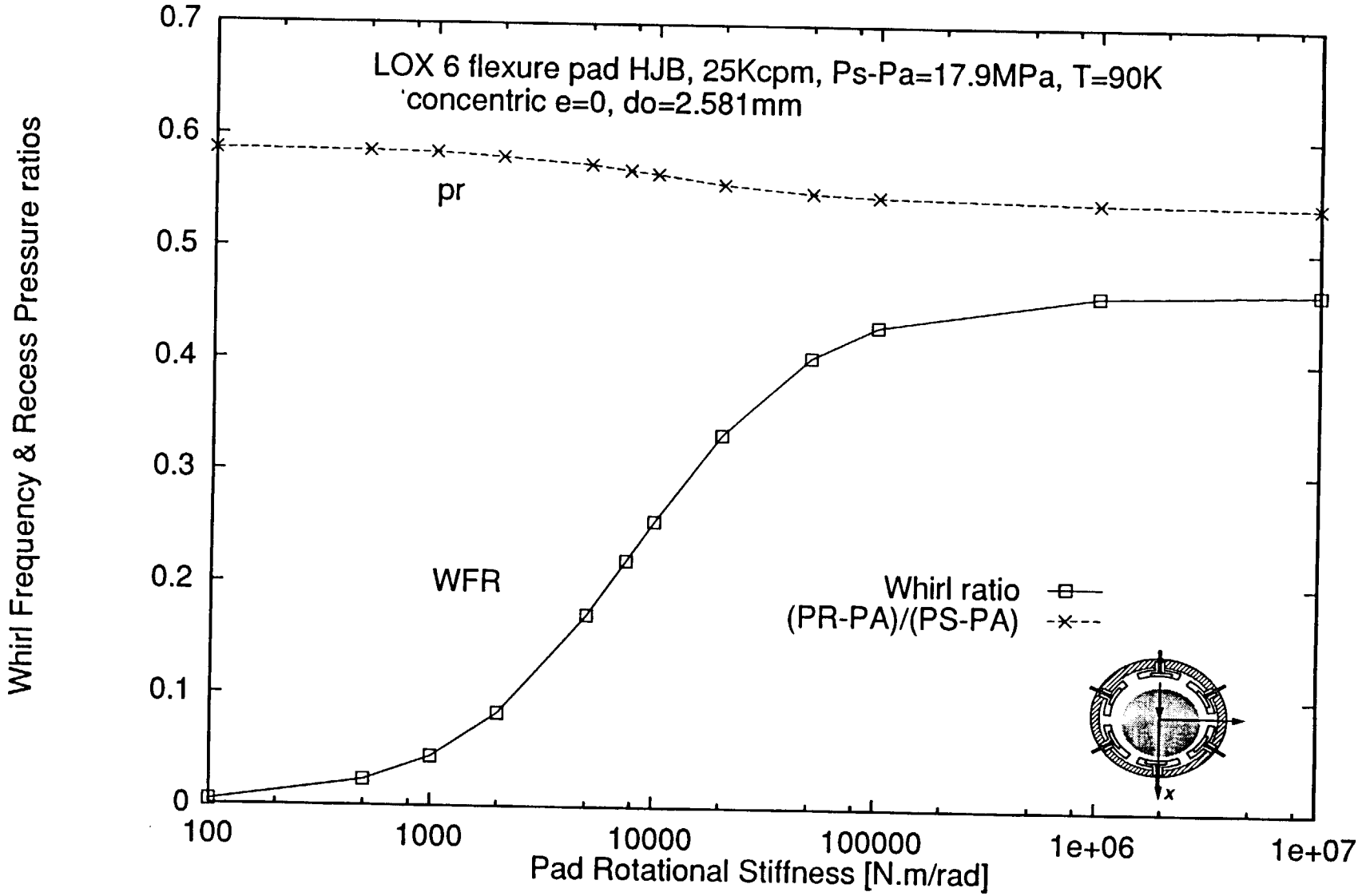

Figure 15. Whirl frequency ratio and recess pressure ratio vs. pad rotational stiffness. LOx flexure-pad hybrid bearing

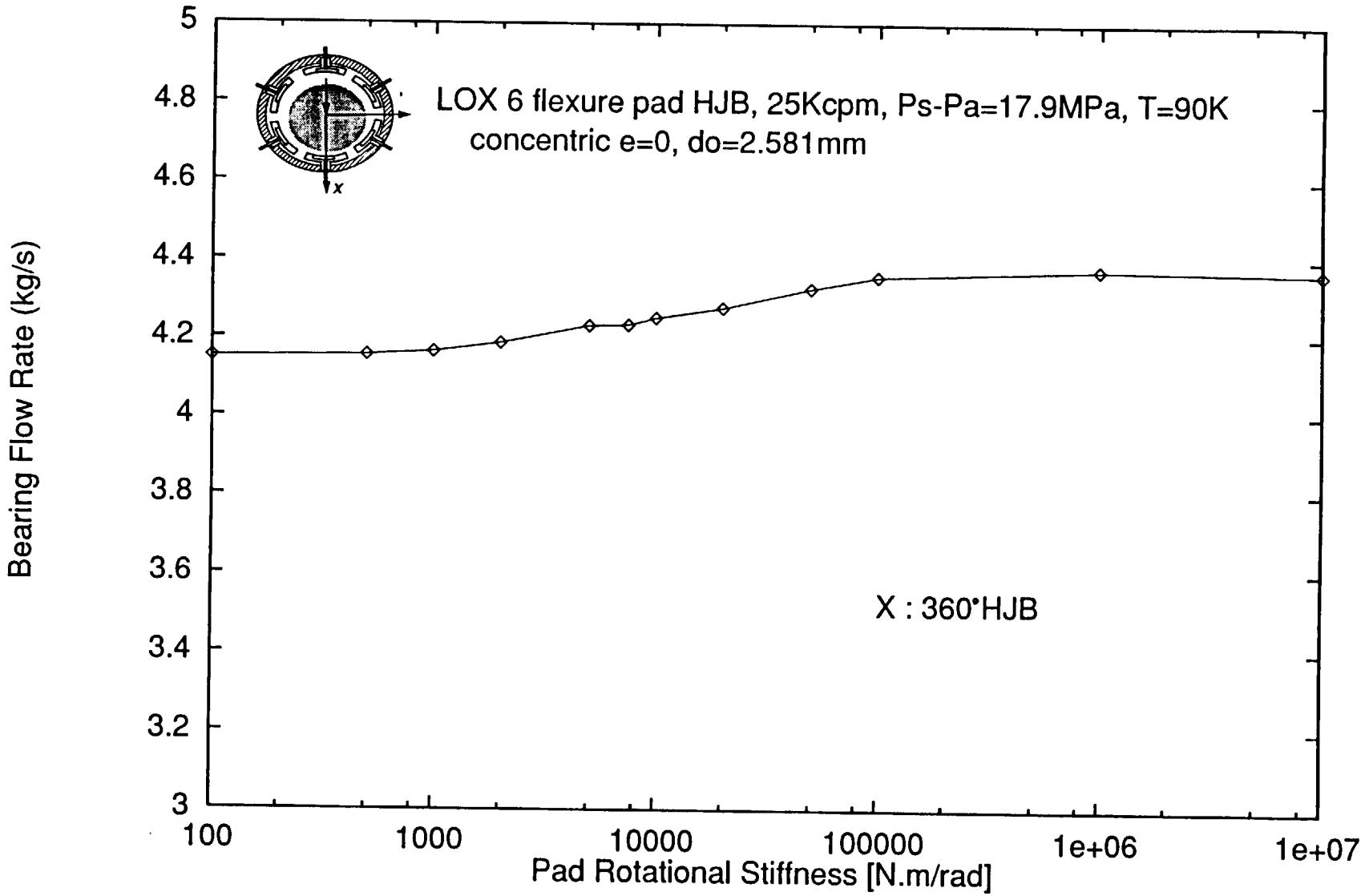

Figure 16. Mass flow rate vs. pad rotational stiffness.

LOx flexure-pad hybrid bearing – concentric operation

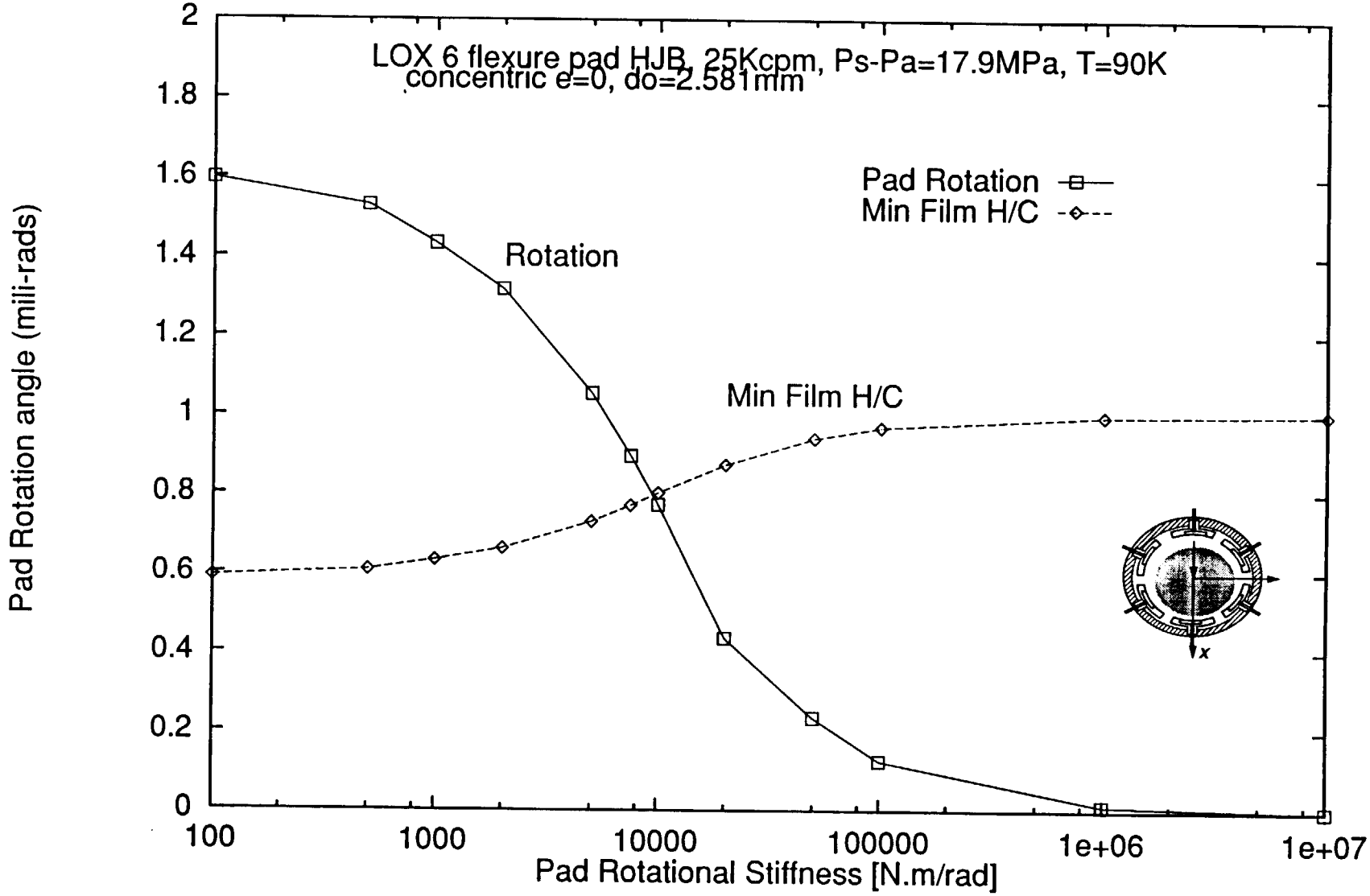

Figure 17. Pad rotation and minimum film thickness vs. pad rotational stiffness. LOx flexure-pad hybrid bearing

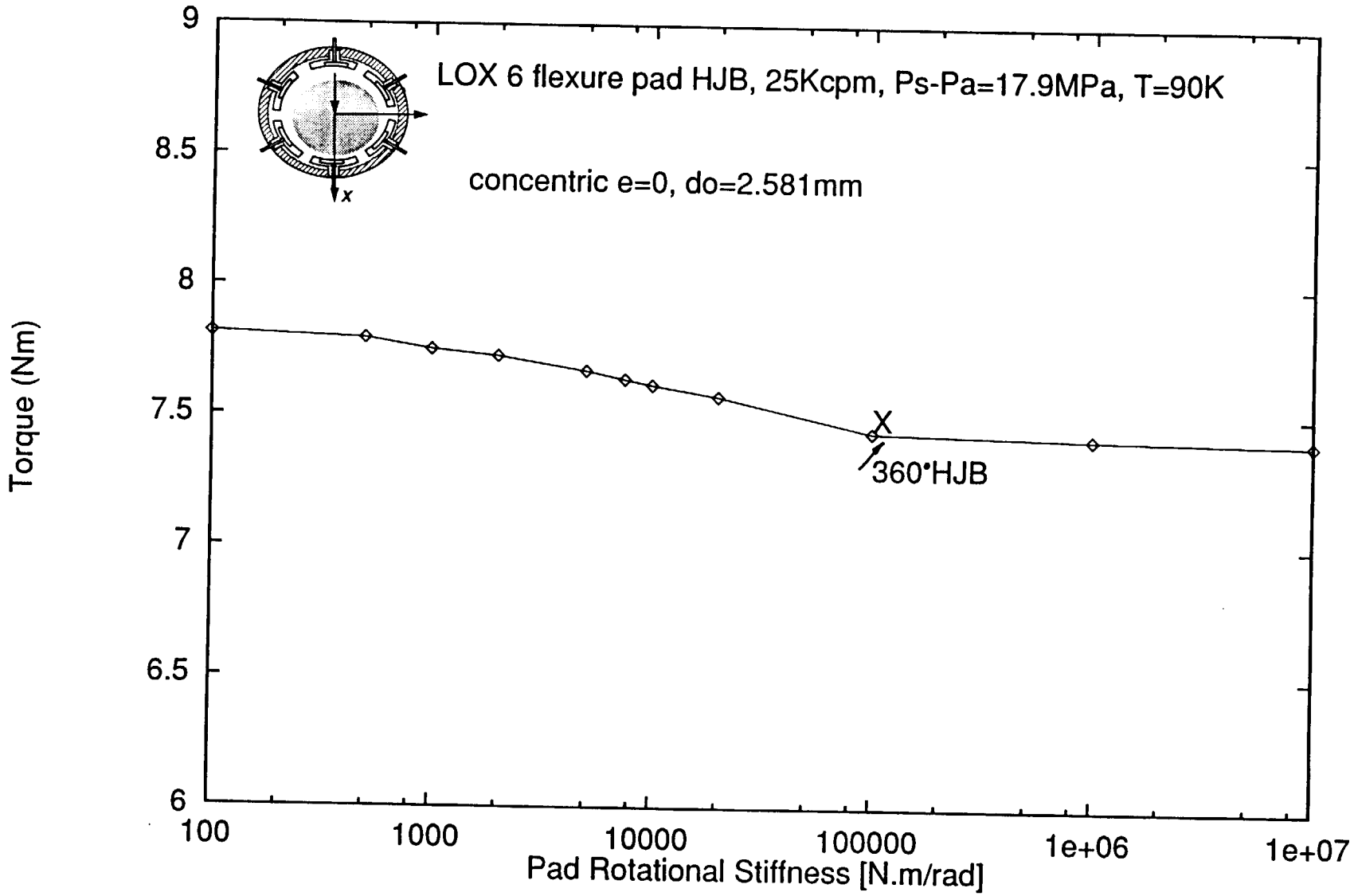

Figure 18. Drag Torque vs. pad rotational stiffness.

LOx flexure-pad hybrid bearing – concentric operation

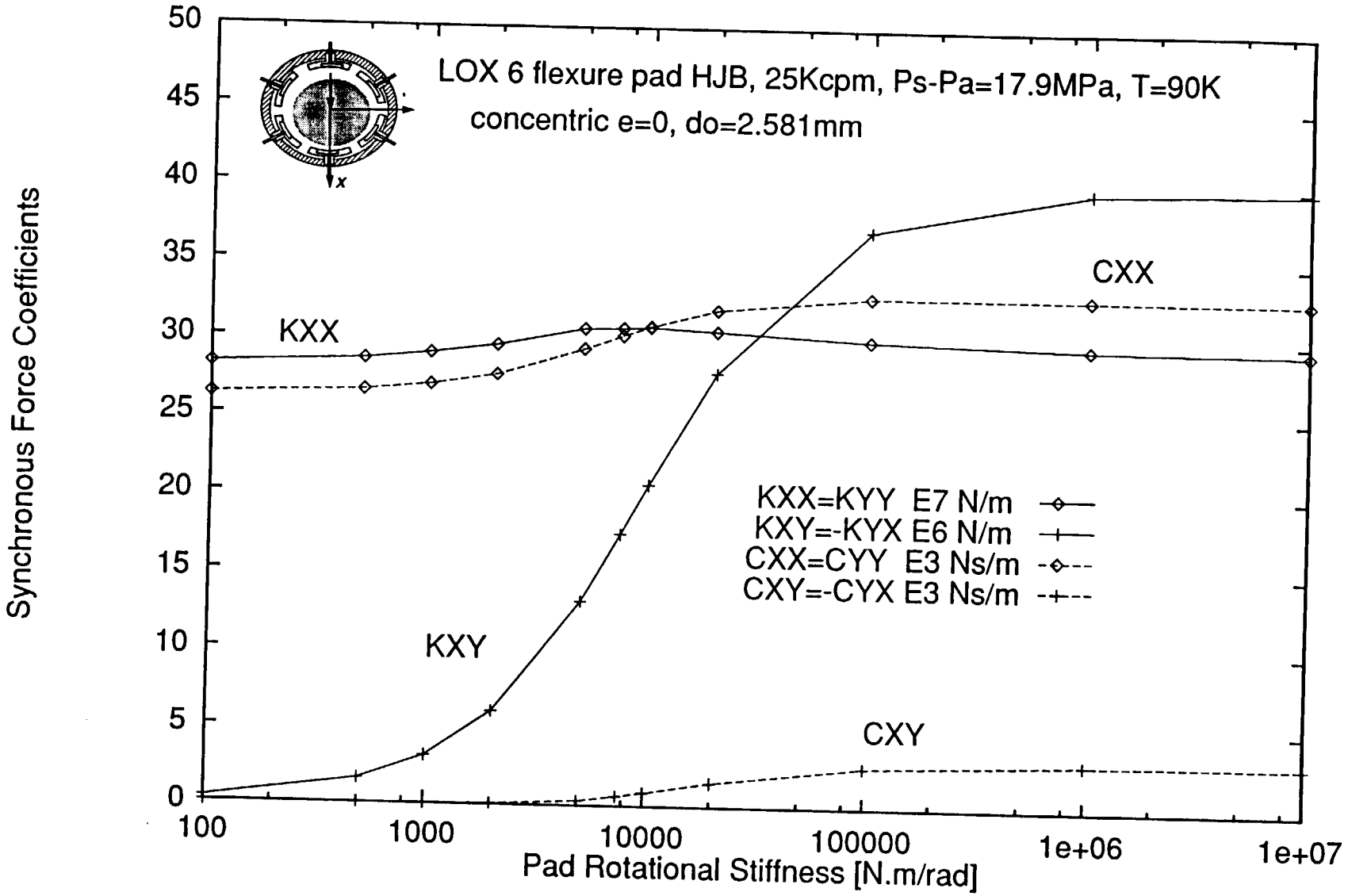

Figure 19. Synchronous force coeffs vs. pad rotational stiffness. LOx flexure–pad hybrid bearing – concentric

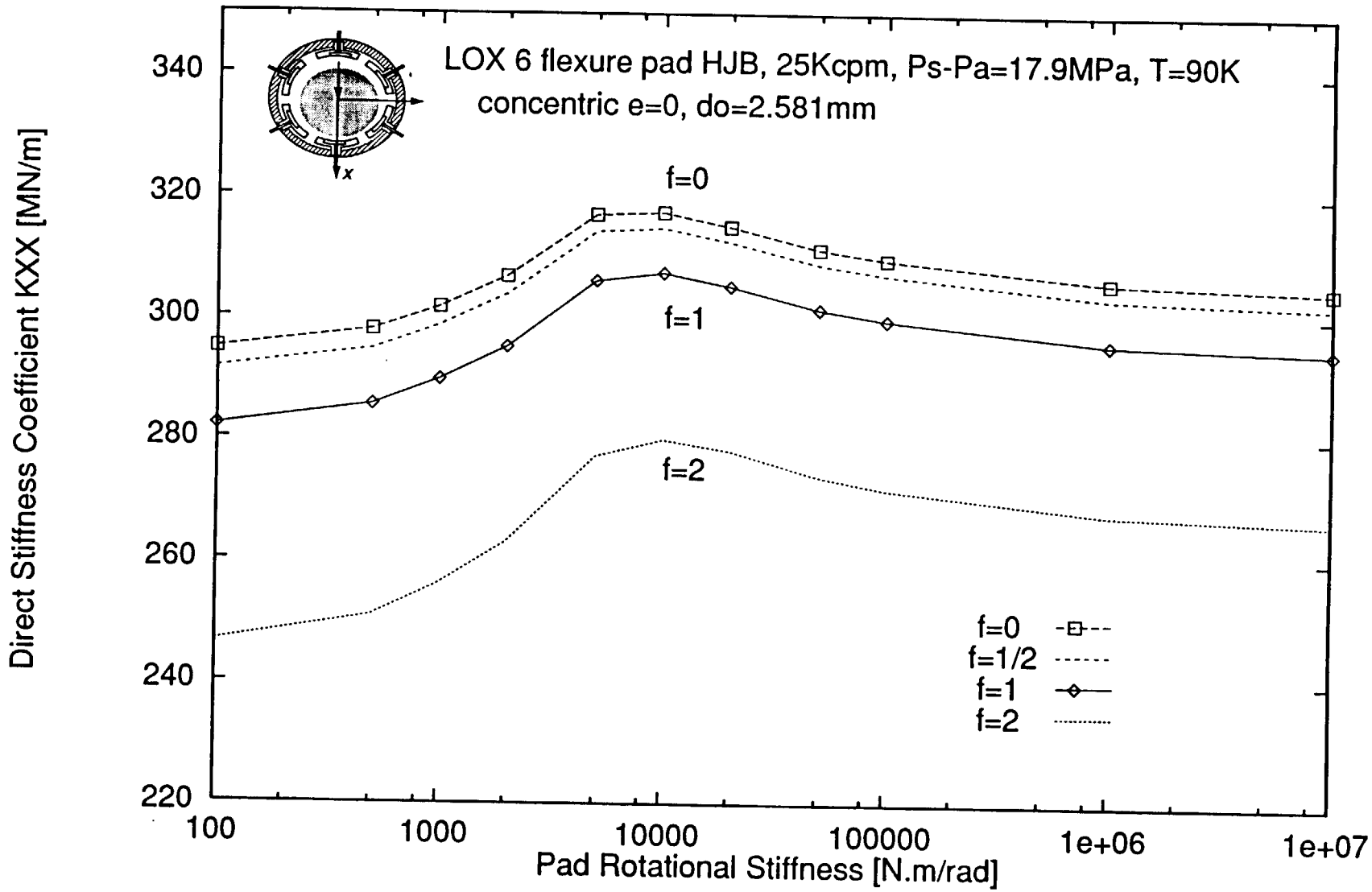

Figure 20. Effect of frequency on direct stiffness $K_{XX}=K_{YY}$

LOx flexure-pad hybrid bearing - concentric operation

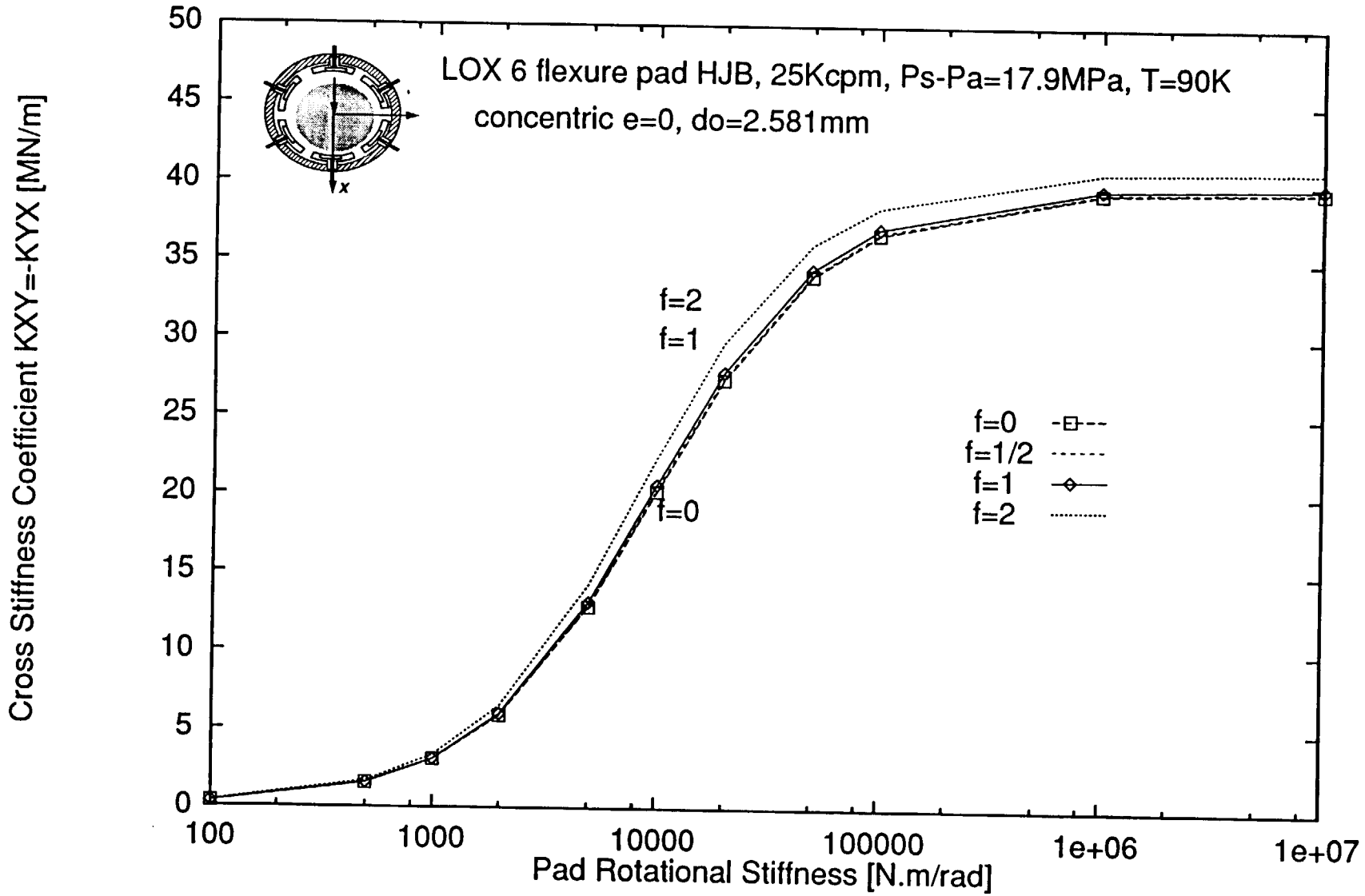

Figure 21. Effect of frequency on cross stiffness $K_{XY}=-K_{YX}$

LOx flexure-pad hybrid bearing – concentric operation

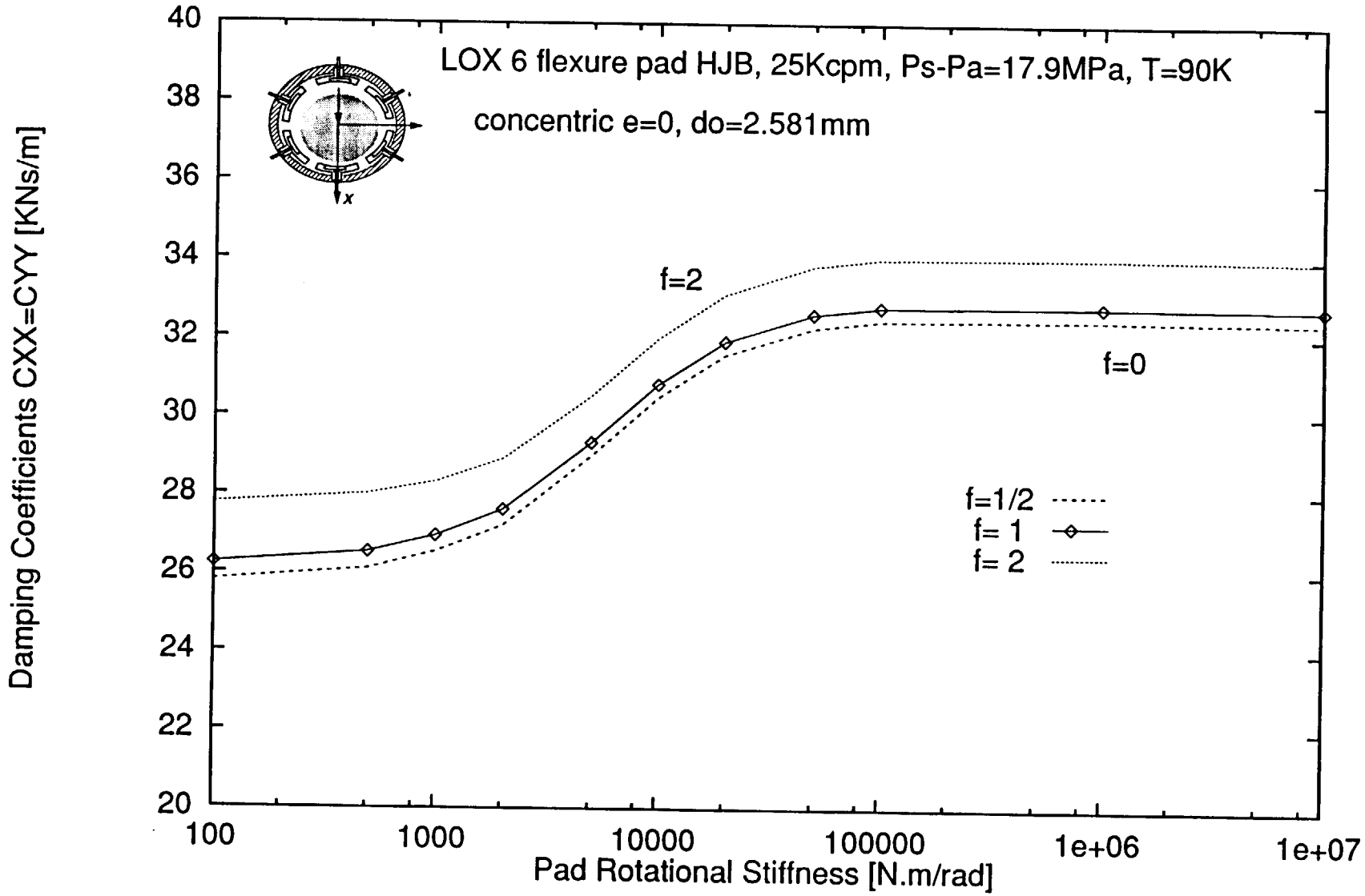

Figure 22. Effect of frequency on direct damping $C_{XX}=C_{YY}$

LOx flexure-pad hybrid bearing – concentric operation

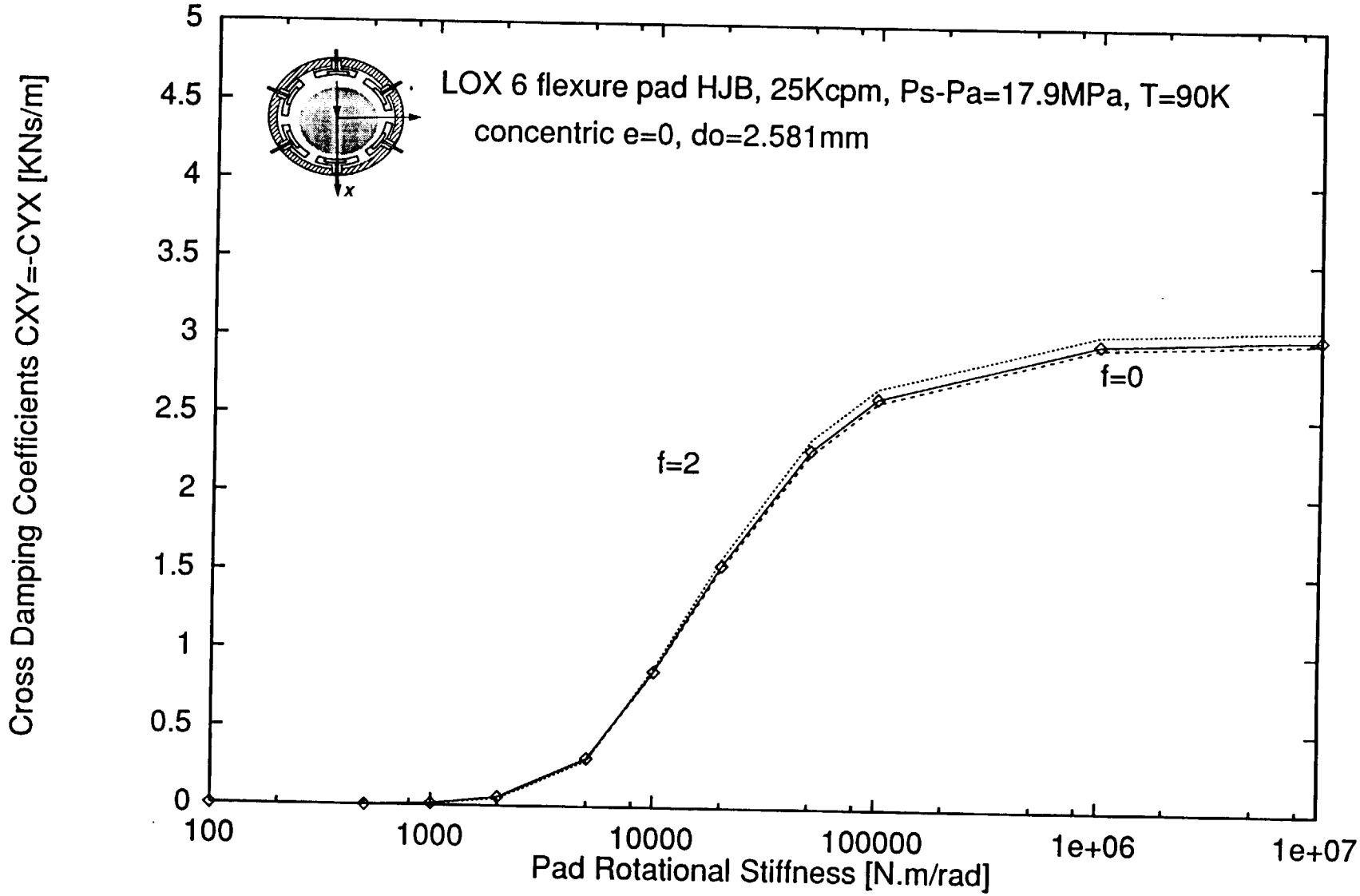

Figure 23. Effect of frequency on cross damping $C_{XY=-CYX}$

LOx flexure-pad hybrid bearing – concentric operation

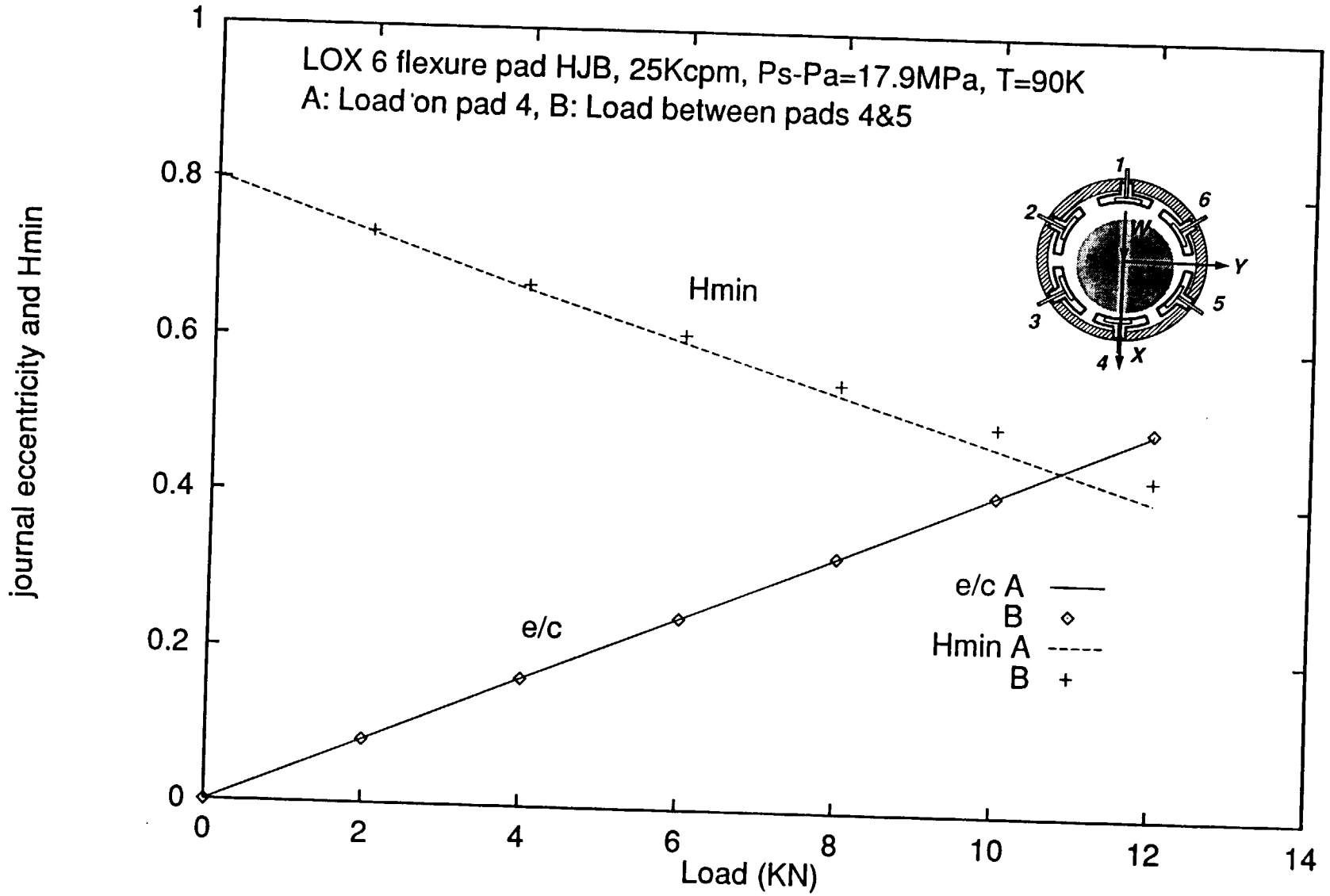

Figure 24. Equilibrium ecentricity vs. load for Kr=10k Nm/rad (A– on pad, B– between pads)

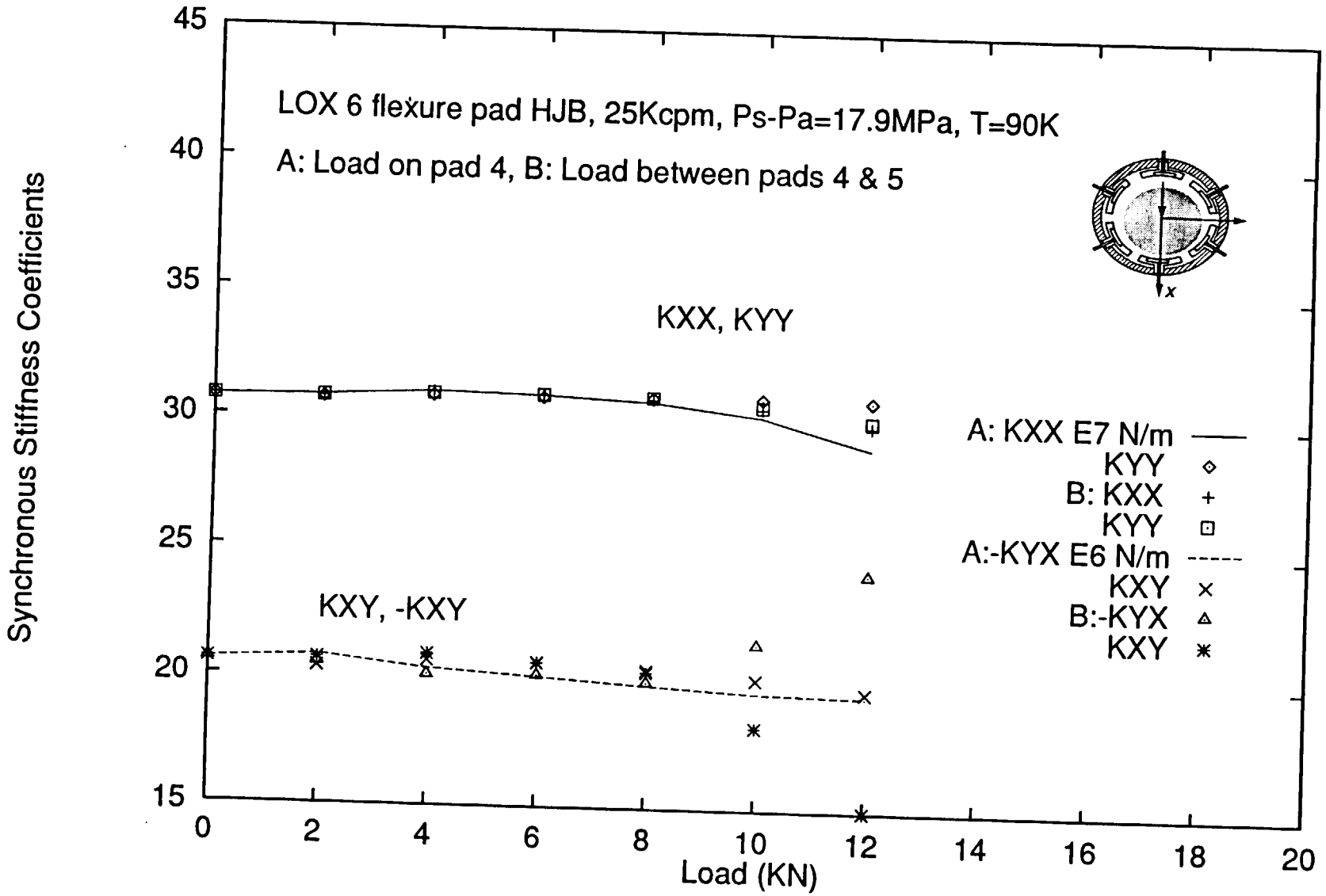

Figure 25. Stiffness Coefficients vs. load for Kr=10k Nm/rad (A– on pad, B– between pads)

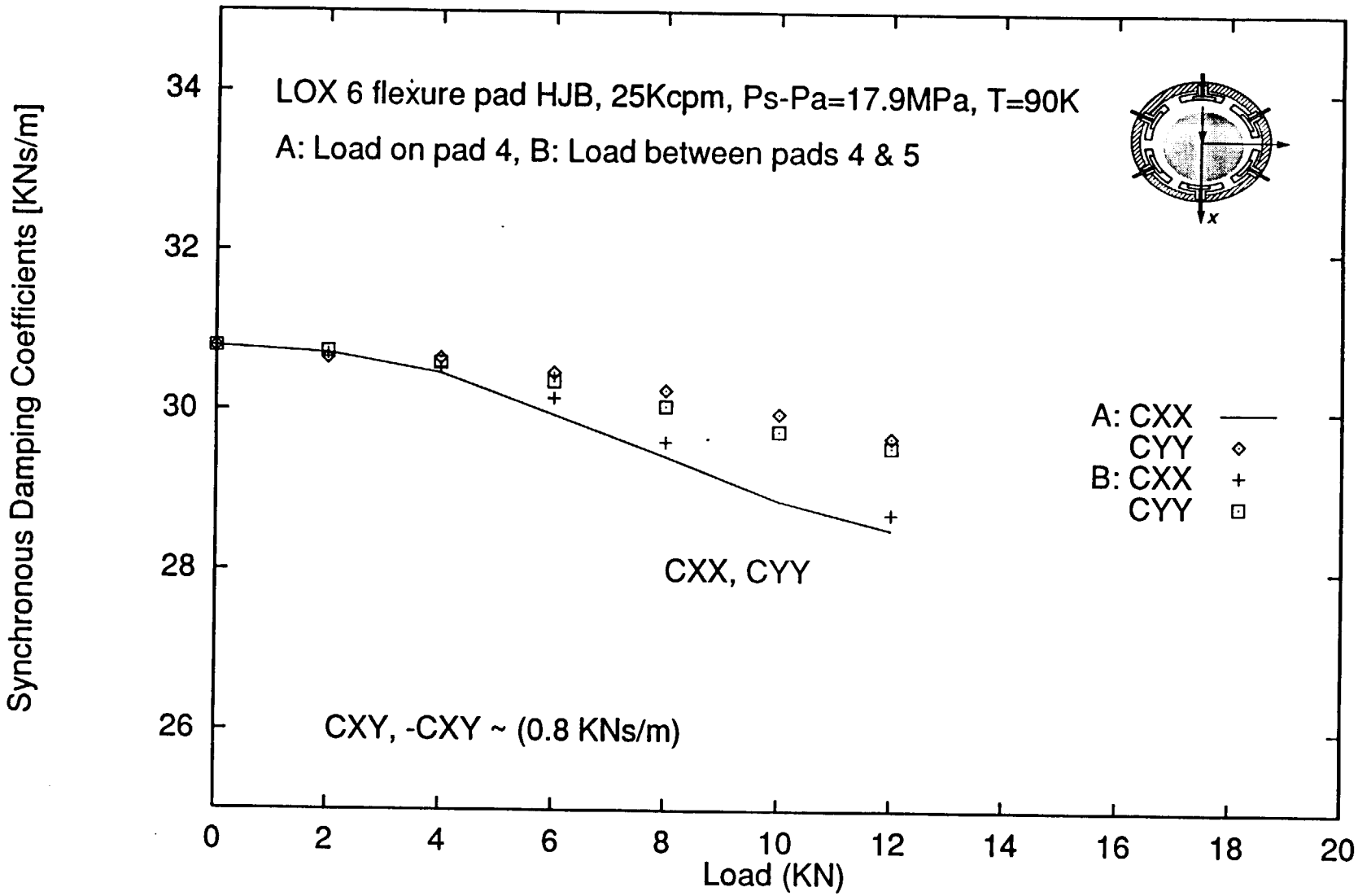

Figure 26. Damping Coefficients vs. load for Kr=10k Nm/rad (A– on pad, B– between pads)

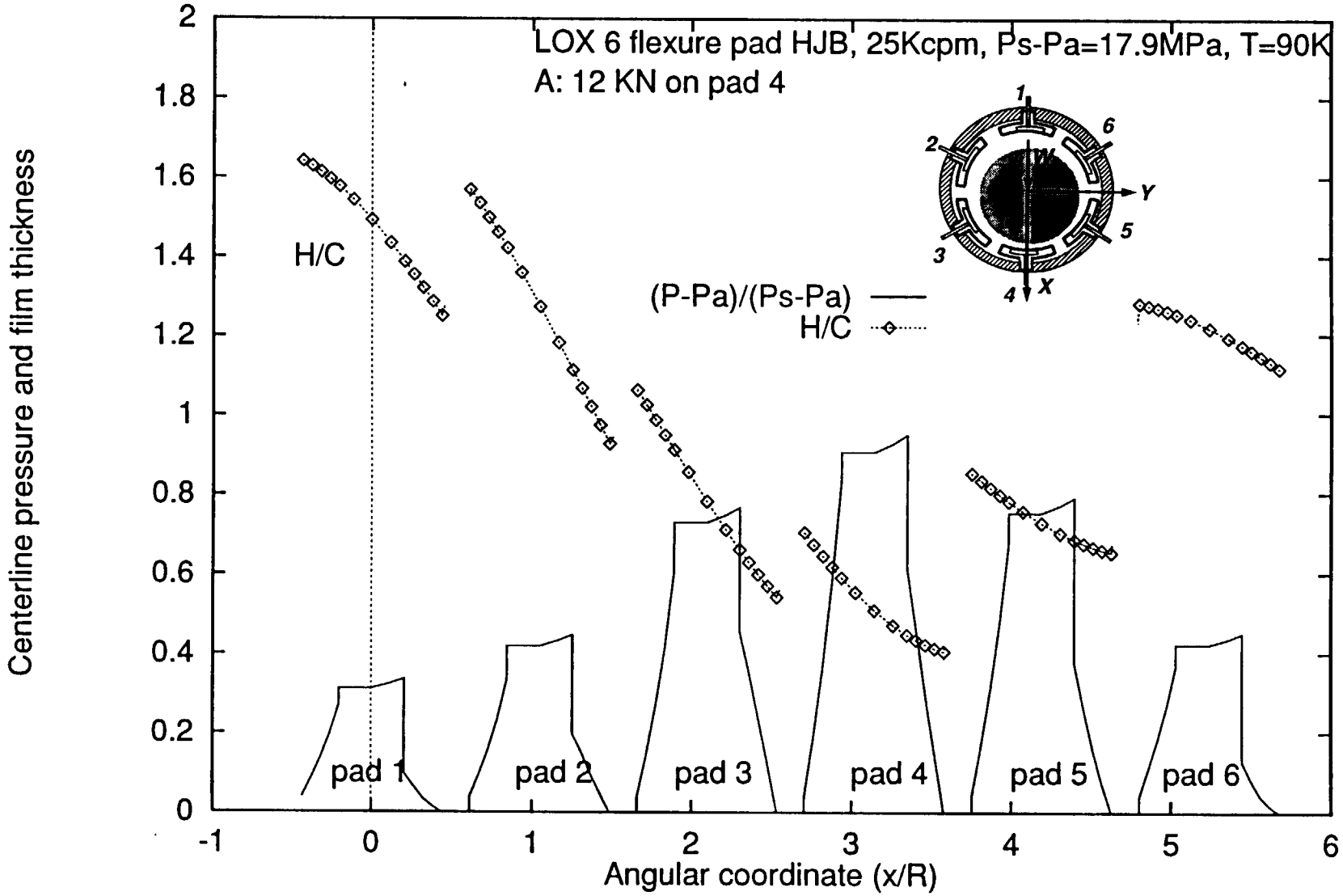

Figure 27. Centerline pressure and film thickness for Kr=10k Nm/rad and 10kN load on pad#4

Texas A&M University
Mechanical Engineering Department

Transient Response of a Rotor Supported on Externally Pressurized Fluid Film Bearings

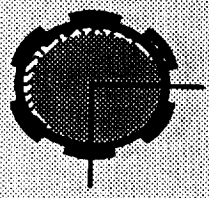

NASA Lewis Research Center
NASA Grant NAG3-1434
Contract Monitor: Mr. James Walker

Luis San Andres
Associate Professor
December 1994

Thermohydrodynamic Analysis of Cryogenic Liquid Turbulent Flow Fluid Film Bearings (Phase II)

Transient Response of a Rotor Supported on Externally Pressurized Fluid Film Bearings

Luis San Andres
Associate Professor
Texas A&M University

December 1994

Prepared for NASA Lewis Research Center
NASA Grant NAG3-1434
Year II
Contract Monitor: Mr. James Walker

ABSTRACT

An analysis for the prediction of the transient response of a rigid rotor supported in turbulent flow, externally pressurized fluid film bearings is presented. The rotor-bearing system nonlinear equations of motion are numerically solved with local linearization at each integration time. Fluid film bearing reaction forces are calculated from the numerical solution of the unsteady bulk-flow equations on the film lands. Analytical perturbations determine linear bulk-flow equations and their solutions allow estimation of rotordynamic force coefficients. The current numerical model is largely based on prior efficient and accurate computational programs for the prediction of the static and rotordynamic force response characteristics of turbulent flow fluid film bearings.

Examples for the transient response of rigid rotors supported on plain journal bearings, annular pressure seals and hydrostatic bearings under a variety of external loads are discussed in detail. Transient responses based on an approximate model which uses rotordynamic force coefficients at an equilibrium position are also presented. The full nonlinear model demands small time steps and is computationally very intensive. For externally pressurized bearings, the linear transient model provides good results in a fraction of the time required for the nonlinear model to compute the rotor-bearing dynamic forced response.

For a lucid discussion on the importance and advantages of fluid film bearings in cryogenic turbomachinery see the Research Progress Report, Year I, to the present project (San Andres, 1993)

Refer to **hydrotran User's Manual and Tutorial** for information and instructions to run the program.

NOMENCLATURE

A_o	Cd π $d_o^2/4$. Equivalent orifice area [m^2].
A_r	$l \cdot R_* \cdot \theta_r$. Recess area [$m^2$].
A_X, A_Y	Rotor accelerations [m/s^2].
C	Radial clearance function [m].
C_p	Fluid specific heat [$J/kg \cdot °K$].
$C_{XX}, C_{XY}, C_{YX}, C_{YY}$	Damping force (linear) coefficients [Ns/m].
C_d	Orifice discharge coefficient
D	$2 \cdot R$. Bearing diameter [m].
d_o	Orifice diameter [m]
$f_{J,B}$	$a_M \left[1 + \left(c_M \frac{r_{J,B}}{H} + \frac{b_M}{R_{J,B}} \right)^{e_M} \right]$; a_M=0.001375, b_M=500,000; c_M=10,000, e_M=1/3.00
	Turbulent flow friction factors at journal and bearing surfaces.
F_X, F_Y	Bearing fluid film forces along {X,Y} axes [N].
H	$C + X(t) \cos(\theta) + Y(t) \sin(\theta)$. Film thickness [m].
H_r	Recess depth [m].
h_B, h_J	heat transfer coefficients to bearing and journal [$W/m^2 °K$]
$K_{XX}, K_{XY}, K_{YX}, K_{YY}$	Bearing force stiffness coefficients [N/m]
K_{eq}	Equivalent linear bearing stiffness [N/m]
L,l	Bearing axial length, recess axial length [m].
M	Point rotor mass [kg].
$M_{XX}, M_{XY}, M_{YX}, M_{YY}$	Bearing inertia force coefficients [kg].
M	$U_x \cdot \sqrt{\beta_p \cdot \rho_r}$. Orifice circumferential velocity Mach number.
N_{recess}	Number of recesses on bearing.
P,Pr	Fluid pressure, recess pressure [N/m^2].
P_e^-, P_e^+	Pressures just before and after recess edge [N/m^2].

P_O, P_L	Discharge pressures on left and right sides of bearing[N/m^2].
P_s	External supply pressure [N/m^2].
Q_s	heat flow to bearing and journal surfaces [W/m^2].
R	Bearing radius [m].
Re	$(\rho \cdot \Omega \cdot C \cdot R/\mu)_*$. Nominal circumferential flow Reynolds number.
Re_s	$(\rho \cdot \omega \cdot C^2/\mu)_*$. Nominal Squeeze film Reynolds number
R_J, R_B	$(\rho/\mu)H\sqrt{[(U_\theta - \Omega \cdot R)^2 + U_z^2]}$; $(\rho/\mu)H\sqrt{[U_\theta^2 + U_z^2]}$ Flow Reynolds numbers relative to journal and bearing surfaces.
r_J, r_B	Roughness depths at journal and bearing surfaces [m].
S_i	$\underline{\Theta} \cdot \Delta t_i$. Extended time step [s].
t, t_o	time coordinate [s], initial time [s].
T, T_s	Temperature, supply temperature [°K].
U_x, U_y	Bulk-flow velocities in circ.(x) and axial (y) directions [m/s].
V_r	$(H_r+H)A_r+V_s$ Total recess volume [m^3].
V_s	Volume of orifice supply line [m^3].
V_X, V_Y	Journal (rotor) velocity components [m/s].
$W_X(t), W_Y(t)$	External loads to rotor-bearing [N].
X(t), Y(t)	journal (rotor) displacements in inertial coordinates [m].
Z	$[X,Y]^T$. Vector of journal displacements [m].
β_P	$(1/\rho)(\partial\rho/\partial P)$. Liquid compressibility coefficient [m^2/N].
β_T	$-(1/\rho)(\partial\rho/\partial T)$. Liquid volumetric expansion coefficient [1/°K].
η	$H/(H_r+H)$. Ratio of land film thickness to recess depth.
θ	x/R. Circumferential or angular coordinate.
θ_r	rth-recess angular length [rad].
$\underline{\Theta}$	time integration parameter, typ=1.42.

$K_z=K_x$	$\frac{1}{2}(K_J+K_B)$. Turbulence shear factors in (y,x) flow directions.
K_J, K_B	$f_J \cdot R_J$, $f_B \cdot R_B$. Turbulent shear parameters at journal and bearing surfaces.
K_r	$\frac{Re_r^{0.681}}{7.753}$. Turbulent shear flow parameter at recess.
ρ, μ	Fluid density [Kg/m^3], viscosity [Ns/m^2].
ξ_{xu}, ξ_{xd}	Empirical recess-edge entrance loss coefficients in circumferential (upstream,downstream) direction.
ξ_y	Empirical recess-edge entrance loss coefficients in axial direction.
Ω, ω	Rotational speed of journal, excitation or whirl frequency [1/s]
ϕ	whirl frequency ratio.
τ	$t-t_i$. Local time coordinate [s].
τ_n	$2\pi/\omega_n$. Natural period of rotor-bearing system [s].
Λ_x	$\Omega \cdot R$. Journal surface velocity [m/s].
Γ_r	recess boundary with outward normal **n**.
Δt	$t_{i+1}-t_i$. Time step [s]
ΔZ_i	$Z_{i+1}-Z_i$. Vector of incremental displacements [m].
ΔV_{Zi}	$V_{Zi+1}-V_{Zi}$. Vector of incremental journal velocities [m/s]
ΔA_{Zi}	$A_{Zi+1}-A_{Zi}$. Vector of incremental journal accelerations [m/s^2]

Subscripts refer to:

x,y	in direction of local circumferential and axial coordinates in plane of bearing.
r,e	bearing recesses and edges (entrance).
i,j	refer to discrete times t_j and t_i.
B,J	refer to bearing and journal surfaces.

LIST OF TABLES

LIST OF FIGURES

LIST OF FIGURES (continued)

INTRODUCTION

The transient forced response of rotor systems supported on fluid film bearings is of importance to study (or to discover) the effect of bearing nonlinearities brought by extreme loading conditions or stringent operating conditions. There is a general belief that classical rotordynamic studies based on linearized bearing force coefficients are unable to predict system time responses for realistic levels of external loads. Some types of fluid film bearing elements such as hydrodynamic bearings, foil bearings and squeeze film dampers are known to be highly nonlinear, and therefore, nonlinear transient analyses are necessary to establish the ranges for safe operation of these rotor - bearing systems. Transient studies including accurate finite length fluid film bearing models can be performed in reasonable amounts of time thanks to the current high speed computing facilities. Furthermore, novel and sound analytical techniques for handling highly nonlinear systems are at the researcher's disposal to study aperiodic responses, jump-phenomena, bifurcation and even "chaotic" responses in certain regimes of operation (Ehrich, 1992).

The development of an all fluid film bearing technology for cryogenic turbopumps has advanced steadily over the past years. Low cost, reliable fluid film bearing elements are needed to provide maximum operating life with optimum and predictable rotordynamic characteristics. San Andres (1990 - 1993) provides the analysis and computational programs for the calculation of static and rotordynamic force characteristics in turbulent flow, cryogenic liquid hydrostatic bearings and pressure seals. Extensive experimental tests performed at the high speed, high pressure, water - bearing test facility at Texas A&M University have validated the numerical predictions (Kurtin et al., 1993, Lindsey, 1993, Franchek et al., 1994). Further analytical and experimental

studies currently address the important issues of fluid compressibility with cryogenic liquids and the limited operating range due to hydrodynamic inestability in conventional bearing designs. The present investigation develops an analysis for computation of the transient dynamics and forced response of a rigid rotor supported on turbulent flow, fluid film bearings. The ultimate aim of the investigation is to provide a sound computational program for the prediction of synchronous unbalance response, rotor lift-off, and response to abnormal shock and maneuvering loads in cryogenic turbomachinery.

LITERATURE REVIEW

The literature related to the transient response of rotating machinery supported in fluid film bearings is quite extensive. From the numerous relevant references I have selected a few of those works which have directly shaped my understanding of the nonlinear rotor - fluid film bearing problem. Booker (1965) and later Childs et al. (1977) developed the mobility and impedances methods for solution of rotor-bearing problems involving transient responses. The impedance formulation applicable to rotordynamic studies expresses the bearing instantaneous reaction loads in terms of a single (squeeze) velocity vector in a particular rotating frame. This simple though fundamental idea allows fast evaluation of the fluid film bearing forces. The mobility and impedance methods are applicable to cylindrical bearings and were quite popular before the advent of the high speed, personal computer. The original methods were graphical in nature and provided the trained engineer with an opportunity to obtain quickly the dynamic response of rotors supported on fluid film bearings with a few calculations.

Kirk and Gunter (1970-1976) and Barrett et al. (1977) pioneered the

numerical study of transient dynamics of simple rigid and flexible rotors supported on short length, cylindrical hydrodynamic bearings. The study confirmed the findings of the classical linear stability analysis of Lund (1965) and detailed the severity of a sudden blade loss in rotor - bearing systems. These early works have left a profound imprint on our current understanding of rotordynamics and shaped many later developments, most notably those relevant to the coupling of floating oil seals to rotor - bearing dynamics (Kirk, 1988, 1994). These early fundamental references are rarely acknowledged today although their examples and methods have been replicated in numerous investigations published on the last decade.

The analysis of the dynamics of rotors supported in squeeze film dampers (SFDs) is perhaps the single topic which has received most attention in terms of its transient response. Current analyses of rotor-disk assemblies supported on SFDs are based on overly simplified analytical expressions for fluid film forces as derived from the short journal bearing model with the so called π-film cavitation assumption (Li and Taylor, 1987, Chen et al. 1993, Sundararajan et al. 1994). Transient responses based on direct numerical integrations, and lately computational solutions based on current nonlinear dynamics models with elegant mathematical methods, show the forced response of rotor-SFDs systems to be highly nonlinear with extreme sensitivity to unbalance levels. Little effort has been placed on finding a combination of operating and design parameters which will avoid the system undesirable response. On the other hand, the richness of the nonlinear (theoretical) behavior has been exploited to prove beyond practical limits the amazing accuracy of the analytical models. However, there is little physical evidence and practical experience attesting to the veracity of the theoretical and computational predictions. In the last four

years, 1990-94, over 20 journal and conference publications have presented extensive theoretical nonlinear transient studies of the problem. Only Zhao et al. (1994) provide fundamental experimental results which demonstrate that current theoretical-computational models fail to predict the observed performance of actual rotor-damper systems. It appears then that the π-film short length SFD model used in these nonlinear analyses has little relationship with reality.

Choy et al. (1990a-b, 1991) present detailed numerical studies on nonlinear effects in plain journal bearings due to journal misalignment, levels of loading and thermal conditions. Most importantly, the authors develop transfer functions for the response of a simple rotor - journal bearing system due to impulse loadings and compare them with transfer functions obtained from the linearized bearing force coefficients. The numerical results show the extent of nonlinear behavior to be of importance for journal operation at low eccentricities where nonlinearities show a marked increase as the journal is suddenly displaced to a larger operating point. Adams et al.(1983, 1994) present transient studies of point mass rotors supported on cylindrical journal bearings and tilting-pad bearings. The analyses address the phenomena of pad flutter at subsynchronous frequencies and the appearance of chaotic phenomena under particular operating and loading conditions. Tichy and Bou-Said (1991) report on the importance of fluid inertia effects on the initial transient response of simple rotors supported in hydrodynamic plain journal bearings and acted upon by impulsive loads. The method extends the application of the film-averaged momentum equations (Elrod et al., 1983) to analyze unsteady flows in fluid film bearings. This type of average-inertia model has been used extensively to address fluid inertia effects in squeeze film dampers (Szeri et al., 1983).

Paranjpe and co-workers have advanced steadily the thermohydrodynamic analysis of dynamically loaded journal bearings for automotive applications. The latest publication (Paranjpe et al., 1994) describes the complexity of their current model and provides a lucid explanation on the time scales for thermal effects in a fluid film bearing and its bounding solids. Desbordes et al. (1994), and Gadangi et al. (1994a,b) include the effects of film temperature and pivot flexibility on the transient response to suddenly applied unbalance loads in rotors supported on tilting-pad bearings. The authors bring to attention a rotor-bearing highly nonlinear behavior for large levels of unbalance, and where a linear rotordynamic model fails to predict the system transient response.

For turbulent flow applications in annular pressure seals, Nordmann and Dietzen (1988), Tam et al. (1988), Baskharone and Hensel (1991a,b), and, Athavale et al. (1994) use time dependent 3-dimensional computational fluid dynamic models to obtain rotordynamic force coefficients for specified small amplitude whirl motions about a journal equilibrium position. The intensive unsteady flow computations are not coupled to the dynamics of a rotating system, and thus, can not yet address effectively the nonlinear aspects of the fluid film bearing element studied. Padavala (1993) recently completed a time dependent analysis for a rigid rotor supported on turbulent flow annular pressure seals. The numerical integration of the unsteady bulk-flow equations is performed in explicit form, and thus, the method requires very small time steps to assure stability of the calculated solution. Padavala concludes that, for most loading cases of interest, annular pressure seals in cryogenic turbomachinery behave as linear elements even for large amplitude motions away from the rotor equilibrium position. The author also notes that fluid inertia forces are unimportant in the unsteady bulk-flow model. However, Padavala fails

to indicate that the test cases studied are relevant to a rotor system operating well below its critical speed. This operating condition alone justifies his major conclusion.

ANALYSIS

Consider a point mass rigid rotor supported on fluid film bearings as shown schematically in Figure 1. The equations describing the motion of the rotor-bearing system are given as:

$$\begin{aligned} M\,A_X &= F_X(t) + W_X(t) + M\cdot g \\ M\,A_Y &= F_Y(t) + W_Y(t) \end{aligned} \qquad (1)$$

where $\{A_X, A_Y\}$ correspond to the rotor accelerations in the X and Y inertial coordinates, and $\{F_\iota, W_\iota\}_{\iota=X,Y}$ correspond to the time dependent fluid film bearing reaction forces and applied external loads, respectively. The solution of equations (1) is unique provided initial conditions on the rotor center displacements $\{X_o, Y_o\}$ and velocities $\{V_{Xo}, V_{Yo}\}$ are specified at some initial time (t_o). In general, the fluid film bearing forces depend on the bearing geometry, operating conditions and the journal (rotor) center displacements and velocities, and expressed in general form as:

$$F_\iota = F_\iota(X, Y, V_X, V_Y), \qquad \iota = X, Y \qquad (2)$$

A local coordinate system is placed on the unwrapped plane of a hybrid (hydrostatic/hydrodynamic) fluid film bearing with the {x,y} axes pointing in the circumferential and axial directions, respectively (see Figure 2). This cartesian coordinate system is a logical consequence of the smallness of the film thickness relative to the bearing diameter and length and constitutes the

fundamental assumption of lubrication theory.

The fluid reaction forces are determined from the film pressure generated by the flow field within the fluid film bearing, i.e.

$$F_\iota = \int_0^L \int_0^{2\pi R} P\, h_\iota \, dx\, dy, \qquad \iota = X, Y \tag{3}$$

where $h_X = \cos\theta$, and $h_Y = \sin\theta$, respectively. The flow field (velocities and pressure) within the bearing is described by a set of equations of motion with appropriate boundary conditions and accompanied by specification of the kinematics of the journal motion and the film thickness.

At operating conditions, the journal position relative to the bearing housing is described with reference to the inertial axes {X,Y,Z=y} by the journal center displacements (X(t),Y(t)). The film thickness and its time derivative in the flow region are given by the following expressions:

$$H(\theta,y,t) = C(y) + X(t)\cos(\theta) + Y(t)\sin(\theta)$$
$$\partial H/\partial t = V_X \cos(\theta) + V_Y \sin(\theta) \qquad \theta = x/R \tag{4}$$

where C is the bearing radial clearance, in general a function of the axial coordinate. Clearance functions of interest range from uniform and tapered (convergent, divergent) to discontinuous functions like steps and more complex forms of the structural wavy type. The film thickness above is representative of a cylindrical bearing. The analysis can also represent film thikness variations due to pad preload in fixed arc or tilting pad bearings, and due to journal misalignment axis conditions. In equation (4), the journal center displacement components (X,Y) are functions only of time and determined by solution of the governing equations (1).

The equations of motion for the fluid film bearing

The unsteady fluid flow on the film lands of a bearing is considered as fully developed with a turbulent character due to the large axial pressure drop, high rotor surface speed and the low viscosity typical of process liquids. Here, "average fluid inertia" equations are used to describe the bulk-flow motion in thin film geometries (Elrod et al., 1983, Szeri et al., 1983). The equations of mass conservation, momentum and energy transport for the turbulent bulk-flow on the thin film lands of a bearing are given by Yang et al.(1992,1993a, 1994) as:

$$\frac{\partial}{\partial x_i}\left(\rho H U_i\right) + \frac{\partial}{\partial t}\left(\rho H\right) = 0 \tag{5}$$

$$-H\frac{\partial P}{\partial x_i} = \frac{1}{H}\left(\kappa_i - \frac{1}{2}\kappa_J \Lambda_j\right) + \frac{\partial}{\partial t}\left(\rho H U_i\right) + \frac{\partial}{\partial x_j}\left(\rho H U_i \cdot U_j\right) \tag{6}$$

$$C_p\left\{\frac{\partial}{\partial t}\left(\rho H T\right) + \frac{\partial}{\partial x_i}\left(\rho H U_i \cdot T\right)\right\} + Q_s = \beta_T H T\left\{\frac{\partial P}{\partial t} + U_i\frac{\partial P}{\partial x_i}\right\} + \Lambda_x H\frac{\partial P}{\partial x} + \frac{\mu}{H}\left\{\kappa_x\left(U_x^2+U_y^2+\frac{1}{2}\Lambda_x\cdot U_x\right) + \kappa_J\Lambda_x\left(\frac{1}{4}\Lambda_x - U_x\right)\right\} \tag{7}$$

$$i=x,y$$

where $\Lambda_x=\Omega\cdot R$ and $\Lambda_y=0$ correspond to the surface rotor speed in the circumfer - ential and axial directions, respectively. $\kappa_x=\kappa_y=(\kappa_J+\kappa_B)/2$ are the wall shear stress difference coefficients as local functions of the turbulent friction factors, bearing and journal surface conditions, and the flow Reynolds numbers relative to the rotating (R_J) and stationary (R_B) surfaces, i.e $\kappa_J=f_J R_J$, $\kappa_B=f_B R_B$ (Hirs, 1973). For cryogenic liquids such as LH_2, LO_2, LN_2, and LCH_4, the fluid

properties are calculated from the Benedict-Web-Rubin equation of state as given in the standard data base of McCarty(1986). And,

$$Q_s = h_B(T-T_B) + h_J\,(T-T_J) \tag{8}$$

denotes the heat flow from the fluid film to the bearing and journal surfaces at temperatures (T_B) and (T_J), respectively, and with (h_B,h_J) as the bulk-flow convection heat transfer coefficients. A description of these parameters in turbulent bulk-flows is given by Yang (1992).

In an orifice-compensated hydrostatic bearing, mass conservation must be satisfied at each bearing recess of area ($l \cdot R \cdot \Theta_r$) and depth H_r. The global balance between the mass flow through the orifice restrictor (Q_{ro}), the mass flow into the film lands and the accumulation of mass within the recess volume (V_r) is given as:

$$Q_{rk}=A_o\sqrt{2\,\rho_r(P_s-P_{rk})} = \int_{\Gamma_{rk}}\left[\rho\, H\, \vec{\mathbf{U}}\cdot\vec{\mathbf{n}}\right]d\Gamma_r + \rho_{rk}\frac{\partial V_{rk}}{\partial t}+\rho_{rk}V_{rk}\left\{\beta_P\frac{\partial P_{rk}}{\partial t} - \beta_T\frac{\partial T_{rk}}{\partial t}\right\} \tag{9}$$

for k=1,2..., Nrecess

where $A_o=C_d\pi d^2/4$ is the effective orifice area, and $\beta_P=(1/\rho)\partial\rho/\partial P$ and $\beta_T=-(1/\rho)\partial\rho/\partial T=$ represent the fluid compressibility and volumetric expansion coefficients, respectively. Γ_r represents the closure (perimeter) of the recess volume with the film lands and with normal **n** along the boundary line. Note that the orifice flow equation is valid only for small changes of the liquid density. A more accurate relationship for highly compressible cryogenic liquids is not readily available, although a complex thermophysical model has been advanced by Hall et al. (1986). Experimental evidence has shown that the predicted

performance of hydrostatic bearings is quite sensitive to the appropriate selection or knowledge of the discharge coefficient (C_d). See Scharrer et al. (1990), Kurtin et al. (1993), and Franchek et al. (1994) for more details on this subject.

The fluid recess-edge pressure at the entrance to the film lands is given by the superposition of viscous shear effects on the recess extent and an entrance drop due to fluid inertia. Figure 3 shows the assumed pressure distribution within the recess volume and details the relevant nomenclature. On the circumferential direction, the pressure rise (P_e^-) downstream of the recess orifice is given by (Constantinescu and DiMofte, 1987, San Andres, 1992):

$$\left[P_e^- = P_r - \mu_r K_r \frac{R \cdot \Theta_r}{2 H_r^2} \left(U_x \left(\rho_e^-/\rho_r\right) \eta - \frac{\Lambda_x}{2} \right) \frac{1}{(1-\mathbf{M}^2)} \right]_k \qquad (10)$$

k=1,2..,Nrecesses

where, $\mathbf{M}$ is the circumferential flow local Mach number at the orifice discharge and defined as the ratio between the azimuthal velocity U_x and the liquid sound speed ($1./\sqrt{[\beta_P \rho_r]}$). The entrance pressures (P_e^+) to the film lands in the circumferential and axial directions are given by:

$$\left[P_e^+ = P_e^- - \frac{\rho_e^+}{2}(1+\xi_i)\left\{1 - \left(\rho_e^+/\rho_e^-\right)^2 \eta^2\right\} U_i^2 \right]_k \qquad i=x,y \qquad (11)$$

for k=1,2..., Nrecess

The analysis generalizes equations (11) for uneven empirical entrance loss factors ξ in the axial direction (y) and also circumferentially(x) upstream(u) and downstream(d) of the recess. The Bernoulli like pressure drop occurs only if

fluid flows from the recess towards the film lands. On the contrary, if fluid enters from the film lands into the bearing recess, then the edge pressure is equal to the recess pressure. This consideration is based on momentum conservation for turbulent shear flows in sudden expansions.

A simplified form of the energy transport equation at the recess volume is easily determined from equation (7). A detailed exposition of the energy transport process in a bearing recess is given by San Andres (1993).

Boundary Conditions

At low rotational speeds, the pressure at the bearing side boundaries is invariant in time and equal to a specified value of ambient or sump pressure, i.e.,

$$P\ (x,0) = P_0; \qquad P\ (x,L) = P_L \tag{12}$$

For multiple-pad bearings, at high journal surface speeds ($\Omega \cdot R$) significant momentum changes at a pad leading edge generate a "ram" pressure which is a fraction of the dynamic head based on the journal surface speed (Burton and Carper, 1967, Ha et al., 1994). Details of the analysis including the inlet fluid speed and energy transfer at the leading edge of a bearing pad are given in a previous publication (San Andres, 1993). The axial velocity U_y is zero if the bearing is symmetric both in geometry and operating conditions. The symmetry condition allows simplification and solution of the flow field in one-half of the bearing.

Numerical Method of Solution for the Fluid Flow Equations

A cell finite-difference scheme is implemented to solve the nonlinear, time dependent differential equations on the film lands. The numerical procedure is based on the forward marching scheme of Launder and Leschziner (1978) and uses

the SIMPLEC algorithm of Van Doormaal and Raithby (1984). At a bearing recess, the flow through the supply orifice is coupled to the flow towards the film lands and to the unsteady accumulation of fluid volume on the recess. A Newton-Raphson scheme is then used to update the recess pressures and to satisfy the transient mass continuity constraint at each bearing recess.

Appendix A details the algebraic difference equations derived on a staggered grid for calculation of the flow velocities and pressure on the bearing film lands. The time marching algorithm is fully implicit with the flow variables (velocities, pressure and temperature) obtained from numerical solution of the equations of motion at the current time step and accounting for the past history of the flow field. The scheme is computationally intensive and requires the satisfaction of boundary conditions and reccess mass flow equations at each time step. The precursor numerical procedures to the present time - dependent implicit scheme have been extensively validated for steady state flow problems with existing measurements of bearing static load performance and rotordynamic force coefficients (San Andres, 1990, 1992). Kurtin et al.(1993), Franchek et al.(1994), Mosher (1992) present detailed experimental vs. theoretical predictions for water lubricated, turbulent flow HJBs. Further validations to experimental force coefficient data for LH_2 HJBs and water HJBs are reported by Yang et al. (1994). San Andres (1993) also presents comparisons to test force coefficients for an oil lubricated HJB from Adams et al. (1992), journal bearing load measurements from Tonnesen and Hansen (1981), and numerical predictions by Braun et al. for the performance of liquid oxygen journal bearings (1987).

In general, computations for journal equilibirum position at steady state operating conditions require a relatively small number of grid points to achieve

grid independent results. For example, less than 2% difference in bearing static and dynamic performance characteristics are determined when comparing the results from a 67 by 16 grid (number of circumferential points x axial points) with those from a 85 by 26 grid for bearing cases reported by Yang (1992). Note that the analysis and program developed can handle also fluid film bearings for industrial applications and operating in the laminar-flow regime with viscous lubricants.

Several empirical parameters are used in the analysis of hydrostatic bearings and annular pressure seals. Entrance loss coefficients (ξ_x, ξ_y) and rotor(journal) and stator(bearing) surface roughnesses (r_J, r_B) are needed for annular seals and HJBs, while orifice discharge coefficients (C_d) are also required for hydrostatic bearings. Lindsey (1993) presents a detailed sensitivity analysis for annular seals, and Kurtin et al. (1993), Mosher (1992), and Franchek et al. (1994) present similar studies for hydrostatic bearings. These references describe comparisons between numerical predictions based on the present model and experimental measurements performed on water lubricated seals and hydrostatic bearings at an existing test facility (Childs and Hale, 1994). The sensitivity analysis involved changing an input parameter by ±10% from its estimated experimental value for each operating condition while the other input parameters were kept invariant. The maximum difference between the numerical prediction and experimental value for each case was then compared with the maximum difference from the original results. Then, a relative sensitivity was determined by dividing the percentage change in maximum difference of the calculated parameter by the percentage change in the input parameter. The studies determined that flow rate and direct stiffness coefficients are particularly sensitive to changes in the orifice discharge coefficient (C_d) for

HJBs and less sensitive to variations in the entrance loss coefficients. On the other hand, flow rate and direct stiffness coefficients for annular pressure seals are highly sensitive to the changes in the inlet loss coefficient (ξ_y) and surface roughness conditions. Other force coefficients and the whirl frequency ratio for HJBs are particularly insensitive to variations in the empirical parameters. The interested reader is encouraged to seek the references cited for further details on the sensitivity analyses and major results.

Numerical Solution of the Equations of Motion for the Coupled Rotor-Bearing System

The general nonlinear equations (1) governing the rotor and bearing motion are numerically solved using the Wilson-$\underline{\theta}$ method as described by Bathe (1982). Selection of this implicit numerical method is based on its stability characteristics and accuracy, in particular for linear systems. A brief description of the method as applied to the present analysis follows.

The time domain is divided into a sequence of discrete times $\{t_j\}_{j=1,\ Nt}$ starting at the initial time t_o, and such that the time step Δt_i is related to the discrete times by $(t_{i+1}-t_i)$. At <u>discrete</u> times t_i and $t_j=t_{i+1}$, the equations of motion (1) are reduced to the following **algebraic** expressions:

$$\begin{aligned} M\,A_{Xi} &= F_{Xi} + W_{Xi} + M\cdot g & MA_{Xj} &= F_{Xj} + W_{Xj} + M\cdot g \\ M\,A_{Yi} &= F_{Yi} + W_{Yi} & MA_{Yj} &= F_{Yj} + W_{Yj} \end{aligned} \qquad (13)$$

where, $A_{Xi}=A_X(t_i)$, and $W_{Xi}=W_X(t_i)$ are the X-direction rotor acceleration and external load evaluated at time t_i. $F_{Xi} \simeq F_X(X_i, Y_i, V_{Xi}, V_{Yi})$ is the X-fluid film bearing force estimated at time t_i. Similar definitions hold for the Y-direction journal displacement and its time derivatives, as well as forces at the calculation times t_i and t_j. Note that in the equations above, the journal

position and velocity and the fluid film forces are to be determined at time t_j, and henceforth all quantities at time t_i are known. Equations for incremental changes in the system acceleration are determined from equations (13) as:

$$\begin{aligned} M\ \Delta A_{Xi} &= \Delta F_{Xi} + \Delta W_{Xi} \\ M\ \Delta A_{Yi} &= \Delta F_{Yi} + \Delta W_{Yi} \end{aligned} \tag{14}$$

where $\Delta AX_i = A_{Xj} - A_{Xi}$, $\Delta WX_i = W_{Xj} - W_{Xi}$, $\Delta F_{Xi} = F_{Xj} - F_{Xi}$, etc. are referred as the incremental changes in accelerations, loads, and bearing forces, respectively. For small time steps Δt_i, the fluid film forces using a Taylor series expansion are approximately given as:

$$\begin{aligned} -\Delta F_{Xi} &= K_{XX}\,\Delta X_i + K_{XY}\,\Delta Y_i + C_{XX}\,\Delta V_{Xi} + C_{XY}\,\Delta V_{Yi} + M_{XX}\,\Delta A_{Xi} + M_{XY}\,\Delta A_{Yi} \\ -\Delta F_{Yi} &= K_{YX}\,\Delta_{Xi} + K_{YY}\,\Delta Y_i + C_{YX}\,\Delta V_{Xi} + C_{YY}\,\Delta V_{Yi} + K_{YX}\,\Delta A_{Xi} + M_{YY}\,\Delta A_{Yi} \end{aligned} \tag{15}$$

where the local or linearized stiffness, damping and inertia coefficients for the fluid film bearing are given as

$$K_{\alpha\beta} = -\left.\frac{\partial F_\alpha}{\partial_\beta}\right|_{(Xi,Yi)} \qquad C_{\alpha\beta} = -\left.\frac{\partial F_\alpha}{\partial V_\beta}\right|_{(X_i,Y_i)} \qquad M_{\alpha\beta} = -\left.\frac{\partial F_\alpha}{\partial A_\beta}\right|_{(X_i,Y_i)} ;\ \alpha,\beta = X,Y \tag{16}$$

and evaluated from analytical perturbations to the nonlinear flow governing equations for the fluid film bearing. Complete details on the derivation and solution for the flow equations for small perturbations about an operating condition have been given in detail in the past (San Andres, 1993, Yang, 1992). In general, for turbulent-flow bearings and seals with compressible fluids, the linearized force coefficients are functions of the excitation whirl frequency.

Substitution of the force coefficients into equations (14) for the incremental accelerations leads to the following linearized equations:

$$\begin{bmatrix} M+M_{XX} & M_{XY} \\ M_{YX} & M+M_{YY} \end{bmatrix} \begin{bmatrix} \Delta A_{Xi} \\ \Delta A_{Yi} \end{bmatrix} + \begin{bmatrix} K_{XX} & K_{XY} \\ K_{YX} & K_{YY} \end{bmatrix} \begin{bmatrix} \Delta V_{Xi} \\ \Delta V_{Yi} \end{bmatrix} + \begin{bmatrix} C_{XX} & C_{XY} \\ C_{YX} & C_{YY} \end{bmatrix} \begin{bmatrix} \Delta X_i \\ \Delta Y_i \end{bmatrix} = \begin{bmatrix} \Delta W_{Xi} \\ \Delta W_{Yi} \end{bmatrix} \qquad (17)$$

In the Wilson-$\underline{\theta}$ method the accelerations are regarded as linear on the extended time interval t_i to $t_i+\underline{\theta}\Delta t_i$. The method depends on the parameter $\underline{\theta}$ with optimum results for a value $\underline{\theta}$=1.42 (Bathe, 1982). Thus, over the local time coordinate τ the accelerations are given as (see Figure 4):

$$\begin{aligned} A_X(\tau) &= AX_i + (\tau/S_i)\ \Delta sA_{Xi} \\ A_Y(\tau) &= A_{Yi} + (\tau/S_i)\ \Delta sA_{Yi}, \quad S_i=\underline{\theta}\Delta t_i \end{aligned} \qquad (18)$$

Integration of these equations over the discrete time $0\leq\tau\leq S_i$ gives the displacements and velocities as quadratic and cubic functions of time τ as:

$$\begin{aligned} V_X(\tau) &= V_{Xi} + \tau\ A_{Xi} + (\tau^2/2S_i)\ \Delta_s A_{Xi} \\ V_Y(\tau) &= V_{Yi} + \tau\ A_{Yi} + (\tau^2/2S_i)\ \Delta_s A_{Yi} \end{aligned} \qquad (19)$$

and,

$$\begin{aligned} X(\tau) &= X_i + V_{Xi}\ \tau + (\tau^2/2)\ A_{Xi} + (\tau^3/6S_i)\ \Delta sA_{Xi} \\ Y(\tau) &= Y_i + V_{Yi}\ \tau + (\tau^2/2)\ A_{Yi} + (\tau^3/6S_i)\ \Delta sA_{Yi} \end{aligned} \qquad (20)$$

Substitution of $\tau=S_i$ on the expressions above leads to relationships for the incremental changes in acceleration and velocities at the end of the extended time interval, i.e.

$$\begin{aligned} \Delta sA_{Xi} &= (6/S_i^2)\ \Delta sX_i - (6/S_i)\ V_{Xi} - 3\ A_{Xi} \\ \Delta sA_{Yi} &= (6/S_i^2)\ \Delta sY_i - (6/S_i)\ V_{Yi} - 3\ A_{Yi} \end{aligned} \qquad (21)$$

and,

$$\begin{aligned} \Delta sV_{Xi} &= (3/S_i)\ \Delta sX_i - 3\ V_{Xi} - (S_i/2)\ A_{Xi} \\ \Delta sV_{Yi} &= (3/S_i)\ \Delta s_{Yi} - 3\ V_{Yi} - (S_i/2)\ A_{Yi} \end{aligned} \qquad (22)$$

From equations (17), the equations for evaluation of the incremental accelerations, velocities and displacements at the end of the extended time interval are given as:

$$\begin{bmatrix} M+M_{XX} & M_{XY} \\ M_{YX} & M+M_{YY} \end{bmatrix} \begin{bmatrix} \Delta sA_{Xi} \\ \Delta sA_{Yi} \end{bmatrix} + \begin{bmatrix} K_{XX} & K_{XY} \\ K_{YX} & K_{YY} \end{bmatrix} \begin{bmatrix} \Delta sV_{Xi} \\ \Delta sV_{Yi} \end{bmatrix} + \begin{bmatrix} C_{XX} & C_{XY} \\ C_{YX} & C_{YY} \end{bmatrix} \begin{bmatrix} \Delta sX_i \\ \Delta sY_i \end{bmatrix} = \begin{bmatrix} W_X(t_i+S_i)-W_X(t_i) \\ W_Y(t_i+S_i)-W_Y(t_i) \end{bmatrix} \tag{23}$$

The expressions for the incremental changes in accelerations ($\Delta sA_{X,Y}$) and velocities ($\Delta sV_{X,Y}$) are substituted into these equations to give:

$$\begin{aligned} &[\mathbf{Mi}] \{(6/S_i^2)\ \Delta sZ_i - (6/S_i)\ V_{Zi} - 3\ A_{Zi}\} \\ &+ [\mathbf{Ci}] \{(3/S_i)\ \Delta sZ_i - 3\ V_{Zi} - (S_i/2)\ A_{Zi}\} \\ &+ [\mathbf{Ki}]\ \Delta sZ_i = \underline{\Theta}\ \{ W(t_j)-W(t_i) \} = \Delta sW_i \end{aligned} \tag{24}$$

where [Ki], [Ci], [Mi] represent the matrices of local stiffness, damping and inertia coefficients evaluated at time t_i. $\Delta sZ = \{\Delta sX, \Delta sY\}^T$ is a vector of incremental displacements, and $\Delta sW = [\underline{\Theta}\cdot\Delta W_X, \underline{\Theta}\cdot\Delta W_Y]^T$ is a vector of incremental external loads. Rearranging equations (24) gives finally the following matrix expression:

$$[K^*]\ \Delta sZ_i = \Delta sW_i^* \tag{25}$$

where,

$$[K_*] = [\mathbf{Ki}] + (3/S_i)\ [\mathbf{Ci}] + (6/S_i^2)\ [\mathbf{Mi}] \tag{26}$$

and

$$\Delta sW_i^* = \underline{\Theta}\left\{W_j-W_i\right\} + \left[(6/S_i)[\mathbf{Mi}] + 3[\mathbf{Ci}]\right]V_{Zi} + \left[3[\mathbf{Mi}]+(S_i/2)[\mathbf{Ci}]\right]A_{Zi} \tag{27}$$

are known as the "pseudo" dynamic stiffness matrix and equivalent load vector,

respectively. Note that equation (25) represents the **dynamic** problem as a "pseudo" static load problem (Bathe, 1982).

Once the incremental displacements over the extended time period S_i are obtained from solution of equation (25), the following formulae are used to estimate the displacements and velocities at the end of the time step $t_j=t_i+\Delta t_i$:

$$V_{Zj} = V_{Zi} + \Delta ti \{ A_{Zi} + (1/2)\ \Delta A_{Zi})$$

$$Z_j = Z_i + \Delta t_i\ V_{Zi} + (\Delta t_i^2/2) \{ A_{Zi} + (1/3)\ \Delta A_{Zi} \} \qquad (28)$$

where

$$\Delta A_{Zi} = (1/\theta)\ \Delta s A_{Zi} = 1/\theta \cdot \left[(6/S_i^2)\ \Delta s Z_i - (6/S_i)\ V_{Zi} - 3\ A_{Zi} \right] \qquad (29)$$

To insure dynamic equilibrium, the accelerations at the end of the time step (t_j) are not determined from the incremental equations but by direct solution of the original equations (1), i.e.

$$A_{Zj} = (1/M)\ [F_{Zj} + W_Z(t_j) + M \cdot g] \qquad (30)$$

where the fluid film forces are calculated from the solution of the flow equations with the updated values of journal displacements and speeds on the film thickness and its time derivative, i.e., $F_Z = F_Z(Z_j, V_{Zj})$.

At the start time (to) for analysis, initial conditions in journal position and speed and the corresponding flow field (pressure, temperature, velocities and fluid material properties) must be given. Then, for time specified variations in the external loads, the procedure follows the scheme outlined above at each time step. A **User's Manual** describes the operation of the computer program developed along with the many options available and bearing geometries analyzed (San Andres, 1994a).

Required time step for the transient analysis.

The computational effort required to solve the entire bearing flow field along with evaluation of forces and local force coefficients is very intensive. It is noted that time steps need to be kept small if accurate results are to be the natural outcome of the numerical algorithm. The minimum required size of the time step is typically related to the fundamental period of motion of the system or the largest frequency intrinsic to the external load. Thus, before calculations are started an estimate of the natural frequency of the system for small amplitude motions about an equilibrium position is required. Note that the notion of a natural frequency here implies linearity of the equations of motion which is not likely to be the same as in a highly non - linear system with large time varying forces applied to it.

The criteria for the threshold speed of instability (Ω_s) and whirl frequency ratio (ϕ) of a rigid rotor supported in fluid film bearings are well known (Lund, 1965). For fluid film bearings where fluid inertia effects are not important the equivalent stiffness and whirl frequency ratio of the rigid rotor - bearing system are given as:

$$K_{eq} = \frac{K_{XX}C_{YY}+C_{XX}K_{YY}-C_{YX}K_{XY}-C_{XY}K_{YX}}{C_{XX}+C_{YY}} \qquad (31)$$

$$\phi^2 = (\omega_n/\Omega_s)^2 = \frac{(K_{eq}-K_{XX})(K_{eq}-K_{YY})-K_{XY}K_{YX}}{\Omega_s^2\,(C_{XX}C_{YY}-C_{XY}C_{YX})} \qquad (32)$$

where the force coefficients $\{K_{\alpha\beta}, C_{\alpha\beta}\}$ are evaluated at an equilibrium journal (rotor) position defined by the applied static load. From these equations, an estimate of the natural period of motion (τ_n) of the rotor-bearing system is

given as:

$$\tau_n = 2\pi/\omega_n = 2\pi\,(M/K_{eq})^{1/2} \qquad (33)$$

If the operating speed (Ω) is larger than Ω_s then the rotor bearing system becomes unstable (in the sense of a linear stability analysis) with unbounded motions of the rotor at its natural frequency (ω_n), i.e. at a fraction ϕ of the rotational speed. For a similar analysis including fluid inertia effects refer to San Andres (1991).

As briefly stated earlier, the time step for the transient analysis must be a fraction of the natural period of motion (τ_n), or a fraction of the period of motion due to rotor angular speed ($2\pi/\Omega$), or a fraction of the smallest period determined by the largest frequency (ω) intrinsic to the time-varying external loads. The time step selected should be the smallest satisfying these three conditions. In practice, the time step is chosen for purposes of accuracy as (Childs et al., 1977):

$$\Delta t \leq [2\pi/\omega_*]/60 \qquad (34)$$

where ω_* is the largest frequency (in Hz) likely to be excited in the system. The less stringent requirement, $\Delta t \leq 2/\omega_*$, guarantees only stability but not necessarily accuracy of the numerical scheme. Note that suddenly applied loads like impulses and step loads are rich in high frequencies, and consequently initial time steps are constrained to be very small in order to capture with accuracy the imposed external actions.

The efficiency of the complex computational model coupling the dynamics of the rotor-bearing system to the flow dynamics within the fluid film bearing is severely reduced due to the stringent requirement of small time steps and the

current limitations in the processing speed of computers. The current program runs on a personal workstation with a clock speed of 35MHz. Times of execution reported later for the examples and test cases analized are particular to the machine used.

For example, calculation of the steady-stated flow field and forces in a water lubricated hydrostatic bearing operating at 30 kcpm and given specified static load is about 60 seconds with an initially assumed flow field close within 20% to the actual solution. This execution time seems small (in my opinion) if a few static load cases are analyzed. In the past this fast execution has allowed the current computational program to be used in an interactive way with the user. However, to describe a transient situation due to a blade loss (sudden unbalance) turns out to be almost prohibitive. If we assume that the entire transient will take about 10 rotor revolutions then the total time of calculation is equal to 10 x 0.002 secs where this last number corresponds to the period of whirl motion (1/500 Hz). With a time step $\Delta t=0.002/60$ (33.3 μsecs) to complete the necessary 600 time steps, the present compufational model would approximately need about 600x60=36,000 secs (10 hours) of computing time. This time value is certainly excessive and addresses to the need of either refining the analysis, coming across with more efficient ways to calculate the system transient response, or simply getting hold of a faster computer.

The recent archival literature presents several transient analyses for rotors supported on inertialess - fluid film bearings, see for example Padavala (1993), Gadangi et al. (1994a,b), Desbordes et al. (1994). These references report advanced models for the prediction of fluid film bearing forces, but however little insight is given in regard to the time steps used and the actual

computational time required to complete a detailed transient analysis. The authors of these scholarly references assert in personal communications that their schemes are time consuming and need to run on the fastest computers available, namely a CRAY machine, for a few hours.

Approximate (linear) transient solution

Externally pressurized bearings like hydrostatic bearings and annular pressure seals are known to provide force coefficients which do not vary greatly with the journal position (or the applied load) at a fixed operational speed (San Andres, 1991). This is not the case, however, for hydrodynamic journal bearings as the technical literature profusely reports. The uniformity of force coefficients in HJBs and pressure seals allows a dramatic simplification of the general nonlinear equations of motions (1) to render:

$$\begin{bmatrix} M+M_{XX} & M_{XY} \\ M_{YX} & M+M_{YY} \end{bmatrix} \begin{bmatrix} \Delta A_X \\ \Delta A_Y \end{bmatrix} + \begin{bmatrix} K_{XX} & K_{XY} \\ K_{YX} & K_{YY} \end{bmatrix} \begin{bmatrix} \Delta V_X \\ \Delta V_Y \end{bmatrix} + \begin{bmatrix} C_{XX} & C_{XY} \\ C_{YX} & C_{YY} \end{bmatrix} \begin{bmatrix} \Delta X \\ \Delta Y \end{bmatrix} = \begin{bmatrix} W_X(t) \\ W_Y(t) \end{bmatrix} \quad (35)$$

or

$$[\mathbf{Mo}]\ \Delta A_Z + [\mathbf{Co}]\ \Delta V_Z + [\mathbf{Ko}]\ \Delta_Z = \mathbf{W}(t) \quad (36)$$

where $\Delta X=X-Xo$, $\Delta V_X=V_X$, $\Delta A_X=A_X$, etc. represent the approximate journal (rotor) center displacements, velocities and accelerations about the (equilibrium) steady-state position (Xo,Yo) defined by the static load ($M \cdot g$). The set of coefficients $\{K_{\alpha\beta},\ C_{\alpha\beta},\ M_{\alpha\beta}\}_{\alpha,\beta=X,Y}$ correspond to the linearized stiffness, damping and fluid inertia force coefficients evaluated at {Xo,Yo}. The numerical solution of the equations above is much faster than the full nonlinear solution described earlier since the matrices of inertia, damping and stiffness are evaluated only once prior to the start of the transient analysis, and

furthermore, the method does not even require the solution of the flow equations at each step. The reader is urged to note that the approximate linear equations of motion become exact for small amplitude journal motions induced by small magnitude loads, and in effect, under these conditions they can even be used for rotors supported on hydrodynamic journal bearings. In fact, the greatest achievements of rotordynamic analysis have become from such a simple and "crude" representation of the system dynamics.

The method selected to solve the approximate **linear** equations is the Wilson-$\underline{\theta}$ scheme described earlier. Execution times for solution of the approximate linearized equations of motion are about 4 orders of magnitude lower than the full nonlinear transient solution. Examples detailed below compare the relative accuracy of the approximate analysis when correlated directly to the full nonlinear transient model.

RESULTS AND DISCUSSION

The computer program named **hydrotran** is the outcome of the fluid film bearing transient analysis. Details on the capabilities and major options available with this program are fully described on its **Manual** (San Andres, 1994a). All the transient cases studied including the input and output files as well as the graphical output are given on the program **Examples** (San Andres, 1994b).

This section discusses the transient response of several point mass rotors supported on different types of fluid film bearings like plain cylindrical bearings, annular pressure seals and hydrostatic bearings, and under a variety of impossed external loads such as step forces, impulsive loads and suddenly applied unbalance forces. First, the examples compare the calculated transient

responses with those given in the literature for some relevant cases. Next, results are presented for a cryogenic application with annular pressure seals (damper seals) and also the time response of a high speed, water lubricated hydrostatic bearing and rotor system. No efforts have been made to compare the numerical predictions to experimental results since there are none reproted in the archival literature.

Table 1 presents the description of a rotor supported on plain journal bearings as given by Childs et al. (1977). The example presents the transient response of the system due to a step load equal to the rotor weight (8 kN). The journal (shaft) operates at a speed of 6,493 rpm and it is released initially from a position at the center of the bearing clearance. Figure 5 shows the the journal center to move rapidly from the centered position towards the bottom of the bearing clearance. At a large eccentricity the journal suddenly reverses its motion and proceeds steadily to its equilibrium static position. The results depicted in the figure are very similar to those of Childs et al. (1977) and also confirmed with a prior transient response on short journal bearings (San Andres, 1984). Figure 6 shows the transient fluid film forces (F_X,F_Y), rotor inertia forces ($M\cdot A_X$,$M\cdot A_Y$) due to the external loads (W_X=8 kN, W_Y=0 N). The numerical results feature very large inertial rotor forces and bearing reaction forces in the direction of the aplied load (X) at the instant of journal reversal motion. The maximum bearing X-force is actually 7 times larger than the applied static load.

Childs et al. (1977) present an interesting example for a rotor bearing system with a highly nonlinear behavior. Table 2 describes the geometry of the rotor and hydrodynamic journal bearings. At the operating conditions the journal is initially located at its equilibrium position due to the rotor weight. Then,

a sudden unbalance load (pressumably due to a blade loss) of a magnitude equal to 697 N is exerted on the system. Numerical predictions for the bearing rotor-dynamic force coefficients at the static equilibrium condition show that the rotor-bearing system is linearly unstable at the rated speed. Figure 7 shows the journal orbital motion to proceed from the static position to describe a large orbit within the bearing clearance. The journal motion is very similar as that reported by Childs et al. (1977). Figures 8 and 9 show the "steady state" journal displacements and bearing reaction forces after 10 rotor revolutions have elapsed, i.e. for times greater than 57.1 msec. The "T" labels on the figures mark a full revolution of the rotor. The numerical predictions show a characterisitic half frequency whirl motion and demonstrate a highly nonlinear behavior. Note in particular the complex functional form of the bearing reaction forces which have a period twice as large as that of the impossed unbalance force.

Tichy and Bou-Said (1991) present a study on the effect of impulsive loads on rotors supported on "short length" plain journal bearings. The thrust of the analysis is to demonstrate the importance of fluid inertia effects on the initial time response of rotor-bearing systems. Table 3 presents the geometry and operating conditions of the rotating system studied by Tichy et al. At the static equilibrium position (due to the rotor weight) the system is linearly stable. Note that the current analysis predicts a different journal equilibrium position if fluid inertia effects are included in the flow model equations. The impulsive load has an exponential character and decreases to 36.7% its initial value after t_o=2.77 msec have elapsed (1/6 rotor period). At the time the rotor has given a full revolution (t=16.6 msec), the impulse load has practically dissapeared. Figure 10 shows the journal orbital motion for the applied

impulsive load along the -Y axis, and Figure 11 depicts the journal center displacements (X,Y) for the time span of numerical integration. Figures 12 and 13 show the bearing reaction forces and rotor inertia forces for the initial transient motion to 40 msec (approximately 2.40 rotor revolutions),respectively. The inertialess flow model "appears" to predict a more rapid decay response than the fluid inertia model; however, note that both flow bearing models approach different equilibrium positions. The inertial flow model does not predict the "ripple" at the end of the journal trajectory in the direction of the applied impulsive load. This condition may be solely due to the smallness of the time step used. The most important conclusion from the example is derived from the initial bearing reaction forces and rotor mass inertia forces which are substantially smaller for the fluid inertia model. The model without fluid inertia predicts bearing forces up to 66% larger than those from the fluid inertia model. The reason for the difference lies on the "added" bearing inertia forces which arise due to fluid inertia effects. It is relatively simple to demonstrate that the apparent mass of the fluid is about 40 kg, and determines an overall increase in the system inertia to 245 kg. Hence, the predicted journal accelerations are smaller for the fluid inertia model, and consequently the rotor inertia force will be substantially reduced. The present transient response results are somewhat different to those reproted by Tichy and Bou-Said (1991). The reference presents an orbital plot where the **fluid inertia** solution shows the "ripple" at the farthest position of the journal trajectory. Furthermore, even their steady-state equilibrium results could not be verified with the exact formulae for the inertialess finite-length bearing model given by Lund (1966).

In the examples for hydrodynamic journal bearings above no comparisons with

the approximate (linear) solutions are presented since these types of fluid film bearings are well known to be highly nonlinear. Furthermore, the magnitude of the external loads applied are large enough to prevent the use of the linear transient solution. The Examples Handbook (San Andres, 1994b) does include a comparison of linear and nonlinear rotor-plain bearing transient responses using a test case from Gadangi et al.(1994a).

Table 4 presents a description of a cryogenic rotor-bearing system. The fluid film bearings are tapered damper seals handling liquid oxygen. Predictions for the static and rotordynamic force coefficients of this type of seal are given in detail by San Andres and Yang (1994). This example compares the transient system response obtained using the nonlinear and linear time integration models. The seal rotordynamic force coefficients at its centered position are used in the linear model. The predicted "linearized" natural frequency of the system is 290 Hz, and therefore, the rotor speed of 26,000 rpm is 1.5 times greater than the system critical speed.

Figures 14 to 16 present the seal nonlinear and linear transient responses for a step and a ramp loads applied in the X-direction. The magnitude of the load is 10 kN with a rise time equal to 11.5 msec for the ramp load. The orbital seal motions are shown in Figure 14, and the transient seal eccentricy is depicted in Figure 15. The results show a forced motion with little damping and at a frequency close to the predicted natural frequency for small amplitude motions. Note that the linear (approximate) transient solution follows the same trend as the nonlinear solution but presents a smaller overshoot and decays faster. The transient bearing forces (F_X) in Figure 16 show also a system with very little damping. For the step load the initial overshoot is large (approximately 100μm or 77% of the minimum clearance). Even for this large

amplitude motion, the approximate solution predicts well the system response since the damper seal has force coefficients which vary very little with the journal position.

Figure 17 shows the rotor-damper seal transient response to an impulse load of magnitude equal to 10 kN and with a characteristic time of 0.57 msec. The seal reaction force (F_Y) in the direction of the applied impulsive load (W_Y) is depicted in Figure 18. Note that after a full rotor revolution (2.3 msec), the applied impulse vanishes. The linear (approximate) solution predicts well the initial seal forces but it presents too much damping and decays faster than the nonlinear transient response.

The time response of the rotor-damper seal to a synchronous periodic load is presented next. The magnitude of the load is 5 kN which corresponds to a rotor unbalance of 13.5 μm. Figure 19 shows the transient seal eccentricity and Figure 20 depicts the magnitude of the damper seal reaction force for the linear and nonlinear models. Figure 21 shows the transient seal center orbital motion for the nonlinear model. The linear model predicts well the transient response but again it shows more damping and reaches faster a steady-state solution which is slightly larger than that of the nonlinear model. The correlation between the linear and nonlinear transient models for the example rotor supported on liquid oxygen damper seals is regarded as satisfactory and demonstrates that externally pressurized bearings can be well represented by linearized models.

Table 5 presents a description of a rotor supported on water lubricated hydrostatic bearings (HJBs). The bearings have five rectangular recesseses and orifice ports evenly distributed around the bearing circumference. Kurtin et al. (1993), Childs and Hale (1994), and Franchek et al. (1994) report experimental results for the bearing flow rate, load capacity and force coefficients of this

bearing for verious supply pressures and speeds. The tests show that the bearing is very stiff at high supply pressures and demonstrate that the force coefficients have a weak dependence on the journal position. Linear and nonlinear transient responses are compared in the discussion that follows. The bearing force coefficients at the journal centered position are used in the approximate (linear) transient model.

Figures 22 and 23 show the hydrostatic bearing transient response to applied (5 kN) ramp loads with rise times equal to 0.2 msec and 2 msec, respectively. Note that the rotor period of motion is 2 msec, and the fast-ramp load reaches its maximum value in 1/10 of a rotor full revolution. Figure 24 depicts the bearing reaction force (F_X) in the direction of the applied ramp load. The numerical predictions show the system to be highly damped with similar responses for both the linear and nonlinear transient models.

Figures 25 and 26 show the transient response of the rotor-HJB system to an impulse load of 5 kN with a characteristic time of 0.5 msec. The bearing reaction force (F_Y) in the direction of the applied impulsive load (W_Y) is depicted in Figure 27. Note that after a full rotor revolution (2 msec), the applied impulse vanishes. The linear (approximate) solution shows slightly more damping than the full nonlinear model. Both models compare well in all aspects of the time response since the maximum journal displacements are small relative to the bearing clearance (76.2 μm). For example, Figure 26 shows that the maximum journal center displacements are 9.8 μm and 9.5 μm for the nonlinear and linear models, respectively. These values represent motions to just 13% of the bearing nominal clearance.

The time response of the rotor supported on hydrostatic bearings due to rotor unbalances is presented next. Two unbalance displacements of 15.2 μm and

40 μm determine loads of magnitude equal to 7,520 N and 19,740 kN, respectively. Figure 28 shows the transient journal eccentricity for 15 rotor revolutions, and Figure 29 depicts the steady-state rotor orbits. For the largest unbalance (U=40 μm), the maximum journal displacements reach to 90% of the bearing clearance. The steady-state orbit magnitudes for the linear model are different (within 4% of the bearing clearance) to those predicted by the nonlinear model. For the largest unbalance, initial and steady-state bearing reaction forces and rotor inertia forces are presented in Figures 30 and 31, respectively. The linear and nonlinear models correlate well and show that operation at 30 kcpm is above the system natural frequency since the rotor inertia forces are almost in phase with the unbalance load.

The linear (approximate) transient model appears adequate to predict the transient response of point mass rotors supported on externally pressurized bearings (damper seals and hydrostatic bearings). However, the most important conclusion is related to the dramatic differences in computing time for the linear and nonlinear transient models. For example, the nonlinear (large) unbalance response of the example rotor-hydrostatic bearings takes 38,380 seconds to compute 450 time steps (85.3 sec/step) in a SGI 35 MHz worksattion, while the approximate solution takes only about a second. The time difference is over four orders of magnitude.

CONCLUSIONS

A detailed analysis for the prediction of the transient response of a rigid rotor supported in fluid film bearings is presented. The nonlinear equations of motion of the rotor-bearing system are numerically solved using the Wilson-$\underline{\theta}$ method with local space linearization at each time step. The fluid film bearing

forces are evaluated from the numerical solution of the unsteady bulk-flow equations on the film lands and with satisfaction of the time-dependent flow constraints at the recesses of a hydrostatic bearing. An implicit computational fluid mechanics algorithm is implemented to solve the bearing bulk-flow equations. Analytical perturbations renders linear bulk-flow equations for estimation of linearized force coefficients. The current numerical model is largely based on efficient and accurate models deviced in the past for the prediction of the static and rotordynamic force response characteristics of turbulent flow fluid film bearings in aerospace applications.

Examples for the transient response of rigid rotors supported on hydrodynamic bearings, annular pressure seals and hydrostatic bearings under a variety of external loads are discussed in detail. Transient responses based on an approximate model which uses constant rotordynamic force coefficients are also presented. The full nonlinear model demands small time steps and is computationally very intensive since it requires solution of the bearing flow equations at each time step.

Externally pressurized bearings generally present rotordynamic force coefficients which depend little on the journal equilibrium position at a constant operating speed. Hence, the linear transient model should be adequate to predict the rotor-bearing system time response due to applied dynamic loads. The numerous comparisons between the linear and nonlinear transient responses support this assertion. Furthermore, the approximate transient model brings dramatic savings on the computing time required to determine the rotor-bearing system time response. On the other hand, hydrodynamic bearings are well known to be highly nonlinear and the linearized transient response would be accurate only for small amplitude loads and at operating conditions well below the stability margin of the rotor-bearing system.

REFERENCES:

Adams, M.L., and S. Payandeh, 1983, "Self Excited Vibration of Statically Unloaded Pads in Tilting-Pad Journal Bearings," ASME Journal of Lubrication Technology, Vol. 105, pp. 377-384.

Adams, M., Sawicki, J.T., and R. Capaldi, 1992, "Experimetal Determination of Hydrostatic Journal Bearing Coefficients," Proc. of IMechE, Paper C432/145, International Conference in Vibrations in Rotating Machinery, IMechE 1992-6.

Adams,, M.L., and I.A. Abu-Mahfouz, 1994, "Exploratory Research on Chaos Concepts as Diagnostic Tools for Assessing Rotating Machinery Vibration Signatures," Proceedings of the IFToMM 4th International Conference on Rotordynamics, Chicago, ILL, September, pp. 29-39.

Athavale, M., A. Przekwas, Hendricks, R., and A. Liang, 1994, "SCISEAL: A 3-D CFD Code for Accurate Analysis of Fluid Flow and Forces in Seals," Proceedings of the Advanced Earth-to-Orbit Propulsion Technology Conference, NASA CP 3282, Vol. 1, pp. 337-345.

Barrett, L. E., P. E. Allaire, and E.J. Gunter, 1977, "Stability and Dynamic Response of Pressurized Journal Bearings with Nuclear Water Pump Applications," Annals of Nuclear Energy, Vol. 4, pp. 115-126.

Baskharone E.A., and S.J. Hensel, 1991a, "Moment Coefficients of Incompressible Flow Seals with Conically Whirling Rotors," International Journal of Mechanical Engineering Science, Vol. 133, 2 , pp. 151-167.

Baskharone E.A., and S.J. Hensel, 1991b, "Interrelated Rotordynamic Effects of Cylindrical and Conical Whirl of Annular Seal Rotors," ASME Journal of Tribology, 113, 3, pp. 470-480.

Bathe, K., 1982, "Finite Element Procedures in Engineering Analysis," Prentice-Hall Pubs., pp. 508-511.

Booker, J. F., 1965, "Dynamically Loaded Journal Bearings, Mobility Method of Solution," ASME Journal of Basic Engineering, pp. 534-546.

Braun, M.J., Wheeler, R. and R. Hendricks, 1987, "Thermal Shaft Effects on Load Carrying Capacity of a Fully Coupled, Variable properties Cryogenic Journal Bearing," STLE Tribology Transactions, 1987, Vol. 130, pp. 282-292.

Burton, R.A., and H.J. Carper, 1967, "An Experimental Study of Annular Flows with Applications in Turbulent Film Lubrication," Journal of Lubrication Technology, pp. 381-391.

Chen, P. Y.P., E.J. Hahn and C.Y. Wang, 1993, "Subharmonic Oscilations in Squeeze Film Damped Rotor Bearing Systems without Centralizing Springs," ASME Paper 93-GT-428.

Childs, D., Moes, H., and H. van Leeuwen, 1977, "Journal Bearing Impedance

Descriptions for Rotordynamic Applications," ASME Journal of Lubrication, Vol. 99, 2, pp. 198-214.

Childs, D. and K. Hale, 1994, "A Test Apparatus and Facility to Identify the Rotordynamic Coefficients of High Speed Hydrostatic Bearings," ASME Journal of Tribology, Vol. 116, 1, pp. 337-344.

Choy, F.K., Braun, M.J., and Y. Hu, 1990a, "Nonlinear Effects in a Plain Journal Bearing: Part 1 - Analytical Study," ASME paper 90-Trib-56.

Choy, F.K., Braun, M.J., and Y. Hu, 1990b, "Nonlinear Effects in a Plain Journal Bearing: Part 1 - Results," ASME paper 90-Trib-57.

Choy, F.K., Braun, M.J., and Y. Hu, 1991, "Nonlinear Transient and Frequqncy Response Analysis of Hydrodynamic Journal Bearings," ASME Journal of Tribology, Vol. 114, pp. 448-454.

Constantinescu, V.N., and F. DiMofte, 1987, "On the Influence of the Mach Number on Pressure Distribution in Gas Lubricated Step Bearings," Rev. Roum. Sci. Tech. - Mec. Appl., Tome 32, No 1, p. 51-56.

Desbordes, H., M. Fillon, J. Frene, and C. Chan Hew Wai, 1994, "The Effects of Three Dimensional Pad Deformations on Tilting-Pad Journal Bearings Under Dynamic Loading," ASME Paper 94-Trib-46.

Ehrich, F., 1992, "handbook of Rotordynamics," McGraw-Hill Pubs., NY.

Elrod, H.G., Anwar, I., and R. Colsher, 1983, "Transient Lubricating Films with Fluid Inertia," ASME Journal of Lubrication Technology, Vol.105, 3, pp. 539-547.

Franchek, N., Childs, D. and L. San Andres, 1994, "Theoretical and Experimental Comparisons for Rotordynamic Coefficients of a High Speed, High Pressure, Orifice Compensated, Hybrid Bearing," ASME Paper 94-Trib-3.

Gadangi, R. K., A. B. Palazzolo, and J. Kim, 1994a, "Transient Analysis of Plain and Tilt Pad Journal Bearings Including Fluid Film Temperature Effects," ASME Paper 94-Trib-30.

Gadangi, R. K., A. B. Palazzolo, 1994b, "Transient Analysis of Tilt Pad Journal Bearings Including Effects of Pad Flexibility and Fluid Film Temperature," ASME Paper 94-Trib-47.

Ha, H., Kim, H., and K.W. Kim, 1994, "Inlet Pressure Effects on the Thermohydrodynamic Performance of a Large Tilting Pad Journal Bearing," ASME Paper 94-Trib-26.

Hall, K.R., P. Eubank, J. Holste, K. Marsh, 1986, "Performance Equations for Compressible Flow Through Orifices and Other ΔP Devices: A Thermodynamics Approach," AIChe Journal, Vol.32, No. 3, pp. 517-519.

Hirs, G.G. , 1973, "A Bulk-Flow Theory For Turbulence in Lubricating Films," ASME Journal of Lubrication Technology, pp. 135-146.

Kirk, R.G., and E.J. Gunter, 1970,"Transient Journal Bearing Analysis," NASA CR 1599, NTIS , Springfield, VA 22151.

Kirk, R.G., and E.J. Gunter, 1975, "Short Bearing Analysis Applied to Rotordynamics, 1: Theory," ASME Paper 75-Lub-30.

Kirk, R.G., and E.J. Gunter, 1975, "Short Bearing Analysis Applied to Rotordynamics, 1: Results of Journal Bearing Response," ASME Paper 75-Lub-31.

Kirk, R.G., and E.J. Gunter, 1976, "Stability and Transient Motion of a Plain Journal Mounted in Flexible Damper Supports," ASME Journal of Engineering for Industry, pp. 576-592.

Kirk, R.G., 1988, "Transient response of Floating Ring Liquid Seals," ASME Journal of Tribology, Vol. 110, 3, pp. 572-588.

Kirk, R.G., 1994, "Analysis and Design of Floating Ring Oil Seals for Centrigugal Compressors," Proceedings of the IFToMM 4th International Conference on Rotordynamics, Chicago, ILL, September, pp. 185-190.

Kurtin, K., Childs, D., San Andres, L.A., and K. Hale, 1993, "Experimental versus Theoretical Characteristics of a High Speed Hybrid (combination Hydrostatic and Hydrodynamic) Bearing," ASME Journal of Tribology, Vol. 115, 2, pp. 160-169.

Launder, B.E., and M. Leschziner, 1978, "Flow in Finite Width Thrust Bearings Including Inertial Effects, I-Laminar Flow, II-Turbulent Flow," ASME Journal of Lubrication Technology, Vol. 100, pp. 330-345.

Li, X., and D. Taylor, 1987, "Nonsynchronous Motion of Squeeze Film Damper Systems," ASME Journal of tribology, Vol. 109. 1, pp 169-176.

Lindsey, T., 1993, "Experimental vs. Theoretical Comparison of the Effects of Taper on the Rotordynamic Coefficients in Short Smooth Annular Seals Used in High Speed Turbomachinery," M.S. Thesis, Texas A&M University.

Lund, J.W., 1965, "The Stability of an Elastic Rotor in Journal Bearings with Flexible, Damped Supports," ASME Journal of Applied Mechanics, pp. 911-920.

Lund, J., 1966, "Self Excited Stationary Whirl Orbits of a Journal in a Sleeve Bearing," Ph.D. Dissertation, Rensselaer Polytechnic Institute.

McCarty, R.D., 1986, NBS Standard Reference Data Base 12, Thermophysical Properties of Fluids, MIPROPS 86, Thermophysics Division, Center for Chemical Engineering, National Bureu of Standards, Colorado.

Mosher, P., 1992, "Experimental vs. experimental and Theoretical Characteristics of Five Hybrid (Combination Hydrostatic and Hydrodynamic)

Bearing Designs for Use in High Speed Turbomachinery," M.S. Thesis, Texas A&M University, December.

Nordmann, R., and F.J. Dietzen, 1988, "A 3-Dimensional Finite-Difference Method for Calculating the Dynamic Coefficients of Seals," Proceedings of the Rotordynamics Instability Problems in High-Performance Turbomachinery," College Station, TX, NASA Conference Publication 3026.

Padavala, S., 1993, "Dynamic Analysis of Arbitrary Profile Liquid Annular Seals and Transient Analysis with Large Eccentric Motion," Ph.D. Dissertation, Texas A&M University, December.

Paranjpe, R., and T. Han, 1994, "A Transient Thermohydrodynamic Analysis Including Mass Conserving Cavitation for Dynamically Loaded Journal Bearings," ASME Transactions, ASME Paper No. 94-Trib-36.

San Andres, L., 1984, "Transient Rotordynamics Simulation Examples," Texas A&M University, Turbomachinery Research Consortium, Report No. 204, May.

San Andres, L., 1990, "Turbulent Hybrid Bearings with Fluid Inertia Effects", ASME Journal of Tribology, Vol. 112, pp. 699-707

San Andres, L., 1991, "Effect of Eccentricity on the Force response of a Hybrid Bearing," STLE Tribology Transactions, Vol. 34, 4, pp. 537-544.

San Andres, L., 1992,, "Analysis of Turbulent Hydrostatic Bearings with a Barotropic Fluid," ASME Journal of Tribology, Vol. 114, 4, pp. 755-765.

San Andres, L., 1993, "Thermohydrodynamic Analysis of Cryogenic Liquid, Turbulent Flow Fluid Film Bearings," Annual Progress Report to NASA Lewis Research Center, NASA Grant NAG3-1434, December.

San Andres, L., 1994a, "**hydrotran**, User's Manual", Thermohydrodynamic Analysis of Cryogenic Liquid Turbulent Flow Fluid Film Bearings, Phase II, NASA LeRC, NASA Grant NAG3-1434, December.

San Andres, L., 1994b, "**hydrotran**, Examples-Hanbook", Thermohydrodynamic Analysis of Cryogenic Liquid Turbulent Flow Fluid Film Bearings, Phase II, NASA LeRC, NASA Grant NAG3-1434, December.

San Andres, L.,and Z. Yang, 1994, "Thermohydrodynamic Analysis of Fluid Film Bearings for Cryogenic Applications, 6th-NASA Conference on Advanced Earth-to-Orbit Propulsion Technology, NASA CP 3282, Vol. II, pp. 421-430.

Scharrer,J,K, R. Hibbs, 1990, "Flow Coefficients for the Orifice of a Hydrostatic Bearing," STLE Tribology Transactions, vo. 33, pp. 543-547.

Sundararajan, P., Noah S., and L. San Andres, 1994, "Fluid Inertia Effects on the Non-Linear Response of a Rigid Rotor Supported on Squeeze Film Dampers," Proceedings of the IFToMM 4th International Conference on Rotordynamics, Chicago, ILL, September, pp. 333-340.

Szeri, A.Z., A.A. Raimondi, and A. Giron-Duarte, 1983, "Linear Force Coefficients for Squeeze Film Dampers," ASME Journal of Lubrication Technology, Vol. 105, 3, pp. 326-334.

Tam, L.T, Przekwas, A.J., A.J. Muszinska, A., Hendricks, R.C., Braun, M.J., and R.L. Mullen, 1988, "Numerical and Analytical Study of Fluid Dynamic Forces in Seals and Bearings,"ASME Journal of Vibration, Acoustics, Stress and Reliability Design, pp. 315-325.

Tichy, J., and B. Bou-Said, 1991, "Hydrodynamic Lubrication and Bearing Behavior with Impulsive Loads," STLE Tribology Transactions, Vol. 34,4, pp. 505-512.

Tonnesen, J., and P.K. Hansen 1981, "Some Experiments on the Steady State Characteristics of a Cylindircal Fluid Film Bearing Considering Thermal Effects," ASME Journal of Lubrication Technology, Vol. 103, pp. 107-114.

Van Doormal, J.P. and G.D. Raithby, 1984, "Enhancements of the SIMPLE Method for Predicting Incompressible Fluid Flows," Numerical Heat Transfer, Vol. 7, pp. 147-163.

Yang, Z., 1992, "Thermohydrodynamic Analysis of Product-Lubricated Hydrostatic Bearings in Turbulent Regime," Ph.D. Dissertation, Texas A&M University, December.

Yang, Z., San Andres, L., and D. Childs, 1993a, "Thermal Effects in Cryogenic Liquid Annular Seals, I: Theory and Approximate Solutions; II: Numerical Solution and Results", ASME Journal of Lubrication Technology, Vol 115, 2, pp. 267-284.

Yang, Z., L. San Andres, and D. Childs, 1993b, "Importance of Heat Transfer from Fluid Film to Stator in Turbulent Flow Annular Seals," WEAR, Vol. 160, pp. 269-277.

Yang, Z., L. San Andres, and D. Childs, 1994, "Thermohydrodynamic Analysis of Process Liquid Hydrostatic Bearings in Turbulent Regime, I: Theory, II: Numerical Results," accepted for publication at ASME Journal of Applied Mechanics.

Zhao, J.Y., I.W. Linett, L.J. McLean, 1994, "Unbalanced Response of a Flexible Rotor Supported by a Squeeze Film Damper," ASME Journal of Vibrations and Acoustics, Paper #JVA-93-016.

Table 1. Description of rotor supported on plain cylindrical bearings. Transient response due to applied static weight. Data from Childs et al. (1977).

Bearing type: cylindrical plain journal bearing
C=127 μm, D=50.8 mm, L=25.4 mm, L/D=0.50
Lubricant: viscosity μ=0.06897 Pa·s, ρ=890 kg/m^3
Supply pressure: 0 MPa (0 psig)

Bearing model: isothermal, incompressible, isoviscous fluid

Rotor: mass M=816.5 kg, weight M·g= 8,0000 N
rotational speed Ω = 680 rad/s (6,493 rpm).
period of rotational motion: 9.2 msec

Initial conditions: $X_o=Y_o=0$ m, $V_{Xo}=V_{Yo}=0$ m/s [centered position]

parameters for time integration: Δt=0.2msec, Tmax=82.8 msec(8 rotor revolutions)
46 time steps per rotor period.

Static equilibrium position for applied weight: X_s=98.2 μm, Y_s=53 μm.

- o -

Table 2. Description of rotor supported on plain cylindrical bearings. Transient response due to sudden unbalance load. Data from Childs et al. (1977).

Bearing type: cylindrical plain journal bearing
C=127 μm, D=50.8 mm, L=25.4 mm, L/D=0.50
Lubricant: viscosity μ=0.06897 Pa·s, ρ=890 kg/m^3
Supply pressure: 0 MPa (0 psig)

Bearing model: isothermal, incompressible, isoviscous fluid

Rotor: mass M=22.68 kg, weight M·g= 222.3 N
rotational speed Ω = 1,100 rad/s (10,504 rpm).
period of rotational motion: 5.71 msec

Unbalance U: 25.4 μm, force magnitude=$M\cdot U\cdot \Omega^2$ = 697 N

Initial conditions: X_o=3.6 μm, Y_o=19.2 μm, $V_{Xo}=V_{Yo}$=0 m/s [equilibrium position]

parameters for time integration: Δt=0.1msec, Tmax=57.1msec(10 rotor revolutions)
57 time steps per rotor period.

Execution time (SGI 35MHz): 2,155 sec (3.8 sec per time step)

- o -

Table 3. Description of rotor supported on plain cylindrical bearings. Transient response due to impulsive load. Data from Tichy and Bou-Said (1991).

Bearing type: cylindrical plain journal bearing
C=300 μm, D=200 mm, L= 100 mm, L/D=0.50
Lubricant: viscosity μ=0.008 Pa·s, ρ=800 kg/m^3
Supply pressure: 0 MPa (0 psig)

Model: isothermal, incompressible, isoviscous fluid
with and without fluid inertia effects

Rotor: mass M=204.1 kg, weight M·g= 2,007 N
rotational speed Ω = 277 rad/s (3,600 rpm).
period of rotational motion: 16.7 msec

External loads: W_X = M·g (rotor weight)
W_Y = -20·exp(-t/t_o) kN, t_o=2.77 msec (impulse)

Initial conditions: equilibrium position due to rotor weight
with fluid inertia X_o=66.3 μm, Y_o=136.2 μm, V_{Xo}=V_{Yo}=0 m/s
without fluid inertia X_o=80.7 μm, Y_o=128.4 μm, V_{Xo}=V_{Yo}=0 m/s

parameters for time integration: Δt=0.2msec, Tmax=166msec(10 rotor revolutions)
83 time steps per rotor period.

Circumferential fow Reynolds number Re_c=ρΩRC/μ =1,131,
Squeeze film Reynolds number Re_s=Re_c·C/R= 3.4

At equilibrium position: Natural frequency ω_n= 35.6 Hz (2,136 rpm)
Critical mass M_c=309.7 kg
system stable

- o -

Table 4. Description of rotor supported on damper seal bearings. Seal data from San Andres and Yang (1994).

Bearing type: tapered damper seals
C(0)=221.3 μm, C(L)=129.1 μm, D=85.1 mm, L= 22.2 mm,
stator (bearing) relative roughness = 0.044 (knurled surface)
Entrance loss factor ξ=0.20, Inlet swirl =0.5·Ω·R

Lubricant: liquid oxygen at Ts=110.5°K
Supply pressure Ps: 39.6 MPa (5,750 psia)
Discharge pressure Pa: 2.09 MPa (303 psia)

Seal model: isothermal, compressible fluid
with fluid inertia effects

Rotor: mass M=50 kg, weight M·g= 490 N
rotational speed Ω = 2,723 rad/s (26,000 rpm).
period of rotational motion: 2.3 msec

Load cases:
a) Ramp load : Wx=10 kN·(t/T*), T*=11.5 msec
b) Step load : Wx=10 kN for t≥0
c) Impulsive load: Wx=M·g=490 N, Wy=10 kN·exp(-t/to), to=0.57 msec
d) Periodic load : Wx=5 kN·cos(Ωt), Wy= 5kN·sin(Ωt), Unbalance=13.5 μm

Initial conditions: equilibrium position due to rotor weight
X_o=2.45 μm, Y_o=0.53 μm, $V_{Xo}=V_{Yo}$=0 m/s

parameters for time integration: Δt=33.3μsec, Tmax=46msec(20 rotor revolutions)
69 time steps per rotor period.

At equilibrium position: Natural frequency ω_n= 290 Hz (17,410 rpm)
system stable

Force coefficients at seal centered position:

$K_{XX}=K_{YY}$	$K_{XY}=-K_{YX}$	$C_{XX}=C_{YY}$	$C_{XY}=-C_{YX}$	$M_{XX}=M_{YY}$	$M_{XY}=-M_{YX}$
E-6N/m	E-6N/m	E-3Ns/m	E-3Ns/m	kg	kg
170.0	34.50	26.63	0.94	0.65	0.00

- o -

Table 5. Description of rotor supported on hydrostatic bearings. Bearing data from Childs and Hale (1994).

Bearing type: orifice-compensated, 5 recess hydrostatic bearing
C=76.2 μm, D=76.2 mm, L= 76.2 mm,
Recess dimensions: square 27 mm x 27 mm x 381μm (depth)
orifice diameter d=1.49 mm, C_d=1.0

Entrance loss factors ξ_x, ξ_y=0.0, Inlet swirl =0.5·Ω·R

Lubricant: water at Ts=330°K
Supply pressure Ps: 6.55 MPa (950 psig)
Discharge pressure Pa: 0.0 MPa (0 psig)

Model: isothermal, compressible fluid
with fluid inertia effects

Rotor: mass M=50 kg, weight M·g= 490 N
rotational speed Ω = 3,141 rad/s (30,000 rpm).
period of rotational motion: 2.0 msec

Load cases:
a) Ramp load : Wx=5 kN·(t/T*), T*=2 msec and 0.2 msec
b) Impulsive load: Wx=M·g=490N, Wy=5 kN·exp(-t/to), to=0.5 msec
c) Periodic load : Wx=Wo·cos(Ωt), Wy= Wo·sin(Ωt).
. Unbalance U=15.2 μm, Wo= 7,520 N = $M \cdot U \cdot \Omega^2$
.. 40.0 μm, Wo=19,740 N

Initial conditions: equilibrium position due to rotor weight
X_o=0.91 μm, Y_o=1.16 μm, $V_{Xo}=V_{Yo}$=0 m/s

parameters for time integration: Δt=66.6μsec, Tmax=30msec(15 rotor revolutions)
30 time steps per rotor period.

At equilibrium position: Natural frequency ω_n= 264 Hz (15,830 rpm) stable system

Force coefficients at bearing centered position:

$K_{XX}=K_{YY}$	$K_{XY}=-K_{YX}$	$C_{XX}=C_{YY}$	$C_{XY}=-C_{YX}$	$M_{XX}=M_{YY}$	$M_{XY}=-M_{YX}$
E-6N/m	E-6N/m	E-3Ns/m	E-3Ns/m	kg	kg
211.6	315.5	206.5	57.26	16.66	-2.847

- o -

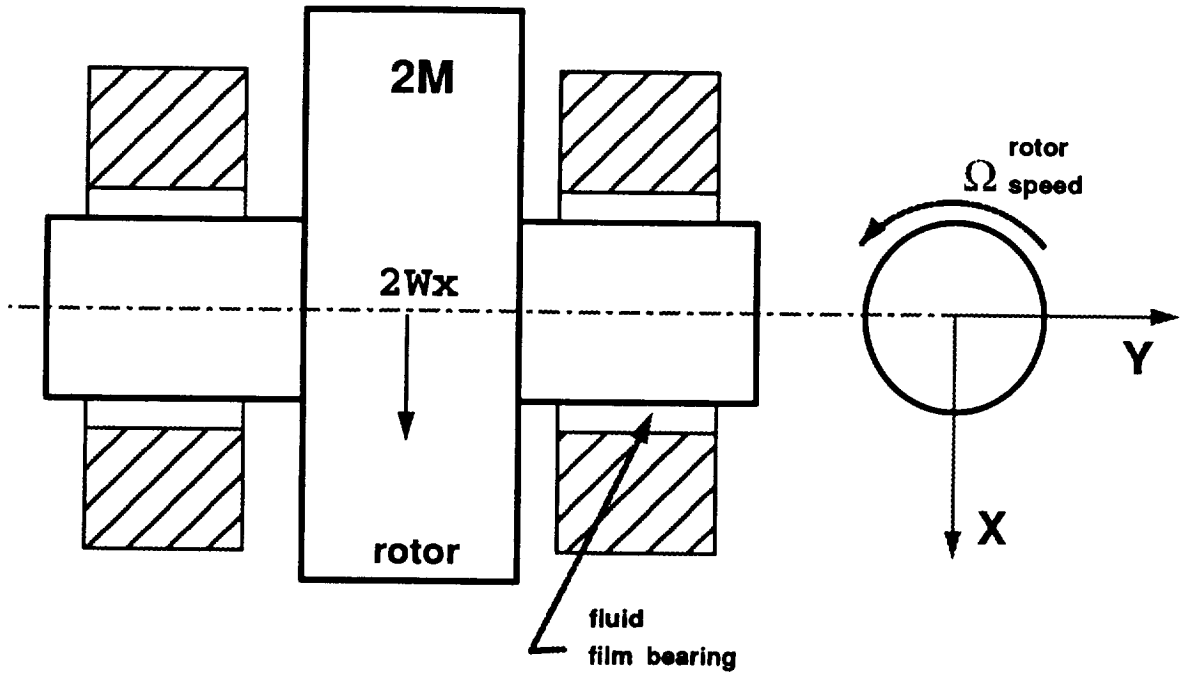

Figure 1. Rigid rotor supported on fluid film bearings

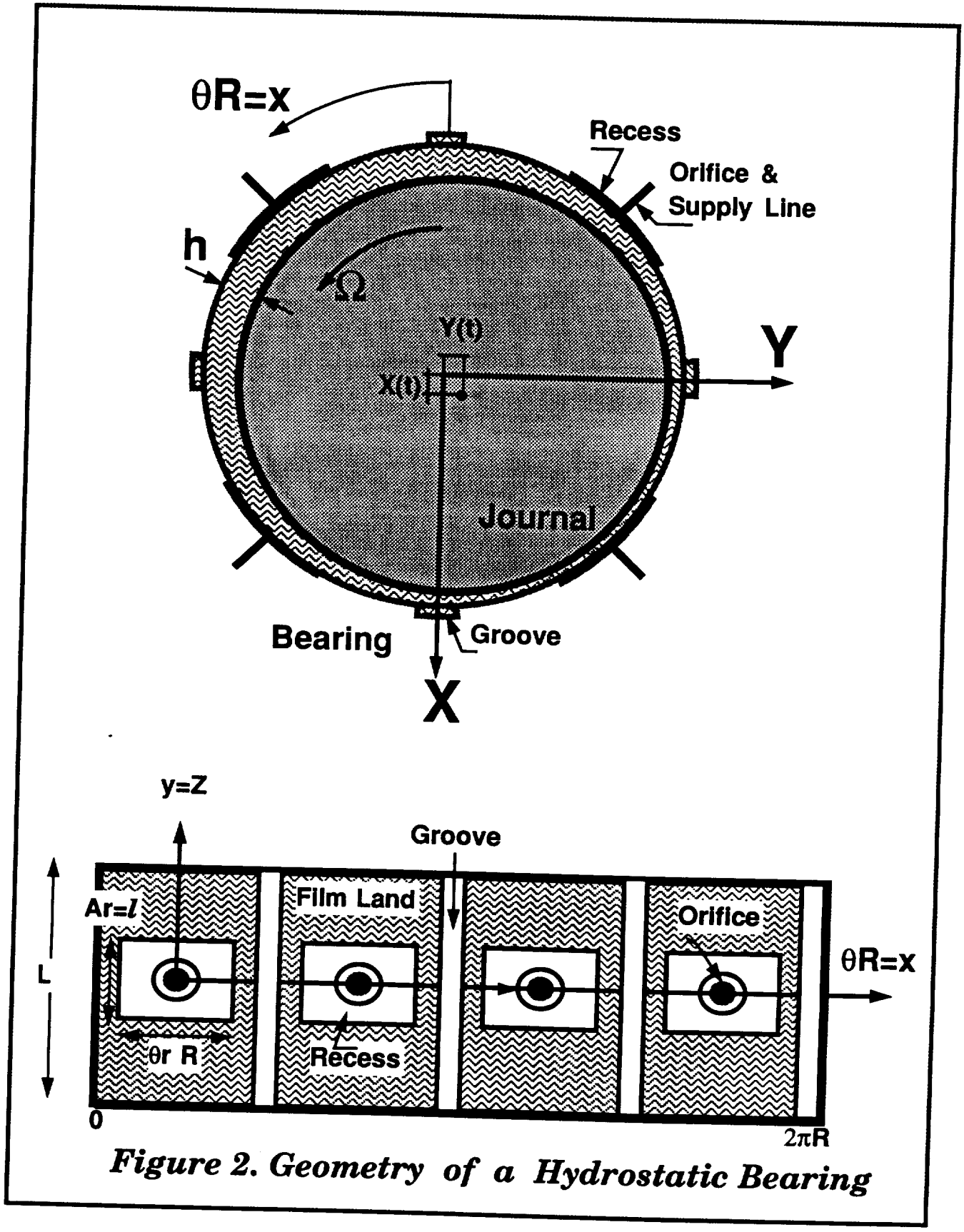

Figure 2. Geometry of a Hydrostatic Bearing

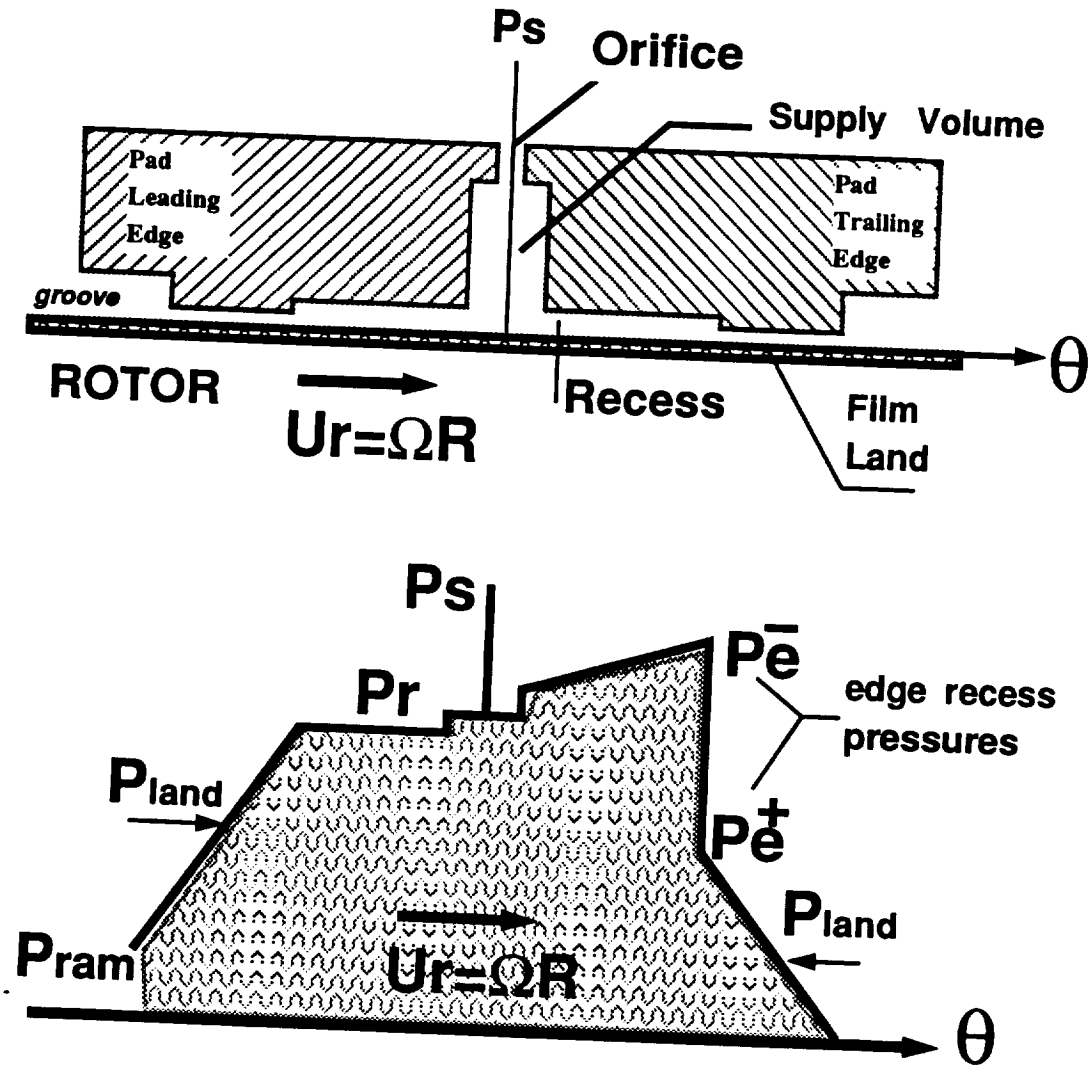

Figure 3. Conceptual description of pressure rise and drop at recess edge of a hydrostatic pad bearing, and pressure ram effect at leading edge of bearing pad.

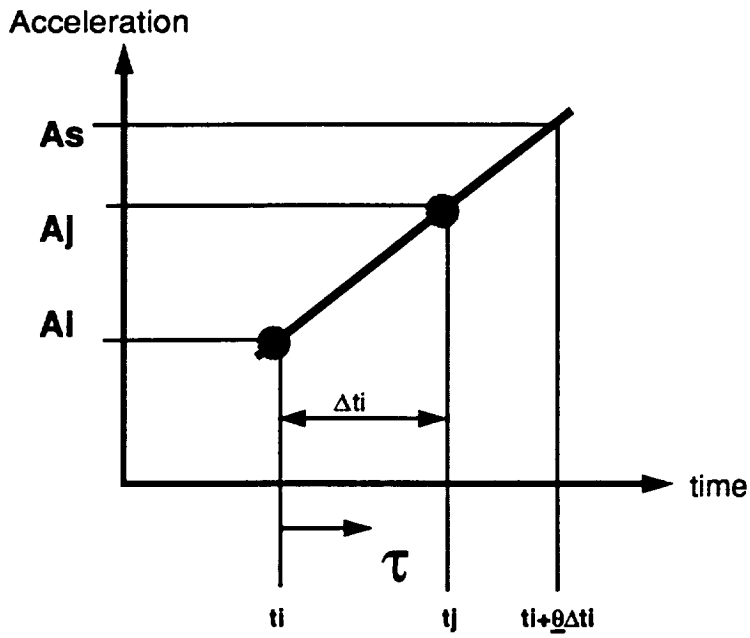

Figure 4. Linear acceleration in numerical integration method

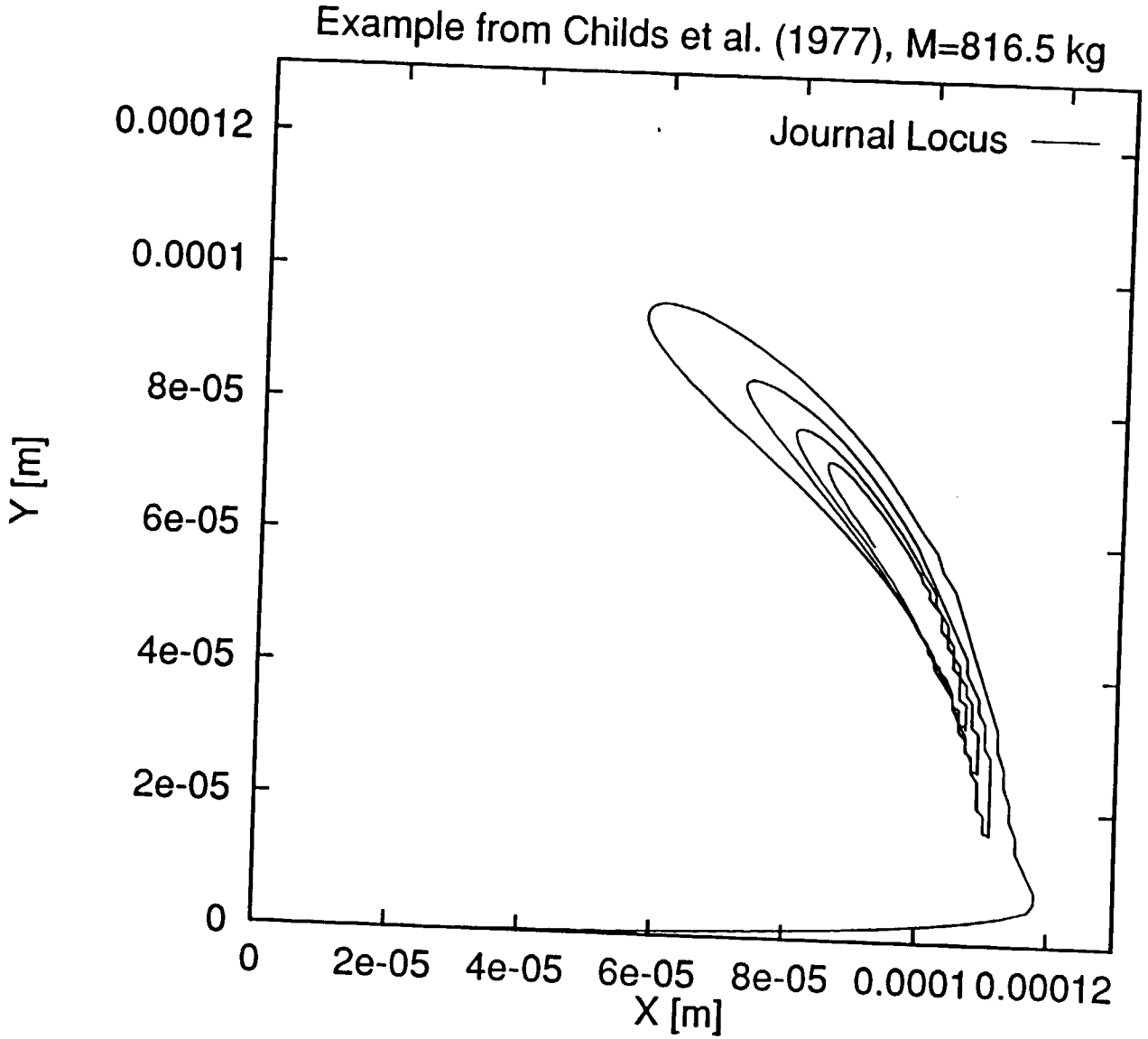

Figure 5. Transient Response of Rigid Rotor on Cylindrical Journal Bearings
Sudden step load Wx=Mg=8,000 [N]

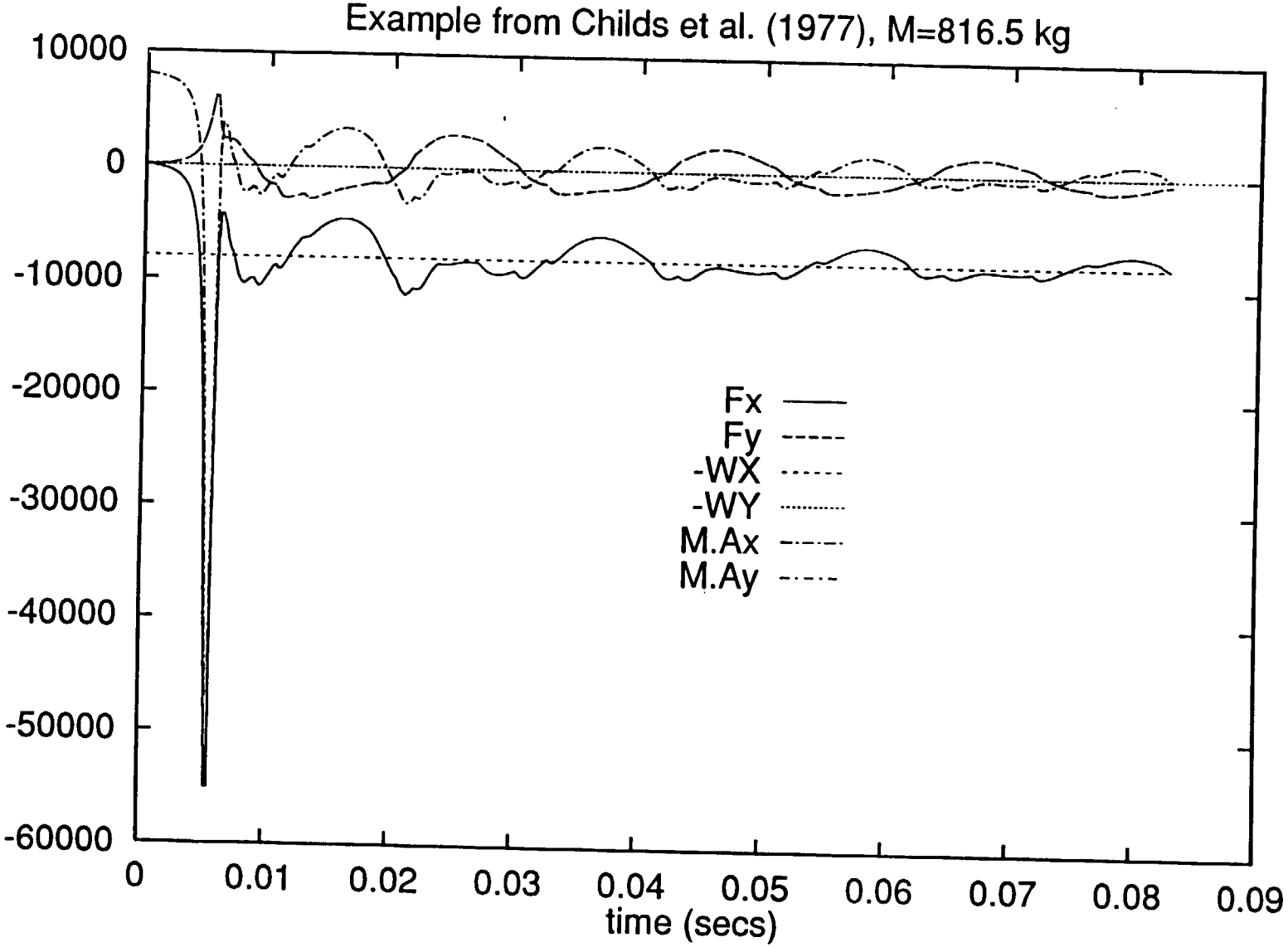

Figure 6. Fluid film forces and inertia forces for transient response

Sudden step load Wx=Mg=8,000 [N] Wy=0

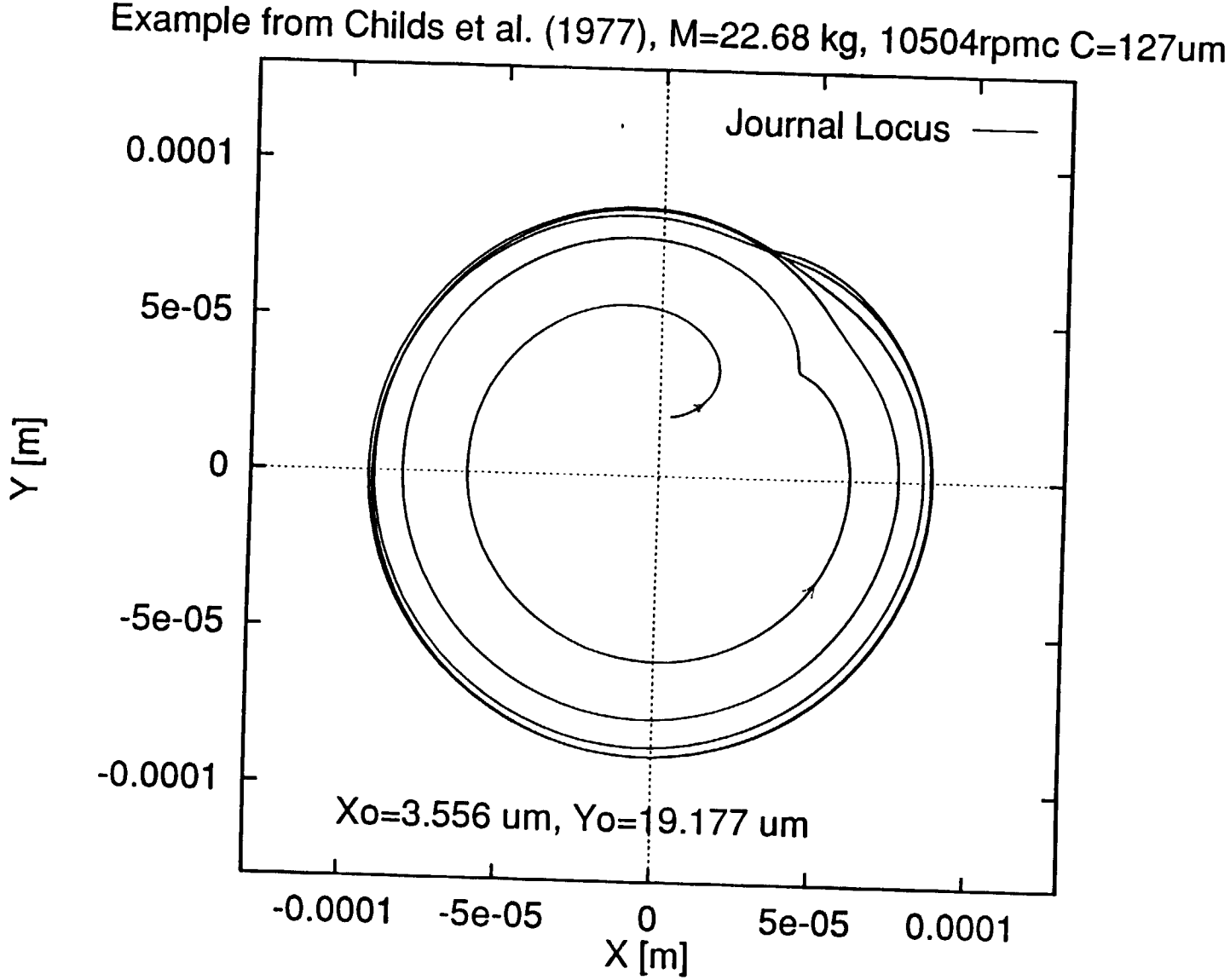

Figure 7. Transient response of Rigid Rotor on Cylindrical Journal Bearings. Sudden unbalance load $Wx=Mg+M\ u\ \omega^2 \cos(\omega t)$, $Wy=M\ u\ \omega^2 \sin(\omega t)$; u=25.4um

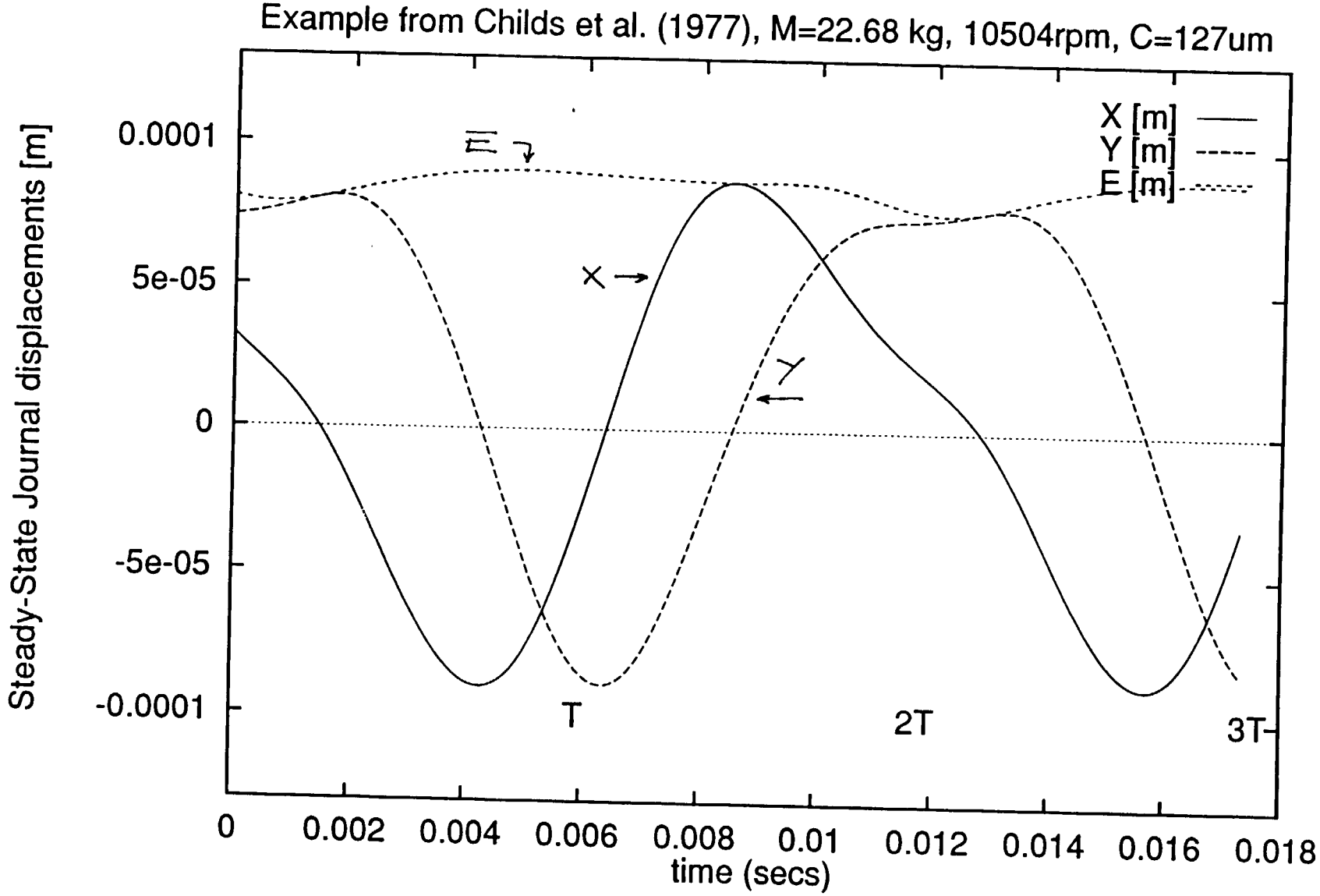

Figure 8. Journal displacements of Rigid Rotor on Cylindrical Journal Bearings. Sudden unbalance load
$Wx=Mg+M\ u\ \omega^2 \cos(\omega t)$, $Wy=M\ u\ \omega^2 \sin(\omega t)$; u=25.4um

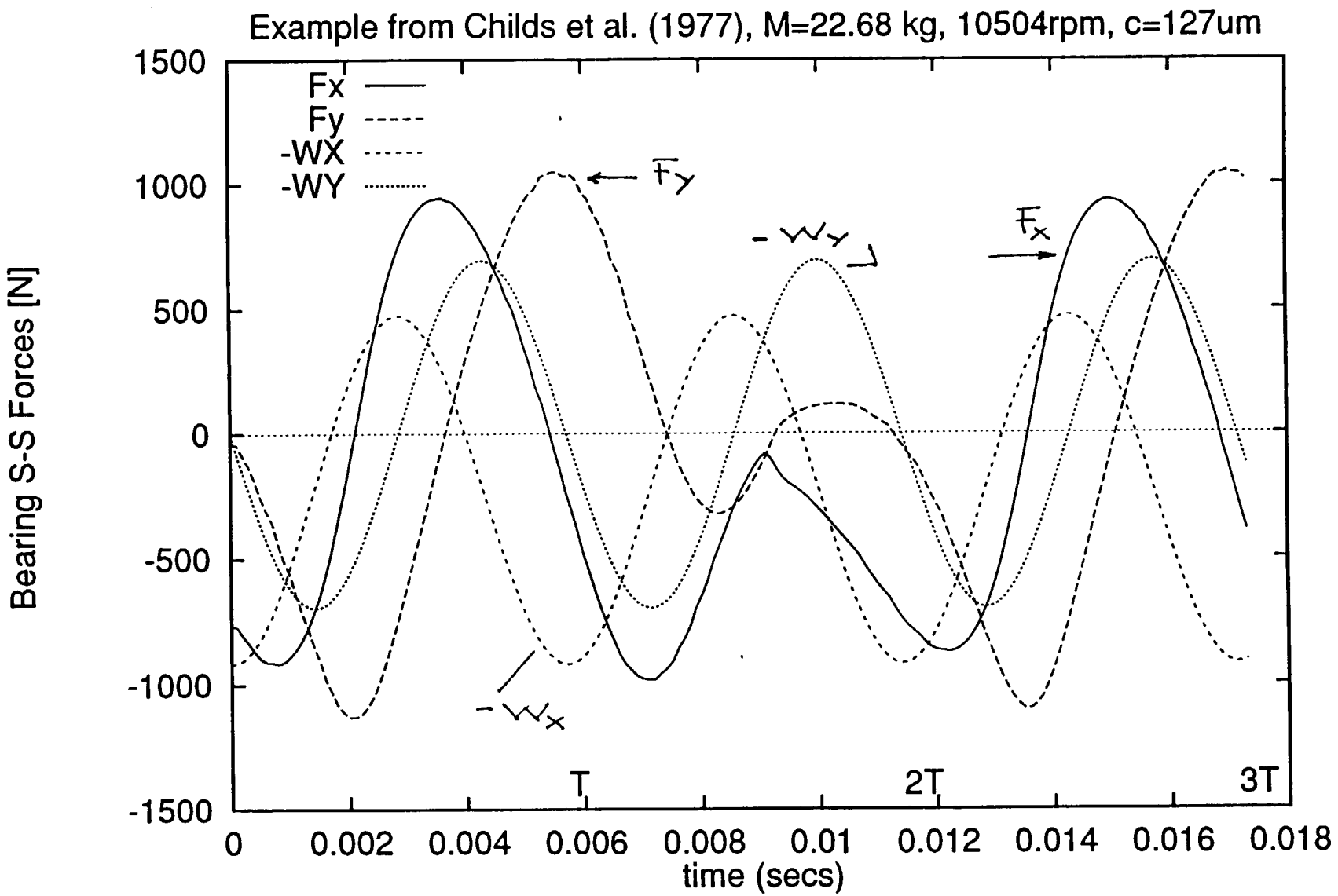

Figure 9. S–S fluid film forces for transient response.
Sudden unbalance load Wx=Mg+M u ω^2 cos(ωt),
Wy=M u ω^2 sin(ωt); u=25.4um

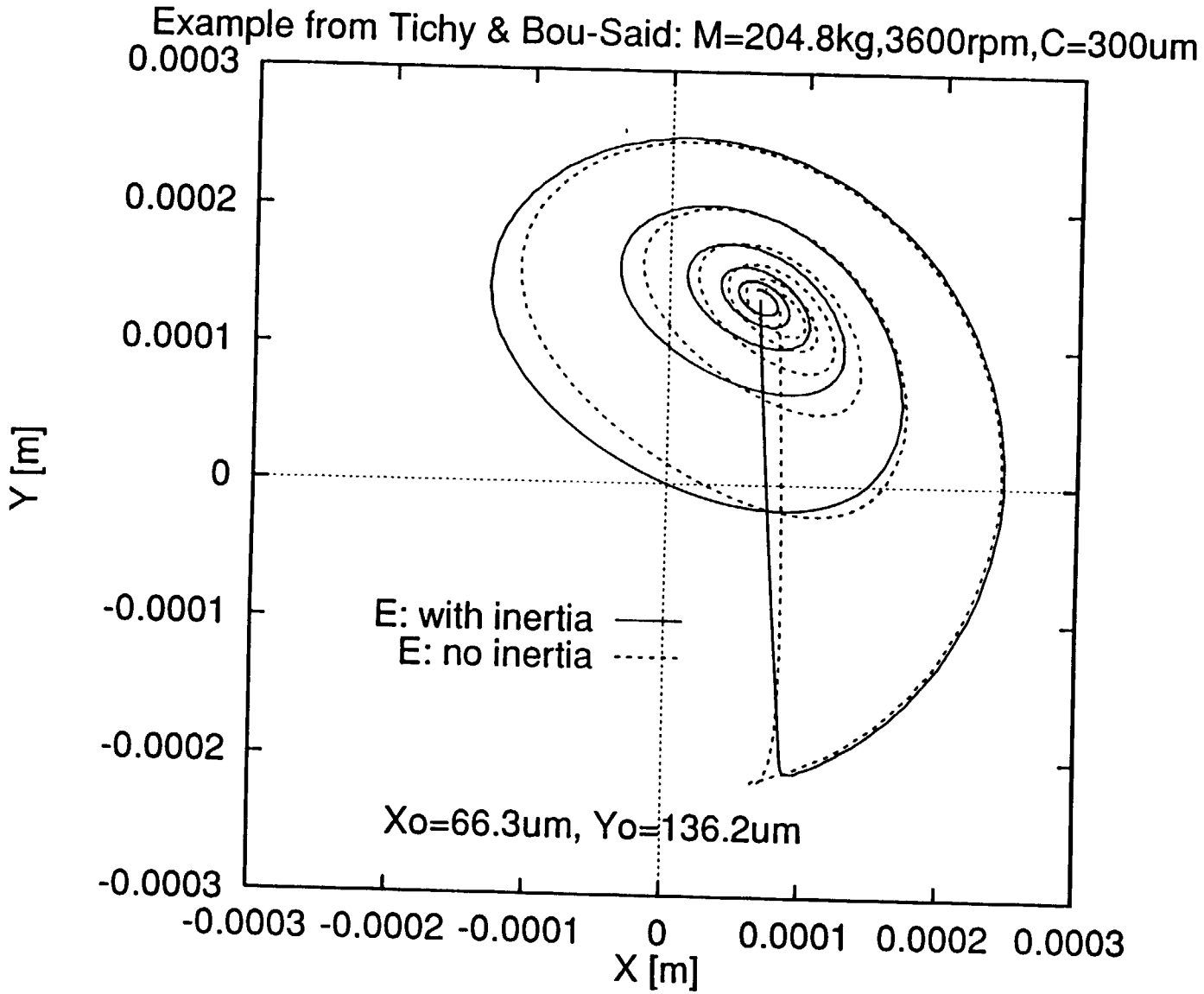

Figure 10 Effect of fluid inertia on transient response
Impulsive load Wx=M.g=2KN, Wy=-20KN over 2.77msec;

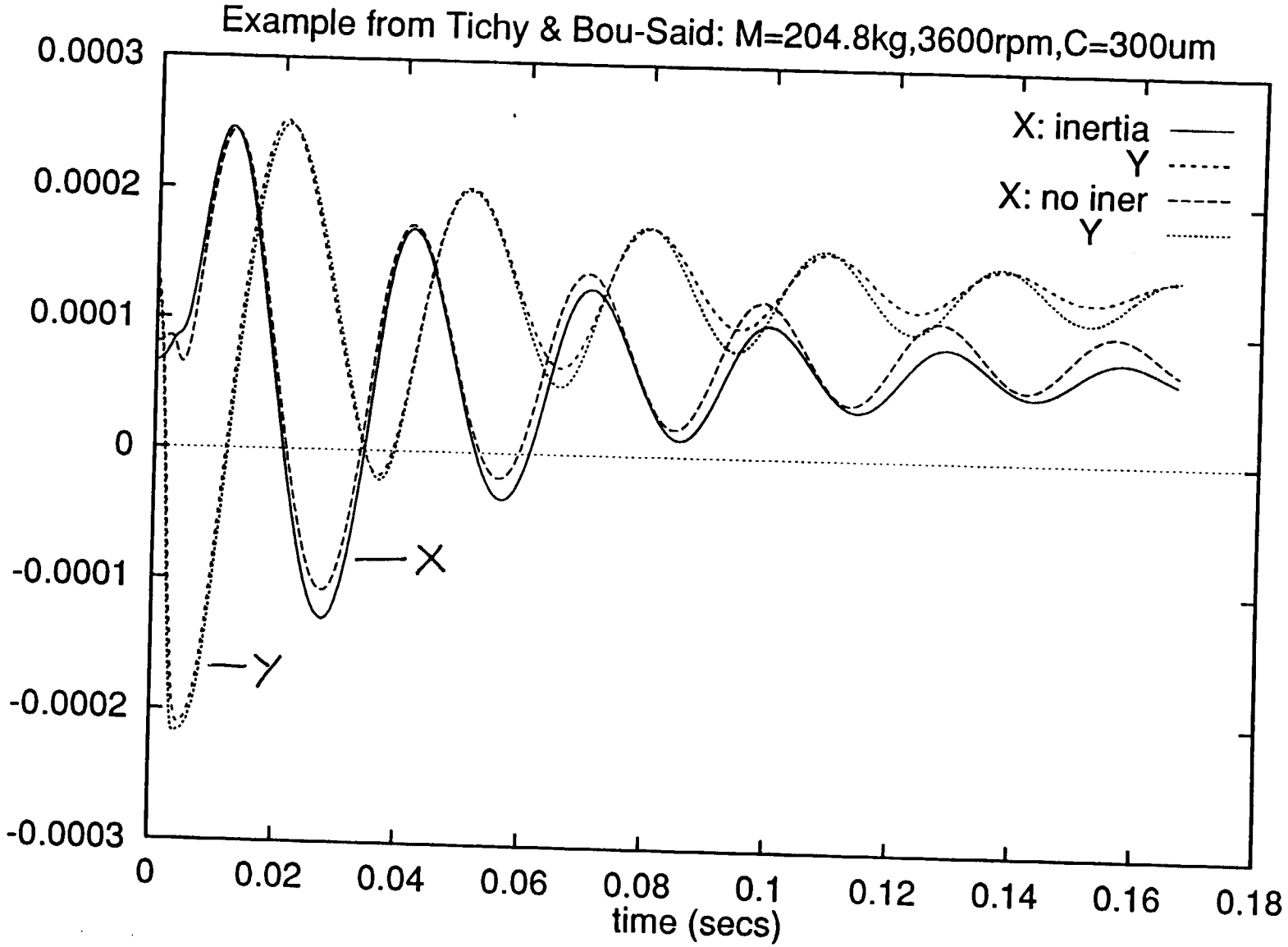

Figure 11. Journal displacements with and without fluid inertia
Impulsive load Wx=M.g=2KN, Wy=-20KN over 2.77msec;

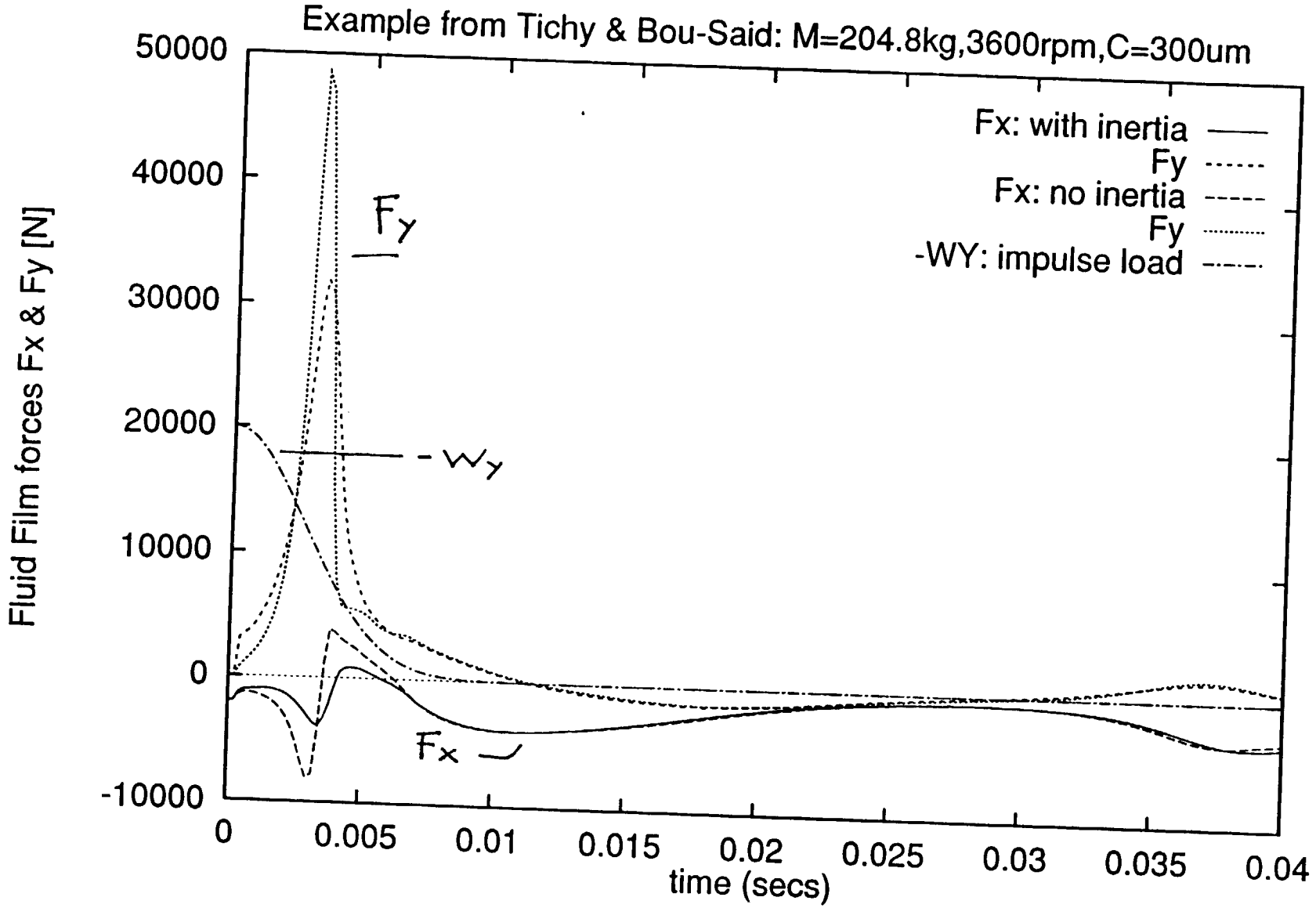

Figure 12. Bearing forces with and without fluid inertia
Impulsive load Wx=M.g=2KN, Wy=-20KN over 2.77msec;

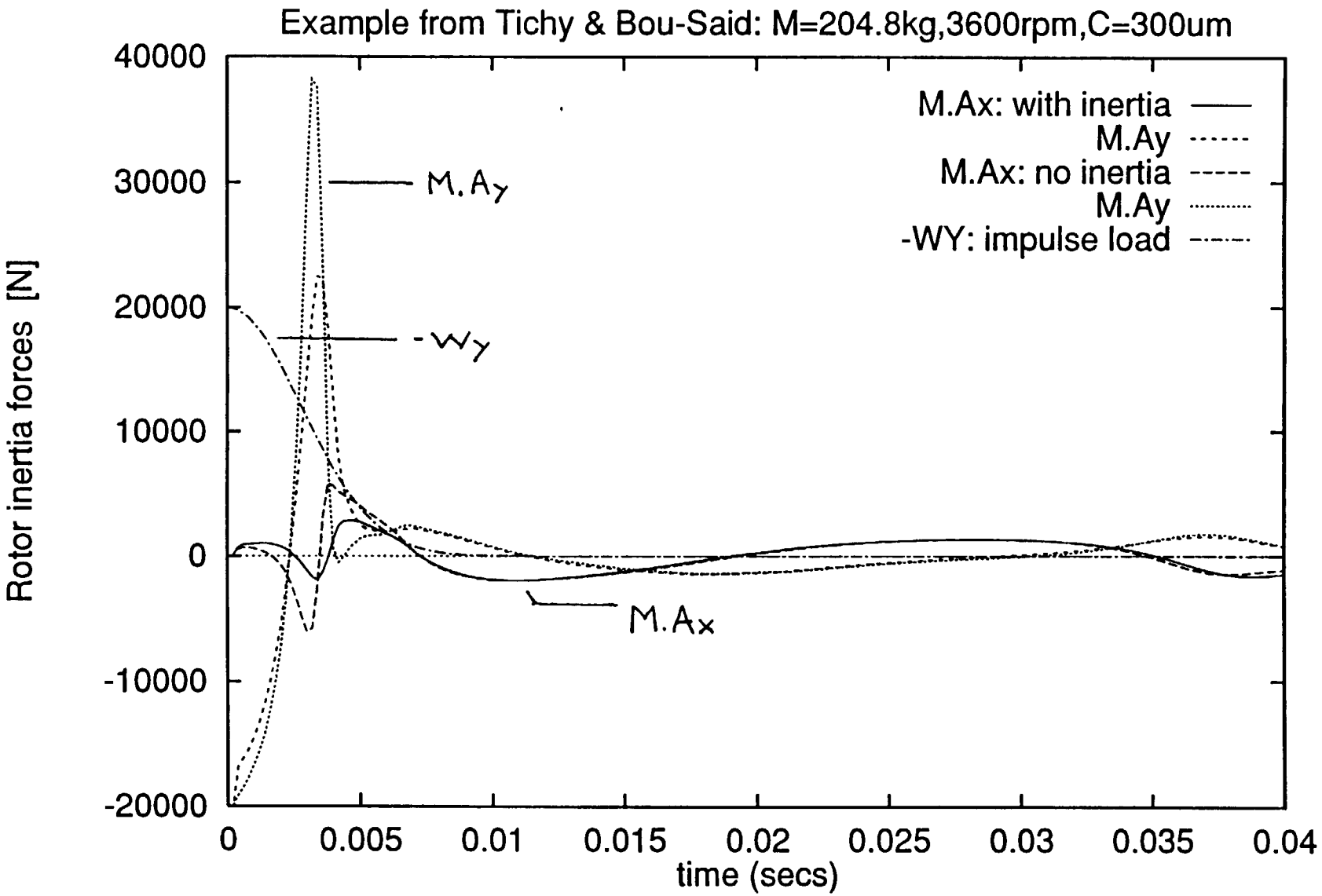

Figure 13. Rotor Inertia forces with and without fluid inertia
Impulsive load Wx=M.g=2KN, Wy=-20KN over 2.77msec;

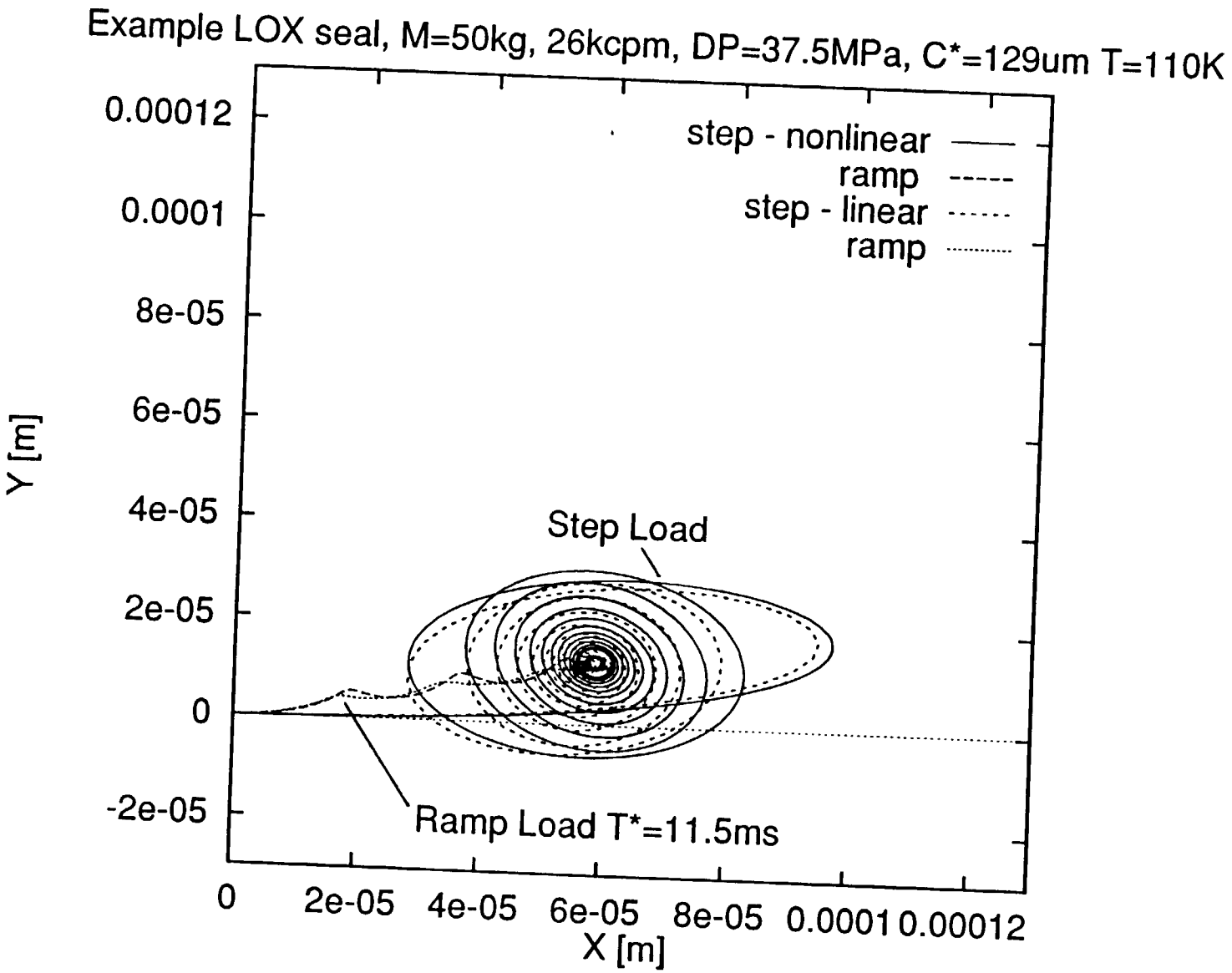

Figure 14. Transient seal locus due to ramp and step loads.
Static load Wx=10,000 N, Wy=0 N.

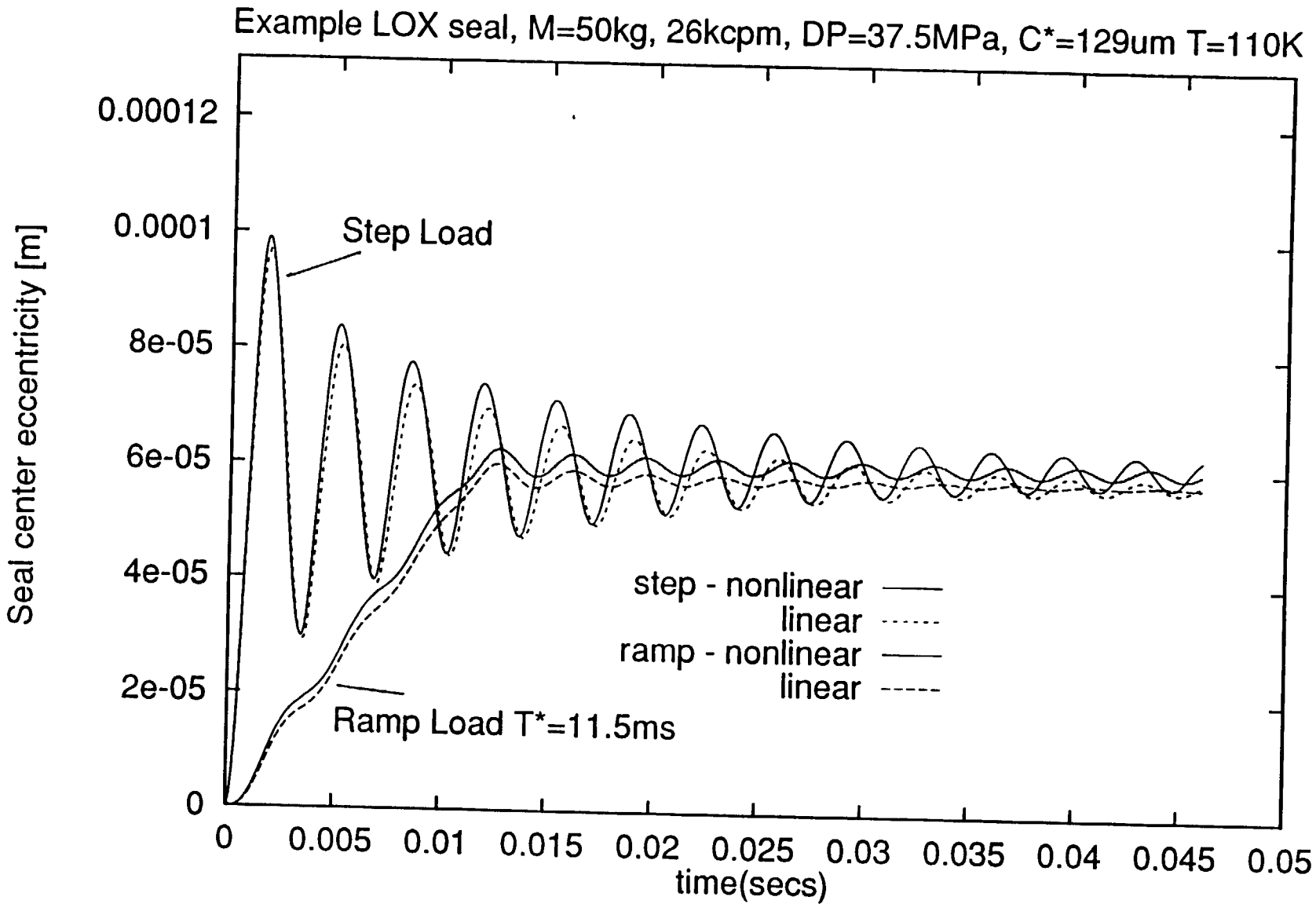

Figure 15. Transient LOX seal eccentricity due to step and ramp loads. Static load Wx=10,000 N, Wy=0 N.

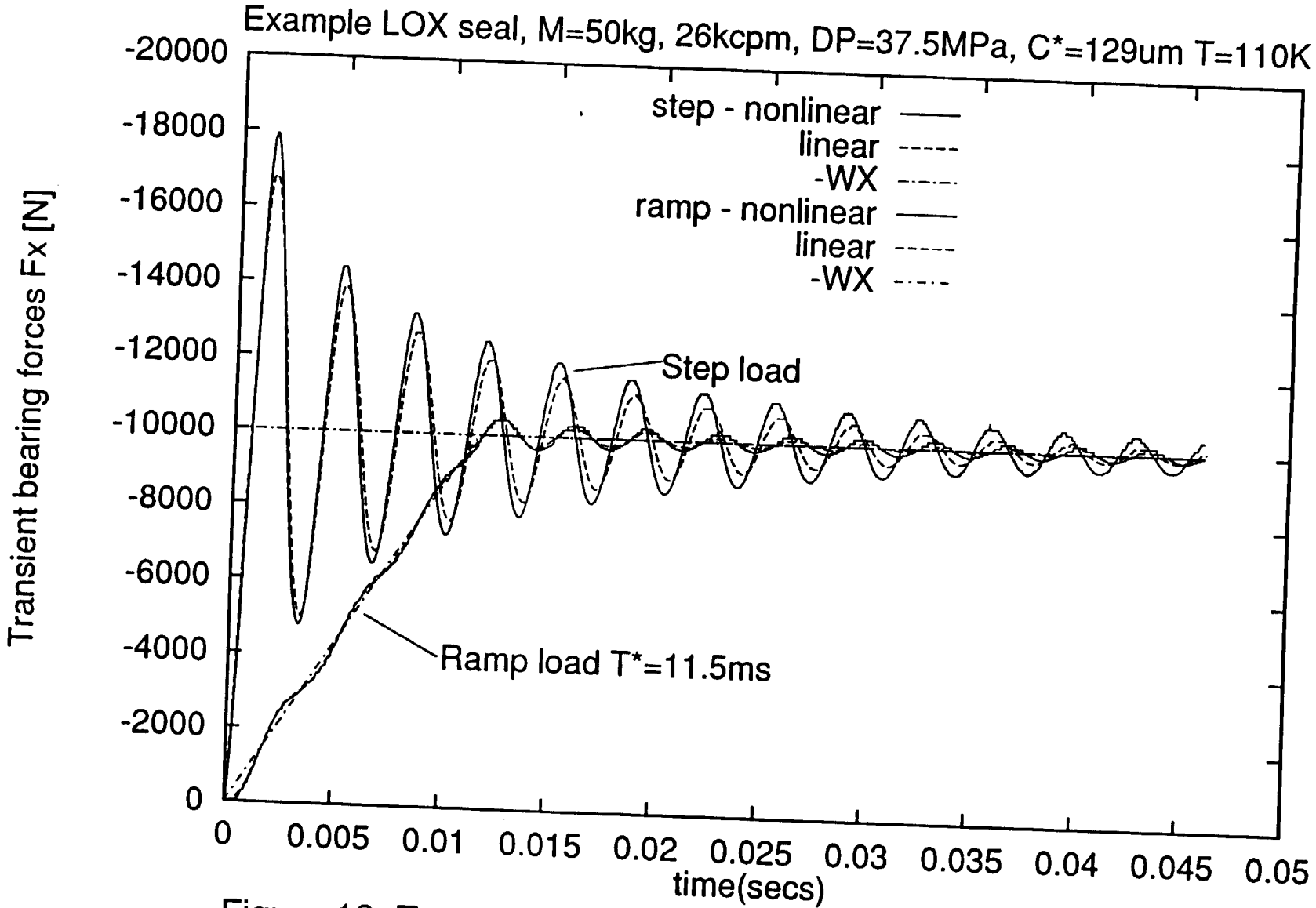

Figure 16. Transient bearing force Fx due to step and ramp loads. Static load Wx=10,000 N, Wy=0 N.

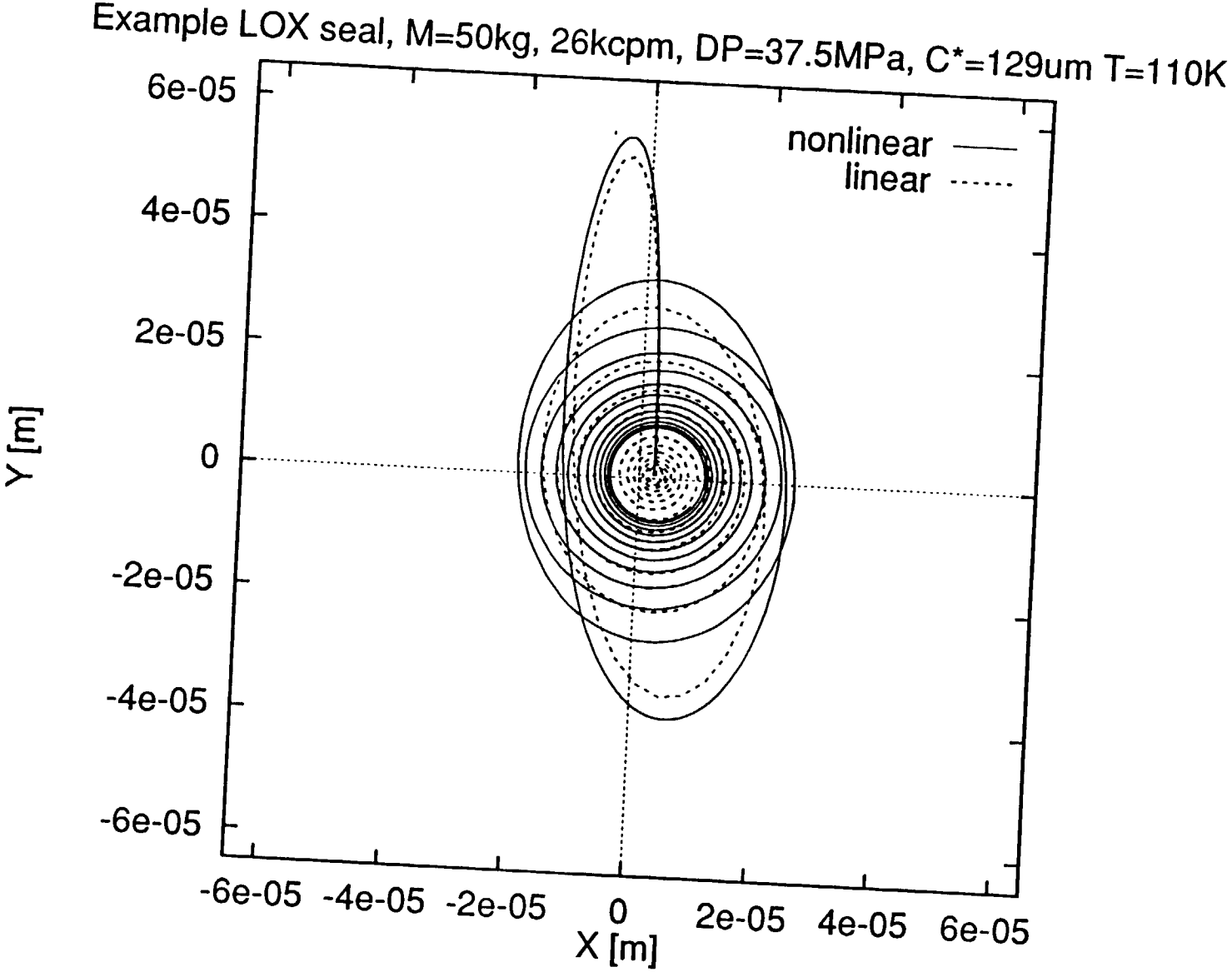

Figure 17. Transient seal center locus due to impulsive load

Wx=M.g=490N, Wy=10KN (impulse), to=0.57ms

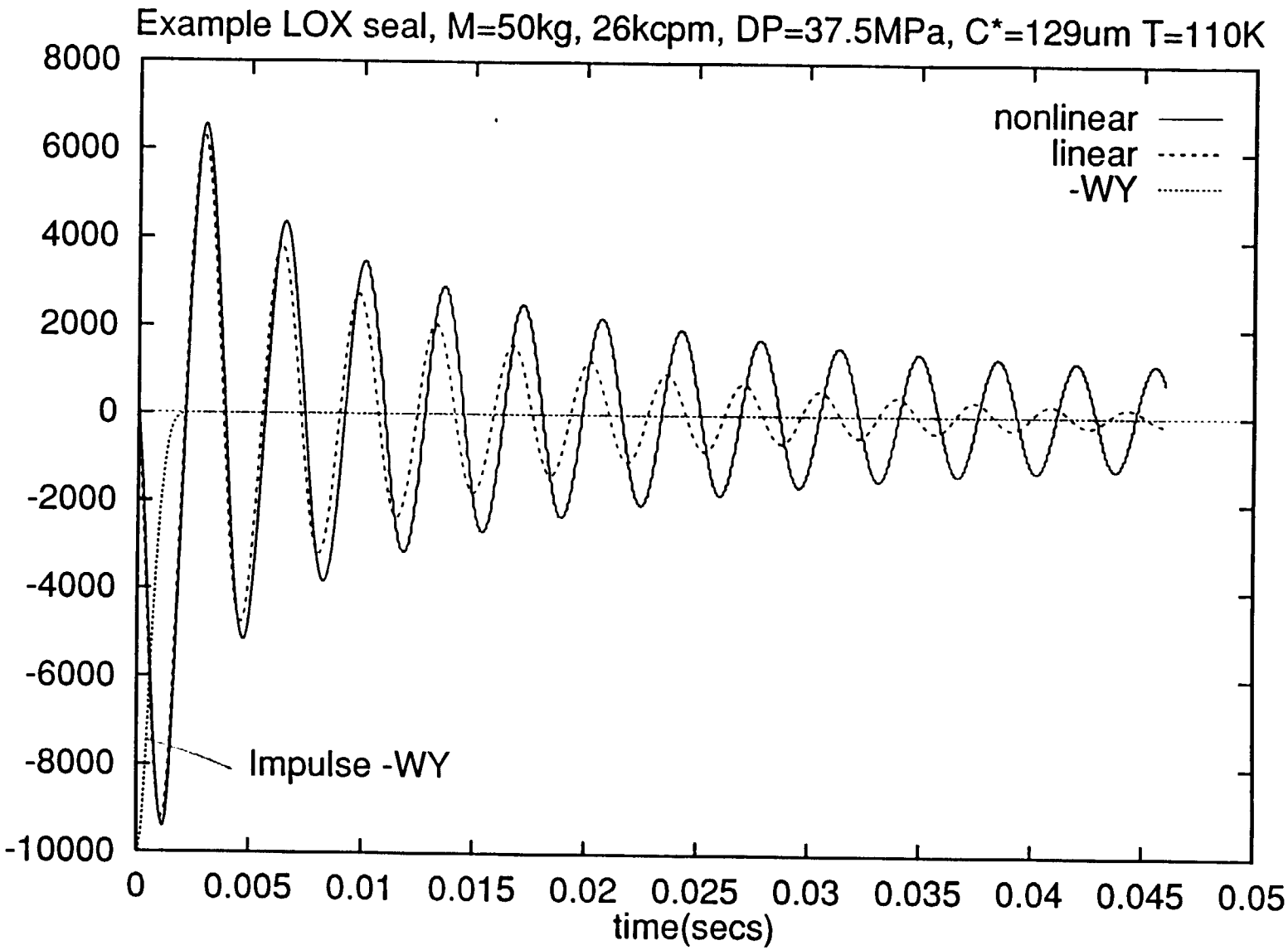

Figure 18. Transient seal force Fy due to impulse load Wy.
Wx=M.g=490 N, Wy=10 kN (impulse), to=0.57 ms.

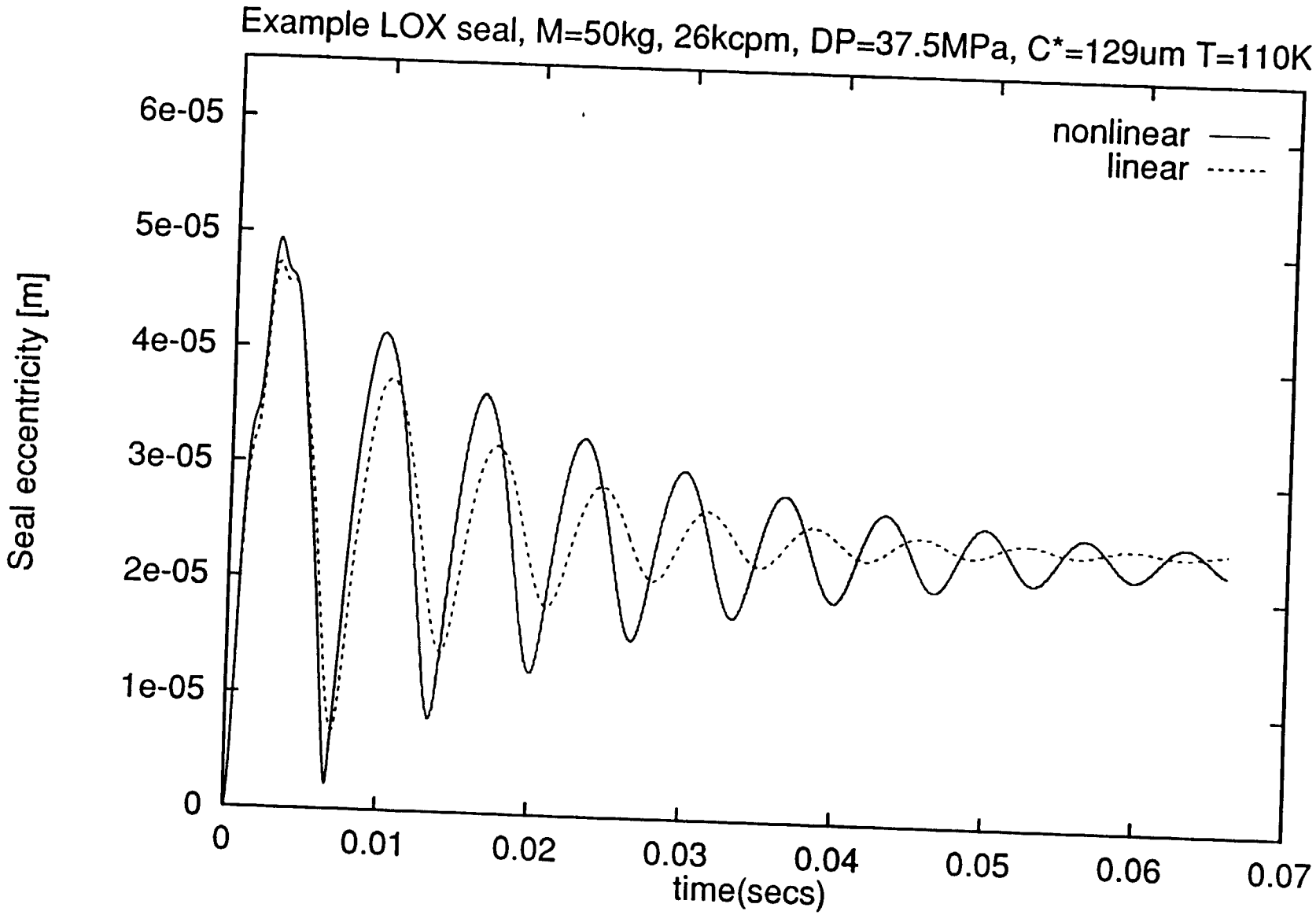

Figure 19. Transient seal eccentricity due to periodic load.
Load 5 KN synchronous (433.3 Hz).

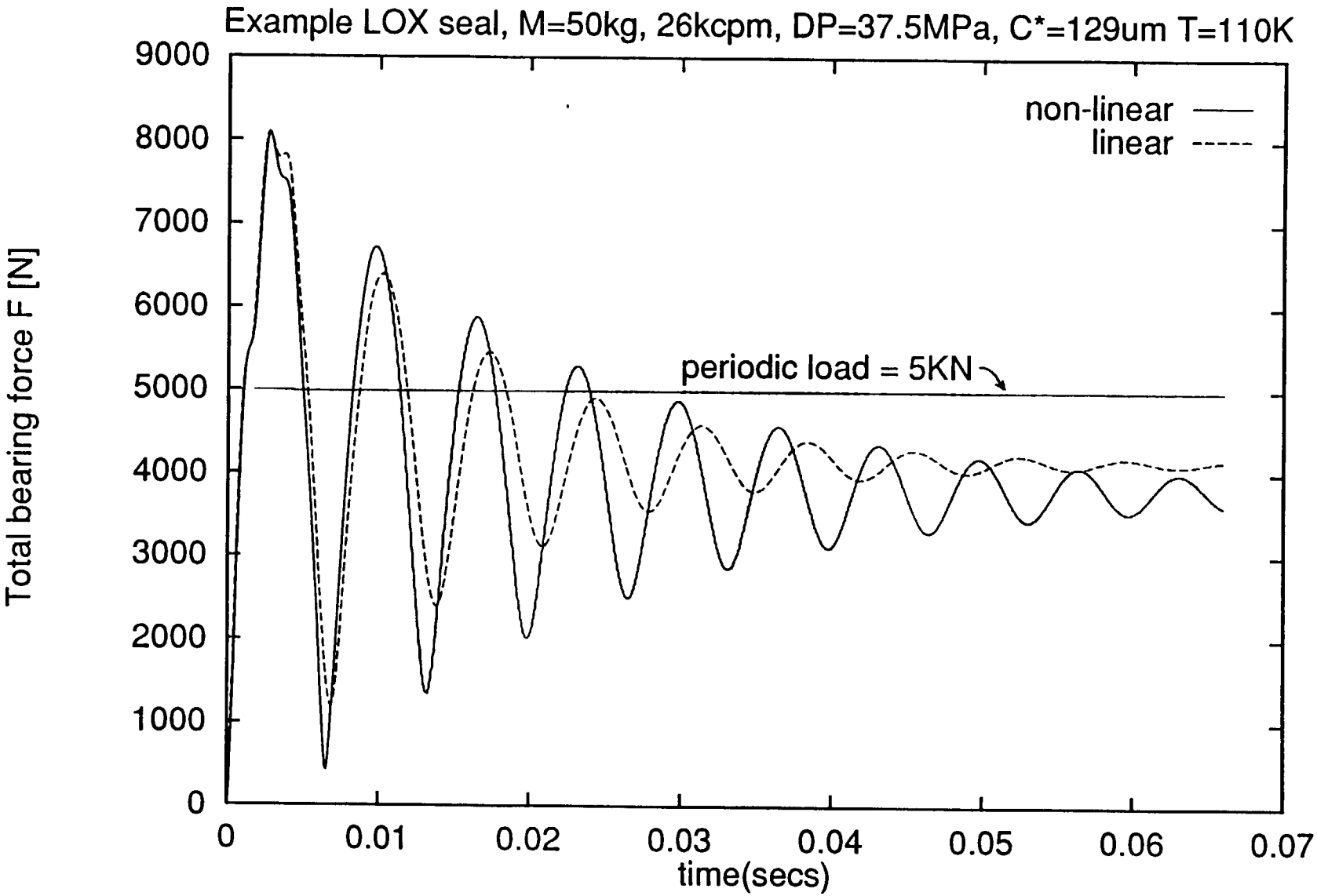

Figure 20. Transient bearing force due to periodic load
Load 5KN synchronous (433.3 Hz)

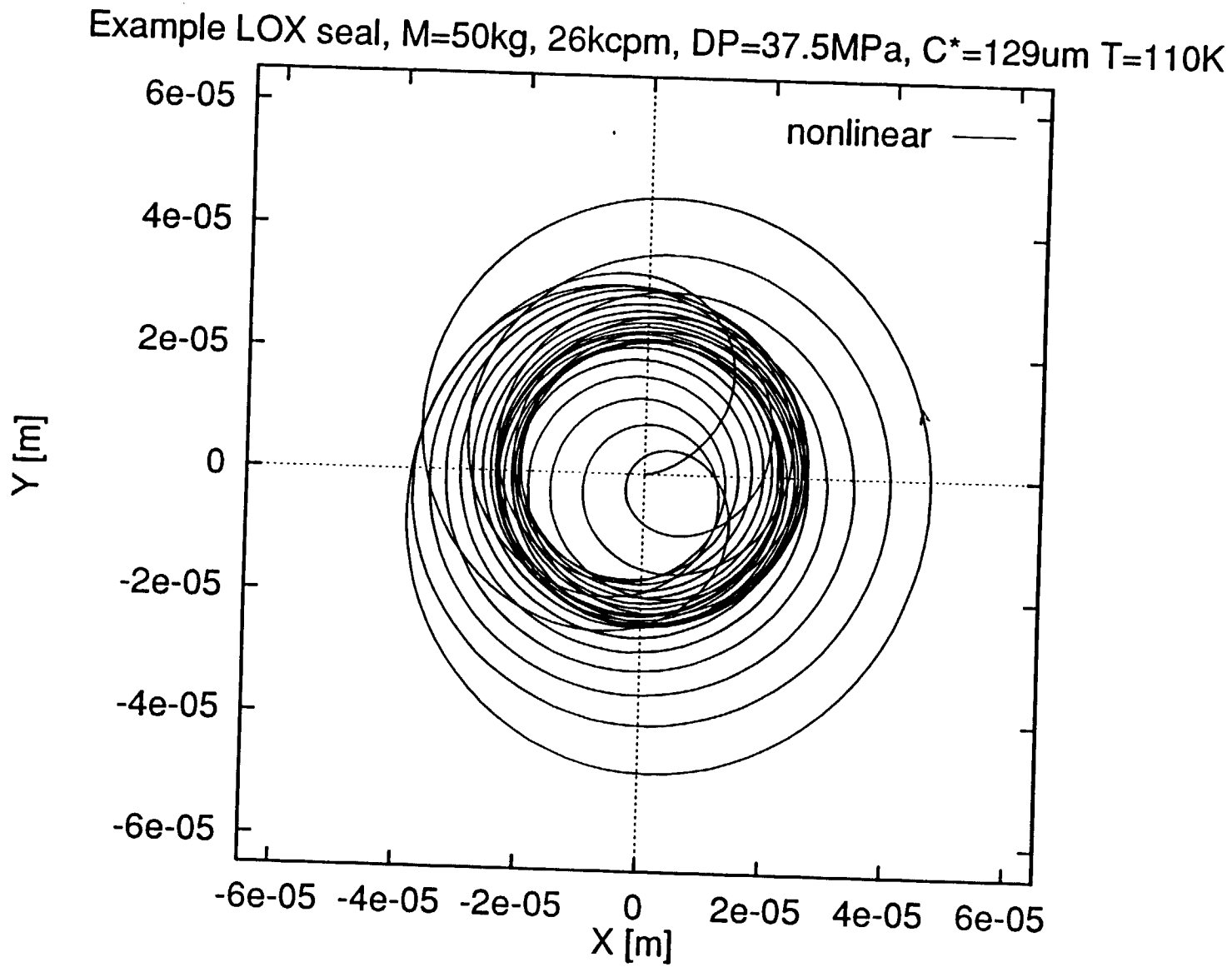

Figure 21. Transient seal center locus due to periodic load

Load 5KN synchronous (433.3 Hz)

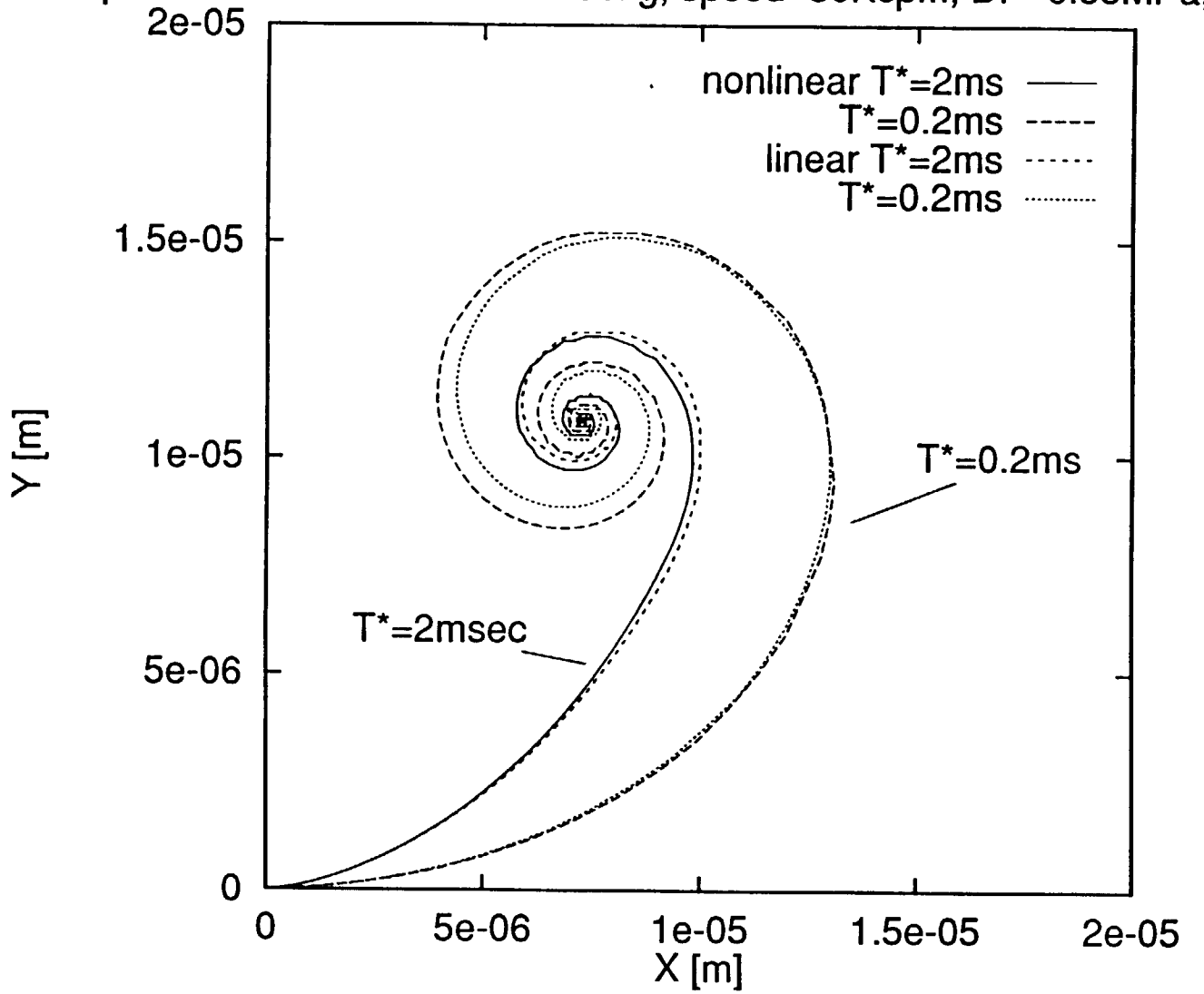

Figure 22. Transient HJB journal center locus due to ramp loads.
Load Wx=5 (t/T*) KN, T*=2 msec, 0.2 msec, Wy=0 N.

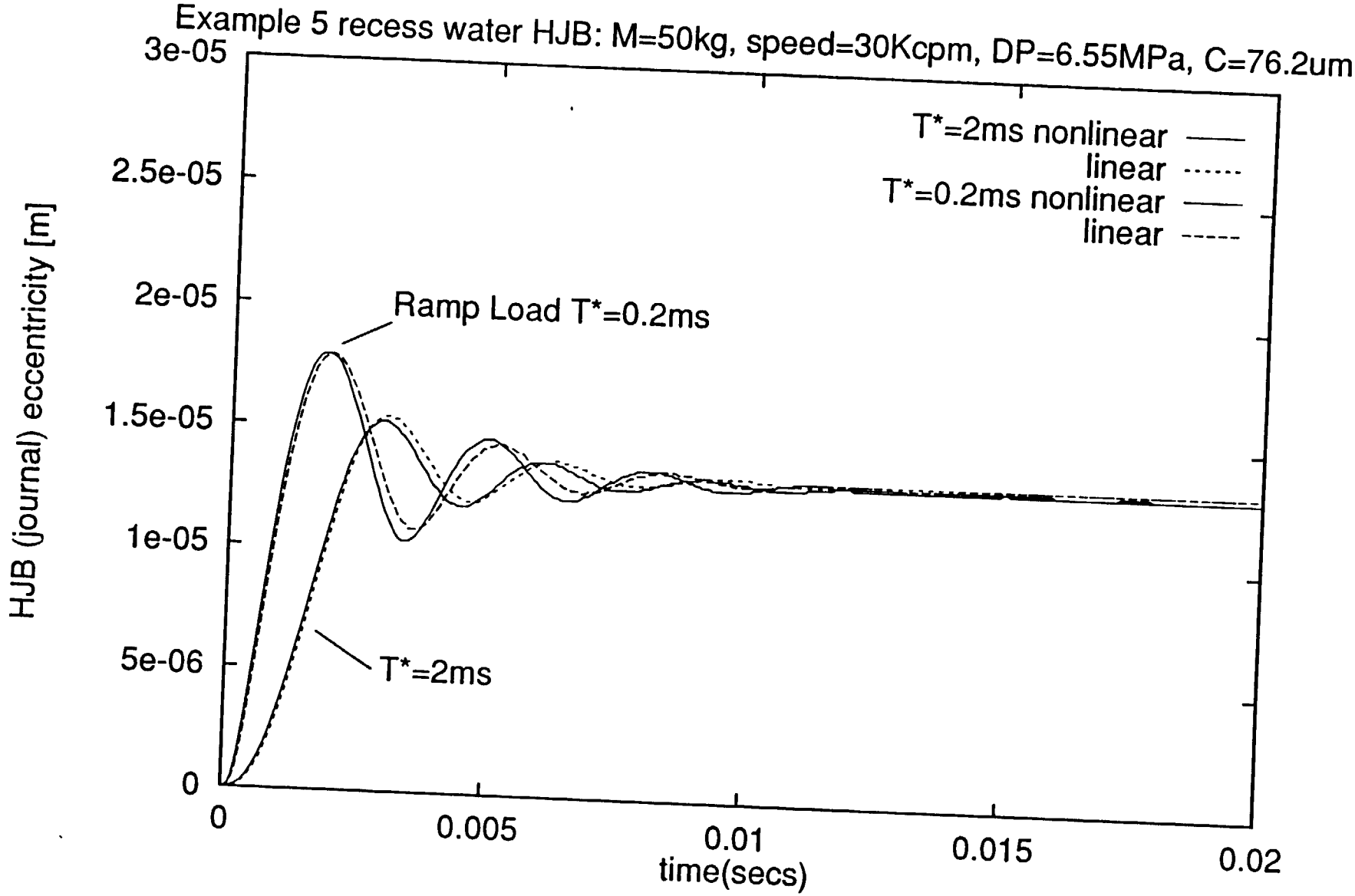

Figure 23. HJB journal eccentricity for ramp loads.
Load Wx=5 (t/T*) KN, T*=2 msec, 0.2 msec, Wy=0 N.

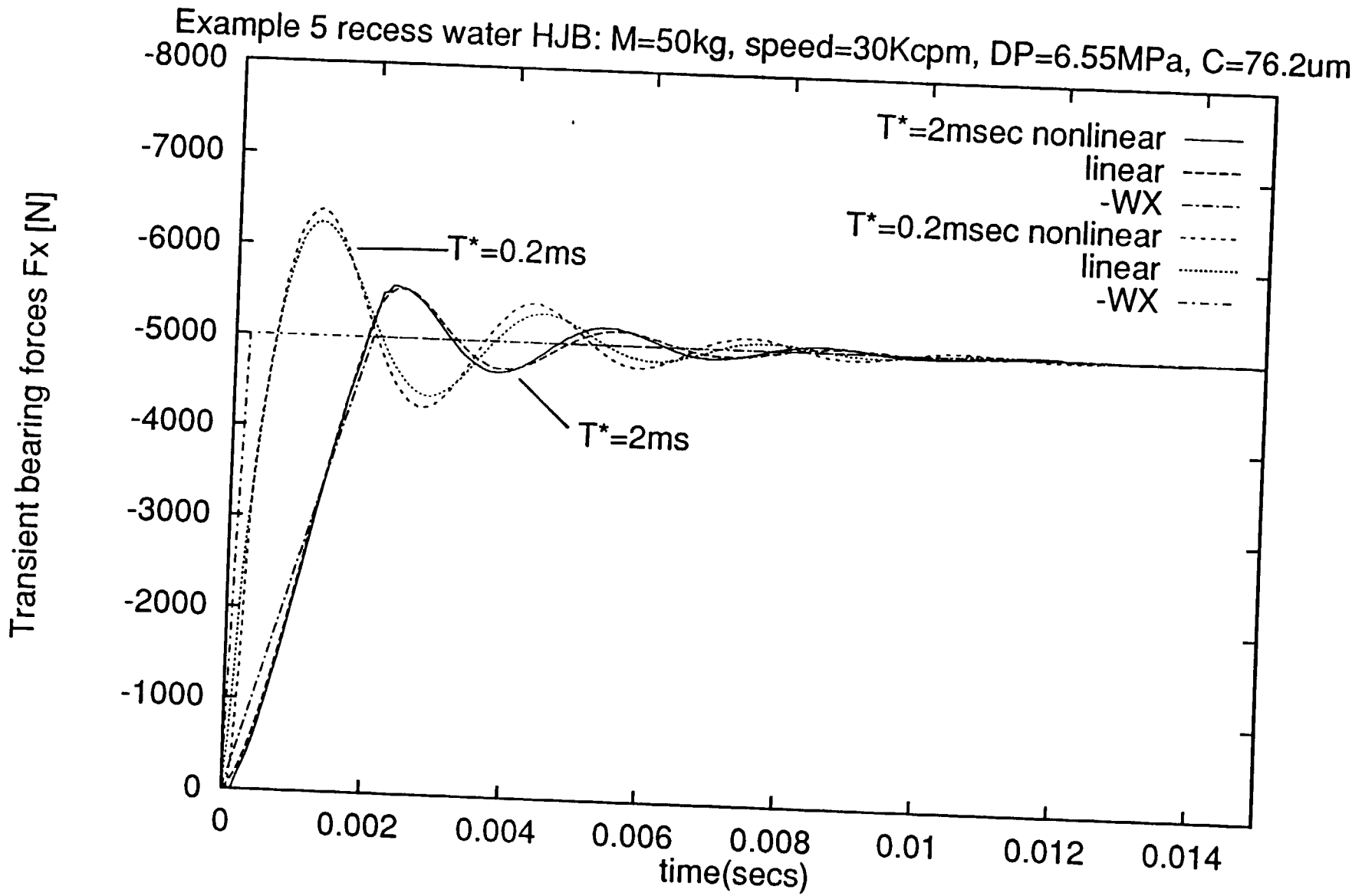

Figure 24. Transient bearing force Fx due to ramp loads.
ramp load Wx=5 KN (t/T*), T*=2 msec, 0.2 msec, Wy=0 N

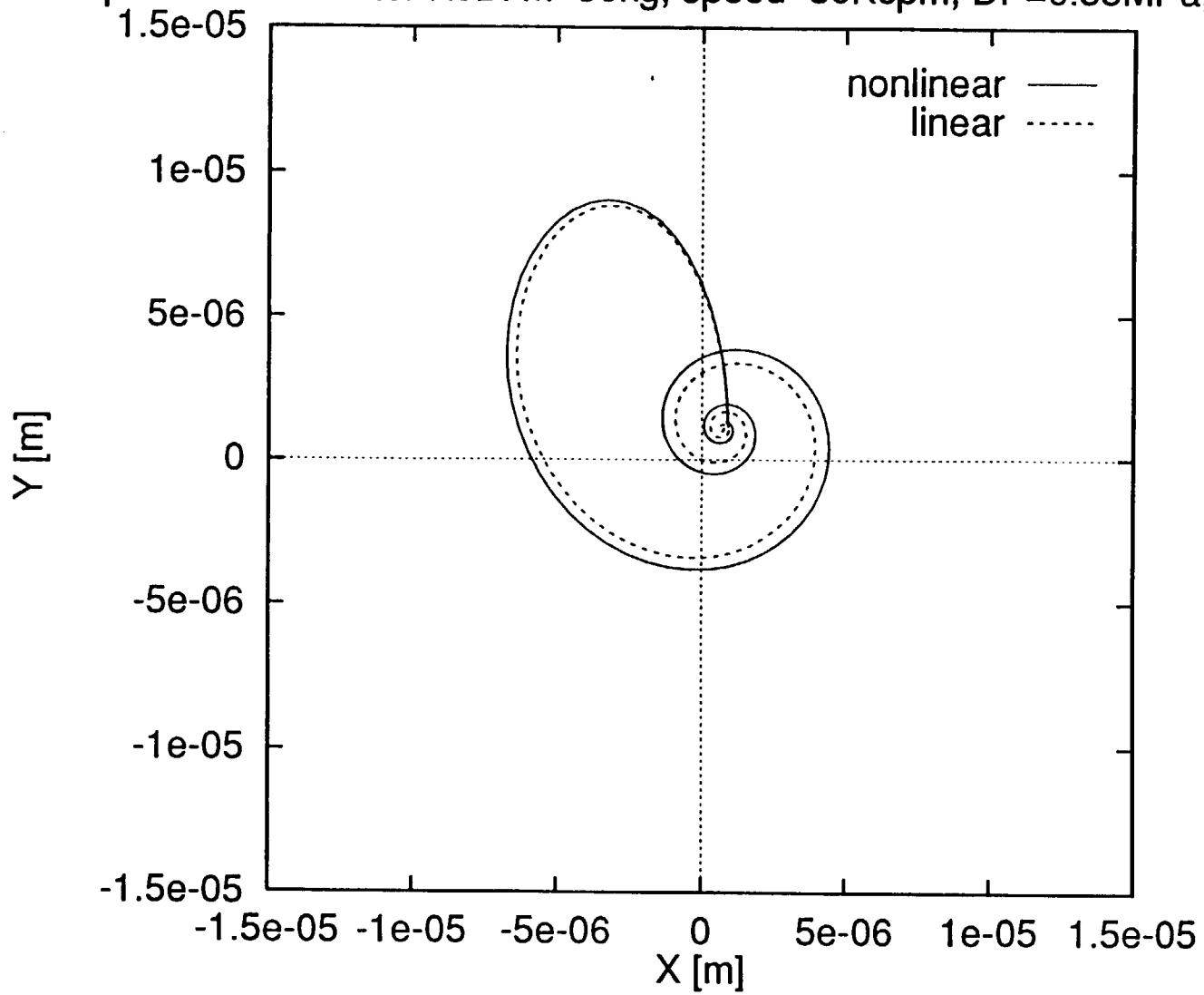

Figure 25. Transient journal locus due to impulsive load

Wx=M.g=490N, Wy=5kN exp(-t/to), to=0.5ms

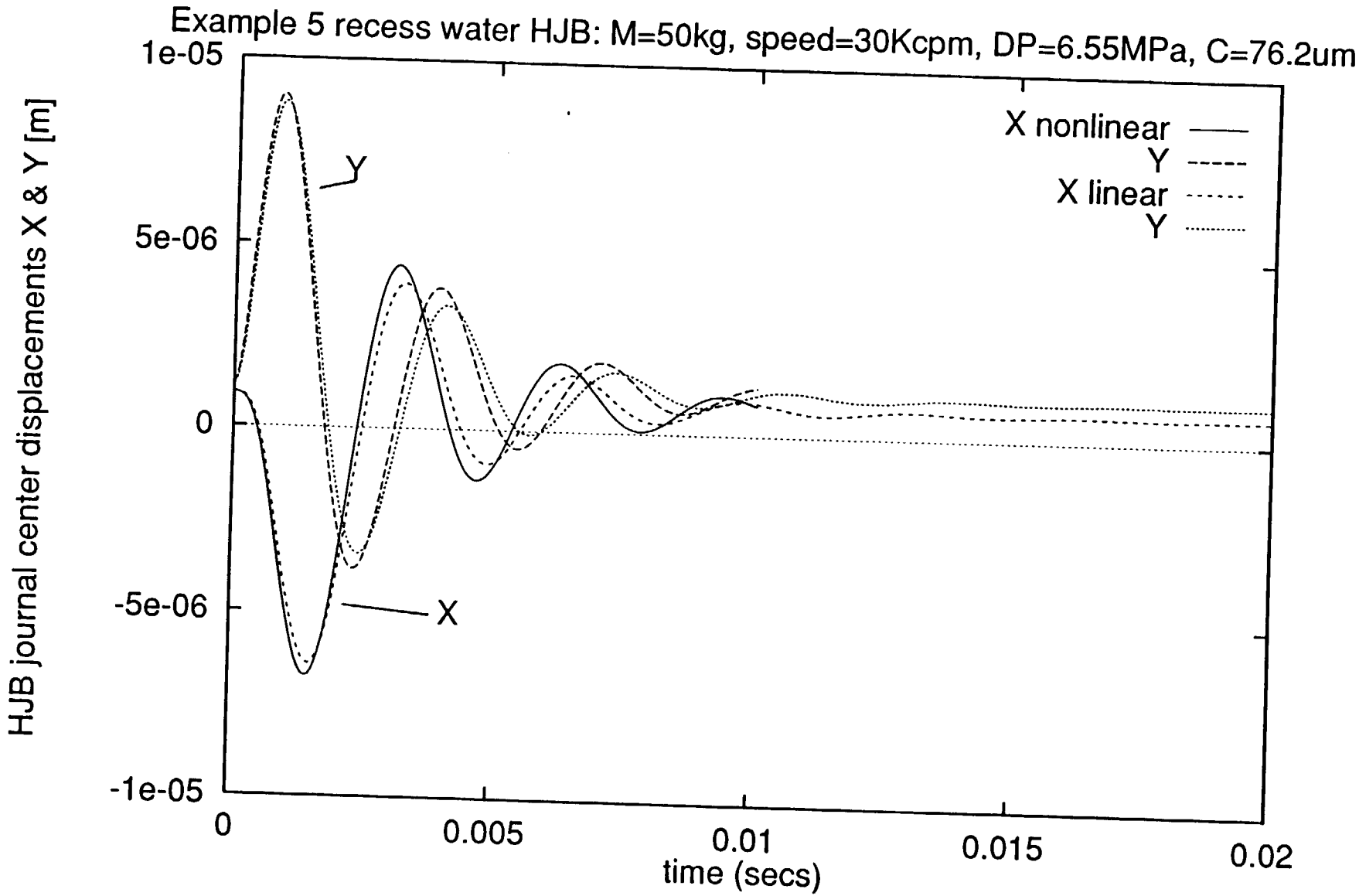

Figure 26. Transient journal center displacements for impulse load
WX=M.g=490N, WY=5kN exp(-t/to), to=0.5msec

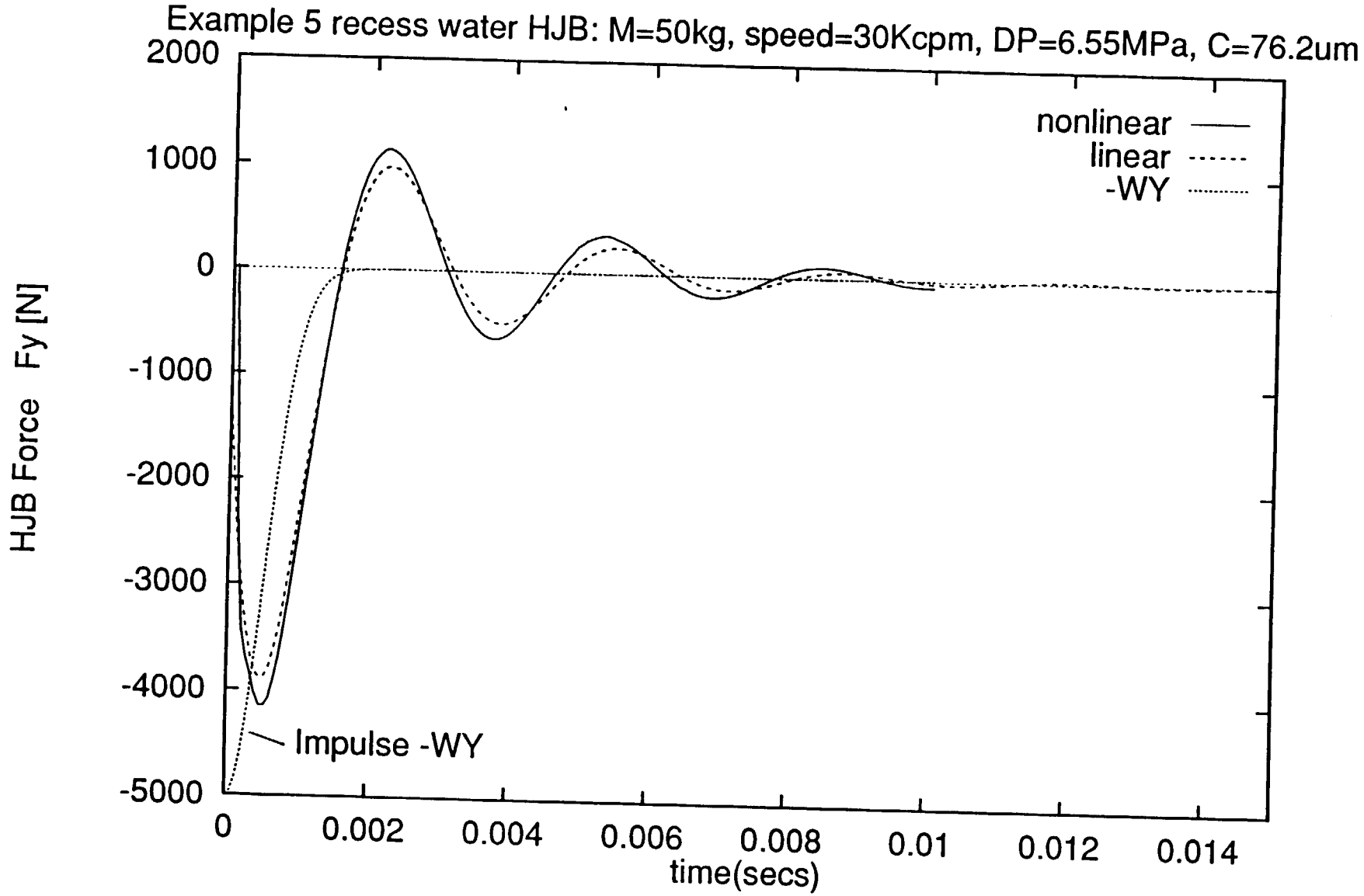

Figure 27. Transient HJB force Fy due to impulsive load Wy.
Wx=M.g=490 N, Wy=5 exp(−t/to) KN, to=0.5 ms.

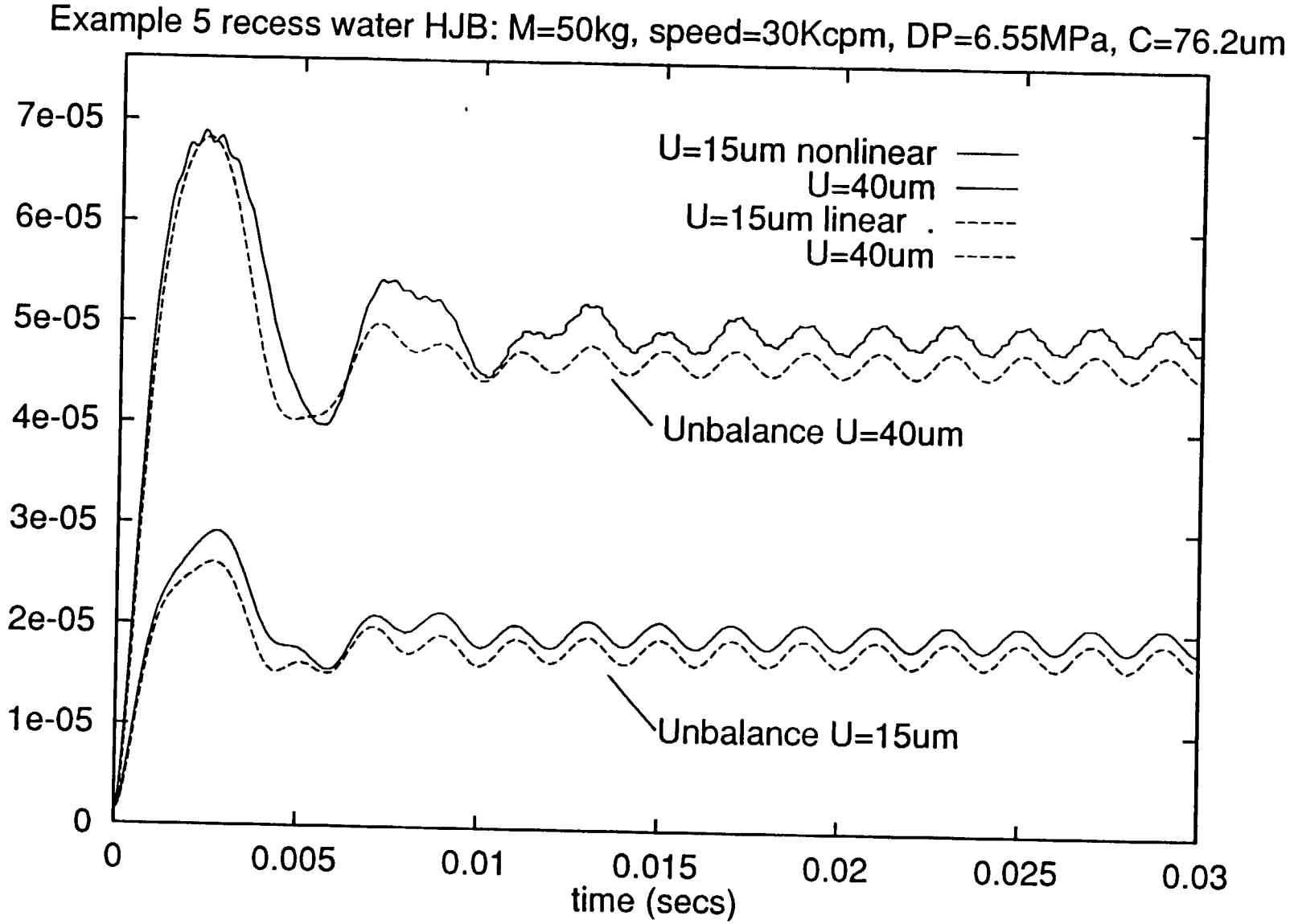

Figure 28. HJB journal eccentricity for unbalance load.
$W_x = Mg + M.U.\omega^2 \cos(\omega t)$, $W_y = M.U.\omega^2 \sin(\omega t)$, U varies.

Example 5 recess water HJB: M=50kg, speed=30Kcpm, DP=6.55MPa, C=76.2um

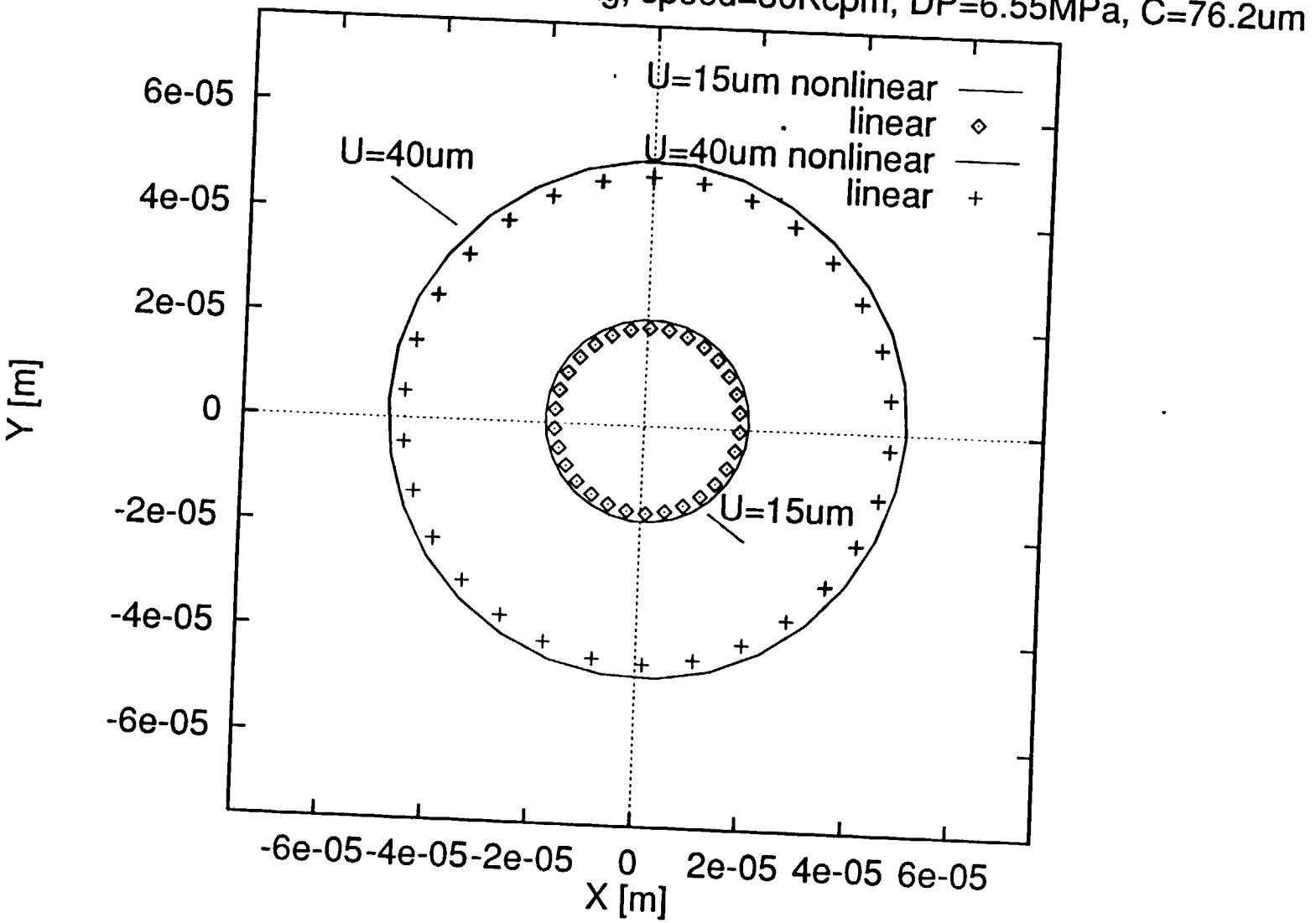

Figure 29. HJB steady state orbit for umbalance load.
$Wx=Mg+M.U.\omega^2 \cos(\omega t)$, $Wy=M.U.\omega^2 \sin(\omega t)$, U varies.

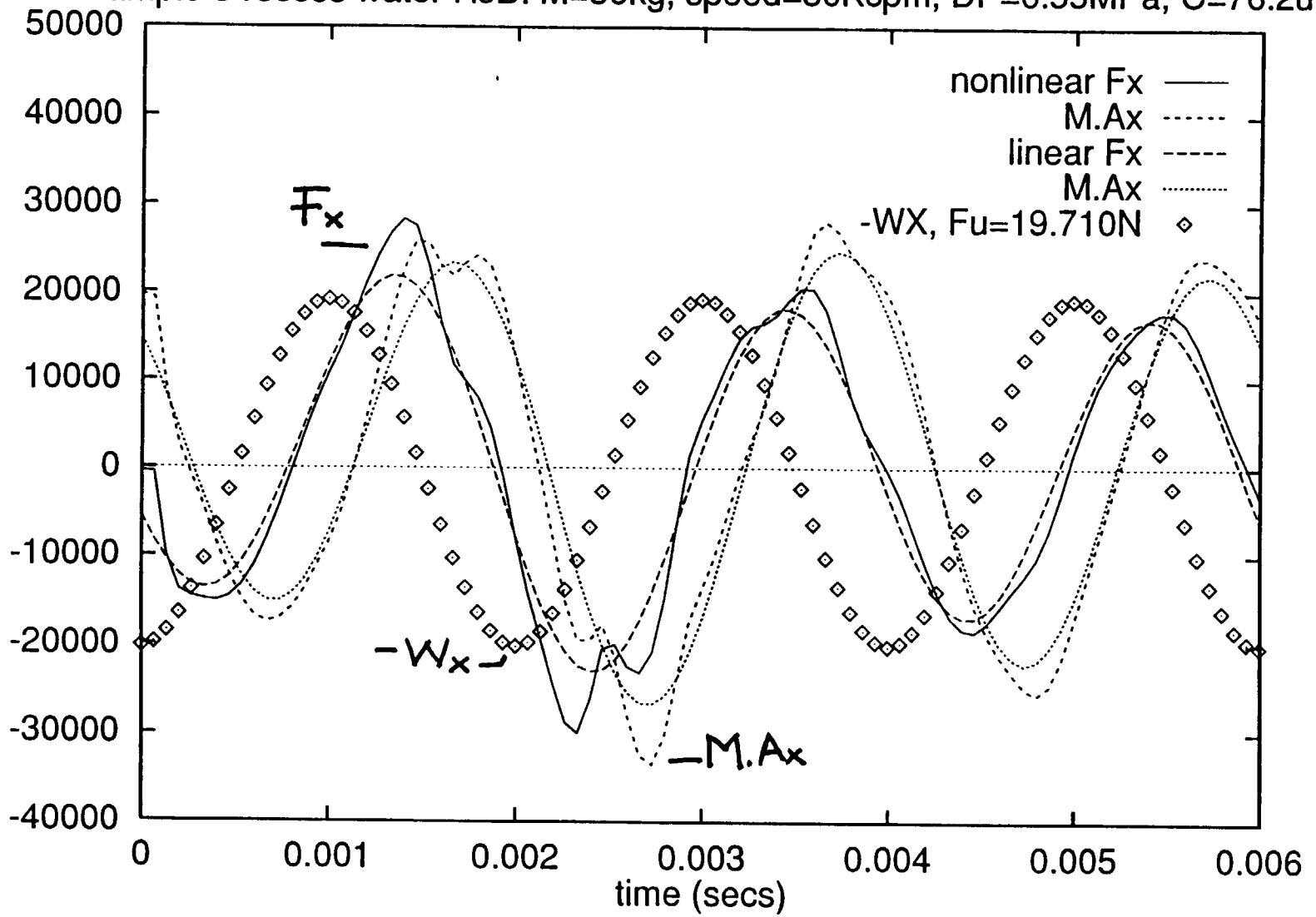

Figure 30. Initial X-forces for unbalance U=40um, Funb=19.71kN

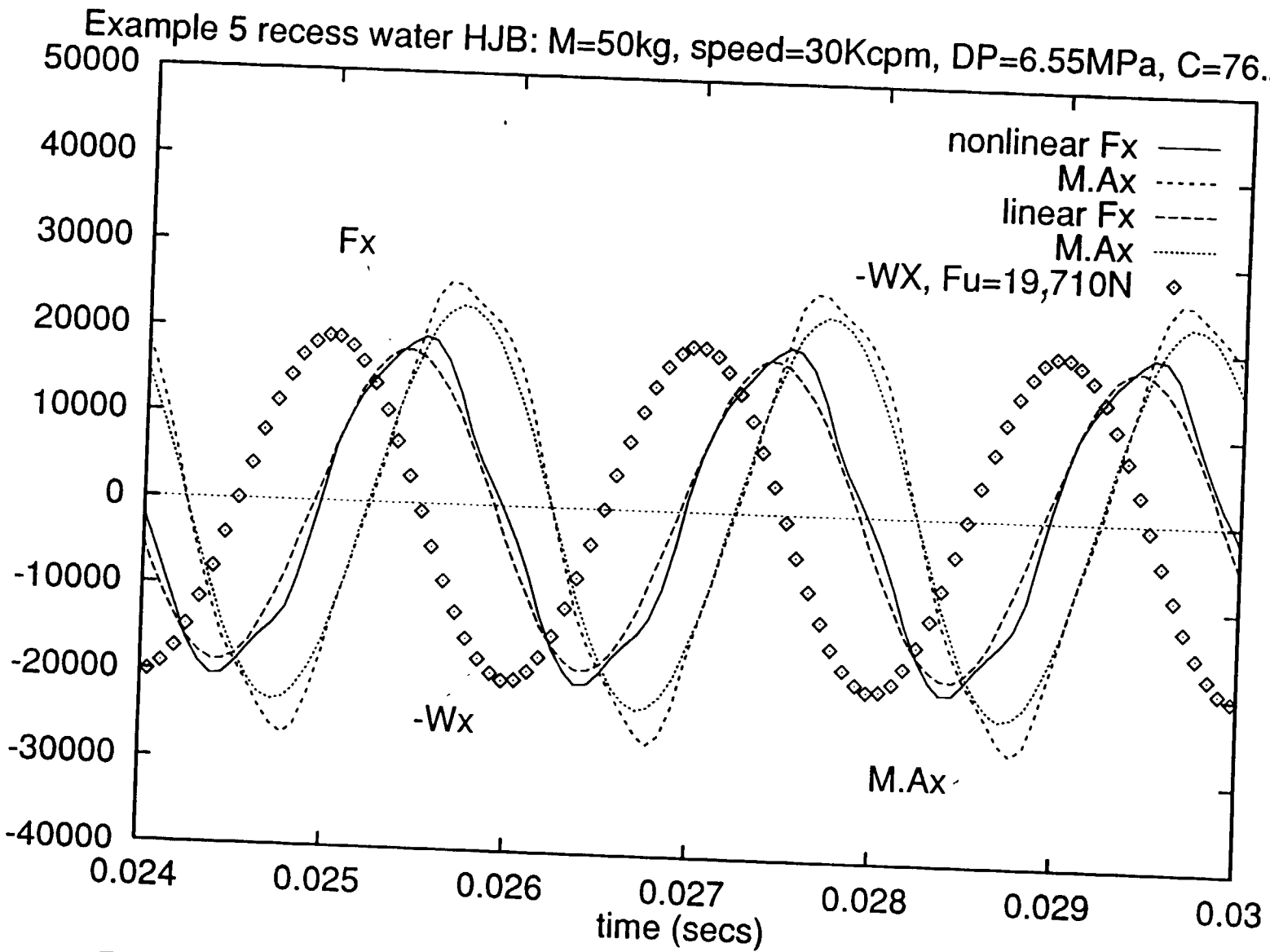

Figure 31. Steady-state X-forces for unbalance U=40um, Funb=19.71kN

Appendix A. Numerical Evaluation of Unsteady Bulk-Flow in Fluid Film Bearings.

Consider the unsteady flow in the thin film lands of a fluid film bearing and governed by the following **bulk-flow equations** (Yang, 1992):
Continuity:

$$\frac{\partial}{\partial x_i}(\rho H U_i) + \frac{\partial}{\partial t}(\rho H) = 0 \tag{1}$$

Momentum:

$$-H\frac{\partial P}{\partial x_i} = \frac{\left(k_i U_i - k_J \frac{\overline{\Lambda}_j}{2}\right)\mu}{H} + \frac{\partial}{\partial t}(\rho H U_i) + \frac{\partial}{\partial x_j}(\rho H U_i U_j) \tag{2}$$

Energy:

$$C_P\left[\frac{\partial}{\partial \tau}(\rho H T) + \frac{\partial}{\partial X_i}(\rho H U_i T)\right] + Q_s = \beta_t H T\left(\frac{\partial P}{\partial t} + U_i\frac{\partial P}{\partial X_i}\right) + \Omega R\frac{H}{2}\frac{\partial P}{\partial X} + \frac{\mu}{H}\left[k_x\left(U_x^2 + U_y^2 + \frac{\Omega R U_x}{2}\right) + k_J\left(\frac{\Omega^2 R^2}{4} - U_x \Omega R\right)\right] \tag{3}$$

where i,j=x,y. circumferential and axial coordinates.
$\overline{\Lambda}_x=\Omega R$; $\overline{\Lambda}_y=0$, journal surface speeds.
k_i, k_J, turbulent shear parameters; and fluid parameters
$C_p=C_p(P,T)$; $\beta_t=\beta_t(P,T)$,
$\rho=\rho(P,T)$; $\mu=\mu(P,T)$
with $Q_s=h_B(T-T_B)+h_J(T-T_J)$ as the heat flow through the bearing and journal surfaces.

The film thickness is typically given as:

$$H = c(x,y) + X(t)\cos\theta + Y(t)\sin\theta \tag{4}$$

where X(t) and Y(t)are time dependent journal center displacements

Dimensionless equations of motion are given as:
Continuity:

$$\frac{\partial}{\partial x}(\overline{\rho} h u_x) + \frac{\partial}{\partial y}(\overline{\rho} h u_y) + \sigma\frac{\partial}{\partial \tau}(\overline{\rho} h) = 0 \tag{5}$$

Circumferential-momentum:

$$-h\frac{\partial p}{\partial x} = \frac{(k_x u_x - k_j\frac{\Lambda}{2})\overline{\mu}}{h} + Re_s\frac{\partial}{\partial \tau}(\overline{\rho} h u_x) + Re_p^*\left[\frac{\partial}{\partial x}(\overline{\rho} h u_x^2) + \frac{\partial}{\partial y}(\overline{\rho} h u_x u_y)\right] \tag{6.a}$$

Axial-momentum:

$$-h\frac{\partial p}{\partial y} = \frac{(k_y u_y)\overline{\mu}}{h} + Re_s\frac{\partial}{\partial \tau}(\overline{\rho} h u_y) + Re_p^*\left[\frac{\partial}{\partial x}(\overline{\rho} h u_x u_y) + \frac{\partial}{\partial y}(\overline{\rho} h u_y^2)\right] \tag{6.b}$$

where,

$\bar{\rho}=\rho/\rho_*$; $\bar{\mu}=\mu/\mu_*$; $x=X/R$; $y=Y/R$; $t=\tau/\omega$
$u_x=U_x/V_*$; $u_y=U_y/V_*$; $\Lambda=\Omega R/V_*$; $V_*=c^2 Psa/\mu_* R$
$\sigma=\omega R/V_*$; $p=(P-Pa)/Psa$;
$h=H/c_*$

$Re_p^*=Re_p c/R=(\rho_*/\mu_*)(V_*/R)c^2$ is a typical advection flow Reynolds number, $Re_s=(\rho_*/\mu_*)\Omega c^2 = Re_p^* \sigma$ is a typical squeeze film Reynolds number, and ω is a characteristic whirl frequency (typically equal to the rotational frequency or a frequency of external excitation).

Integration of Axial Momentum Equation on the Axial Velocity Control Volume (V-C∀)

The axial momentum transport equation (6.b) is integrated on the axial velocity control volume (V-C∀) shown in figure A.1.

$$\int_w^e\int_s^n -h\frac{\partial p}{\partial y}dxdy = \int_w^e\int_s^n \frac{(k_y u_y)\bar{\mu}}{h}dxdy + \int_w^e\int_s^n Re_s\frac{\partial}{\partial \tau}(\bar{\rho}hu_y)\,dxdy + \int_w^e\int_s^n Re_p^*\{\frac{\partial}{\partial x}(\bar{\rho}hu_x u_y)+\frac{\partial}{\partial y}(\bar{\rho}hu_y^2)\}dxdy \qquad (7)$$

consider the following approximations for the different terms in equation (7).

$$\int_w^e\int_s^n -h\frac{\partial p}{\partial y}dxdy \approx \int_w^e -h_P^v\,[\delta p]_s^n dx \approx h_P^v(p_s-p_p)\,\delta x^v \qquad (8.a)$$

i.e., assume the pressure as uniform over the **s** and **n** faces, and an average uniform film thickness evaluated at the center of the V-C∀. Let,

$$\int_w^e\int_s^n \frac{k_y\bar{\mu}u_y}{h}dxdy \approx \left(\frac{k_y\bar{\mu}}{h}\right)_P^v V_P\,\delta x^v\,\delta y^v \qquad (8.b)$$

i.e., assume average film thickness, viscosity and shear coefficient k_y on V-C∀. And,

$$\int_w^e\int_s^n \frac{\partial}{\partial x}(\bar{\rho}hu_x u_y)\,dxdy = \int_s^n (\bar{\rho}hu_x u_y)_w^e\,dy \approx (\bar{\rho}hu_x u_y)_w^e\,\delta y^v \qquad (8.c)$$

i.e., assume uniform circumferential flow ($\rho hu_x\delta y^v$) across the east (**e**) and west (**w**) faces of the V-C∀. Also,

$$\int_w^e\int_s^n \frac{\partial}{\partial y}(\bar{\rho}hu_y u_y)\,dxdy = \int_w^e (\bar{\rho}hu_y u_y)_s^n\,dx \approx (\bar{\rho}hu_y u_y)_s^n\,\delta x^v \qquad (8.d)$$

i.e., regard the axial flow as uniform across the south (**s**) and north (**n**) faces of the V-C∀. And,

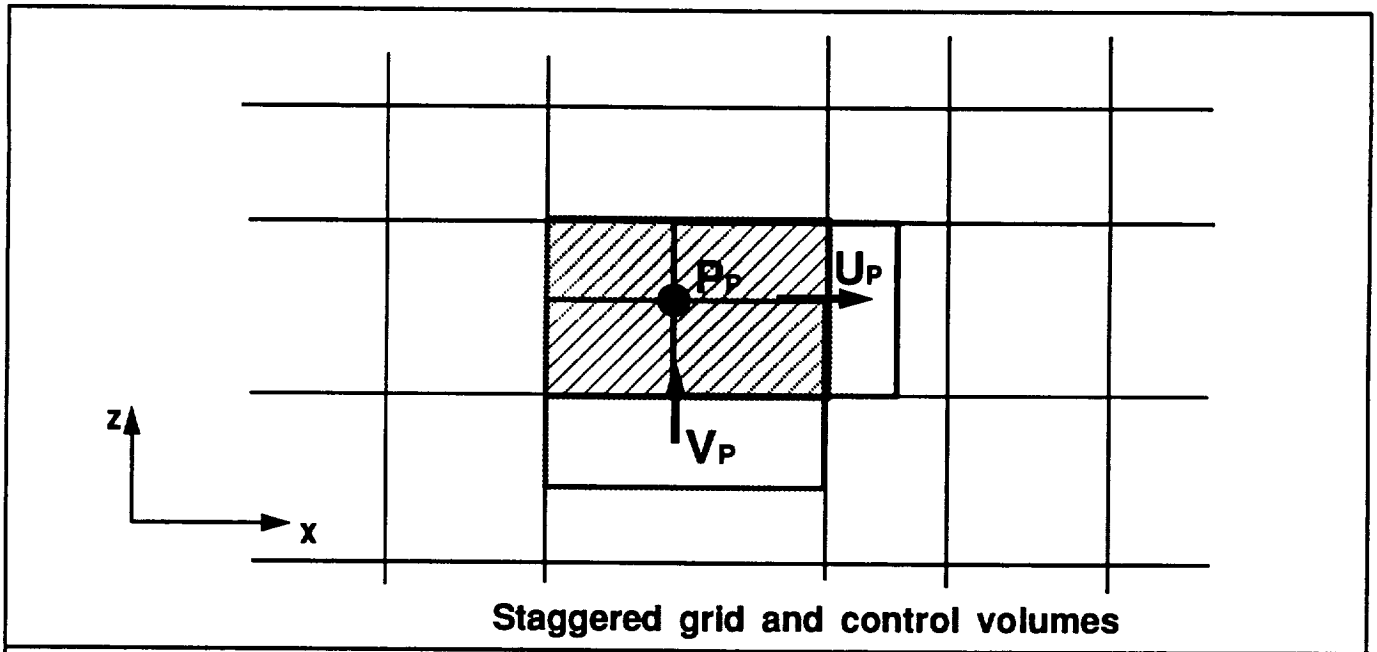

Staggered grid and control volumes

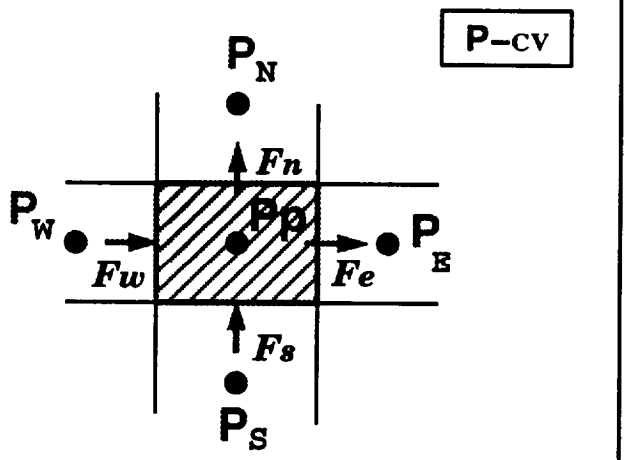

Pressure control-volume

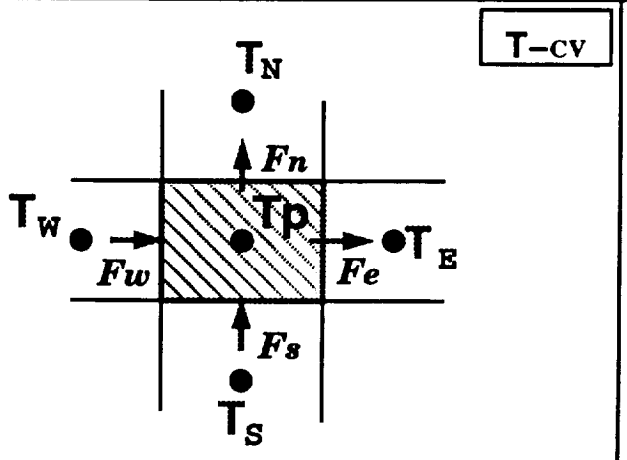

Temperature control volume

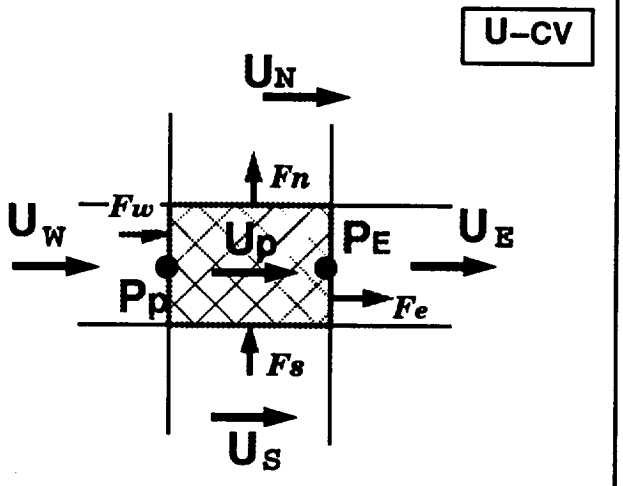

Circumferential velocity control volume

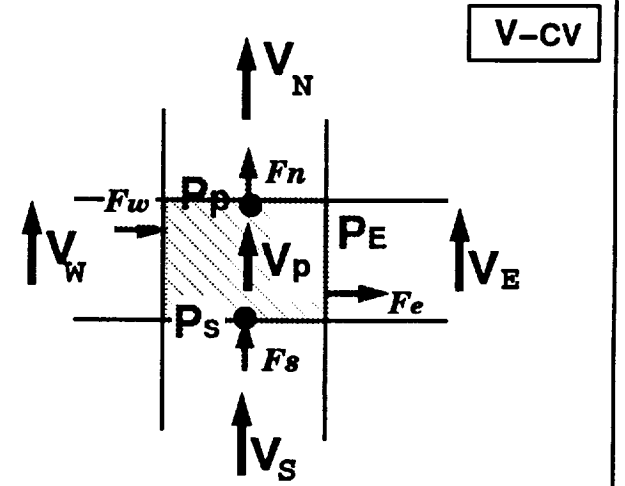

Axial velocity control volume

Figure A.1. Control volumes for integration of equations

$$\iint_{ws}^{en} \frac{\partial}{\partial \tau}(\bar{\rho} h u_y)\, dxdy = \frac{\partial}{\partial \tau}\iint_{ws}^{en} (\bar{\rho} h u_y)\, dxdy \qquad (8.e)$$

since the control volume size is fixed in space.

Thus, equation (7) can be written over the control volume as:

$$h_P^v (p_s - p_p)\, \delta x^v = \left(\frac{k_y \bar{\mu}}{h}\right)_p^v u_{y0}\, \delta x^v\, \delta y^v + Re_s \frac{\partial}{\partial \tau}\iint (\bar{\rho} h u_y)\, dxdy + \left[(\bar{\rho} h u_x u_y)_w^e\, \delta y^v + (\bar{\rho} h u_y u_y)_s^n\, \delta x^v\right] Re_p^* \qquad (9)$$

Integration of the continuity equation (1) on the V-C$\forall$ gives:

$$(\bar{\rho} h u_x)_w^e\, \delta y^v + (\bar{\rho} h u_y)_s^n\, \delta x^v + \sigma \frac{\partial}{\partial \tau}\iint_{ws}^{en} (\bar{\rho} h)\, dxdy = 0 \qquad (10)$$

Let the flow rates across the control volume faces be expressed as

$$F_e^v = (\bar{\rho} h u_x)^e\, \delta y^v; \quad F_w^v = (\bar{\rho} h u_x)^w\, \delta y^v;$$
$$F_n^v = (\bar{\rho} h u_y)^n\, \delta x^v; \quad F_s^v = (\bar{\rho} h u_y)^s\, \delta x^v; \qquad (11)$$

Then equation (10) is rewritten as

$$F_e^v - F_w^v + F_n^v - F_s^v + \sigma \frac{\partial}{\partial \tau}\iint_{ws}^{en} (\bar{\rho} h)\, dxdy = 0 \qquad (12)$$

which establishes a bulk-flow balance including the rate of mass accumulation on the V-C$\forall$.

The momentum flux terms in equation (9) are treated using the upwind scheme of Launder and Leschziner (1978). This scheme establishes a selection of velocities based on whether the flow is <u>into</u> or <u>out</u> of the C$\forall$.

For example

$$(\bar{\rho} h u_x u_y)^e \delta y^v = F_e u_y^e = \begin{cases} F_e\, V_P & \text{if } F_e < 0 \\ F_e\, V_E & \text{if } F_e > 0 \end{cases} \quad \text{where } F_e = \bar{\rho}(h u_x)^e \delta y^v$$

and can be written as

$$F_e u_y^e = [\![F_e, 0]\!] V_P - [\![-F_e, 0]\!] V_E \qquad \textit{where } [\![a, 0]\!] = \max(a, 0)$$

Thus, it can be stated that the momentum fluxes are equal to:

$$
\begin{aligned}
(\overline{\rho} h u_x u_y)^w \, \delta y^v &= F_w u_y^w = [\![F_w, 0]\!] V_W - [\![-F_w, 0]\!] V_P \\
(\overline{\rho} h u_x u_y)^e \, \delta y^v &= F_e u_y^e = [\![F_e, 0]\!] V_P - [\![-F_e, 0]\!] V_E \\
(\overline{\rho} h u_y u_y)^s \, \delta x^v &= F_s u_y^s = [\![F_s, 0]\!] V_S - [\![-F_s, 0]\!] V_P \\
(\overline{\rho} h u_y u_y)^n \, \delta x^v &= F_n u_y^n = [\![F_n, 0]\!] V_P - [\![-F_n, 0]\!] V_N
\end{aligned}
\tag{13}
$$

The momentum flux difference terms in equation (9) are written as

$$
\begin{aligned}
(\overline{\rho} h u_x u_y)_w^e \, \delta y^v + (\overline{\rho} h u_y u_y)_s^n \, \delta x^v &= F_e u_y^e - F_w u_y^n + F_n u_y^n - F_s u_y^s \\
&= V_P \, ([\![F_e, 0]\!] + [\![-F_w, 0]\!] + [\![F_n, 0]\!] + [\![-F_s, 0]\!]) \\
&\quad - [\![-F_e, 0]\!] V_E - [\![F_w, 0]\!] V_W - [\![-F_n, 0]\!] V_N - [\![F_s, 0]\!] V_S
\end{aligned}
\tag{14}
$$

Let,

$$
\begin{aligned}
a_E^v &= Re_p^* \, [\![-F_e, 0]\!] \; ; \quad a_W^v = Re_p^* \, [\![F_w, 0]\!] \; ; \\
a_N^v &= Re_p^* \, [\![-F_n, 0]\!] \; ; \quad a_S^v = Re_p^* \, [\![F_s, 0]\!]
\end{aligned}
\tag{15}
$$

and using the identities:

$$
[\![\alpha, 0]\!] = \frac{1}{2} [\alpha + |\alpha|] \; ; \quad [\![-\alpha, 0]\!] = \frac{1}{2} [-\alpha + |\alpha|]
$$

the following identity is obtained

$$
\begin{aligned}
F_e + [\![-F_e, 0]\!] - F_w + [\![F_w, 0]\!] + F_n + [\![-F_n, 0]\!] + F_s + [\![-F_s, 0]\!] &= (F_e - F_w + F_n - F_s) \\
&\quad + \frac{1}{Re_p^*} [a_E^v + a_W^v + a_S^v + a_N^v]
\end{aligned}
\tag{16.a}
$$

And using the continuity equation (12),

$$
\begin{aligned}
F_e + [\![-F_e, 0]\!] - F_w + [\![F_w, 0]\!] + F_n + [\![-F_n, 0]\!] - F_s + [\![F_s, 0]\!] &= -\sigma \frac{\partial}{\partial \tau} \iint_{w\,s}^{e\,n} (\overline{\rho} h) \, dxdy \\
&\quad + \frac{1}{Re_p^*} \sum_{nb} a_{nb}^v
\end{aligned}
\tag{16.b}
$$

where nb refers to the neighbor nodes (e,w,n,s).

Substitution of (16.b) into the axial momentum equation (9) gives:

$$
\begin{aligned}
h_P^v (p_s - p_p) \, \delta x = & \left(\frac{k_y \overline{\mu}}{h} \right)_p^v \delta x^v \delta y^v + Re_s \frac{\partial}{\partial \tau} \iint (\overline{\rho} h u_y) \, dxdy \\
& + Re_p^* [V_P \, ([\![F_e, 0]\!] + [\![-F_w, 0]\!] + [\![F_n, 0]\!] + [\![-F_s, 0]\!])] \\
& - Re_p^* \, ([\![-F_e, 0]\!] V_E - [\![F_w, 0]\!] V_W - [\![-F_n, 0]\!] V_N - [\![F_s, 0]\!] V_S)
\end{aligned}
\tag{17}
$$

and substituting equation (16.b),

$$h_P(p_s-p_P)\,\delta x^v+\sum_{nb} a_{nb}^v V_{nb} = \left[\left(\frac{k_y\bar{\mu}}{h}\right)_P^v+\sum_{nb} a_{nb}^v\right]V_P+Re_s\frac{\partial}{\partial\tau}\iint(\bar{\rho}hu_y)\,dxdy$$
$$-V_pRe_s^*\frac{\partial}{\partial\tau}\iint(\bar{\rho}h)\,dxdy \qquad (18)$$

Hence, the difference form of the momentum equation is obtained as

$$h_P(p_s-p_P)\,\delta x^v+\sum_{nb} a_{nb}^v V_{nb} = \left[\left(\frac{k_y\bar{\mu}}{h}\right)_P^v+\sum_{nb} a_{nb}^v\right]V_P$$
$$+Re_s\left[(\bar{\rho}h)_P^v\delta x^v\delta y^v\right]\frac{\partial}{\partial\tau}V_P \qquad (19)$$

A suitable approximation for the time derivative has to be found. An <u>implicit scheme</u> is used for the unsteady term, i.e.,

$$\frac{\partial V_P}{\partial\tau} = \frac{V_P-V_P^*}{\Delta\tau} \qquad (*)$$

where $V_P = V_P$ is the axial velocity at time $t+\Delta t$, and
$V_P^* = V_P$ is the axial velocity at time t, respectively.

Note that all variables (velocity and pressure) in equation (19) are to be evaluated at time $t+\Delta t$.

Finally, the discrete form of the axial momentum transport equation is given as:

$$\left[h_P^v(p_s-p_P)\,\delta x^v+\sum_{nb} a_{nb}^v V_{nb}\right]+\frac{Re_s(\bar{\rho}h)_P^v\delta x^v\delta y^v}{\Delta\tau}V_P^* = a_P^v\,V_P \qquad (20)$$

where:

$$a_P^v = \left(\frac{k_y\bar{\mu}}{h}\right)_P^v\delta x^v\,\delta y^v+\sum_{nb} a_{nb}^v+Re_s(\bar{\rho}h)_P^v\,\frac{\delta x^v\,\delta y^v}{\Delta\tau}$$

<u>Integration of Circumferential Momentum Equation</u>

Integration of the circumferential momentum transport equation (6.a) on the control volume (U-C∀) shown in figure A.1, and use of the continuity equation to simplify some terms (same as for the V-C∀ equation) leads to the following algebraic equation:

$$h_P^u(p_P-p_E)\,\delta y^u+a_E^uU_E+a_W^uU_W+a_S^uU_S+a_N^uU_N$$
$$+\left[\frac{k_J\bar{\mu}}{h}\frac{\Lambda}{2}\right]_P^u\delta x^u\,\delta y^u+\frac{Re_s}{\Delta\tau}(\bar{\rho}h)_P^u\,\delta x^u\,\delta y^uU_P^* = a_P^u\,U_P \qquad (21)$$

where: $U_P^* = U$ at time t

$$a_P^u = \sum_{nb} a_{nb}^u + \left(\frac{k_x\bar{\mu}}{h}\right)_P^u \delta x^u\,\delta y^u + Re_s(\bar{\rho}h)_P^u\,\frac{\delta x^u\,\delta y^u}{\Delta\tau}$$

$$a_E^u = Re_P^*\,[\![-F_e, 0]\!]\;; \quad a_W^u = Re_P^*\,[\![F_w, 0]\!]\;;$$
$$a_N^u = Re_P^*\,[\![-F_n, 0]\!]\;; \quad a_S^u = Re_P^*\,[\![F_s, 0]\!]$$

$$F_e^u = (\bar{\rho}hu_x)^e\,\delta y^u; \quad F_w^u = (\bar{\rho}hu_x)^w\,\delta y^u;$$
$$F_n^u = (\bar{\rho}hu_y)^n\,\delta x^u; \quad F_s^u = (\bar{\rho}hu_y)^s\,\delta x^u;$$

The difference equations for momentum transport are summarized as

Circumferential-momentum (on U C∀):

$$h_P^u(p_P - p_E)\,\delta y^u + \sum_{nb} a_{nb}^u\,U_{nb} + S_P^u + S_\tau^u U_P^* = a_P^u U_P \qquad (22)$$

Axial-momentum (on V C∀):

$$h_P^v(p_S - p_P)\,\delta x^v + \sum_{nb} a_{nb}^v\,V_{nb} + S_P^v + S_\tau^v V_P^* = a_P^v V_P \qquad (23)$$

where:

$$a_P^v = \left[\frac{k_y\bar{\mu}}{h}\right]_P^v \delta x^v\,\delta y^v + \sum_{nb} a_{nb}^v + S_\tau^v\;; \quad S_\tau^v = Re_s(\bar{\rho}h)_P^v\,\frac{\delta x^v\,\delta y^v}{\Delta\tau}$$

$$a_P^u = \left[\frac{k_x\bar{\mu}}{h}\right]_P^u \delta x^u\,\delta y^u + \sum_{nb} a_{nb}^u + S_\tau^u\;; \quad S_\tau^u = Re_s(\bar{\rho}h)_P^u\,\frac{\delta x^u\,\delta y^u}{\Delta\tau}$$

$$S_P^u = \left[\frac{k_f\bar{\mu}}{h}\,\frac{\Lambda}{2}\right]\frac{\delta x^u\,\delta y^u}{\Delta\tau}\;; \quad S_P^v = 0$$

in general:

$$a_E^r = Re_P^*\,[\![-F_e^r, 0]\!]\;; \quad a_W^r = Re_P^*\,[\![F_w^r, 0]\!]\;;$$
$$a_N^r = Re_P^*\,[\![-F_n^r, 0]\!]\;; \quad a_S^r = Re_P^*\,[\![F_s^r, 0]\!]$$

with

$$F_e^r = (\bar{\rho}hu_x)_e^r\,\delta y^r; \quad F_w^r = (\bar{\rho}hu_x)_w^r\,\delta y^r;$$
$$F_n^r = (\bar{\rho}hu_y)_n^r\,\delta x^r; \quad F_s^r = (\bar{\rho}hu_y)_s^r\,\delta x^r;$$

r= u or v

Derivation of the pressure correction equation

Integration of the continuity equation (5) on the pressure control volume(P-C∀) shown in figure A.1 leads to

$$F_e^P - F_w^P + F_n^P - F_s^P + \sigma \frac{\partial}{\partial \tau} \int_w^e \int_s^n (\overline{\rho} h)\, dxdy = 0 \qquad (24)$$

where the flow rates across the faces of the P-C∀ are:

$$\begin{aligned} F_e^P &= (\overline{\rho} h u_x)_e^P \delta y^P \approx (\overline{\rho} h)_e^P U_p \delta y^P \ ; \\ F_w^P &= (\overline{\rho} h u_x)_w^P \delta y^P \approx (\overline{\rho} h)_w^P U_w \delta y^P \ ; \\ F_n^P &= (\overline{\rho} h u_y)_n^P \delta x^P \approx (\overline{\rho} h)_n^P V_N \delta x^P \ ; \\ F_s^P &= (\overline{\rho} h u_y)_s^P \delta x^P \approx (\overline{\rho} h)_s^P V_p \delta x^P \end{aligned} \qquad (25)$$

The unsteady integral term is approximately given by

$$\frac{\partial}{\partial \tau} \int_w^e \int_s^n (\overline{\rho} h)\, dxdy \approx \left[\frac{\partial}{\partial \tau} (\overline{\rho} h)_P \right] \delta x^P \, \delta y^P = \left[\overline{\rho}_P^P \frac{\partial h_P^P}{\partial \tau} + h_P^P \frac{\partial \overline{\rho}_P^P}{\partial \tau} \right] \delta x^P \, \delta y^P$$

which implies that the size of the P C∀ is fixed in space, and that the values of h and $\overline{\rho}$ are uniform within the control volume.

The algebraic form of the continuity equation establishes the flow balance on a finite size control volume as

$$F_e^P - F_w^P + F_n^P - F_s^P + \sigma \delta x^P \, \delta y^P \left[\overline{\rho}_P^P \frac{\partial h_P^P}{\partial \tau} + h_P^P \frac{\partial \overline{\rho}_P^P}{\partial \tau} \right] = 0 \qquad (26)$$

Since $h = \bar{c}(x,y) + \bar{x}(\tau)\cos\theta + \bar{y}(\tau)\sin\theta$, then

$$\frac{\partial h_P^P}{\partial \tau} = \frac{\partial \overline{x}_{(\tau)}}{\partial \tau} \cos\theta_P + \frac{\partial \overline{y}_{(\tau)}}{\partial \tau} \sin\theta_P$$

where the time derivatives of $\bar{x}$ and $\bar{y}$ are given by the solution of the rotor-bearing equations of motion. Also,

$\frac{\partial \overline{\rho}_P^P}{\partial \tau} = \frac{\overline{\rho}_P^P - \overline{\rho}_P^{P^*}}{\Delta \tau}$ where $\bar{\rho}^* = \bar{\rho}(t)$ and $\bar{\rho} = \bar{\rho}(t+\Delta\tau)$.

The continuity equation in the P C∀ is then written as

$$F_e^P - F_w^P + F_n^P - F_s^P + \sigma \delta x^P \, \delta y^P \left[\overline{\rho}_P^P \dot{h}_P + h_P \frac{\overline{\rho}_P^P - \overline{\rho}_P^*}{\Delta \tau} \right] = 0 \qquad (27)$$

Using the pressure correction method, (Launder and Leschziner, 1978):

$$U = \overline{U} + u' \ ; \quad V = \overline{V} + v' \ ; \quad p = \overline{p} + p' \qquad (28)$$

where U, V satisfy the momentum equations (22 and 23), and
u', v', p' are correction fields

Substituting (28) into the momentum equations (20) and (21) leads to

$$h_P^u\ (\overline{p}_P-\overline{p}_E)\,\delta y^u + \sum_{bn} a_{nb}^u\ \overline{U}_{nb} + S_P^u + S_\tau^u U_P^*$$
$$+h_P^u\ (p'_P-p'_E)\,\delta y^u + \sum_{nb} a_{nb}^u\ \overline{u}'_{nb} = a_P^u \overline{V}_P + a_P^u u'_P \qquad (29)$$

then,

$$h_P^u\ (p'_P-p'_E)\,\delta y^u + \sum_{nb} a_{nb}^u\ u'_{nb} = a_P^u u'_P \qquad (30.a)$$

and identically

$$h_P^v\ (p'_S-p'_P)\,\delta x^v + \sum_{nb} a_{nb}^v\ v'_{nb} = a_P^v v'_P \qquad (30.b)$$

Let, using the SIMPLEC procedure (Van Doormaal & Raithby, 1984)

$$\sum a_{nb}^u\ u'_{nb} \simeq \sum a_{nb}^u\ u'_P$$
$$\sum a_{nb}^v\ v'_{nb} \simeq \sum a_{nb}^v\ v'_P \qquad (31)$$

Equations (30) then become:

$$u'_P \simeq \frac{d_P^u\ (p'_P-p'_E)}{a_P^u - \sum a_{nb}^u} \quad ; \quad d_P^u = h_P^u \delta y^u$$
$$v'_P \simeq \frac{d_P^v\ (p'_S-p'_P)}{a_P^v - \sum a_{nb}^v} \quad ; \quad d_P^v = h_P^v \delta x^v \qquad (32)$$

where,

$$a_P^u = \left(\frac{k_x \overline{\mu}}{h}\right)_P^u \delta x^u\,\delta y^u + \sum a_{nb}^u + S_\tau^u \quad ; \quad S_\tau^u = Re_s\,(\overline{\rho} h)_P^u\ \frac{\delta x^u\,\delta y^u}{\Delta\tau}$$

$$a_P^v = \left(\frac{k_y \overline{\mu}}{h}\right)_P^v \delta x^v\,\delta y^v + \sum a_{nb}^v + S_\tau^v \quad ; \quad S_\tau^v = Re_s\,(\overline{\rho} h)_P^v\ \frac{\delta x^v\,\delta y^v}{\Delta\tau}$$

Let,

$$D_P^u = \frac{d_P^u}{a_P^u - \sum a_{nb}^u}$$
$$D_P^v = \frac{d_P^v}{a_P^v - \sum a_{nb}^v}$$

Substitution of the correction fields, equation (28), into the continuity equation (27) gives:

$$(\overline{F}_e+F'_e)^P-(\overline{F}_w+F'_w)^P+(\overline{F}_n+F'_n)^P-(\overline{F}_s+F'_s)^P+\sigma\,\delta x^P\,\delta y^P\left[\overline{\rho}_P\dot{h}_P+h_P\frac{\overline{\rho}_P^P-\overline{\rho}_P^*}{\Delta\tau}\right]=0 \tag{33}$$

where

$$\begin{aligned}\overline{F}_e &= (\overline{\rho}h\overline{u}_x\delta y)_e^P = (\overline{\rho}h)_e^P\,\overline{U}_P\delta y^P\\ \overline{F}_s &= (\overline{\rho}h\overline{u}_y\delta x)_s^P = (\overline{\rho}h)_s^P\,\overline{V}_P\delta x^P \quad , \; etc\end{aligned} \tag{34}$$

and

$$\begin{aligned}F'_e &= (\overline{\rho}h)_e^P u'_P\delta y^P = (\overline{\rho}h)_e^P D_P^u(p'_P-p'_E)\,\delta y^P\\ &= a_E^P(p'_P-p'_E) \;;\quad a_E^P=(\overline{\rho}h)_e^P\delta y^P\,D_P^u\\ F'_s &= (\overline{\rho}h)_s^P v'_P\delta x^P = (\overline{\rho}h)_s^P D_P^v(p'_S-p'_P)\,\delta x^P\\ &= a_S^P(p'_S-p'_P) \;;\quad a_S^P=(\overline{\rho}h)_s^P\delta x^P\,D_P^v\\ F'_w &= a_W^P(p'_W-p'_P)\\ F'_n &= a_N^P(p'_P-p'_N)\end{aligned} \tag{35}$$

Let

$$\overline{F}_e^P-\overline{F}_w^P+\overline{F}_n^P-\overline{F}_s^P+\sigma\delta x^P\,\delta y^P\left[\overline{\rho}_P\dot{h}_P+h_P\frac{\overline{\rho}_P^P-\overline{\rho}_P^*}{\Delta\tau}\right]\equiv\overline{S}_P^* \tag{36}$$

So equation (33) becomes

$$F'_e-F'_w+F'_n-F'_s=-\overline{S}_P^* \tag{37.a}$$

or

$$a_E^P(p'_P-p'_E)-a_N^P(p'_W-p'_P)+a_N^P(p'_P-p'_N)-a_S^P(p'_S-p'_P)\equiv-\overline{S}_P^* \tag{37.b}$$

or

$$a_P^P\,p'_P=\sum_{nb}a_{nb}^P\,p'_{nb}-\overline{S}_P^* \tag{37.c}$$

where

$$a_P^P=(a_E+a_W+a_N+a_S)^P=\sum_{nb}a_{nb}^P \tag{38}$$

Note that if $p'_{nb} = p'_P = 0$ then $S_P^* = 0$ and mass continuity is satisfied. Then the momentum equations are also satisfied and conversion of the flow field is achieved.

Once the p'_P field is obtained, correction to the u and v fields are done using equations (27). Typically the pressure is underelaxed as,

$$\begin{aligned}p^{new} &= p^{old}+\alpha_p\,p'\\ u^{new} &= u^{old}+u'\\ v^{new} &= v^{old}+v'\end{aligned} \tag{39}$$

with α_p as a parameter typically less than one.

Discretization of Energy Transport Equation

The dimensionless equation for turbulent bulk-flow energy transport is given as (Yang, 1992)

$$\frac{\overline{C}_p Re_s}{E_c}\frac{\partial}{\partial\tau}(\overline{\rho}h\overline{T}) + \frac{\overline{C}_p Re_p^*}{E_c}\left[\frac{\partial}{\partial x}(\overline{\rho}hu_x\overline{T}) + \frac{\partial}{\partial y}(\overline{\rho}hu_y\overline{T})\right] + \frac{Re_p^*}{E_c}\overline{Q}_s$$
$$= \overline{\beta}_t h(\sigma\frac{\partial p}{\partial\tau}+u_x\frac{\partial p}{\partial x}+u_y\frac{\partial p}{\partial y})\overline{T} + \frac{h\Lambda}{2}\frac{\partial p}{\partial x} + \frac{\overline{\mu}}{h}\left(k_x(u_x^2+u_y^2+\frac{1}{2}u_x\Lambda)+k_J(\frac{\Lambda^2}{4}-u_x\Lambda)\right) \quad (40)$$

where,

$x=X/R$; $y=Y/R$; $t=\tau/\omega$

$u_x=U_x/U_*$; $u_y=U_y/U_*$; $\Lambda=\Omega R/U_*$; $\overline{T}=T/T_*$

$\sigma=\omega R/U_*$; $p=(P-Pa)/Psa$; $h=H/c$

$\beta_t = \beta_t T_*$

and, $E_c = U_*2/(T_*C_p^*)$ is the Eckerd number,

$Re_p^*=Re_p\ c/R = (\rho_*/\mu_*)(U_*/R)c^2$ is the advection Reynolds number,

$Re_s=(\rho_*/\mu_*)\omega c^2$ is the squeeze film Reynolds number, and

$\bar{Q}s = \bar{h}_B(\bar{T}-\bar{T}_B)+\bar{h}_J(\bar{T}-\bar{T}_J)$ is the heat flow to bearing and journal surfaces

Define the following source terms,

$$S_1 = [\overline{\beta}_t h(\sigma\frac{\partial p}{\partial\tau}+u_x\frac{\partial p}{\partial x}+u_y\frac{\partial p}{\partial y})\overline{T}$$
$$S_2 = \frac{h\Lambda}{2}\frac{\partial p}{\partial x} + \frac{\overline{\mu}}{h}\left(k_x(u_x^2+u_y^2+\frac{1}{2}u_x\Lambda)+k_J(\frac{\Lambda^2}{4}-u_x\Lambda)\right) \quad (41)$$

Integration of equation (40) over the temperature control volume (T-C$\forall$) shown in figure A.1 leads to

$$\frac{\overline{C}_p Re_s}{E_c}\int\int_{TC\forall}\frac{\partial}{\partial\tau}(\overline{\rho}h\overline{T})\,dxdy + \frac{\overline{C}_p Re_p^*}{E_c}\left[\int_s^n(\overline{\rho}hu_x\overline{T})_w^e\,dy + \int_w^e(\overline{\rho}hu_y\overline{T})_s^n\,dx\right]$$
$$+ \frac{Re_p^*}{E_c}\overline{Q}_s\Delta x\Delta y = (S_1\Delta x\Delta y)\overline{T}_P + S_2\Delta x\Delta y \quad (42)$$

Implementation of the upwind scheme for the thermal flux terms gives:

$$(\overline{\rho}hu_x\overline{T})^e\Delta y = F_e\overline{T}_e = [\![F_e, 0]\!]\,\overline{T}_P - [\![-F_e, 0]\!]\,\overline{T}_E$$

$$(\overline{\rho}hu_x\overline{T})^w\Delta y = F_w\overline{T}_w = [\![F_w, 0]\!]\,\overline{T}_W - [\![-F_w, 0]\!]\,\overline{T}_P$$

$$(\overline{\rho}hu_y\overline{T})^n\Delta x = [\![F_n, 0]\!]\,\overline{T}_P - [\![-F_n, 0]\!]\,\overline{T}_N \quad (43)$$

$$(\overline{\rho}hu_y\overline{T})^s\Delta x = [\![F_s, 0]\!]\,\overline{T}_S - [\![-F_s, 0]\!]\,\overline{T}_P$$

where

$$F_e = (\overline{\rho}u_x\Delta y)_e\ ; \quad F_n = (\overline{\rho}hu_y\Delta x)_n\ ;$$
$$F_w = (\overline{\rho}u_x\Delta y)_w\ ; \quad F_s = (\overline{\rho}hu_y\Delta x)_s$$

Using these expressions the LHS of equation (42) is rewritten as:

$$LHS_{42} = \frac{\overline{C}_p Re_s}{E_c}\int\int_{TC\forall}\frac{\partial}{\partial\tau}(\overline{\rho}h\overline{T})\,dxdy + \frac{\overline{C}_p Re_P^*}{E_c}[[-F_e,0]+[F_w,0]+[-F_n,0]+[F_s,0]]\overline{T}_P$$
$$- \frac{\overline{C}_p Re_P^*}{E_c}[[-F_e,0]\overline{T}_E+[F_w,0]\overline{T}_W+[-F_n,0]\overline{T}_N+[F_s,0]\overline{T}_S]$$
$$+ \frac{\overline{C}_p Re_P^*}{E_c}[F_e-F_w+F_n-F_s]\overline{T}_P + \frac{Re_P^*}{E_c}Q_s\Delta x\Delta y$$

or

$$LHS_{42} = \frac{\overline{C}_p Re_s}{E_c}\int\int_{TC\forall}\frac{\partial}{\partial\tau}(\overline{\rho}h\overline{T})\,dxdy + \left(\sum a_{nb}\right)\overline{T}_P - \sum a_{nb}\overline{T}_{nb}$$
$$+ \frac{\overline{C}_p Re_P^*}{E_c}[F_e-F_w+F_n-F_s]\overline{T}_P + \frac{Re_P^*}{E_c}Q_s\Delta x\Delta y \qquad (44)$$

where

$$a_E = \frac{\overline{C}_p Re_P^*}{E_c}[[-F_e,0]] \;;\quad a_W = \frac{\overline{C}_p Re_P^*}{E_c}[[F_w,0]] \;;$$
$$a_N = \frac{\overline{C}_p Re_P^*}{E_c}[[-F_n,0]] \;;\quad a_S = \frac{\overline{C}_p Re_P^*}{E_c}[[F_s,0]] \qquad (45)$$

The discrete form of the continuity equation on the T C∀ gives

$$[F_e-F_w+F_n-F_s] = -\sigma\int\int_{TC\forall}\frac{\partial}{\partial\tau}(\overline{\rho}h)\,dxdy \qquad (46)$$

Substitution of equation (46) into (44) gives

$$LHS_{42} = \frac{\overline{C}_p Re_s}{E_c}\int\int_{TC\forall}\frac{\partial}{\partial\tau}(\overline{\rho}h\overline{T})\,dxdy - \frac{\overline{C}_p Re_P^*}{E_c}\overline{T}_P\sigma\int\int_{TC\forall}\frac{\partial}{\partial\tau}(\overline{\rho}h)\,dxdy$$
$$+ \left(\sum a_{nb}\right)\overline{T}_P - \sum a_{nb}\overline{T}_{nb} + \frac{Re_P^*}{E_c}Q_s\Delta x\Delta y$$

$$LHS_{42} = \frac{\overline{C}_p Re_s}{E_c}\int\int_{TC\forall}\overline{\rho}h\frac{\partial\overline{T}}{\partial\tau}dxdy + \left(\sum a_{nb}\right)\overline{T}_P - \sum a_{nb}\overline{T}_{nb} + \frac{Re_P^*}{E_c}Q_s\Delta x\Delta y$$
$$+ \frac{\overline{C}_p}{E_c}\overline{T}_P\left[Re_s\int\int_{TC\forall}\frac{\partial(\overline{\rho}h)}{\partial\tau}dxdy - Re_P^*\sigma\int\int_{TC\forall}\frac{\partial}{\partial\tau}(\overline{\rho}h)\,dxdy\right] \qquad (47)$$

Since $Re_s = Re_P^*\sigma$, the last two term on the RHS of the previous expression is add to zero. Then,

$$LHS_{42} = \frac{\overline{C}_p Re_s}{E_c}\int\int_{TCV}\overline{\rho}h\frac{\partial\overline{T}}{\partial\tau}dxdy + \left(\sum a_{nb}\right)\overline{T}_P - \sum a_{nb}\overline{T}_{nb} + \frac{Re_P^*}{E_c}Q_s\Delta x\Delta y \qquad (48)$$

The integral form of the energy transport equation (42) is now expressed as:

$$\frac{\overline{C}_p Re_s}{E_c}\int\int_{TCV}\overline{\rho}h\frac{\partial\overline{T}}{\partial\tau}dxdy + \left(\sum a_{nb}\right)\overline{T}_P - \sum a_{nb}\overline{T}_{nb} + \frac{Re_P^*}{E_c}Q_s\Delta x\Delta y = (S_1\Delta x\Delta y)\overline{T}_P + S_2\Delta x\Delta y \qquad (49)$$

Let,

$$\frac{\partial\overline{T}}{\partial\tau} = \frac{\overline{T}_P - \overline{T}_P^*}{\Delta\tau}$$

$$\overline{Q}_S = \overline{T}_P(\overline{h}_B+\overline{h}_J) - (\overline{h}_B\overline{T}_B+\overline{h}_J\overline{T}_J)$$

where $\overline{T}_P^*$ is the film temperature at the previous time step. Then, the discrete form of equation (49) becomes:

$$\left[\sum a_{nb} + \frac{\overline{C}_p Re_s}{E_c}\frac{\overline{\rho}_P h_P}{\Delta\tau}\Delta x\Delta y + \frac{Re_P^*}{E_c}(\overline{h}_B+\overline{h}_J)\Delta x\Delta y\right]\overline{T}_P - (S_1\Delta x\Delta y)\overline{T}_P = \sum a_{nb}\overline{T}_{nb} + S_2\Delta x\Delta y + \frac{\overline{C}_p Re_s}{E_c}\frac{\overline{\rho}_P h_P}{\Delta\tau}\Delta x\Delta y\overline{T}_P^* + \frac{Re_P^*}{E_c}(\overline{h}_B\overline{T}_B+\overline{h}_J\overline{T}_J)\Delta x\Delta y \qquad (50)$$

The algebraic energy transport theory equation is finally written as

$$a_P^t\,\overline{T}_P = a_E^t\,\overline{T}_E + a_W^t\,\overline{T}_W + a_N^t\,\overline{T}_N + a_S^t\,\overline{T}_S + S_C^t \qquad (51)$$

where

$$a_E^t = \frac{\overline{C}_p Re_P^*}{E_c}[\![-F_e^t, 0]\!] \;\; ; \;\; a_W^t = \frac{\overline{C}_p Re_P^*}{E_c}[\![F_w^t, 0]\!] \;\; ;$$
$$a_N^t = \frac{\overline{C}_p Re_P^*}{E_c}[\![-F_n^t, 0]\!] \;\; ; \;\; a_S^t = \frac{\overline{C}_p Re_P^*}{E_c}[\![F_s^t, 0]\!] \qquad (52.a)$$

$$a_P^t = a_E^t+a_W^t+a_N^t+a_S^t+S_{P1}^t+[\![S_{P2}^t, 0]\!]+S_{P3}^t \qquad (52.b)$$

$$S_C^t = S_{C1}^t+S_{C2}^t+S_{C3}^t+S_{C4}^t+[\![-S_{P2}^t, 0]\!]\,\overline{T}_P^* \qquad (52.c)$$

$$
\begin{aligned}
S_{P1}^{t} &= \frac{Re_p^*}{E_c}\left(\overline{h}_B+\overline{h}_J\right)\Delta x\Delta y \\
S_{P2}^{t} &= \overline{\beta}_{tP}h_P\left[\frac{\sigma\left(p_P-p_P^*\right)}{\Delta\tau}\Delta x\Delta y+U_P\left(p_e-p_w\right)\Delta y+V_P\left(p_n-p_s\right)\Delta x\right] \\
S_{P3}^{t} &= \frac{\overline{C}_P Re_s}{E_c}\frac{\overline{\rho}_P h_P}{\Delta\tau}\Delta x\Delta y
\end{aligned}
\qquad \text{(52.d)}
$$

$$
\begin{aligned}
S_{C1}^{t} &= \left[\frac{\overline{\mu}}{h}\left(k_x\left(u_x^2+u_y^2+\frac{1}{2}u_x\Lambda\right)+k_J\left(\frac{\Lambda^2}{4}-u_x\Lambda\right)\right)\right]_P\Delta x_P\Delta y_P \\
S_{C2}^{t} &= \frac{\Lambda}{2}h_P\left(p_e-p_w\right)\Delta y \\
S_{C3}^{t} &= \frac{Re_p^*}{E_c}\left(\overline{h}_B\overline{T}_B+\overline{h}_J\overline{T}_J\right)\Delta x_P\Delta y_P \\
S_{C4}^{t} &= \frac{\overline{C}_P Re_s}{E_c}\frac{\overline{\rho}_P h_P}{\Delta\tau}\Delta x\Delta y\overline{T}_P^*
\end{aligned}
\qquad \text{(52.e)}
$$

Note that the terms involving $\Delta\tau$ correspond to unsteady flow conditions.

As for the source term $-(S_1\Delta x\Delta y)\bar{T}_P$:
1) $(-S_1\Delta x\Delta y)$ goes into a_P if $(-S_1\Delta x\Delta y)>0$, or
2) $(S_1\Delta x\Delta y)T_P$ into the source term of the RHS if $(-S_1\Delta x\Delta y)<0$.

Texas A&M University
Mechanical Engineering Department

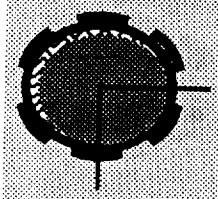

A Literature Review on Two-Phase Flow in Fluid Film Bearings

NASA Lewis Research Center
NASA Grant NAG3-1434
Contract Monitor: Mr. James Walker

Grigory Arauz
Research Assistant

December 1994

Thermohydrodynamic Analysis of Cryogenic Liquid Turbulent Flow Fluid Film Bearings (Phase II)

A Literature Review on Two-Phase Flow in Fluid Film Bearings

Grigory Arauz
Research Assistant

December, 1994

Prepared for NASA Lewis Research Center
NASA Grant NAG3-1434
Year II
Contract Monitor: Mr. James Walker

INTRODUCTION

The classical lubrication theory, derived originally by Reynolds (1886), assumes that the lubricant is a single-phase, isoviscous, newtonian fluid. However, this assumption is commonly violated in practical cases. In some processes like metal forming, a mixture of water and oil is used as lubricant and provide an additional cooling mechanism (Al-Sharif, 1992). Dust and other impurities difficult or expensive to avoid in practical applications will turn the lubricant into a solid-liquid two-phase mixture (Chamniprasart, 1992). In devices like squeeze film dampers entraintment of air, or air dissolved in the oil, will convert the lubricant into a gas-liquid two-phase mixture (Zeidan and Vance, 1989,1990). Operation close to the fluid critical point (like in some damper seals using cryogenic fluids) may result in fluid vaporization and the consequent formation of a single component two-phase fluid (Yang et al., 1993a). In any case, the transformation from a single-phase to a two-phase fluid implies considerable variations in the overall material properties of the fluid such as its viscosity and density. Thus, a pronounced change

in the performance characteristic of the fluid film bearing element is expected under two-phase flow conditions.

LITERATURE REVIEW

The study the two-phase flow phenomena in fluid film bearings such as seal, dampers and bearings commonly used in turbomachinery is of current interest. Therefore, this brief literature review focusses on the behavior of a mixture of a liquid and a dispersed compressible fluid (gas or vapor). A two-phase flow condition is attained when the critical point of the gaseous (compressible) phase is reached. A gaseous phase may be present in hydrodynamic bearings and dampers by two processes: fluid vaporization (vapor cavitation) and gas trapped in the fluid (gaseous cavitation).

There have been two main streams in the study of two-phase flows as a direct result of their practical applications. The first of them considers the fluid as a two-component mixture with no mass transfer between the constituents (for lubrication with emulsions or for contaminated lubricants). The second trend of research regards the fluid as a one-component, two-phase fluid where the vaporization of the liquid requires mass transfer between the phases (face seals and annular seals). The following is a review of the relevant research on two-phase flow under these two approaches.

The continuum theory of mixtures

One of the approaches used to model a two-phase fluid is through the continuum theory of mixtures where the fluid is regarded as a homogeneous mixture of two immiscible components. This method has been applied to lubrication problems in order to

analyze the behavior of oil on water (O/W) emulsions used in metal forming processes. Nakahara et al. (1988) present an experimental study on the droplet behavior on O/W emulsion lubrication on a metal rolling process. Their observations show that the oil droplets which penetrate into the elasto-hydrodynamic-lubrication zone (EHL) form an "oil pool", i.e. an oil zone containing water droplets. In other words, a phase inversion occurs producing a water on oil (W/O) emulsion with a higher mixture viscosity in the EHL zone. The extension of this oil pool was found to be influenced by the oil concentration and the roller speed. However, at high roller speeds, coarse oil droplets cannot enter to the EHL zone because of back flow in the water phase. Only the fine droplets close to the moving surfaces enter the EHL zone producing a very fine O/W emulsion.

Szeri and co-workers (Al-Sharif 1992, Al-Sharif, et al. 1993, Wang, et al. 1993) apply the continuum theory of mixtures to the lubrication problem with liquid-liquid emulsions. In Al-Sharif's work, the continuum theory of mixtures developed by Atkin et al. (1976) and Muller (1968) are thoroughly discussed. The main assumption of this theory relates to the "equipresence principle", which states that every spatial position of a N component mixture is occupied by N particles, one per each component. Conservation equations for each component are derived and coupled by the mutual interaction of the components. The authors develop a set of constitutive equations, which when combined with material functions for viscosity, thermal conductivity and Helmholtz free energy lead to the mixture energy transport equation. The lubrication

approximation (thin films) is applied to the mass and momentum equations to render an extended Reynolds equation for mixtures. When applied to a journal bearing, the model shows some results that agree qualitatively with Nakahara et al. (1988) observations, e.g. a "filtration" phenomenon occurred in the converging region of the fluid film. Due to the difference in viscosity of the components, the one with higher viscosity flows easier to the minimum film thickness section of the fluid film increasing the mixture viscosity. The model also predicts that the maximum peak bearing pressure increases as the oil content increases.

In Wang et al. (1993), the continuum mixture theory is applied to elasto-hydrodynamic conjunctions. The model intends to represent emulsions with suspended deformable particles small enough within the minimum film thickness. An expression for the film thickness as function of velocity, load and material properties is obtained. Results of the proposed model applied to a oil-in-water emulsion show that the film thickness varies linearly with the inlet volume fraction of the oil. An increase in the concentration of oil is observed close to the minimum film thickness (oil pooling). Under this phenomenon the film thickness in the EHD conjunction is defined by the viscosity of the oil.

The next advancement in the mixture theory approach is related to gas-liquid mixtures. This type of mixture usually termed as a "bubbly" mixture may be present in applications such as fluid film bearings like seals, squeeze film dampers and journal bearings vented to ambient conditions and under dynamic loading. Tonder (1975, 1976a) presents a model for a homogeneous mixture of bubbles

and lubricant where the size of the bubbles is small compared to the film thickness and with a low bubble solubility. The model neglects temperature changes and viscosity variations due to the presence of bubbles, i.e. it regards the mixture as isoviscous. This model shows that infinitely wide parallel-surface hydrodynamic bearings cannot carry load when lubricated by a bubbly oil in the absence of large temperature changes. The author concludes that "the presence of bubbles in an oil does not generate load carrying capacity, it can only modify one produce otherwise." Tonder also shows there is a gain in load capacity in externally pressurized bearings when bubbles are trapped in the lubricant (to 10% in gas-to-lubricant volume ratio). This load gain is proportional to bubble content, bearing load factor, and inversely proportional to pressure drop. Tonder's model presents only qualitative agreement with load capacity experimental data presented by Cameron (1966) and with findings of Tonder (1976b).

Khalil et al. (1980) extended Tonder's model to account for variation in lubricant properties due to changes in pressure and temperature along the flow. The model combines continuity, momentum and energy transport equations to obtain expressions for the bearing mass flow and temperature and pressure gradients. The expressions derived are functions of the variable fluid properties, film thickness, bearing geometry, and of course, pressure and temperature gradients. Application of the model to externally pressurized bearings shows that the pressure distribution and load-carrying capacity improve with air bubble content for both rotating and non-rotating bearings.

Chamniprasart et al. (1992, 1993) extend the research of Szeri and co-workers on binary mixtures to bubbly-oil mixtures. The model considers the fluid as a mixture of a newtonian fluid and an ideal gas (typically air). However, the analysis does not account for mass transfer between component and makes the model unsuitable to handle oil vapor cavitation. The analysis when applied to a finite hydrodynamic journal bearing shows that the concentration of air (gas) affects significantly the bearing pressure distribution. The bubble size seems not to have a significant effect on the bearing pressure, although it does affect the size of the two-phase region. Comparison of numerical predictions with the experimental pressure measurements of Braun et al. (1981) show moderate qualitative agreement.

In general the models based on the continuum theory of mixtures present qualitative agreement with experimental and practical observations. Results depend on how close the modeled flow process (laminar flow with isothermal, isoviscous, adiabatic conditions) resembles the actual flow. Note that these models do not account yet for mass transfer between phases, and therefore, they are not suitable for two-phase flows where fluid vaporization/condensation is present. Furthermore, a number of yet unknown experimental parameters are needed for accurate results. It is important to note that all the models referred consider the fluid flow as laminar. This is not an appropriate assumption in applications with cryogenic fluids where the trend to higher rotational speeds as well as the tendency to roughen the surface to improve dynamic stability lead to turbulent flow conditions.

Vapor Cavitation

Zuber et al. (1982) present an early attempt to treat the two-phase flow problem arising from fluid vaporization as a homogeneous mixture in thermodynamic non-equilibrium. The model considers the conservation equations for each component and a "constitutive equation of condensation or of evaporation" specifying the mass rate of liquid formation or extraction per unit volume of mixture. The inclusion of this sink or source term is the only difference with the standard Reynolds equation for compressible fluids. Results from the analysis show that this added term has a significant effect on the static and dynamic bearing force characteristics. Unfortunately, according to the authors, the equation of evaporation and condensation which governs this source/sink term "is not known for some flow regimes and only in a rudimentary way manner for others."

Feng, et. al (1986) present density and viscosity models for two-phase homogeneous fluids used in dynamically loaded hydrodynamic bearings and squeeze film dampers. Expressions for the mixture density as a function of the volume fraction and the vapor pressure are derived for two limiting cases: full-collapse (solubility equilibrium) and non-collapse (no solubility over a load cycle). The authors show that when the fluid vapor pressure is low it has little influence in the gas phase and can be safely regarded as zero (absolute). An empirical correlation for viscosity of certain oil products known as the Hayward model (1961) is used to represent the mixture viscosity.

Pinkus (1990) rises the issue of the differences in the heat

transfer process in each flow region. In the all-liquid region heat generation is high and its temperature is slightly higher than the stator wall temperature. Thus, heat is transferred from the fluid to the walls. In the two-phase region the temperature is lower than that of the walls and the heat generation drops with the increments of quality. The mixture then extracts heat from the walls to maintain the vaporization. In the all-vapor section the heat generation is minimum, which when added to the low temperature at the end of the two-phase region cause a heat transfer from the walls and the temperature of the vapor increases.

Two-Phase Flow in Annular Pressure Seals and Face Seals

The theoretical treatment of multi-phase flow in annular seal applications is only recent. Several analysis have presented modifications to the classical lubrication theory to account for the multi-phase phenomena. Unfortunately, due to the lack of experimental data and the variety of approaches used, most of these efforts show very different results.

Hughes et al. (1978) study the vaporization of a lubricant in liquid face seals. The flow through the seal is divided into two separate regions, one liquid and one gaseous with separate equations of motion for pressure, temperature and mass flow rate in each fluid phase. The two flow zones are coupled by the conditions at the interphase surface. Hughes et al. further assume that both phases are at the same temperature (vaporization temperature). The model predicts that the maximum flow rate is reached when the fluid is fully liquid, and when two-phase flow occurs most of the pressure drop takes place in the vapor phase. The temperature

variations across the film are found not to be significant, with the main cause for liquid boiling as due to "flashing" occuring as the pressure decreases along the seal. However, the theoretical predictions for fluid pressure and temperature show evidence of a transition region where both liquid and vapor phases coexist.

Yasuna and Hughes (1990) present a "continuous boiling" model as opposed to the previous "discrete boiling" analysis. In the novel model the flow along the seal is divided into three regions: all-liquid, liquid-gas, and all-gas. The two-phase region is considered as an homogeneous mixture of saturated liquid and vapor. Results show the extent of the two-phase region to be considerable in all cases, even when the flow is nearly isothermal (discrete model). For nearly isothermal and dissipation dominated conditions, the quality of the mixture is very low (close to zero), and explains why the mixture behaves as a saturated liquid. Results also show that energy convection effects are important and often dominant with respect to the dissipation effects for the typical range of clearances used in laminar flow face seals. The "discrete boiling" model is then inadequate is such situation.

Yasuna and Hughes (1992) present an analysis for two-phase face seals including squeeze film effects and thermal transients. The model is based on the "discrete boiling" model referred earlier. Results for simulations of step perturbations of the film thickness are presented. For step increments the response decays as the rotor approaches the initial steady state conditions. For large enough film thickness step decrements the seal collapses due to the onset of an unstable vibration. For small step decrements of film

thickness the rotor approaches the steady state asymptotically in a stable oscillatory motion. The assumption of discrete boiling and laminar flow are appropriate only for small film thicknesses (low leakage rate) and limit greatly Yasuna et al.'s model. As the film thickness increases, thermal convection gains importance and a two-phase zone may appear. For even larger film thickness the flow will certainly become turbulent, and at this increased velocity condition the thermal transport process may be considered as adiabatic.

Beatty and Hughes (1987) present a turbulent flow, steady and adiabatic flow model for concentric annular pressure seals. Here the fluid flow is also divided into three regions: all liquid, liquid-vapor, and all vapor. Numerical results for the interstage seal of the Space Shuttle Main Engine High-Pressure Oxidizer Turbopump show that the leakage rate is reduced by clearance reduction, increment of rotational speed, lengthening of the seal, and vapor production (due to pressure drop). It is concluded that subcooling of the liquid before the seal inlet will reduce vapor production, and therefore, it will increase the leakage rate.

Beatty and Hughes (1990) present a different approach in a model for turbulent flow annular seals based on the stratified flow of the boiling liquid and vapor phases. Stratification of the phases is attributed to the centrifugal inertia due to shaft rotation. Governing equations for film-averaged liquid and vapor properties are presented. The model assumes the streams to be adiabatic and moving at different bulk-flow velocities, with the vapor layer closer to the shaft. Variations of the leakage rate

with speed, seal length, vapor generation, etc, are similar to that predicted with the previous "homogeneous mixture" model. However, the stratified model predicts larger leakage rates and it is less sensitive to rotational speed than the homogeneous-mixture model.

Hendricks (1987) presents a unique experimental study on uniform clearance, nonrotating, cylindrical seals for high performance turbomachines like the Space Shuttle Main Engine Fuel Pump. This report focusses in the measurement of leakage rates and pressure profiles for several fluid conditions, and for concentric and fully eccentric seal positions. The experiments demonstrate that low back pressures may lead to a two-phase flow condition within the seal. A model based on one-dimensional, steady state isentropic, two-phase momentum and energy equations provides expressions for the mass flux and pressure. These expressions are normalized to use the corresponding-states theory (Hendricks et al., 1973) to compare results using different fluids. Experimental results show two-phase choked flow near the seal exit, denoted by a positive slope of the pressure profiles in that region. The work of Hendricks is relevant because it presents useful experimental data for cryogenic fluids, namely nitrogen and hydrogen. Hydrogen test data are quite sensitive to the inlet temperature for concentric seal configuration. For eccentric operation both, liquid hydrogen and liquid nitrogen, are very sensitive to the inlet temperature.

One of the weaknesses of the analyses for two-phase flow models referred so far is the lack of firm theoretical grounds for the multi-phase transport phenomena (mass, momentum and energy).

Gray, W.G. (1975) presents a general equation for multi-phase transport of a fluid material property. This work demonstrates the importance of the correct definition of the convective and diffusive components of the transport process. Gros D'Aillon et al. (1981) present a experimental study of two-phase flow through nozzles. The measurements, representing the flow under steep pressure gradients in nuclear reactors, show the great influence that interface mass and momentum transfer have in critical flows. It seems that an appropriate treatment of the interface mass, momentum and energy transfer could be the key to a more accurate prediction of two-phase flows.

PROPOSED WORK

The importance of two-phase flow on the performance of fluid film bearings is detailed in the previous section. Operation under two-phase flow condition is likely to occur in cryogenic liquid annular seals operating close to the critical point due to the steep variations of pressure and temperature along the seal (Yang et al., 1993a). An accurate theoretical analysis for such operating conditions is yet to be developed.

The objective of this research is to advance a bulk-flow analysis for the prediction of the dynamic response of annular pressure liquid seals operating under two-phase flow conditions. The starting point of this research will be the analysis of two-phase flow of a concentric liquid annular seal working with cryogenic fluids. As for the structure of the flow, the Beaty and Hughes approach (1987) of dividing the flow inside the seal into three sections: all-liquid, vapor-liquid, and all-gas ("continuous

boiling" model) will be assumed.

Since the film thickness is very small compared to the seal radius, curvature effects can be neglected and the flow domain can be unwrapped into a cartesian coordinate system, as shown in Figure 1. Due to the large axial velocity typical of a turbulent cryogenic annular seal, the heat transfer to the walls is much smaller than the heat carried by convection, and therefore the flow can be regarded as adiabatic (Yang et al. 1993b).

The turbulent bulk-flow of a variable properties fluid inside an annular pressure seal is described by the continuity, momentum and energy transport equations given by Yang, (1992):

Continuity:

$$\frac{\partial}{\partial x_i}(\rho H U_i) + \frac{\partial}{\partial t}(\rho H) = 0 \qquad (1)$$

Momentum:

$$-H\frac{\partial P}{\partial x_i} = \frac{\left(k_i U_i - k_J \frac{\overline{\Lambda}_j}{2}\right)\mu}{H} + \frac{\partial}{\partial t}(\rho H U_i) + \frac{\partial}{\partial x_j}(\rho H U_i U_j) \qquad (2)$$

Energy:

$$C_p\left[\frac{\partial}{\partial \tau}(\rho H T) + \frac{\partial}{\partial X_i}(\rho H U_i T)\right] = \beta_t H T\left(\frac{\partial P}{\partial t} + U_i\frac{\partial P}{\partial X_i}\right) + \Omega R\frac{H}{2}\frac{\partial P}{\partial X} + \frac{\mu}{H}\left[k_x\left(U_x^2 + U_y^2 + \frac{\Omega R U_x}{2}\right) + k_J\left(\frac{\Omega^2 R^2}{4} - U_x \Omega R\right)\right] \qquad (3)$$

where: i,j=x,y. circumferential and axial coordinates.

$\overline{\Lambda}_x=\Omega R$; $\overline{\Lambda}_y=0$, journal surface speeds.

k_i, k_j, turbulent shear parameters

$\rho=\rho(P,T)$; $\mu=\mu(P,T)$,

$C_p=C_p(P,T)$; $\beta_t=\beta_t(P,T)$ for a variable properties fluid.

These equations are valid for any single-phase compressible fluid, and thus can be applied directly to the all- liquid or the all-vapor regions. For the vapor-liquid region the transport equations have to be specialized to account for the variation of the mixture properties such as density, viscosity, etc. The two-phase mixture will be considered as homogeneous, and thus, its properties will be expressed as a function of the mixture quality. Additionally, if the heat of vaporization is significant relative to the dissipation energy, i.e. appreciable amounts of heat are taken from the fluid to maintain the vaporization, the mixture properties will be a function of the heat transfer process (Pinkus, 1990).

The present research will bring special attention to the interphase interaction (mass and energy transfer) expressed by the mixture quality. The limited understanding of this phenomenon accounts for a great deal of the discrepancies among the different two-phase flow models.

As in previous analyses (San Andres, 1991, and Yang et al., 1993a,b), equations (1-3) will be subject to a perturbation analysis to obtain the dynamic response of the seal. The rotor is considered to describe small amplitude translational motions about an equilibrium position. For such small motions the flow velocity, temperature and pressure along with the fluid properties are expressed as the superposition of a zeroth order and a first order fields. The zeroth order equations describe the equilibrium

condition and their solution will provide static parameters like leakage, torque and temperature rise. The first order equations describe the perturbed dynamic motion of the rotor, and their solution will render the linearized force coefficients due to journal lateral motions.

REFERENCES

Al-Sharif, A., 1992, "Hydrodynamic Lubrication with Emulsion," Ph.D. Dissertation, Department of Mechanical Engineering, University of Pittsburgh.

Al-Sharif, A., Chamniprasart K., Rajagopal K.R., Szeri A.Z., 1993, "Lubrication with Binary Mixtures: Liquid-Liquid Emulsion," *ASME Journal of Tribology*, Vol. 115, pp. 46-55.

Atkin, R.J., Craine, R.E., 1976, "Continuum Theories of Mixtures: Basic Theory and Historical Development," Quarterly Journal of Mechanics and Applied Mathematics, Vol. 29, pp. 209-244.

Beatty, P.A., and Hughes, W.F., 1987, "Turbulent Two-Phase Flow in Annular Seals," *ASLE Trans.*, Vol. 30,1, pp. 11-18.

Beatty, P.A., and Hughes, W.F., 1990, "Stratified Two-Phase Flow in Annular Seals," *ASME Journal of Tribology*, Vol. 112, pp. 372-381.

Braun, M. and Hendricks, R., 1981, "An Experimental Investigation of the Vaporous / Gaseous Cavity Characteristics of an Eccentric Journal Bearing," ASLE Trans., Vol. 27, pp. 1-14.

Cameron, A., 1966, "Principles of Lubrication," Longman, Harlow, Essex.

Chamniprasart K., 1992, "A Theoretical Model of Hydrodynamic Lubrication with Bubbly Oil," Ph.D. Dissertation, Department of Mechanical Engineering, University of Pittsburgh.

Chamniprasart K., Al-Sharif A., Rajagopal K.R., Szeri A.Z., 1993, "Lubrication with Binary Mixtures: Bubbly Oil," *ASME Journal of Tribology*, Vol. 115, pp. 253-260.

Feng N.S. and Hahn E.J., 1986, "Density and Viscosity Models for Two-Phase Homogeneous Hydrodynamic Damper Fluids," *ASLE Trans.*, Vol. 29, pp. 361-369.

Gray, W.G., 1975, "A Derivation of the Equations for Multi-phase Transport," Chemical Engineering Science, Vol.30, pp. 229-233.

Gros D'Aillon, L., and Jeandey, C., 1981, "Two Phase Flow under Steep Pressure Gradients," Proceedings of the Third CSNI Specialist Meeting on Transient Two-Phase Flow, Pasadena, California, Mar 23-35, 1981, pp. 123-132.

Hayward, A.T.J., 1961, "Viscosity of Bubbly Oil," Fluids Report No. 99, National Engineering Laboratory.

Hendricks, R.C. and Simoneau, R.J., 1973, "Application of the

Principle of Corresponding States to Two-Phase Choked Flow," NASA TM X-68193.

Hendricks, R.C., 1987, "Straight Cylindrical Seals for High Performance Turbomachinery," NASA TP-1850.

Hughes, W.F., Winowich, N.S., Birchak, M.J., Kennedy, W.C., 1978, "Phase Change in Liquid Face Seals,", *ASME Journal of Tribology*, Vol. 100, pp. 74-80.

Khalil, M.F. and Rhodes, E., 1980, "Effect of Air Bubbles on Externally Pressurized Bearing Performance," WEAR, Vol. 65, pp. 113-123.

Muller, I., 1968, "A Thermodynamic Theory of Mixture of Fluids," Archive for Rational Mechanics and Analysis, Vol. 28, pp. 1-39.

Nakahara, T., Makino, T., Jyogoku, K., 1988, "Observations of Liquid Droplet Behavior and Oil Film Formation in O/W Type Emulsion Lubrication," ASME Journal of Tribology, Vol. 110, pp. 348-353.

Pinkus, O., 1990, "Thermal Aspects of Fluid Film Tribology," ASME Press, New York, pp. 326-340.

Reynolds, O., 1886, "On the Theory of Lubrication and its Application to Mr. Beauchamp Tower's Experiments Including Experimental Determination of the Viscosity of Olive Oil," Philosophical Transactions, Vol. 177, pp. 157-234.

San Andres, L.A., 1991, "Analysis of Variable Fluid Properties, Turbulent Annular Seals," ASME Journal of Tribology, Vol. 113, pp. 694-702.

Tonder,K., 1975, "Parallel Surfaces Lubricated by a Bubbly Oil," WEAR, Vol. 35, pp. 23-34.

Tonder, K., 1976a, "Thermal Model of Effects of Gas Bubbles on the Lubrication of Parallel Surfaces," WEAR, Vol. 40, pp. 37-50.

Tonder, K., 1976b, "Effect on bearing performance of a bubbly lubricant'" JSLE-ASLE Int. Lubr. Conf., Tokyo, 1975, Elsevier, Amsterdam, 1976.

Wang S.H., Al-Sharif A., Rajagopal K.R., Szeri A.Z., 1993, "Lubrication with Binary Mixtures: Liquid-Liquid Emulsion in an EHL Conjunction," *ASME Journal of Tribology*, Vol. 115, pp. 515-522.

Yang, Z., 1992, "Thermohydrodynamic Analysis of Product-Lubricated Hydrostatic Bearings in Turbulent Regime," PhD. Dissertation, Department of Mechanical Engineering, Texas A&M University.

Yang, Z., San Andres, L.A., Childs, D., 1993a, "Thermal Effects in Cryogenic Liquid Annular Seals. Part II: Numerical Solutions and Results," *ASME Journal of Tribology*, Vol. 115, pp. 277-284.

Yang, Z., San Andres, L.A., Childs, D., 1993b, "Thermal Effects in Cryogenic Liquid Annular Seals. Part I: Theory and Approximate Solution ," *ASME Journal of Tribology*, Vol. 115, pp. 267-276.

Yasuna, J.A., Hughes, W.F., 1990, "A Continuous Boiling Model for Face Seals," *ASME Journal of Tribology*, Vol. 112, pp. 266-274.

Yasuna, J.A., Hughes, W.F., 1992, "Squeeze Film Dynamics of Two-Phase Seals," *ASME Journal of Tribology*, Vol. 114, pp. 236-247.

Zeidan, F.Y., Vance, J.M., 1989, "Cavitation Leading to a Two Phase Fluid in a Squeeze Film Damper," *ASLE Trans.*, Vol. 32, pp. 100-110.

Zeidan, F.Y., Vance, J.M., 1990, "A Density Correlation for a Two Phase Lubricant and its Effect on the Pressure Distribution," *ASLE Trans.*, Vol. 33, pp. 641-647.

Zuber N. and Dougherty D.E., 1982, "The Field Equations for Two-Phase Reynolds Film Flow with a Change of Phase," *ASLE Trans.*, Vol. 25, pp. 108-116.

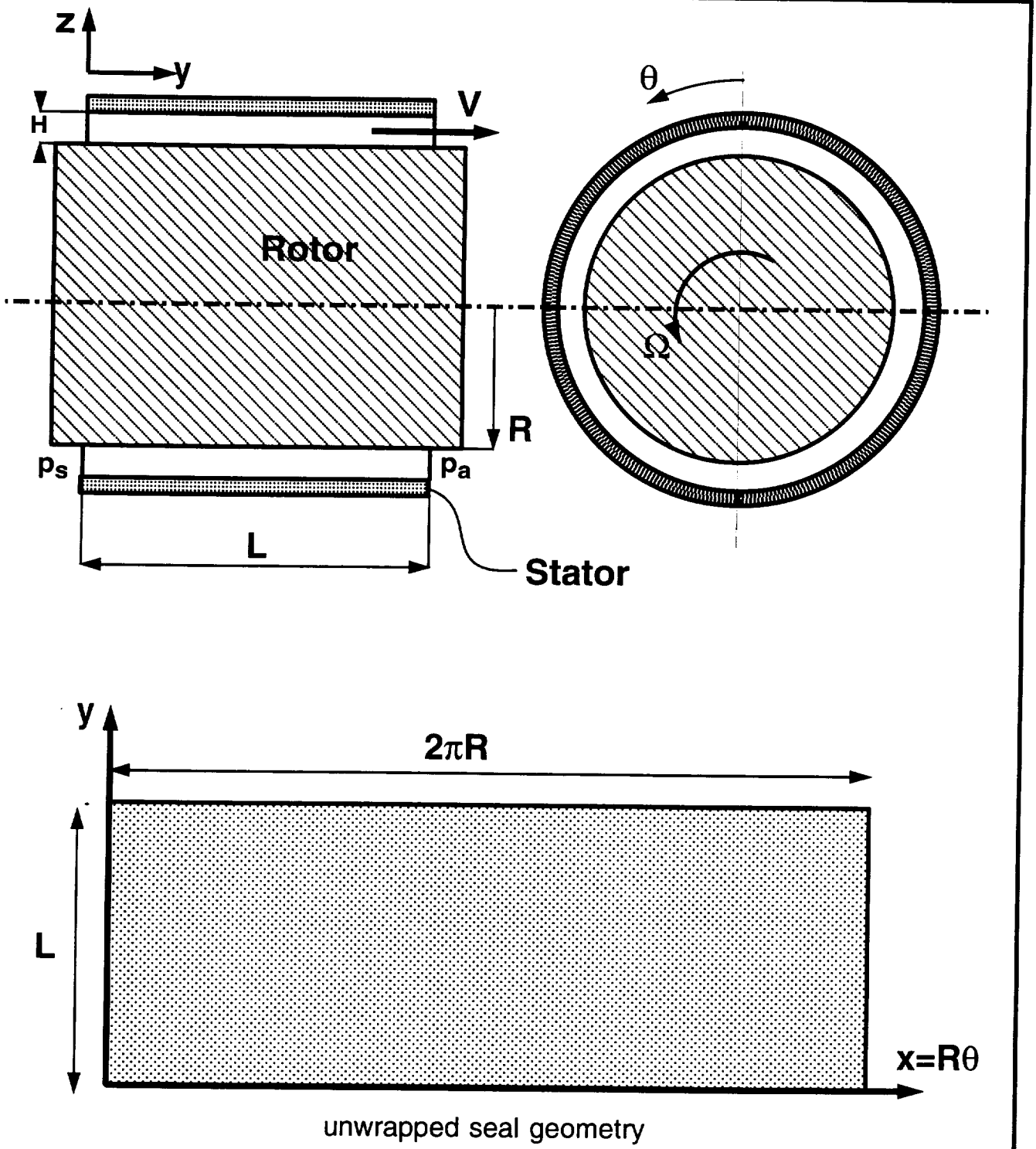

Figure 1. Annular pressure seal geometry and coordinate system.